On the Indeterminates of Glaucoma

Pappelis, Konstantinos

DOI:
10.33612/diss.217111330

University of Groningen

On the Indeterminates of Glaucoma

The Controversy of Arterial Blood Pressure and Retinal Perfusion

Konstantinos Pappelis

On the Indeterminates of Glaucoma. The Controversy of Arterial Blood Pressure and Retinal Perfusion

PhD dissertation, University of Groningen, The Netherlands

Authored by Konstantinos Pappelis, M.D.; 2022

Cover design: K. Pappelis & WOMBO dream (www.wombo.art)

Printed by: Gildeprint - The Netherlands (www.gildeprint.nl)

DOI: <to be completed>

ISBN: <to be completed>

This PhD dissertation was supported by the European Union's Horizon 2020 Innovative Training Networks Program, under the Marie Sklodowska–Curie grant, Project ID 675033 and by the University of Groningen Graduate School of Medical Sciences (GSMS). The publication of this PhD dissertation was generously supported by the Research School of Behavioural and Cognitive Neurosciences (BCN) and the Professor Mulder Stichting.

rijksuniversiteit
groningen

On the Indeterminates of Glaucoma

The Controversy of Arterial Blood Pressure and Retinal Perfusion

Proefschrift

ter verkrijging van de graad van doctor aan de
Rijksuniversiteit Groningen
op gezag van de
rector magnificus prof. dr. C. Wijmenga
en volgens besluit van het College voor Promoties.

De openbare verdediging zal plaatsvinden op

donderdag 7 juli 2022 om 11:00 uur

door

Konstantinos Pappelis

geboren op 1 september 1991
te Amarousio, Griekenland

Promotores
Prof. N.M. Jansonius
Prof. P. van Dijk

Beoordelingscommissie
Prof. dr. J.M.C. van Dijk
Prof. dr. C.A.B. Webbers
Prof. dr. G. Garhöfer

Table of Contents

Preface

This dissertation is the intellectual product of a four-year scientific journey that took place as part of the multidisciplinary European Glaucoma Research Education Training and Training Plus (EGRET/EGRET+) endeavor (https://www.egret-program.eu/, https://egret-plus.eu/). As such, it was conceptualized, stimulated, and realized within a wider setting of academic discourse. This context, together with the external peer review process, the inspiration drawn from previous work, and the perpetual inner self-questioning have contributed an additional dimension to the standard monological argumentation that is naturally dominant in this type of treatise. This dialectical aspect includes not only the exchanges with my fellow peers and mentors, but also with the constantly evolving versions of myself. Indeed, substantial interdisciplinarity is present in the research behind this thesis, which required that I undertook several roles, in addition to that of the prospective ophthalmologist. For all these reasons, although this dissertation is presented as a collection of publications telling one story, my hope is that it will not be merely regarded as such.

Nevertheless, the interested reader can hereunder find the list of all publications that were produced during this period and that either directly compose or support this dissertation:

Chapter 2 published as:

Pappelis K, Loiselle AR, Visser S, Jansonius NM. Association of Systemic Medication Exposure With Glaucoma Progression and Glaucoma Suspect Conversion in the Groningen Longitudinal Glaucoma Study. *Invest Ophthalmol Vis Sci*. 2019;60(14):4548-4555.

Chapter 3 published as:

Pappelis K, Jansonius NM. Quantification and Repeatability of Vessel Density and Flux as Assessed by Optical Coherence Tomography Angiography. *Transl Vis Sci Technol*. 2019;8(3):3.

Chapter 4 published as:

Pappelis K, Choritz L, Jansonius N. Microcirculatory model predicts blood flow and autoregulation range in the human retina: in vivo investigation with Laser Speckle Flowgraphy. *Am J Physiol Heart Circ Physiol*. 2020;319(6):H1253-1273.

Chapter 5 published as:

Pappelis K, Jansonius NM. U-shaped Effect of Blood Pressure on Structural OCT Metrics and Retinal Perfusion in Ophthalmologically Healthy Subjects. *Invest Ophthalmol Vis Sci*. 2021;62(12):5.

Chapter 6 published as:

Pappelis K, Jansonius NM. Retinal Oxygen Delivery and Extraction in Ophthalmologically Healthy Subjects With Different Blood Pressure Status. *Transl Vis Sci Technol*. 2022;11(2):9.

Supporting publication:

Al-Nosairy KO, Prabhakaran GT, Pappelis K, Thieme H, Hoffmann MB. Combined Multi-Modal Assessment of Glaucomatous Damage With Electroretinography and Optical Coherence Tomography/Angiography. *Transl Vis Sci Technol*. 2020;9(12):7.

While this dissertation would likely mainly appeal to ophthalmologists (and hopefully also to cardiologists and vascular internists), I would like to think that it might contain something for everyone: from standard clinical research and epidemiology to state-of-the-art ophthalmic imaging and from biophysical models to vascular physiology and principles of oxygen transport.

In the hope that all readers will find something interesting in the next pages,

Konstantinos Pappelis

Athens, Feb. 20th 2022

Chapter 1

BACKGROUND – INTRODUCTION TO RETINAL PERFUSION

1.1. Abstract

The retina is a layered, posterior ocular structure, responsible for the complex task of producing visual outputs. As such, its function is intrinsically dependent on efficient, well-regulated perfusion mechanisms and on adequate tissue oxygen supply. The innermost retinal layers extend to form the optic nerve and are directly linked to the pathology of the insidious, neurodegenerative eye disease known as glaucoma.

Although the pathogenesis of glaucoma is essentially multidimensional and mainly centered around increased intraocular pressure, compiling evidence over the past decades hints towards a vascular component of the disease. Systemic arterial blood pressure, in particular, has long been thought to be implicated in retinal and glaucomatous pathology, since it could disrupt the mechanisms through which the local microcirculation ensures sufficient tissue perfusion.

Recent advancements in imaging techniques have enabled the detailed depiction of retinal vascularisation, along with retinal neural structure. Nevertheless, although different methods have been proposed for the quantification of retinal blood flow and oxygen extraction in absolute terms, none have found their way to the clinical routine, mostly due to technical shortcomings. As a result, our understanding of the interplay between arterial blood pressure, inner retinal perfusion, and oxygenation and their pertinence to glaucoma remains largely incomplete.

As a whole, this dissertation aims to address this knowledge gap from different perspectives, utilizing a variety of tools, namely epidemiological evidence, retinal image analysis techniques, theoretical modeling, and findings from the clinical setting. We use this introductory chapter to provide the readers with the necessary background, in order to guide them through the complete rationale of this dissertation.

1.2. Overview of the Retina

1.2.1. Structural Anatomy

The posterior, internal surface of the eye (also known as the fundus) is coated by the retina, a layered structure consisting of a multitude of neuronal and non-neuronal cells.[1] The retina extends circumferentially and anteriorly to the ciliary body, ending with the ora serrata, a scalloped border roughly equidistant from the eye equator and the corneal limbus (Fig. 1). The anterior retinal surface lies in direct contact with the vitreous body by means of the internal limiting membrane (ILM), formed by the basal membrane of retinal glial cells, known as Müller cells. The posterior retinal surface is covered by the acellular Bruch's membrane, a thin layer of extracellular matrix separating the retina from the choroid (Fig. 2). The full retinal thickness, that is, the average distance between the anterior and posterior retinal surface, is ~250 μm.[2]

In almost all its span, the retina is composed by ten layers (Fig. 2).[1] The innermost layer, the *retinal nerve fiber layer (RNFL)*, contains the axons of the retinal ganglion cells (RGCs), whose bodies are found in the adjacent *ganglion cell layer (GCL)*. The *inner plexiform layer (IPL)* comprises a dense network of synapses between RGC dendrites and axons of cells belonging to the *inner nuclear layer (INL)*. Together, the RNFL, GCL, and IPL form the ganglion cell complex (GCC). Within the INL, the bodies of various intermediate neurons can be found, namely bipolar, horizontal, and amacrine

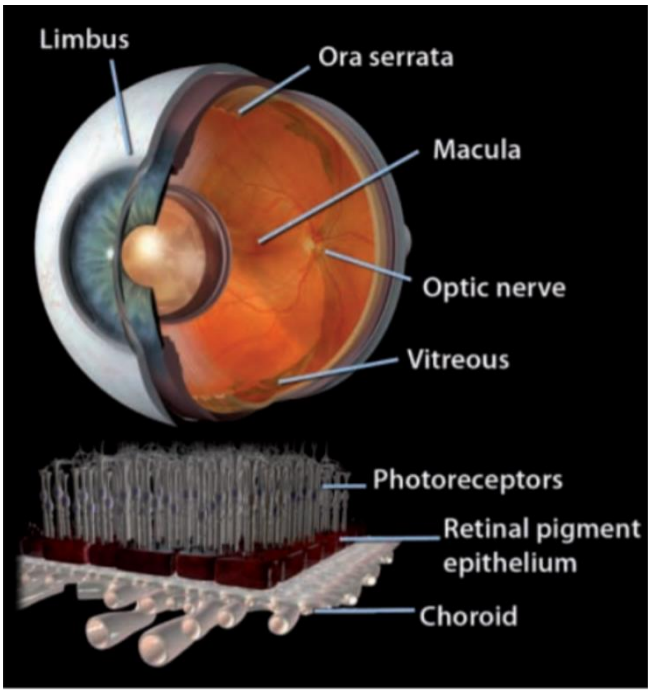

Fig. 1. The retina lines the internal surface of the posterior two thirds of the globe. It is thickest around the optic nerve and ends at the ora serrata, 5-7 mm behind the limbus. The macula lies temporal to the optic nerve, bordered by the vascular arcades; the fovea is a depression at its centre that provides fine visual acuity. The outermost layer of the retina contains photoreceptors (rods and cones), loosely attached to the retinal pigment epithelium; they depend on the retinal pigment epithelium and choroid for support. The vitreous completely fills the vitreous cavity and is firmly attached to the retina near the ora serrata, over the optic nerve and macula, along the blood vessels, and around degenerative retinal lesions. Reproduced from Management of retinal detachment: a guide for non-ophthalmologists, Kang HK, Luff AJ, 336, p. 1235, 2008, with permission from BMJ Publishing Group Ltd.

cells. The Müller cell bodies are also present in this layer. The *outer plexiform layer (OPL)* is the second synaptic layer, where bipolar and horizontal cells interconnect with the two kinds of photoreceptors (rods and cones). The *outer nuclear layer (ONL)* contains the photoreceptor granules and cell bodies, whose bases are lined on the *external limiting membrane (ELM)*. Below the ELM lies the *photoreceptor layer*, where the outer photoreceptor segments are found. The outermost retinal layer is the *retinal pigment epithelium (RPE)*, a single layer of tightly-packed, hexagonal cells containing melanin granules. Tight junctions between the RPE cells form the outer blood-retinal barrier.

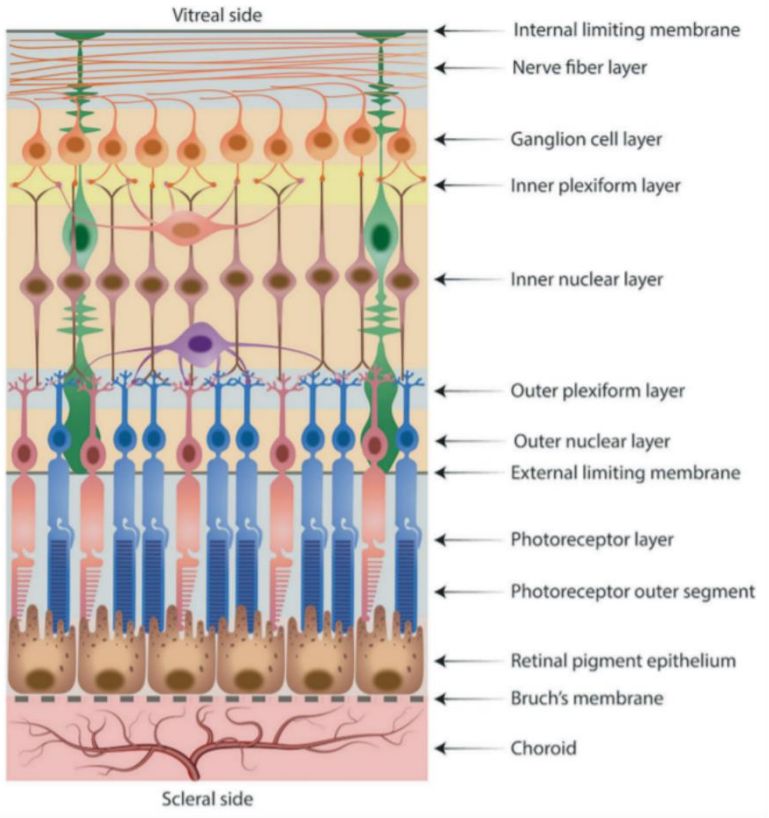

Fig. 2. Retina and choroid. Schematic diagram of retinal layers, Bruch's membrane and choroid. Reprinted from Eye, 35, Ferrara M, Lugano G, Sandinha MT, Kearns V, Geraghty B, Steel DHW, Biomechanical properties of retina and choroid: a comprehensive review of techniques and translational relevance, pp. 1818-1832, 2021, with permission from http://creativecommons.org/licences/by/4.0/.

In emmetropic eyes, that is, eyes with no refractive anomalies, the entering light rays are focused on the retina and form an image, according to optical principles. The light signal induces an electrical response by the photoreceptors, which is sequentially transmitted to the intermediate neurons and RGCs.[3,4] This electric signal subsequently travels to the visual center of the brain for higher processing via the optic nerve, which is essentially formed by the posteriorly extending axons of the RNFL.

The macula, an oval-shaped area with a diameter of ~5.5 mm at the center of the retina, is responsible for central vision.[1] Fine visual acuity (VA) is achieved by the fovea, a ~1.5-mm-diameter central depression, where the photoreceptors are directly exposed (Fig. 3). An avascular zone inside the fovea contains the foveola (or ‘fovea centralis’), the retinal location with the highest density of cone photoreceptors. About 4.5 mm nasally with respect to the macula lies the optic disc (also known as optic nerve head [ONH]), an opening of the

retina at the level of Bruch's membrane, which corresponds to the blind spot, due to the absence of photoreceptors (Fig. 3). The center of the ONH is, on average, situated slightly higher than the macula with respect to the horizontal meridian, at ~2° of visual angle.[5,6]

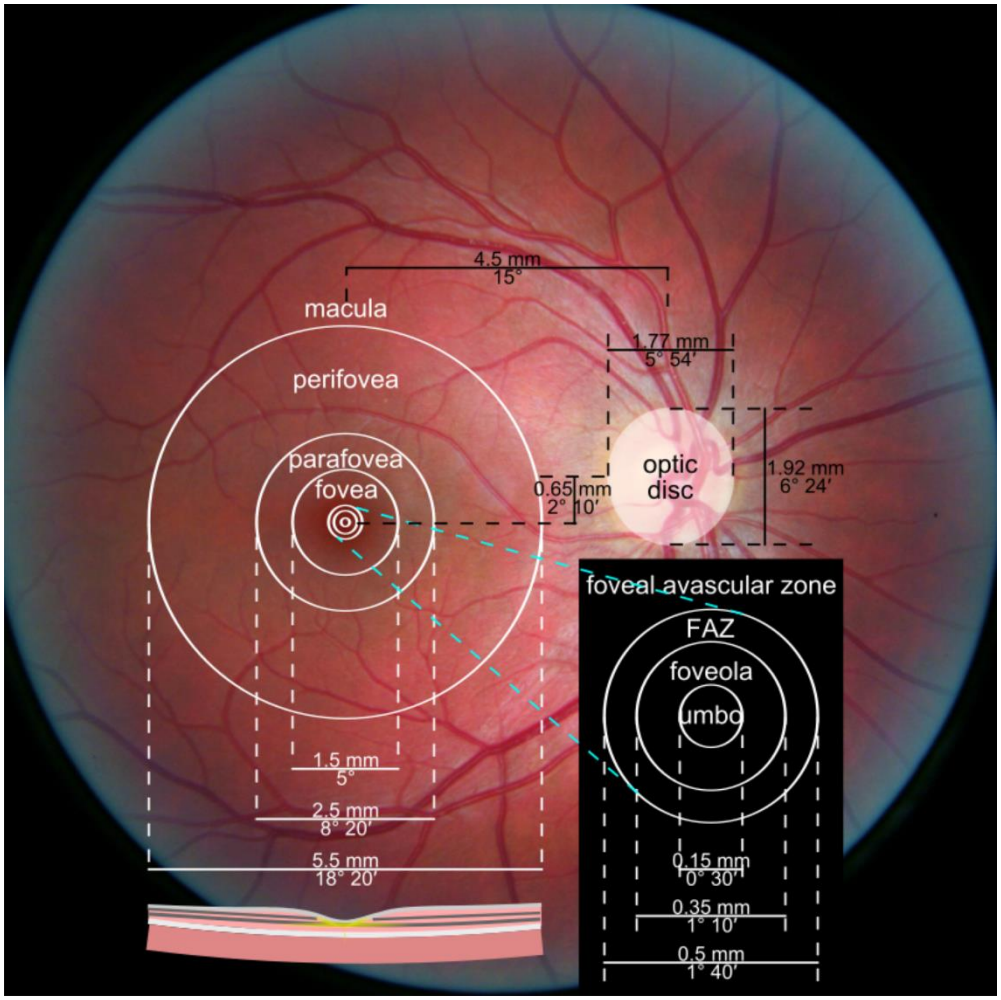

Fig. 3. Retinal image of a right eye (OD), obtained with a fundus camera at a 45° field of view, with overlay diagrams showing the standard dimensions and topography of the macula, fovea, and optic disc. The retina is thinner at the fovea (cross-section), due to lateral displacement of the inner layers, up to the outer plexiform layer. The optic disc lies nasally to the macula, at a distance of ~15° of visual angle. Photograph by Danny Hope (Brighton & Hove, UK), reproduced with permission from https://creativecommons.org/licenses/by/2.0/.

1.2.2. Structural Imaging: Optical Coherence Tomography (OCT)

Optical coherence tomography (OCT) is currently the gold-standard imaging technique for the assessment of retinal structure, because of its non-invasive nature and its ability to produce three-dimensional high-resolution images.[7] Utilizing a broadband light source and interferometry principles, longitudinal (z-axis) scans are acquired for each retinal location (A-scans), which are then combined laterally in the second dimension (B-scans) and third dimension (volumetric scans). Currently, commercial OCT systems fall under the category

of Fourier domain OCT (FD-OCT), which is further subdivided into spectral domain OCT (SD-OCT) and swept source OCT (SS-OCT), based on the underlying technology.

The tomograms (cross-sections) produced by OCT allow for segmentation of the retinal layers and quantification of their thickness. Structures of the ONH, such as the neuroretinal rim (i.e., the posteriorly extending RNFL fibers at the border of the ONH) and the optic cup (i.e., the depression at the center of the optic disc, starting at the edge of the neuroretinal rim) can also be visualized and measured (Fig. 4). The lateral resolution of OCT scans is usually better than 20 µm, while the axial resolution is ~5 µm.[7] While not always necessary, pupil dilation with mydriatic agents usually results in less artifacts and improved image quality.

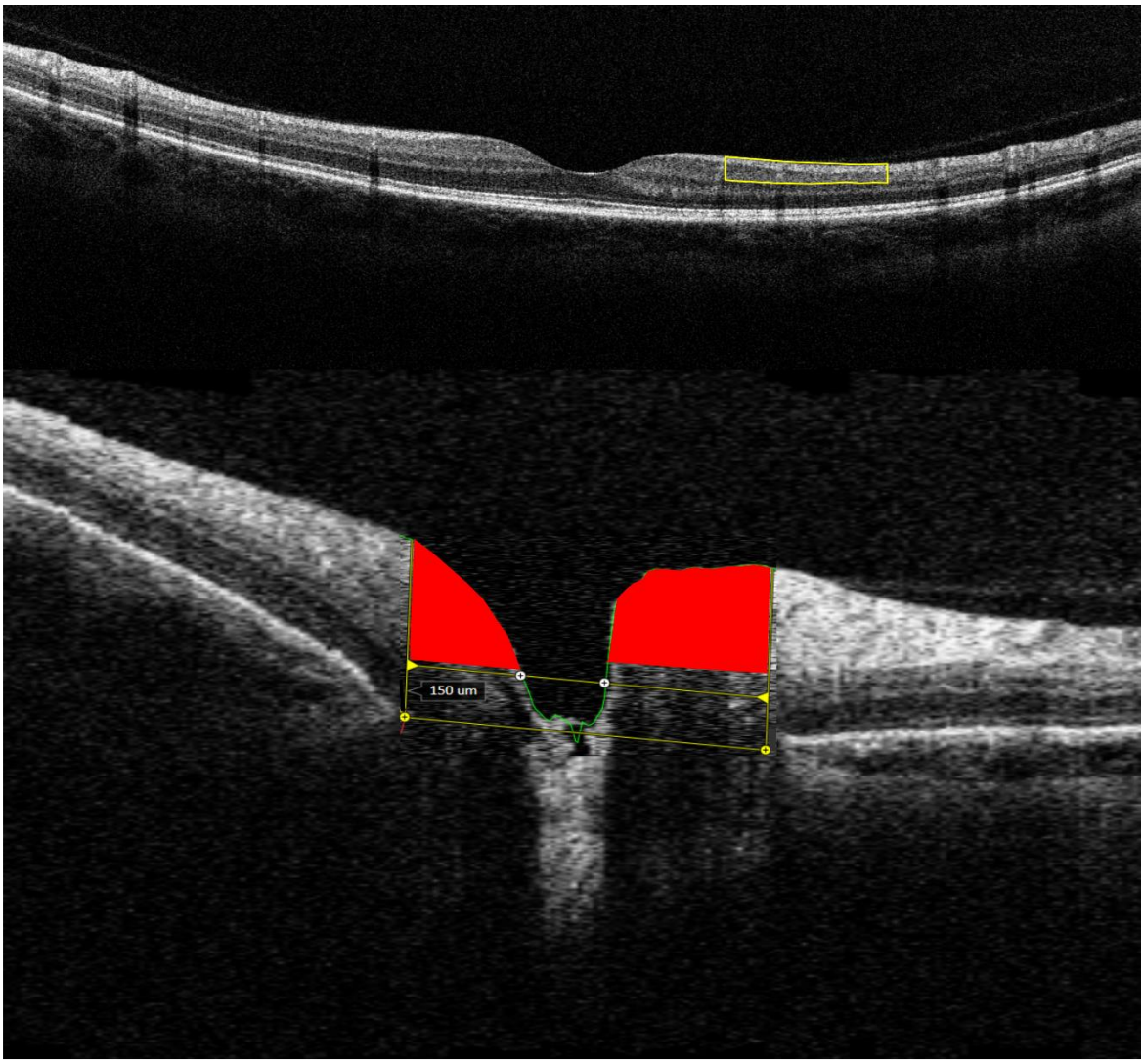

Fig. 4. Top image: B-scan centered at the macula. The retinal layers are discernible and can be segmented because of differences in signal strength. The region surrounded by yellow borders corresponds to the ganglion cell complex (RNFL+GCL+IPL). Blood vessel shadows projecting to the outer layers appear as vertical lines crossing the retina. Bottom image: B-scan centered at the optic nerve. The optic disc is located at the opening of Bruch's membrane (yellow circles). The neuroretinal rim is shown in red. The optic cup is measured 150 µm anteriorly to the opening of Bruch's membrane (white circles), at the edge of the neuroretinal rim. Images were obtained with the Canon HS100 SD-OCT (Canon, Inc., Tokyo, Japan).

1.2.3. Vascular Anatomy

The human vascular system consists of the macrocirculation, which comprises the larger arteries and veins, and the microcirculation, which comprises vessels of smaller caliber (diameter usually less than 100-200 μm), namely arterioles, venules, and capillaries. The compliant (i.e., elastic) arteries of the macrovasculature are responsible for transporting blood to the microvasculature, which nourish and deliver oxygen to terminal organs, such as the retina.

The inner two-thirds of the retina receive blood supply from the retinal circulation, while the photoreceptors and RPE are nourished by the choroidal circulation.[9] The retinal circulation originates from the central retinal artery (CRA), a branch of the ophthalmic artery that penetrates the optic nerve sheath ~10 mm posterior to the globe (Fig. 5). Despite its name, the CRA is classified as an arteriole, because of its relatively small caliber (~160 μm).[10] After passing through the mesh-like scleral opening known as the lamina cribrosa, the CRA enters the retina through the optic disc. At this location, tangentially to the RNFL, four principal branches emerge, each one spanning a different retinal quadrant (superotemporal, inferotemporal, superonasal, inferonasal).

Sequential bifurcations give rise to two distinct capillary networks, the superficial capillary plexus (SCP) and the deep capillary plexus (DCP) (Fig. 6). The SCP is located at the level of the GCL and is responsible for nourishing the RGCs. The DCP is located at the level of the INL and OPL and is the result of vertical anastomoses from the SCP.[11] Recent imaging studies have revealed the existence of a third, in-between network, known as the intermediate capillary plexus (ICP).[12] Most, but not all, evidence supports that the SCP, ICP, and DCP are connected in series, rather than in parallel, with the arteriolar branches mostly located in the SCP and the venular branches in the DCP.[11-14] A fourth plexus of the retinal circulation, known as the radial peripapillary capillary plexus (RPCP), runs parallel to the RNFL axons, after emerging from the ONH. The RPCP is denser in the peripapillary area (i.e., the region extending ~3-4 mm around the center of the ONH) and extends towards and around the fovea, following axon trajectories.

The walls of the larger retinal arterioles consist of as many as seven layers of smooth muscle cells, but become much thinner at the peripheral arterioles of higher order.[9] A layer of endothelium (tunica interna) lies directly in contact with the vessel lumen. The inner blood-

retinal barrier is formed because of the existence of tight junctions between endothelial cells, in combination with an increased density of pericytes and glial cells.

Because of the aforementioned ‘in series’ arrangement, the venular drainage of the retinal circulation mainly occurs at the level of the DCP, with venules of gradually higher order

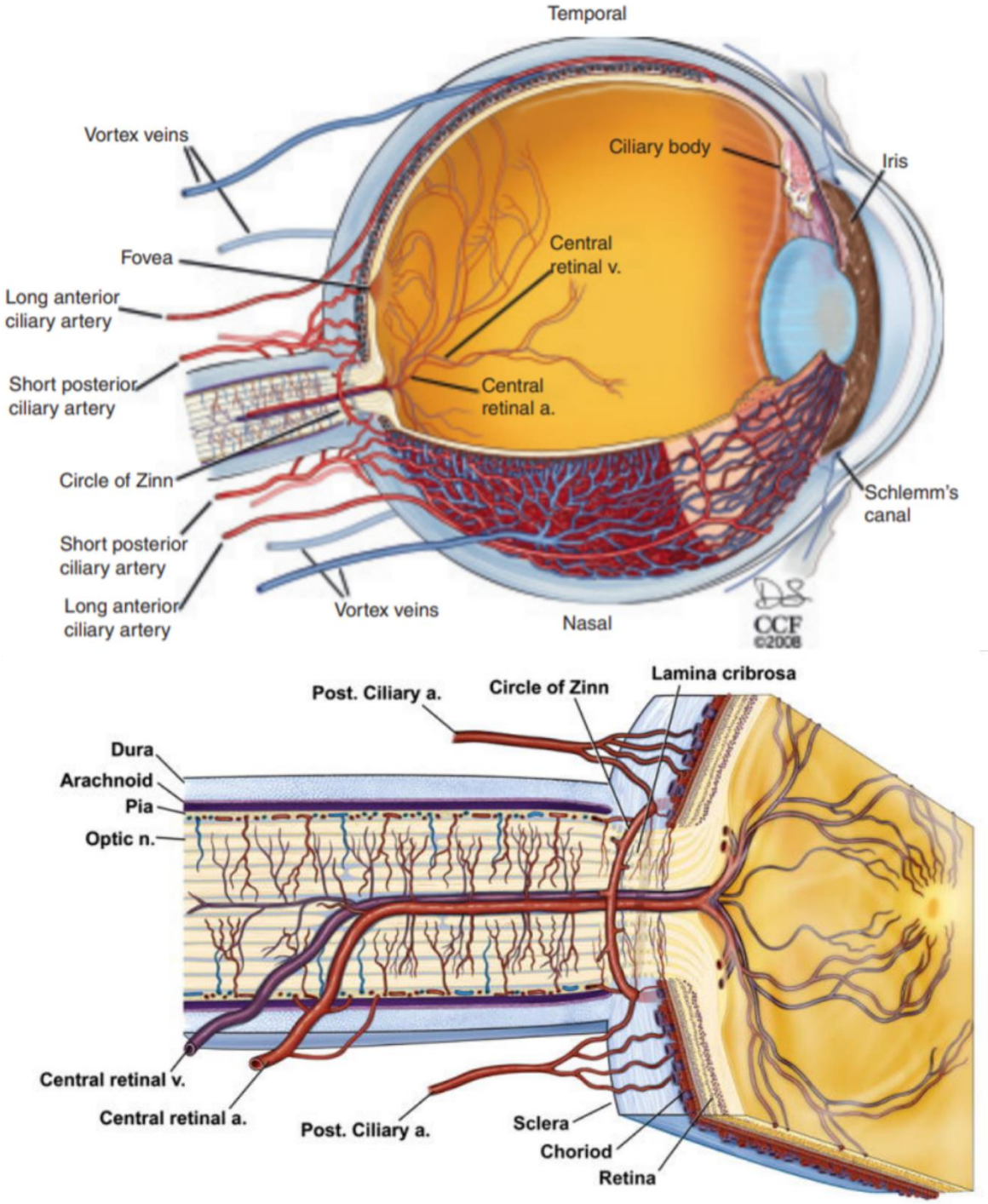

Fig. 5. Top image: A cutaway drawing of the human eye showing the major blood vessels supplying the retina, choroid, and anterior segment. The view is from a superior position over the left eye and the horizontal section passes through both the optic nerve and the fovea. Bottom image: A cutaway drawing along the superior-inferior axis of a left human eye through the optic nerve, showing details of the vascular supply in this location. The fovea is present on the right side of the drawing at the center of the termination of the central retinal vessels. Drawings by Dave Schumick. Reprinted from Encyclopedia of the Eye. Academic Press, Anand-Apte B, Hollyfield JG, Developmental anatomy of the retinal and choroidal vasculature, pp. 9–15, Copyright (2009), with permission from Elsevier and from the Cleveland Clinic Center for Medical Art & Photography © 2008. All Rights Reserved.

emerging to the RNFL and combining to form the central retinal vein (CRV).[11,14] The CRV has a larger lumen (diameter ~235 μm) than the CRA.[10] The two run parallel as the CRV exits the retina through the optic disc and the lamina cribrosa, eventually draining in the cavernous sinus through the ophthalmic vein (Fig. 5).

The choroidal circulation is mainly derived from the long and short ciliary arteries, also branching off the ophthalmic artery.[9] It accounts for ~85% of the ocular circulation. Higher order branches compose the outermost Haller's layer, while medium-sized vessels are located in Sattler's layer. The innermost dense network of terminal choriocapillaris supplies the deeper retinal layers (Fig. 6). An anastomotic ring formed by the short posterior ciliary arteries, known as the circle of Zinn-Haller, is responsible for the blood supply of the ONH. As opposed to retinal vessels, choroidal vessels are fenestrated, that is, endothelial cells do not form tight junctions. Venular return occurs through the vortex veins, which, similar to the retinal circulation, drain in the cavernous sinus through the ophthalmic vein.

A variety of imaging techniques have been developed to depict the retinal microvasculature. For the sake of brevity, in the next subsection we only introduce the ones that are relevant to this treatise.

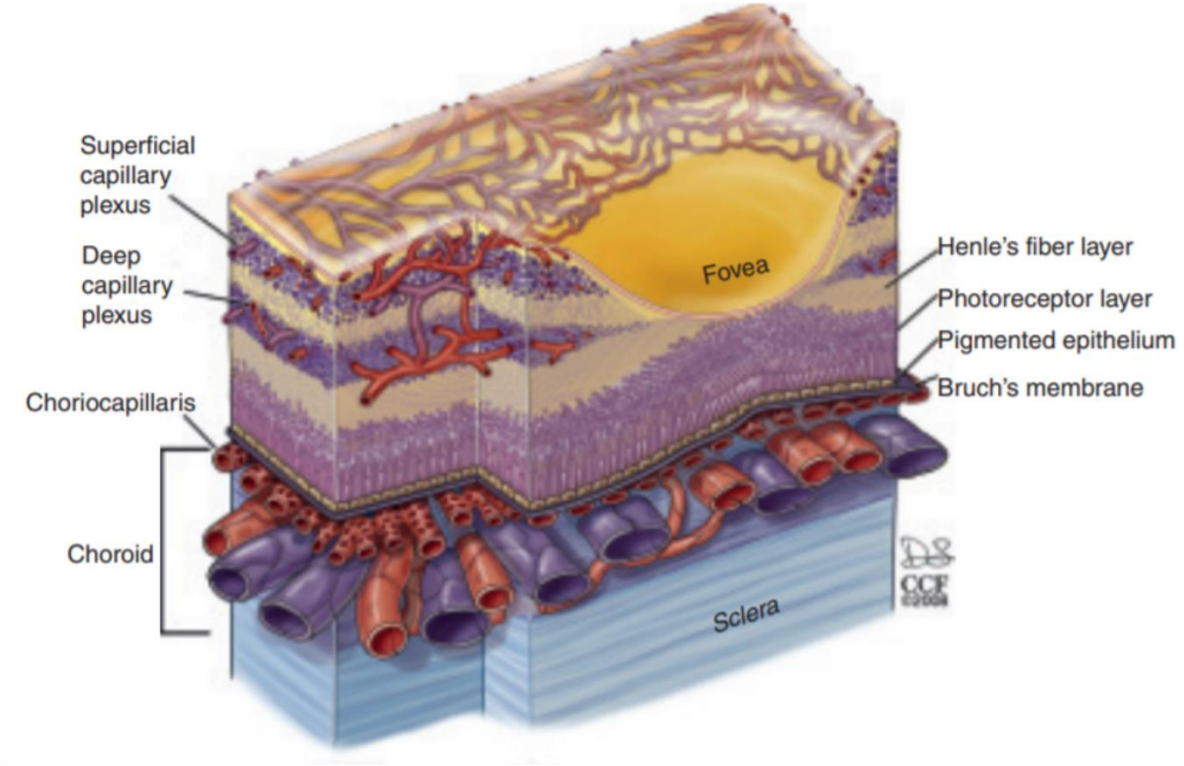

Fig. 6. A diagram showing details of the retinal and choroidal vasculature and changes that occur at the level of the human fovea. The branches from the central retinal circulation form two distinct capillary plexi within the ganglion cell layer (the superficial capillary plexus) and in the inner nuclear layer (the deep capillary plexus). These two vascular plexi end as the ganglion cell and inner nuclear layer disappear in the foveal slope. The choroid contains a dense vascular network terminating with the fenestrated choriocapillaris adjacent to Bruch's membrane. Drawing by Dave Schumick. Reprinted from Encyclopedia of the Eye, Academic Press, Anand-Apte B, Hollyfield JG, Developmental anatomy of the retinal and choroidal vasculature, pp. 9-15, Copyright (2009), with permission from Elsevier and from the Cleveland Clinic Center for Medical Art & Photography © 2008. All Rights Reserved.

1.2.4. Vascular Imaging

A) Fundus imaging

Fundus imaging is a modality extensively used in the clinical setting, serving as an equivalent to ophthalmoscopy, but with the possibility of widefield image acquisition. It produces two-dimensional digital images, depicting prominent retinal features (Fig. 3). Conventional fundus cameras use flood-illuminated imaging, whereas scanning laser ophthalmoscopes (SLOs) implement raster techniques.[8] In both cases, the lateral resolution of modern apparatus usually reaches ~6-7 μm, limited by the resolution of the eye optics.

Abundance of static information on the structure and branching pattern of the large retinal vessels can be extracted and quantified from fundus photographs. When contrast agents in the form of fluorescent dyes are introduced to the systemic circulation, modalities such as fluorescein angiography and indocyanine-green angiography enable the visualization of smaller vessels and the evaluation of certain dynamic components, such as vascular blockage or leakage.

Tailored fundus cameras and SLOs have also been used as tools for retinal oximetry, by making use of the reflectance obtained from the retinal blood vessels over multiple wavelengths. Hemoglobin is the iron-containing protein of the blood responsible for binding with oxygen, facilitating its transport and exchange in tissues. The oxygen saturation, SO_2 (%), that is, the percentage of oxyhemoglobin over total hemoglobin in retinal vessels, can be estimated by quantifying differences in the spectral absorption

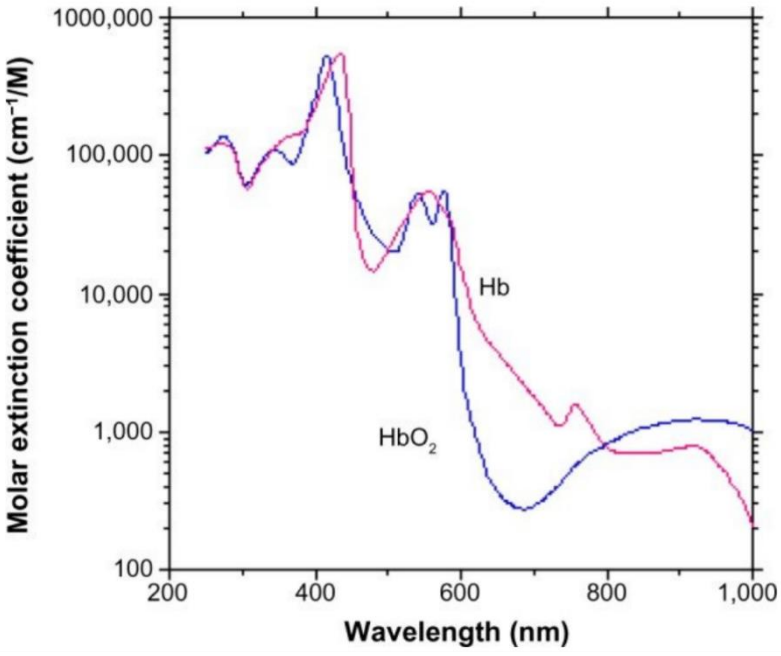

Fig. 7. Absorption spectra of the oxygenated (HbO_2) and deoxygenated (Hb) hemoglobin molecules. When combined with reflectance values obtained from retinal vessels, the intravascular oxygen saturation can be estimated. Reproduced from Optical absorption of hemoglobin, Prahl S, Copyright © 1999. Available from: http://omlc.ogi.edu/spectra/hemoglobin/index.html.

of oxygenated versus deoxygenated hemoglobin (Fig. 7). The principles behind retinal oximetry are extensively analyzed in Chapter 6.

B) OCT-angiography

OCT-angiography (OCTA) is an extension of OCT developed over the last decade.[15] The movement of erythrocytes between consecutive B-scans creates a decorrelation signal, separating the blood vessels from the surrounding static nerve tissue. This enables the visualization of the higher-order arterioles, venules, and capillaries, without the need for contrast agents, as opposed to invasive methods, such as fluorescein angiography. Another crucial advantage of OCTA is its ability to provide depth-resolved signals, generating images of every capillary plexus, including the choriocapillaris. Figure 8 displays 6 × 6 mm OCTA images of the SCP, centered at the macula and the ONH.

Apart from their qualitative assessment, OCTA images can be used to objectively quantify parameters, such as the size of the foveal avascular zone, the vessel density, the vessel branching complexity, and flow voids in the choriocapillaris. While still limited by numerous artifacts during acquisition and processing and by the lack of harmonization between different algorithms and different devices, these biomarkers are already recognized

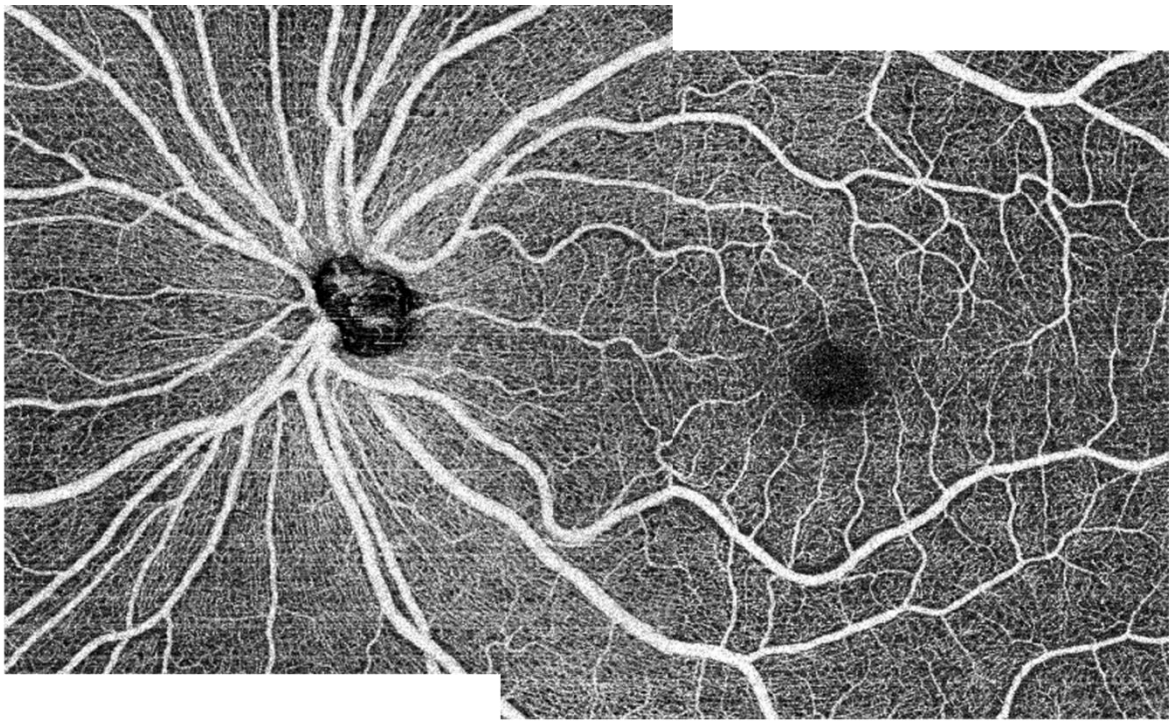

Fig. 8. Overlayed 6 × 6 mm OCTA images of the superficial capillary plexus, centered at the optic nerve head and the macula (left eye). Larger vessels appear brighter, while darker pixels indicate absent (or undetected) flow. The avascular zone at the center of the fovea can be clearly visualized. Images were obtained with the Canon HS100 SD-OCT, Angio eXpert, OCTA version 2.0 (Canon, Inc., Tokyo, Japan).

as a useful tool in the arsenal of the clinical ophthalmologist. It must be noted that, although OCTA is based on the dynamic properties of blood transit, it offers little dynamic information itself. As such, it falls under the category of static retinal imaging. Chapter 3 is entirely dedicated to OCTA.

C) Assessing blood motion

Another extension of OCT, namely Doppler OCT, is used (currently only in the research setting) for the dynamic assessment of the retinal microvasculature.[9] According to the Doppler effect, when backscattered by erythrocytes, the incident beam undergoes a shift in frequency (Doppler shift), which can then be used to estimate blood velocity in absolute values, provided measurements are obtained in two different directions. If the caliber of the examined vessel is simultaneously measured, the volume of blood traversing in the unit of time, that is, blood flow (BF), can be calculated. Summing partial blood flows from all arteries (or veins) emerging from the optic disc (Fig. 9) allows for the calculation of total retinal blood flow (RBF), that is, blood flow in the CRA (or CRV).[16] Some disadvantages of Doppler OCT are its suboptimal reproducibility and its inability to assess BF in branches of higher order, due to aliasing.

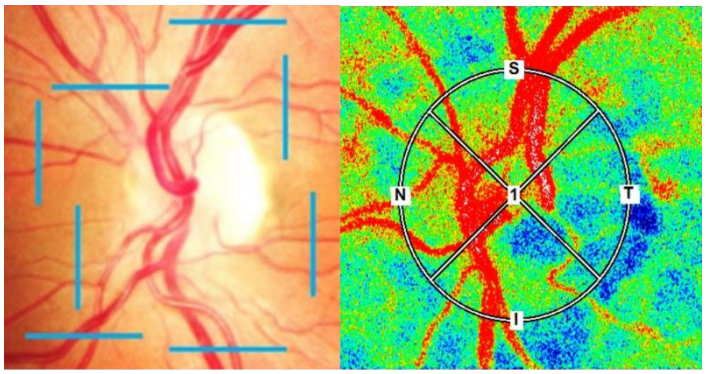

Fig. 9: Left image: Rectangular scanning pattern to assess absolute blood flow in each retinal vessel and total retinal blood flow (left eye). The blood velocity and caliber of each vessel segment is estimated by means of Doppler OCT. Adapted from Invest Ophthalmol Vis Sci, 58, Aschinger GC, Schmetterer L, Fondi K, et al., Effect of Diffuse Luminance Flicker Light Stimulation on Total Retinal Blood Flow Assessed With Dual-Beam Bidirectional Doppler OCT, pp. 1167-1178, 2017, with permission from https://creativecommons.org/licenses/by-nc-nd/4.0/. Right image: Laser speckle flowgraphy snapshot of the peripapillary area (left eye). Regions with larger mean blur rate values (higher relative blood velocity) are depicted in red. Regions with smaller mean blur rate values (lower relative blood velocity) are depicted in blue. Parapapillary microvascular dropout is noticeable on the temporal side.

Laser Speckle Flowgraphy (LSFG) is an imaging method allowing for the relative assessment of blood motion.[9] When the retina is illuminated with coherent light, the movement of erythrocytes creates a characteristic disruption (‘blurring’) to the speckled pattern of stationary tissues. Quantification of this speckle contrast yields a proxy of blood velocity, known as the mean blur rate. Areas with higher contrast correspond to areas of higher relative velocity (Fig. 9). The main limitation of LSFG is its inability to produce absolute values for blood velocity and RBF.

More details about LSFG and *in vivo* RBF quantification can be found in Chapter 4. Notably, by combining RBF measurements with the arterial and venous SO_2 (%) values obtained from retinal oximetry, it is possible to produce estimations for the total volume of oxygen delivered by the circulation (DO_2) and extracted by the tissues (VO_2) per unit time.[8] We demonstrate this in Chapter 6.

1.3. Physiology of Retinal Perfusion

The retina is characterized by relatively low levels of blood flow, compensated by increased tissue oxygen extraction.[9] Hereunder, we provide a short overview of the contributing factors that are implicated in the physiology and pathophysiology of RBF and VO_2.

1.3.1. Ocular Perfusion Pressure

Ocular perfusion pressure (OPP) is the driving force of BF through the microvascular network. It is defined as the difference in pressures between the arteriolar and venular ends of the ocular circulation.[18] Although it is possible to get good estimates of these two pressures by means of ophthalmodynamometric techniques, in practice OPP is approximated as a function of the arterial blood pressure (BP) and intraocular pressure (IOP). Detailed information on OPP is provided in Chapter 4.

A) Blood pressure

BP is a major determinant of perfusion pressure. Due to the heart's pulsatility, BP is not constant throughout the cardiac cycle, but is actually a complex waveform whose amplitude is determined by the systolic blood pressure (SBP) and the diastolic blood pressure (DBP). Specifically, SBP and DBP are the pressures exerted to the aortic walls during heart systole and diastole, respectively. The pulse waveform is responsible for generating a corresponding flow waveform that is transmitted to the ocular circulation.[19]

Due to the capacitive properties of the compliant arteries of the macrovascular network, significant dampening of the pulse waveform occurs when transitioning from the central to the peripheral circulation. In addition, owing to frictional losses during blood transit,

attributed to vascular resistance, a significant drop exists between the central BP and the pressure in the ophthalmic artery, with the latter usually assumed to be around 2/3 of the former. However, the largest pressure drop occurs at the level of the retinal arterioles, where the increased contact surface between blood volume and vessel walls and the simultaneous lack of sufficient channels, as opposed to the terminal capillaries, result in maximal energetical losses due to friction (Fig. 10).

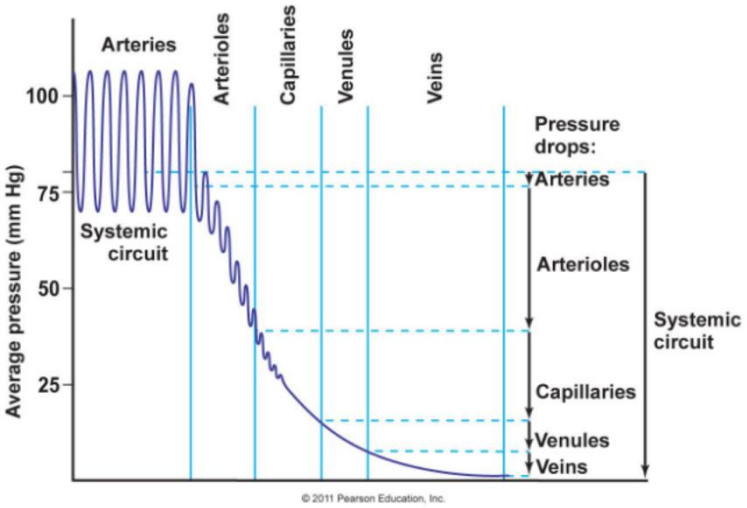

Fig. 10. Illustration of the pressure drop and pulse waveform dampening, as blood traverses the vascular network. The largest pressure drop occurs at the level of the arterioles, due to the increased vascular resistance.

In clinical practice, BP is measured at the level of the brachial artery. Although an increase in BP exists with age, SBP/DBP of 120/80 mmHg or lower are generally accepted as optimal BP values.[17] Low BP is defined as SBP/DBP of 90/60 mmHg or less and does not usually require treatment, when asymptomatic. On the other hand, arterial hypertension (AHT), defined as SBP ≥ 140 mmHg or DBP ≥ 90 mmHg, requires chronic treatment in the form of antihypertensive (AH) medication. Generally, AH medication falls under five major categories: 1) angiotensin-converting enzyme inhibitors (ACEIs), 2) angiotensin II receptor blockers (ARBs), both also referred to as renin-angiotensin-system-acting agents, 3) calcium channel blockers (CCBs), 4) beta blockers, and 5) thiazide diuretics.

B) Intraocular pressure

Aqueous humour is a water-like fluid circulating in the anterior chamber of the eye, a space located between the cornea and the iris.[20] It is produced in the posterior chamber (i.e., the space between the iris and the lens) by the ciliary body, a ring-shaped muscle responsible for the focusing of the lens. It drains into the systemic circulation at the level of the iridocorneal angle, through the spongy trabecular meshwork and Schlemm's canal (Fig. 11).

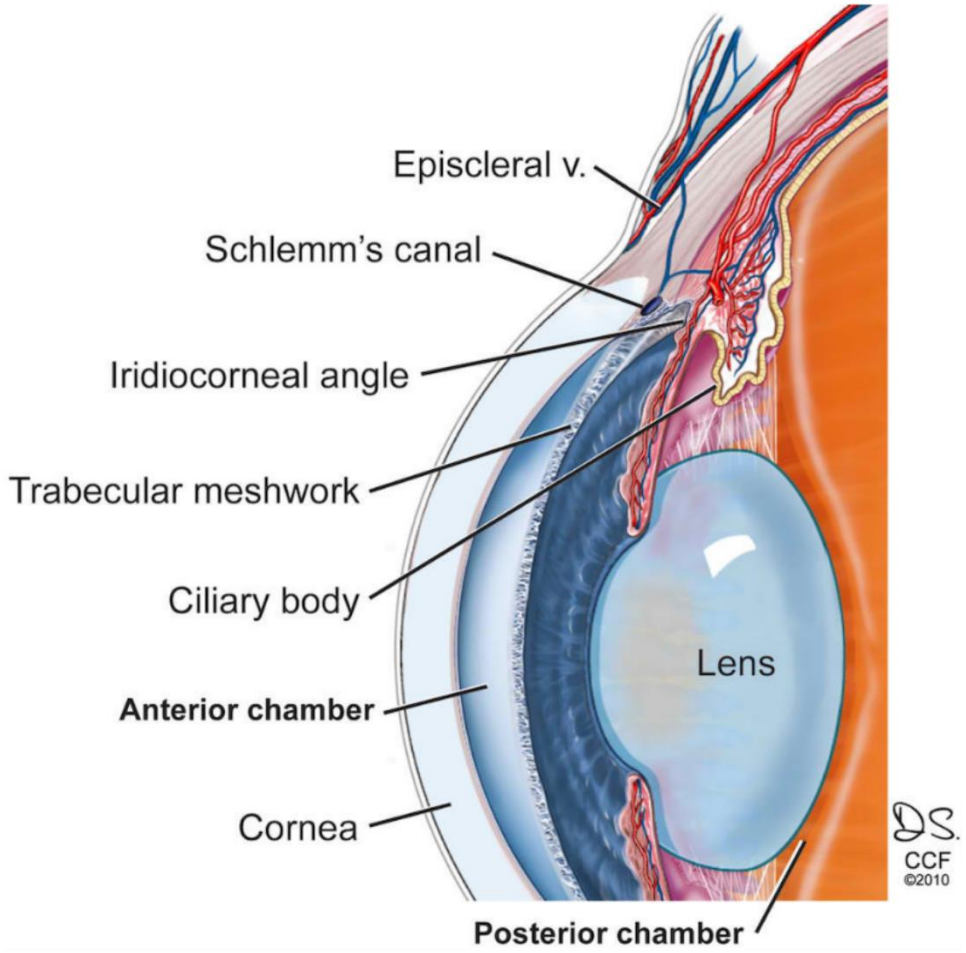

Fig. 11. Human trabecular meshwork. Aqueous humor (AH) is actively produced by the ciliary epithelium in the posterior chamber of the eye and circulates through the pupil to the anterior chamber where it drains through the TM into Schlemm's canal and the episcleral veins. Reprinted from Mol Vis, 18, Bollinger KE, Crabb JS, Yuan X, Putliwala T, Clark A, Crabb JW, Proteomic similarities in steroid responsiveness in normal and glaucomatous trabecular meshwork cells, pp. 2001-2011, Copyright © 2012, with permission from the Cleveland Clinic. Illustration by David Schumick. All rights reserved.

IOP is determined by the rates of aqueous humour production and outflow, as well as the pressure in the thin veins of the sclera (episcleral veins). The normal IOP range is 11-21 mmHg. The gold standard method for measuring IOP is Goldmann applanation tonometry, with non-contact tonometry and rebound tonometry being popular alternatives.[21] All three techniques initially implement an applanation of the cornea, but subsequently utilize different biophysical principles to yield an IOP estimate. Central corneal thickness confounds IOP estimations, with thicker corneas yielding falsely higher IOP readings.

To prevent veins from collapsing, the pressure at the venous end of the ocular circulation must exceed IOP.[18] Therefore, IOP is the second major determinant of OPP, because it is used as an approximation of the effective venous pressure.

1.3.2. Poiseuille's Law

When a number of assumptions is met, the estimated blood flow (Q) through a vessel is given by Poiseuille's Law:

$$Q = \frac{\pi \Delta P r^4}{8 \mu l}$$

where ΔP is the pressure difference between the two ends of the vessel, r is the vessel radius, μ is the blood viscosity, and l is the vessel length.[8]

In the microcirculation, where blood behaves as a non-Newtonian fluid, additional factors need to be taken into account. Fluid dynamics are extensively analyzed in Chapter 4.

1.3.3. Autoregulation

In contrast to the choroidal blood flow, which is mostly controlled by innervation from the autonomic nervous system, RBF is relatively low and tightly regulated by local mechanisms.[9] According to Poiseuille's law (see 1.3.2), a decrease in the pressure difference (OPP), as a consequence to a decrease in BP or to an increase in IOP, would theoretically result in a decrease in flow. Conversely, an increase in OPP would result in increased flow. However, the retinal arterioles are able to modify their resistance by

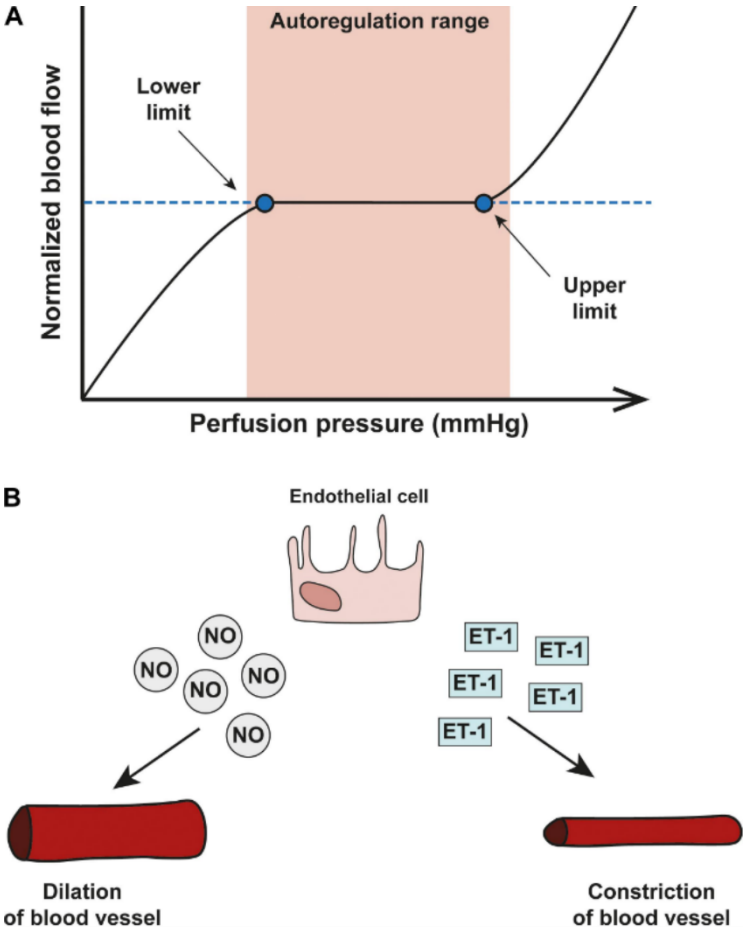

Fig. 12. Blood flow autoregulation in the eye. (A) A schematic showing an autoregulation curve that describes the relationship between normalized blood flow (y-axis) and perfusion pressure (x-axis). Autoregulation can only operate within a critical range of OPP and once OPP surpasses the optimal range (shown in pink), autoregulatory systems start to break down. (B) The two important vasoactive substances released by endothelial cells are nitric oxide (NO) and endothelin-1 (ET-1) and autoregulation of the vascular system in the eye relies on a delicate balance between the two; NO is a potent vasodilator released by smooth muscle cells and endothelial cells which acts via pericytes to dilate capillaries. Opposite in function is ET-1, a potent vasoconstrictor. Reprinted from Front Cell Dev Biol, 8, Wareham LK, Calkins DJ, The Neurovascular Unit in Glaucomatous Neurodegeneration, p. 452, Copyright © 2020 Wareham and Calkins, with permission from: https://creativecommons.org/licenses/by/4.0/

adjusting their diameter, after sensing changes in circumferential wall stress (transmural pressure). This phenomenon intrinsic to smooth muscle cells, known as the myogenic response or Bayliss effect, results in RBF being kept relatively constant, despite changes in OPP. The control of vascular tone is not fully understood, but is largely mediated by vasoactive substances, such as nitric oxide and endothelin-1.[23] Additional local mechanisms, such as pure oxygen breathing or variations in carbon dioxide partial pressure, have been also shown to contribute to RBF regulation.

RBF autoregulation is known to be in effect over a wide range of perfusion pressures (autoregulation plateau), but will eventually fail below or above OPP threshold values, known as the autoregulation limits (Fig. 12). At these points the vasculature has reached its maximum potential for dilation or constriction and any further OPP change will result in a concomitant change in RBF. Autoregulation has a static and a dynamic component, with the former evaluating the complete response of the vasculature over several minutes of stepwise OPP manipulation and the latter assessing the latency of this response to transient changes in OPP. More insight on RBF autoregulation can be found in Chapters 4 and 5.

1.3.4. Oxygen Delivery and Extraction

The most vital function served by RBF is the delivery of oxygen to the retinal tissues.[24] Because of its unique function, the retina has a high metabolic demand (consumption), which is met by the extraction of a significant amount of oxygen from the circulating blood. According to the Fick principle, the volume of extracted oxygen depends on the RBF and the difference in oxygen content between the arteriolar and venular side of the vascular bed. Because retinal RBF is relatively low, a high arteriovenous SO_2 (%) difference is present. Oxygen tension studies combined with modeling have demonstrated that the retinal layers with the highest consumption are the inner segments of the photoreceptors and regions with synaptic activity, that is, the OPL and the deep portions of the IPL.

Evidence from the retina and other tissues suggests that an increase in oxygen extraction forms the last line of defense against tissue hypoxia, suggesting little dependence of oxygen delivery and consumption within a wide range of OPP. In Chapter 6, we shed more light into the mechanisms surrounding retinal oxygen delivery and extraction.

1.4. The Vascular Theory of Glaucoma

1.4.1. Primary Open-Angle Glaucoma

Glaucoma is a multifactorial optic neuropathy causing progressive damage to the RGCs and thinning of their axons, eventually leading to severe and irreversible visual impairment.[25] In reality, the term glaucoma refers to a group of diseases whose common denominator is elevated IOP, one of the two most important risk factors of glaucoma (the other one being old age). An increased IOP is usually caused by an obstruction in the drainage of the aqueous humour. Lowering of the IOP is currently the only available treatment option for glaucoma.[26] This is usually performed by chronic instillation of topical medications, with laser treatment, mainly selective laser trabeculoplasty, being a popular alternative. Selected patients with deteriorating VF deficits may also undergo surgery, in the form of trabeculectomy, implant surgery, or, in some cases, minimally invasive glaucoma surgery.

Primary open-angle glaucoma (POAG) is the most common form of glaucoma and is characterized by an open anterior chamber (iridocorneal) angle and structural and visual field (VF) defects that cannot be otherwise explained. The complete etiology of POAG is unknown, but a variety of clinical and biological risk factors have been identified.[25] Nevertheless, an increased IOP is neither sufficient nor necessary for the development of glaucoma. Indeed, patients may have a higher than normal IOP, but no other signs of the disease, a condition known as ocular hypertension. In addition, normal-tension glaucoma (NTG) is a subtype of POAG in which IOP is within the normal range, but damage to the RGCs is still present. Therefore, it is evident that certain components of the disease remain elusive or insufficiently addressed.

1.4.2. Structure, Function, and Vasculature in Glaucoma

VF evaluation, also known as perimetry, is an interactive test in which stimuli of varying intensity are presented sequentially in a pre-determined portion of the VF, whilst maintaining central fixation.[27] The Humphrey Field Analyzer (HFA) is the most popular commercial device used for VF testing. Each test location is assigned a sensitivity value in dB, based on the patient's performance, and each sensitivity is subsequently compared to a

normative database, producing the total deviation plot. The average of all total deviation values yields the mean deviation (MD). A pattern standard deviation (PSD) plot is also generated, measuring irregularity in the depression of the VF sensitivities. PSD allows for differentiation with conditions in which the VF exhibits homogeneous depression, such as cataract.

Contemporary glaucoma diagnostics and progression monitoring primarily rely on visual VF (functional) assessment, as well as neural tissue thickness (structural) assessment, by means of OCT. Topographical correlation exists between location of structural deficits on the retina and vision sensitivity loss. Structural loss in glaucoma is often depicted as a deviation from the normative peripapillary RNFL or macular GCIPL thickness (Fig. 13). Glaucomatous VF defects tend to respect the horizontal meridian, due to the separation (raphe) of the retinal nerve fibers belonging to the superior and inferior retinal hemifields (Fig. 13). The nasal step, that is, a scotoma in the nasal VF is frequently defined as an early glaucoma manifestation, but VF defects can also manifest in the parafoveal area. A glaucomatous VF defect, according to the Anderson-Patella criteria is defined as a cluster of three or more points in the PSD plot within a single hemifield with a *P* value < 5%, one of which must have a *P* value < 1%.[28]

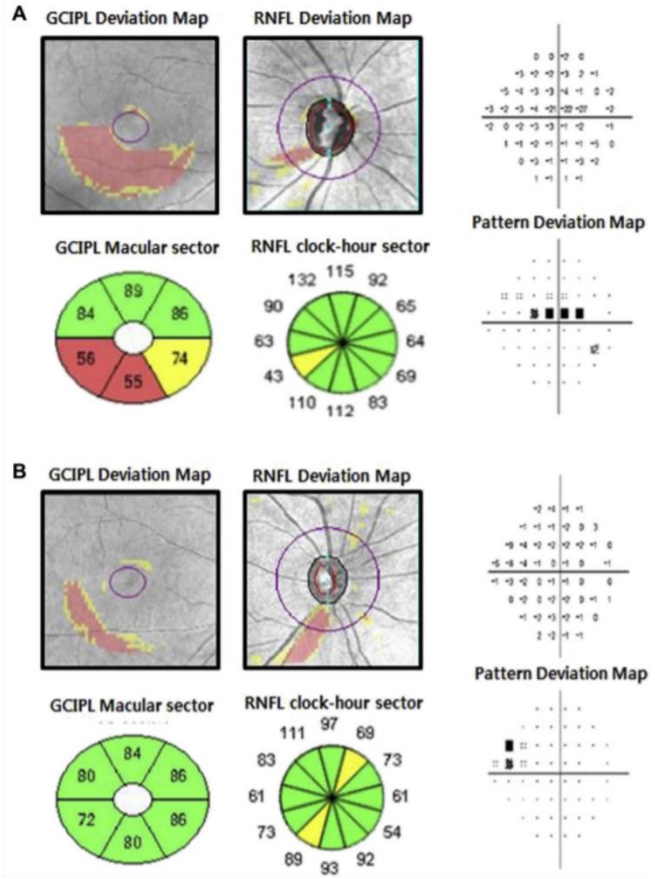

Fig. 13. Two representative cases of the eye with (A) superior parafoveal scotoma (PFS) and (B) superior peripheral nasal step (PNS). A, The clock-hour 8 retinal nerve fiber layer (RNFL) thickness is borderline in the RNFL clock-hour sector map, and the inferotemporal and inferior ganglion cell-inner plexiform layer (GCIPL) thicknesses are outside the normal limits in the GCIPL macular sector map of the eye with superior PFS. B, The clock-hour 7 RNFL thickness is borderline in the RNFL clock-hour sector map, whereas GCIPL thicknesses are all within normal limits in the GCIPL macular sector map of the eye with superior PNS. Reprinted from Ophthalmology, 121, Shin HY, Park HL, Jung KI, Choi JA, Park CK, Glaucoma diagnostic ability of ganglion cell-inner plexiform layer thickness differs according to the location of visual field loss, pp 93-99, Copyright (2014), with permission from Elsevier.

Recently, the additional value of the retinal microvasculature and OCTA in glaucoma diagnostics has been demonstrated. RGC loss has been associated with a decrease in peripapillary and parafoveal vascular density of the SCP and of deeper

layers, as well as with choroidal microvasculature dropout.[29] Vascular metrics have been shown to correlate with glaucoma severity and can sometimes outperform structural metrics in glaucoma diagnostics.

1.4.3. Blood Pressure and Retinal Perfusion in Glaucoma

The mechanisms behind the death of RGCs and their axons are poorly understood. The vascular theory of glaucoma has been a subject of debate for many decades. It has been established that, following the death of RGCs, the decreased oxygen need results in a concomitant decrease in BF. However, compiling evidence suggests that a reduced blood supply and consequent ischemia may well be an additional cause and not merely a consequence of RGC apoptosis. This is known as the 'chicken-egg' dilemma in glaucoma.[11]

Despite the existence of abundant conflicting results, a number of observations support this vascular theory. Indeed, various systemic vascular risk factors have been linked to POAG. This relationship is stronger in NTG than in POAG and has been attributed by research groups to the frequent coexistence of NTG with vascular dysregulation.[11,30] In addition, several epidemiological studies have documented the existence of a complex relationship between BP and glaucomatous prevalence, incidence, or progression, with the majority of evidence pointing towards both low and high BP as being related to glaucoma.[11] As discussed earlier in this chapter, a low BP, sometimes even secondary to intensive antihypertensive treatment, causes a reduction in OPP. If the triggered autoregulatory response of the retinal vasculature is unable to counteract this OPP drop, hypoperfusion of the RGCs is likely to occur. In addition, chronic exposure of the vasculature to detrimentally high pressures in AHT will eventually damage the vessel walls. Therefore, despite the sufficiently large OPP present in AHT, the tissues are still liable to perfusion deficits. In view of these findings, in Chapter 2 we seek to investigate the association between the use of AH medication and unfavorable glaucomatous outcomes.

Nevertheless, after the onset of glaucoma, it is impossible to disentangle the 'chicken-egg' dilemma, owing to lack of information regarding the temporality in this causal cascade of events. In addition, assessing retinal perfusion in the clinical setting is far from an easy task. Consequently, a lot of pertinent issues on the role of BP and retinal perfusion in glaucoma remain insufficiently addressed. These aspects are the central subject matter of this treatise.

1.5. Aim of this Thesis

As a whole, this dissertation aims to enhance our current knowledge on the interplay between BP, retinal perfusion, and retinal structure, in order to understand how these factors pertain to the pathogenesis of glaucoma. It may come as a surprise to the reader that, with the exception of Chapter 2, most of the research presented focuses on (what we perceive as) healthy eyes. The complete rationale behind this approach is explained throughout this thesis. In short, it is based on the realization that, before making any conclusions about potential contribution to disease mechanisms, one first needs to fully comprehend the baseline interaction between the variables in question. Although very simple in its nature, this logical and necessary step has not been implemented in previous efforts to address the vascular theory of glaucoma.

1.6. References

1. Remington LA. Retina. In: *Clinical Anatomy and Physiology of the Visual System*, 3rd. Ed. Philadelphia: Elsevier; 2012:61-92.

2. Alamouti B, Funk J. Retinal Thickness Decreases with Age: An OCT Study. *Br J Ophthalmol*. 2003;87(7):899-901.

3. Grossniklaus HE, Geisert EE, Nickerson JM. Introduction to the Retina. *Prog Mol Biol Transl Sci*. 2015;134:383-396.

4. Hoon M, Okawa H, Della Santina L, Wong ROL. Functional architecture of the retina: development and disease. *Prog Retin Eye Res*. 2014;42:44-84.

5. Resch H, Pereira I, Hienert J, et al. Influence of disc-fovea angle and retinal blood vessels on interindividual variability of circumpapillary retinal nerve fibre layer. *Br J Ophthalmol*. 2016;100(4):531-6.

6. Jonas RA, Wang YX, Yang H, et al. Optic Disc – Fovea Angle: The Beijing Eye Study. PLoS One. 2015;10(11):e0141771.

7. Everett, M, Magazzeni, S, Schmoll, T, Kempe, M. Optical coherence tomography: From technology to applications in ophthalmology. *Transl Biophotonics*. 2021;3:e202000012.

8. Burns SA, Elsner AE, Gast TJ. Imaging the Retinal Vasculature. *Annu Rev Vis Sci*. 2021;7:129-153.

9. Kur J, Newman EA, Chan-Ling T. Cellular and physiological mechanisms underlying blood flow regulation in the retina and choroid in health and disease. *Prog Retin Eye Res*. 2012;31:377–406.

10. Lee KE, Klein BE, Klein R, Meuer SM. Association of retinal vessel caliber to optic disc and cup diameters. *Invest Ophthalmol Vis Sci*. 2007;48(1):63-7.

11. Harris A, Guidoboni G, Siesky B, et al. Ocular blood flow as a clinical observation: Value, limitations and data analysis. *Prog Retin Eye Res*. 2020;24:100841.

12. Campbell JP, Zhang M, Hwang TS, et al. Detailed Vascular Anatomy of the Human Retina by Projection-Resolved Optical Coherence Tomography Angiography. *Sci Rep*. 2017;7:42201.

13. Fouquet S, Vacca O, Sennlaub F, Paques M. The 3D Retinal Capillary Circulation in Pigs Reveals a Predominant Serial Organization. *Invest Ophthalmol Vis Sci*. 2017;58(13):5754-5763.

14. Freund KB, Sarraf D, Leong BCS, Garrity ST, Vupparaboina KK, Dansingani KK. Association of Optical Coherence Tomography Angiography of Collaterals in Retinal Vein Occlusion With Major Venous Outflow Through the Deep Vascular Complex. *JAMA Ophthalmol*. 2018;136(11):1262-1270.

15. Kashani AH, Chen C-L, Gahm JK, et al. Optical coherence tomography angiography: A comprehensive review of current methods and clinical applications. *Prog Retin Eye Res.* 2017;60:66–100.

16. Aschinger GC, Schmetterer L, Fondi K, et al. Effect of Diffuse Luminance Flicker Light Stimulation on Total Retinal Blood Flow Assessed With Dual-Beam Bidirectional Doppler OCT. *Invest Ophthalmol Vis Sci* 2017;58:1167–1178.

17. Williams B, Mancia G, Spiering W, et al. 2018 ESC/ESH Guidelines for the management of arterial hypertension. The Task Force for the management of arterial hypertension of the European Society of Cardiology (ESC) and the European Society of Hypertension (ESH). *G Ital Cardiol* 2018;19:3–73.

18. Kiel JW. Chapter 4, Ocular perfusion pressure, IOP and the ocular Starling resistor effect. In: *The Ocular Circulation*, San Rafael (CA): Morgan & Claypool Life Sciences; 2010.

19. Puyo L, Paques M, Fink M, Sahel JA, Atlan M. Waveform analysis of human retinal and choroidal blood flow with laser Doppler holography. *Biomed Opt Express*. 2019;10:4942–4963.

20. Cunningham AJ, Barry P. Intraocular pressure--physiology and implications for anaesthetic management. *Can Anaesth Soc J*. 1986;33(2):195-208.

21. Chen M, Zhang L, Xu J et al. Comparability of three intraocular pressure measurement: iCare pro rebound, non-contact and Goldmann applanation tonometry in different IOP group. *BMC Ophthalmol.* 2019;19:225.

22. Tonnu PA, Ho T, Newson T, et al. The influence of central corneal thickness and age on intraocular pressure measured by pneumotonometry, non-contact tonometry, the Tono-Pen XL, and Goldmann applanation tonometry. *Br J Ophthalmol*. 2005;89(7):851-4.

23. Wareham LK, Calkins DJ. The Neurovascular Unit in Glaucomatous Neurodegeneration. *Front Cell Dev Biol*. 2020;8:452.

24. Yu DY, Cringle SJ. Oxygen distribution and consumption within the retina in vascularised and avascular retinas and in animal models of retinal disease. *Prog Retin Eye Res*. 2001;20:175–208.

25. Janssen SF, Gorgels TG, Ramdas WD, et al. The vast complexity of primary open angle glaucoma: disease genes, risks, molecular mechanisms and pathobiology. *Prog Retin Eye Res*. 2013;37:31-67.

26. Heijl A, Leske MC, Bengtsson B, et al. Reduction of intraocular pressure and glaucoma progression: results from the Early Manifest Glaucoma Trial. *Arch Ophthalmol*. 2002;120(10):1268-1279.

27. Aref AA, Budenz DL. Detecting Visual Field Progression. *Ophthalmology*. 2017;124(12S):S51-S56.

28. Anderson DR Patella, VM. Automated Static Perimetry. 2nd Ed., St. Louis Mosby; 1990:121-190.

29. Aghsaei Fard M, Ritch R. Optical coherence tomography angiography in glaucoma. *Ann Transl Med*. 2020 Sep;8(18):1204.

30. Funk RO, Hodge DO, Kohli D, Roddy GW. Multiple Systemic Vascular Risk Factors Are Associated With Low-Tension Glaucoma. *J Glaucoma*. 2022;31(1):15-22.

Chapter 2

ANTIHYPERTENSIVE MEDICATION AND GLAUCOMA*

* Pappelis K, Loiselle AR, Visser S, Jansonius NM. Association of Systemic Medication Exposure With Glaucoma Progression and Glaucoma Suspect Conversion in the Groningen Longitudinal Glaucoma Study. *Invest Ophthalmol Vis Sci*. 2019;60(14):4548-4555.

2.1. Abstract

Purpose: To determine the association of statins, five classes of antihypertensive medication, and proton pump inhibitors with (1) primary open angle glaucoma (POAG) progression and (2) conversion of POAG suspects to POAG.

Methods: We retrospectively investigated the records of a cohort with POAG cases and suspects from the Groningen Longitudinal Glaucoma Study. To quantify visual field (VF) deterioration in cases, we used the rate of progression of the mean deviation (MD). Suspects were considered to have converted at the time point after which two consecutive VF tests for at least one eye were abnormal (glaucoma hemifield test outside normal limits). Progression and conversion were analyzed with quantile and logistic regression, respectively, with the systemic medications as predictors, controlling for age, gender, body mass index, pretreatment intraocular pressure (IOP), corneal thickness, and baseline MD. The multivariable models were built with and without IOP intervention.

Results: No systemic medications were associated with POAG progression in the final IOP/treatment-adjusted or unadjusted model. However, angiotensin II receptor blockers (ARBs) appeared to slow progression in older patients ($b_{interaction} = 0.014$, $P = 0.0001$). ACE-inhibitors (ACEIs) were significantly associated with a decrease in POAG suspect conversion in both the IOP/treatment-adjusted and -unadjusted model [odds ratio (OR) = 0.23, 95% CI: 0.07-0.79, $P = 0.012$; OR = 0.24, 95% CI: 0.07-0.78, $P = 0.021$, respectively], as were ARBs (OR = 0.12, 95% CI: 0.01-0.98, $P = 0.014$; OR = 0.11, 95% CI: 0.01-0.87, $P = 0.005$, respectively).

Conclusions: No overall association of VF progression with systemic medication was found; ARBs delayed progression in older patients. ACEIs and ARBs were associated with lower risk of suspect conversion. The pathophysiology of this relationship is to be disentangled.

2.2. Introduction

Glaucoma is a chronic and progressive eye disease characterized by cupping of the optic disc, thinning of the retinal nerve fiber layer, loss of retinal ganglion cells (RGCs), and loss of visual function.[1,2] A high intraocular pressure (IOP) is an important risk factor for glaucoma and IOP-lowering medications, laser, or surgery are currently the only available options to delay, but not inhibit, glaucomatous progression.[3,4] However, not every person with ocular hypertension will convert to the disease, and glaucoma also may develop in those with an apparently normal IOP.[5] These observations imply that other risk factors exist that are not being addressed in current treatment decisions.

Several other factors may contribute to the development and progression of the disease, including systemic medications used to treat other pathologies. Specifically, a protective role of statins, possibly unrelated to their cholesterol-lowering effect, has been reported in primary open-angle glaucoma (POAG).[6–9] Moreover, numerous studies have examined the effect of antihypertensive (AH) medication on glaucoma, due to the fact that the disease is believed to contain a vascular component.[10–12] This suggests that drugs able to modify vascular events could pertain to the outcome of glaucoma. In this regard, proton pump inhibitors (PPIs), a medication class used to lower the levels of stomach acid in gastric and esophageal pathologies, could influence unfavorably the course of the disease because of their documented inhibition of nitric oxide (NO) production.[13] To make it even more complicated, these drugs could simultaneously have a beneficial effect because they create an unfavorable gastric environment for *Helicobacter pylori*, a bacterium for which an association with increased risk for POAG has been suggested.[14]

However, the results of studies examining the role of statins and AH medication in POAG are conflicting.[15,16] A neuroprotective property of statins as well as of certain AH medications has been suggested, but not all studies confirm such an effect.[17,18] Even from a pathophysiological perspective, although hypertension has been suggested as a risk factor for glaucoma, aggressive treatment with blood pressure (BP) medication could also result in ischemic damage to the RGCs mediated by a low diastolic BP.[19] In addition, to the best of our knowledge, there currently exists only scarce evidence addressing a potential effect of PPIs on POAG development. Last, some study designs in the literature incorporate a loose definition of POAG (e.g., prescription of glaucoma medication) based on national registries

or insurance claim data.[11,16] As a result, it is impossible to differentiate the impact of systemic medication on glaucoma suspects from the corresponding impact on those with a glaucoma diagnosis.

Therefore, the aim of this study was to determine the association of statins, five main classes of AH medication, and PPIs with (1) POAG progression and (2) conversion of POAG suspects to a POAG diagnosis. For this purpose, we retrospectively looked into the information of the Groningen Longitudinal Glaucoma Study (GLGS) to determine exposure to the aforementioned systemic medications in a cohort of POAG patients and POAG suspects.

2.3. Methods

2.3.1. Study Population

Patients were selected from the GLGS database. The GLGS began in 2000 and was originally a prospective, observational cohort study conducted in the clinical setting of the University Medical Center Groningen (UMCG), comprising both glaucoma patients and glaucoma suspects (predominantly Caucasians). In 2000, the UMCG served both as an academic and as a community hospital; the majority of patients in the current study should be considered community hospital patients. The objectives and methods of the GLGS have been previously described.[20,21] After the onset of the original GLGS, we continued adding newly diagnosed glaucoma patients, making the GLGS a dynamic population. From those patients who visited the clinic in 2015, we recorded their current and past systemic medications, and height and weight. This is the subset used in the current study. For the glaucoma patients, we associated the rate of progression (RoP; defined below) with systemic medication use, making the study design a retrospective follow-up study. For glaucoma suspects, we compared systemic medication use between those who converted to glaucoma and those who did not, making the study design a case-control study. The study protocol was approved by the ethics board of the University Medical Center Groningen and followed the tenets of the Declaration of Helsinki. All patients provided written informed consent.

To be eligible, subjects had to be followed with standard automated perimetry (see next subsection). Those with pseudoexfoliative or pigment dispersion glaucoma or a history of

angle closure or secondary glaucoma were excluded (leaving POAG and POAG suspects). For being a glaucoma patient, glaucomatous visual field (VF) loss had to be present at baseline in at least one eye.[20] For glaucomatous baseline VF loss, two consecutive tests had to be abnormal (see next subsection) in at least one eye. Defects had to be compatible with glaucoma and without any other explanation. A VF test before the two baseline tests was discarded to reduce the influence of learning. Thus, at least three tests had to be performed at baseline before glaucomatous VF loss could be diagnosed. Glaucoma suspects were those who had an intact VF when entering the study and were followed in our outpatient department because of ocular hypertension (IOP above 20 mmHg on at least two separate visits), a positive family history of glaucoma (glaucoma reported in father, mother, brother, or sister), or a suspected optic disc (cup-to-disc ratio above 0.6), or combinations thereof.[22]

2.3.2. Perimetry, Progression, and Conversion

Perimetry was performed using the Humphrey Field Analyzer (Carl Zeiss, Jena, Germany) 30-2 Swedish interactive threshold algorithm fast strategy with 30-2 grid. An abnormal test result was defined as a glaucoma hemifield test ‘outside normal limits’. Test results were included only if they were reliable; a test result was considered unreliable if false positives exceeded 10% or if both false negatives and fixation losses exceeded 10% and 20%, respectively. We pooled false negatives and fixation losses because they were reported to have a much smaller influence on the mean deviation (MD) and the false negatives, especially, are not informative in glaucoma.[23,24]

In glaucoma patients, the RoP was calculated as the slope of the MD over time, after a minimum of 5 years of perimetric follow-up.[25] For the conversion analysis, subjects who were glaucoma suspects were considered to have converted to a glaucoma diagnosis at the time point after which all subsequent VF tests (at least two) for at least one eye were abnormal.

2.3.3. Risk Factors

The possible risk factors for glaucoma progression that were included in this study were: age at baseline, sex, body mass index (BMI), highest pretreatment IOP, central corneal thickness (CCT), baseline MD (dichotomized above and below the median of -9.4 dB),[26] mean IOP

during follow-up, surgery for glaucoma (yes/no), number of glaucoma medications, and systemic medications. Systemic medications included were statins, diuretics, angiotensin II receptor blockers (ARBs), ACE inhibitors (ACEIs), calcium channel blockers (CCBs), beta blockers, and PPIs. For the number of glaucoma medications, topical and oral were included, and if the patient underwent laser treatment, this was considered as an additional medication.[27]

2.3.4. Systemic Medication Exposure Ascertainment

To verify systemic medication exposure, the complete medical file of each patient was examined, in combination with a semi-structured interview that took place in 2015 (at or towards the end of the follow-up). An interviewer (blinded to the study question and taking no other part in the study procedures) asked each participant to list his or her current medications, guiding them with additional questions, such as: "What medications are you currently taking for high blood pressure/high cholesterol/your heart/your stomach?". To ascertain prior or subsequent use of the reported or other relevant medications we recorded all medication listings until the end of the patient's follow-up from the patient's hospital file, which included letters to his or her primary care doctors detailing prescribed medications. We defined the 'oldest recorded exposure date' as the very first date a drug appeared in this listing (or mentioned in the interview), while being absent from all listings of previous reports. We used this date (1) to approximate the duration of systemic medication use during follow-up for the progression analysis and (2) to ascertain that systemic medication exposure occurred before the conversion date in the conversion analysis.

2.3.5. Data Analysis

For the progression analysis, only one eye per patient was included. If a patient met the inclusion criteria with both eyes, a randomly chosen eye was included. Conversion was based on a by-patient basis: those who converted with at least one eye were considered to have converted; for analysis, the first converted eye was used and if no conversion took place, a random eye was chosen. The patient characteristics were described with mean and standard deviation (SD) for normally distributed variables. For variables with a skewed distribution, we used median and interquartile range (IQR) instead. In the multivariable analysis (see

below), missing data for CCT (2 cases) and BMI (3 cases) were imputed from the median value. There were no other missing values for any other risk factor.

Because of the non-normality of the RoP distribution, quantile regression was performed using a saturated model with RoP as the outcome variable and all predictor variables included. The least significant variable was then removed, and the models with and without the least significant variable were compared using the Akaike information criterion (AIC). If the model without the concerning variable was the better fit for the data, the same process was repeated for the next least significant variable, and this process was continued until we reached a minimal model. Coefficients and *P* values were reported. The saturated model for the RoP regression can be found in the supplementary material (Supplementary Table S1).

Conversion of glaucoma suspects to a glaucoma diagnosis was analyzed using a logistic regression model. The saturated model included all the predictor variables included above, except for glaucoma surgery and baseline MD, which would both be irrelevant for those not yet diagnosed with glaucoma. Mean IOP during follow-up was calculated either until the point at which the patient converted, or for the entire follow-up duration if the patient never converted. Again, using the AIC, covariates were removed and a minimal model was created. Odds ratios (ORs) with 95% confidence intervals (CIs) and *P* values were reported. The saturated model for the conversion logistic regression model can be found in the supplementary material (Supplementary Table S2).

All analyses were performed using R (version 3.3.3; R Foundation for Statistical Computing, Vienna, Austria). A *P* value of 0.05 or less was considered statistically significant. According to the AIC, inclusion in the final model implies $P < 0.16$.

2.4. Results

We included 250 patients in the RoP analysis and 112 glaucoma suspects for the conversion analysis. Of the 112 glaucoma suspects, 21 were included because of ocular hypertension, 4 because of a positive family history of glaucoma, 6 because of a suspected optic disc, and 81 because of combinations thereof. Table 1 shows the characteristics of the study population.

Table 1. Demographics of the Study Population

	Glaucoma Patients	Glaucoma Suspects	
		Converted	Not Converted
Number of patients	250	53	59
Age at baseline, y; mean ± SD	61.8 ± 9.9	58.3 ± 10.0	55.4 ± 11.3
Sex, % female	46.0	56.6	54.2
BMI, kg/m^2; mean ± SD	26.2 ± 4.2	25.6 ± 3.8	27.2 ± 4.5
IOP before treatment, mm Hg; median (IQR)	26.0 (22.0 to 31.0)	26.0 (23.0 to 30.0)	29.0 (24.0 to 32.0)
CCT, µm; median (IQR)	537.0 (512.5 to 566.0)	543.0 (519.0 to 558.0)	551.0 (539.5 to 576.0)
VF MD at baseline, dB; median (IQR)	−9.4 (−15.6 to −5.1)	−1.1 (−3.9 to 0.0)	−0.8 (−1.8 to 0.2)
Follow-up duration, y; median (IQR)	12.0 (9.0 to 15.0)	7.0 (4.0 to 12.0)	16.0 (13.0 to 18.0)
Mean IOP during follow-up, mm Hg; median (IQR)	13.2 (11.3 to 15.5)	15.5 (13.9 to 17.3)	17.1 (14.6 to 18.2)
ROP, dB/y; median (IQR)	−0.27 (−0.55 to −0.08)	NA	NA
Statins, % (*n*)	37.2 (93)	15.1 (8)	40.7 (24)
Statin duration, percentage of follow-up years; median (IQR)	45.6 (25.3 to 82.5)	NA	NA
Diuretics, % (*n*)	27.6 (69)	9.4 (5)	33.9 (20)
ARBs, % (*n*)	15.2 (38)	1.9 (1)	15.2 (9)
ACE inhibitors, % (*n*)	24.8 (62)	7.5 (4)	25.4 (15)
CCBs, % (*n*)	19.2 (48)	11.3 (6)	20.3 (12)
Beta blockers, % (*n*)	27.2 (68)	18.8 (10)	30.5 (18)
AH duration, percentage of follow-up y; median (IQR)	50.0 (27.3 to 100.0)	NA	NA
PPIs, % (*n*)	33.2 (83)	22.6 (12)	32.2 (19)
PPI duration, percentage of follow-up y; median (IQR)	44.4 (25.8 to 90.4)	NA	NA

NA, not applicable; VF MD, standard automated perimetry mean deviation.

Median follow-up duration of the glaucoma patients was 12 years; median RoP -0.27 dB/year. Table 2 depicts the univariable quantile regression analysis with median RoP as the dependent variable. Older age, lower BMI, lower IOP before treatment, and a higher number of glaucoma medications were significantly associated with faster progression.

Table 3 shows the final multivariable model for median RoP, along with a model built without the variables that account for intervention by the treating ophthalmologist (by excluding mean IOP during follow-up, number of glaucoma medications, and glaucoma surgery from the saturated model) to account for any systemic medication-mediated IOP changes. In both final models, older age

Table 2. Univariable Quantile Regression Analysis for Glaucoma Patients With Median ROP as Dependent Variable

	Coefficient	*P* Value
Age, y	−0.006	0.003
Sex, female	0.080	0.15
BMI, kg/m^2	0.010	0.050
IOP before treatment, mm Hg	0.005	0.008
CCT, µm	−0.0002	0.76
VF MD at baseline, dB	0.000	1.0
Mean IOP during follow-up, mm Hg	−0.005	0.52
Glaucoma surgery, 0 = No	0.040	0.44
Number of glaucoma medications	−0.046	0.028
Statins	−0.060	0.27
Diuretics	−0.010	0.87
ARBs	0.020	0.74
ACE inhibitors	−0.060	0.23
CCBs	−0.080	0.31
Beta blockers	−0.080	0.16
PPIs	0.010	0.86

Table 3. Final Models for Glaucoma Patients With Median ROP as Dependent Variable

	Final Model		Final Model (Not Adjusted for IOP Intervention)	
	Coefficient	*P* Value	Coefficient	*P* Value
Age, y	−0.007	0.001	−0.006	0.010
Sex, female	0.122	0.018	0.128	0.004
BMI, kg/m^2	0.010	0.032	0.006	0.14
IOP before treatment, mm Hg	0.004	0.12	0.004	0.077
CCT, µm	−0.0008	0.14	−0.0007	0.16
Number of glaucoma medications	−0.036	0.056	NA	NA
Statins	−0.083	0.086	NA	NA
ARBs	0.089	0.097	NA	NA

and male sex were significantly associated with faster progression. Specifically, for each 10 years of age, the median RoP was 0.07 dB/year faster (0.06 dB/year for the model excluding intervention). Statins and ARBs remained in the model but were not significantly associated with RoP.

For these two systemic medications, we completed a secondary dose-response relationship analysis in which we created categories based on duration of medication use, defined as follows: no use, duration of use below the median, and duration of use above the median. Compared with nonusers of statins, there was a trend toward faster progression with prolonged statin use (6 years or less, b = -0.083, $P = 0.06$; more than 6 years, b = -0.130, $P = 0.009$). There was no dose-response relationship found for ARBs.

We also repeated the analysis using a variable with the cumulative number of AHs (in place of the different classes) as a marker for the severity of hypertension, but this variable was the first to leave the model, suggesting the number of AHs was not associated with progression.

Interactions between the two systemic medications remaining in the final model (ARBs and statins) and both pretreatment IOP and age also were investigated, with a Bonferroni-adjusted significance cutoff of $P = 0.0125$. The only significant interaction effect on RoP was between ARBs and age (b = 0.014, $P = 0.0001$). For each additional 10 years of age, ARB takers had a median RoP that was 0.14 dB/year slower than non-ARB takers. In addition, tests for collinearity between systemic medications revealed only a moderate collinear relationship between beta blockers and ACEIs (phi = 0.42, $P < 0.001$), all other phi coefficients were similar or lower.

Of the 112 glaucoma suspects, 53 converted during follow-up. The median follow-up duration until conversion was 7 years for those who converted; those who did not convert were followed for a median of 16 years. The survival curve is displayed in the Figure. From this curve, it can be predicted that it will take 15 years for 50% of the suspects to convert.

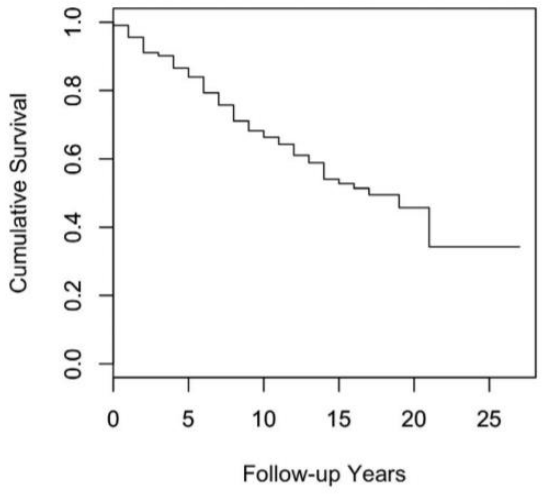

FIGURE. Survival curve for the glaucoma suspect population. Conversion to POAG is defined as the time point after which all subsequent VF tests (at least two) for at least one eye were abnormal.

Tables 4 and 5 present the univariable and final multivariable logistic regression models, respectively, for glaucoma suspect conversion. In the univariable analysis, a higher BMI, a higher number of glaucoma medications, and the use of statins, diuretics, ARBs, and ACEIs were associated with a significant decrease in conversion. Again, multivariable models were built with and without mean IOP during follow-up and number of glaucoma medications. In the final model, a higher number of glaucoma medications and the use of ARBs and ACEIs were associated with a significant decrease in conversion to a glaucoma diagnosis. Even in the final model without mean IOP and IOP treatment, the rate of conversion of suspects on ARBs and ACEIs was 89% and 76% lower, respectively, than those not taking the drugs, suggesting the possible protective association is not mediated by IOP. Tests for collinearity between systemic medications revealed a moderate collinear relationship between beta blockers and CCBs (phi = 0.53, $P < 0.001$), all other phi coefficients were similar or lower.

Table 4. Univariable Analysis With Glaucoma Suspect Conversion as Dependent Variable

	OR (95% CI)	*P* Value
Age, y	1.03 (0.99–1.06)	0.14
Sex, female	1.1 (0.52–2.32)	0.80
BMI, kg/m^2	0.91 (0.83–1.00)	0.043
IOP before treatment, mm Hg	0.98 (0.94–1.03)	0.44
CCT, µm	0.99 (0.98–1.00)	0.058
Mean IOP during follow-up, mm Hg	0.90 (0.80–1.01)	0.078
Number of glaucoma medications	0.53 (0.34–0.85)	0.004
Statins	0.26 (0.1–0.65)	0.002
Diuretics	0.20 (0.07–0.59)	0.001
ARBs	0.11 (0.01–0.87)	0.008
ACE inhibitors	0.24 (0.07–0.78)	0.009
CCBs	0.50 (0.17–1.44)	0.19
Beta blockers	0.53 (0.22–1.28)	0.15
PPIs	0.62 (0.26–1.43)	0.26

Table 5. Final Models With Glaucoma Suspect Conversion as Dependent Variable

	Final Model		Final Model (Not Adjusted for IOP Intervention)	
	OR (95% CI)	*P* Value	OR (95% CI)	*P* Value
Age, y	NA	NA	1.03 (0.99–1.07)	0.14
BMI, kg/m^2	NA	NA	0.93 (0.83–1.07)	0.15
CCT, µm	0.99 (0.98–1.00)	0.063	0.99 (0.98–1.00)	0.069
Number of glaucoma medications	0.59 (0.37–0.94)	0.025	NA	NA
ARBs	0.12 (0.01–0.98)	0.014	0.11 (0.01–0.87)	0.005
ACE inhibitors	0.23 (0.07–0.79)	0.012	0.24 (0.07–0.78)	0.021

2.5. Discussion

No systemic medications were associated with POAG progression in the final IOP-intervention adjusted or unadjusted model; statins and ARBs remained in the final IOP-intervention adjusted model without reaching significance, but an interaction term revealed a significantly slower progression associated with ARBs for older ages. ACEIs and ARBs were significantly associated with a decrease in POAG suspect conversion in the final model, regardless of IOP-intervention adjustment.

Regarding the effect of statins on POAG progression, other studies have given varying results. Iskedjian *et al.* reported no significant differences in the need for adjunct topical IOP-lowering medications between statin users and nonusers.[12] Leung *et al.* found that significantly more nonprogressors were using statins. In contrast to our study, their study concerned only normal tension glaucoma (NTG) subjects (256 subjects followed for 3 years; 31 taking statins).[8] An interaction term between statin use and pretreatment IOP added to our model did not uncover a significant association, suggesting that statins don't have a selective association with NTG in our study population. De Castro *et al.* assessed progression with structural parameters and reported that statin users, albeit only the ones not receiving aspirin treatment simultaneously, had lower progression rates (n = 76; smallest group n = 12; follow-up duration: 5.5 years).[28] This observation suggests that early structural changes might be more sensitive to the effect of statins compared to VF parameters, but a study assessing both structure and function would be needed to clarify this hypothesis. McCann *et al.* could not perform a meta-analysis on these studies because the definitions of glaucoma differed.[15] Lastly, a propensity score analysis by Whigham *et al.* reported that a history of statin use resulted in slower VF progression (847 subjects followed for 3.5 years; 629 taking statins).[6] However, their propensity score was limited to age, gender, baseline glaucomatous severity, and systemic medical conditions; hence, it did not include some important variables present in our analysis, especially the variables related to IOP. Notably, in our study, the relevant RoP coefficient for the IOP-intervention adjusted model suggests a faster progression (-0.083 dB/year for statin users compared with nonusers), but this result did not reach significance ($P = 0.086$). Our secondary dose-response analysis suggested faster progression for POAG patients using statins for more than 6 years (-0.130 dB/year compared with nonusers, $P = 0.009$), but according to a recent publication this is more likely a result of higher serum cholesterol.[29] All these studies, including ours, were observational studies, that is, the statins were not prescribed as part of a randomized control trial (RCT).

With regard to statin use and POAG incidence, most observational studies, but not all, agree that short-term statin use (2 years or less) does not significantly affect the risk.[7,16,30–33] Among them, Stein *et al.* also examined the conversion of glaucoma suspects (n = 49,628) within a retrospective longitudinal cohort design. They found that POAG suspects who used statins for 1 or 2 years had a smaller hazard for conversion (HR = 0.907, 95% CI: 0.846-0.973), but not for the need for glaucoma surgery.[7] It is possible, of course, that any beneficial effect, is only a result of longer exposure to the medication.[7,30,32] Interestingly, a

large observational prospective study by Talwar *et al.* (25,420 subjects; 15,898 taking statins) showed reduced POAG incident risk after 2 years of statin use (HR = 0.79, 95% CI: 0.66-0.96), independent of the cholesterol-lowering effect, dosage, and statin type.[9] It has been suggested that this effect may be mediated by neuroprotective mechanisms.[17,34,35] Albeit significant in these studies with very large sample sizes, the effect sizes were actually small. This illustrates that a visible effect size in large samples does not immediately imply clinical relevance. Notably, in the univariate analysis of our study, statins are shown to be associated (after Bonferroni correction) with a reduced odds ratio for suspect conversion [OR = 0.26, 95% CI: 0.1-0.65, *P*(adjusted) = 0.014]; however, the multivariate model reveals that this association is mediated by concomitant use of AH medications.

A recent observational study from insurance claim data suggested a causal, protective effect of AH medication, especially those in the renin-angiotensin category, with respect to incident glaucoma.[11] Hirooka *et al.* reported a similar finding in a NTG sample treated with ACEIs, while Yang *et al.* found a neuroprotective effect of ARBs in a rat model.[18,36] The authors hypothesized that the decrease in angiotensin II levels reduces the activity of the NADPH-dependent oxidase complex, thus reducing oxidative stress and the subsequent RGC apoptosis. They also discussed that the increase in plasma bradykinin caused by the ACEIs offers extra possibilities: improved blood flow through activation of the L-arginine NO pathway, or protection from glutamate-induced neurotoxicity. In our study, ACEIs and ARBs were significantly associated with lower odds of suspects converting to POAG, which is in agreement with these results. In addition, the highly significant interaction term between age and ARBs in our progression analysis suggests that the older the glaucomatous patient, the more they could benefit from an ARB, as far as their glaucomatous progression is concerned.

The effects of other AH medications are less clear. Beta blockers have been associated with decreased POAG incidence in some studies, whereas the opposite has been reported for CCBs and, sometimes, even ARBs.[16,37,38] Diuretics were associated with increased conversion risk of ocular hypertensives in the European Glaucoma Prevention Study and increased risk of POAG in other studies.[31,38,39] A protective effect of the cumulative number of AH drugs was reported by Horwitz *et al.*; in addition, Iskedjian *et al.* showed that the use of AH medication reduced the need for adjunct topical IOP-lowering medication.[11,12] Overall, these results suggest that AH medication classes might contribute differently to the course of glaucoma; this points towards the fact that pathways other than the BP-lowering effect could

be involved.[40,41] Protection could be mediated by an IOP-lowering effect[42–46]; additional neuroprotective mechanisms have been attributed to medication in the renin-angiotensin category, as discussed in the previous paragraph.[47–49]

There are several reasons for these conflicting results. POAG treatment is a dynamic procedure in which the clinician's decisions interfere with the true (untreated) disease progression. Therefore, explanatory variables such as mean IOP during follow-up or number of glaucoma medications could mediate or antagonize effects observed in other studies. Furthermore, a threshold effect could exist for certain AH drugs, or a ceiling effect with no further increase in risk for glaucomatous damage after this ceiling has been reached, hampering consistent dose-response findings.[16,37] Last, it is possible that AH treatment is beneficial only when started timely and harmful if started after many years of untreated hypertension. This, however, is impossible to address in an observational study with limited information regarding the time course of BP and its treatment. Interestingly, overtreatment of hypertension leading to hypotension has been reported as a risk factor for glaucoma.[19,50] Noticeably, data extracted from a large cohort study (Lifelines Biobank) reveal that aggressive AH treatment is hardly the case in our region, the northern Netherlands.[51] Indeed, average (SD) systolic BP/diastolic BP values for users and nonusers of AH medication are, within Lifelines, 135(17)/79(10) and 128(15)/76(9), respectively.

PPIs appear to both mitigate and worsen glaucoma. In a study investigating systemic medication use and glaucoma in insurance claims data,[16] it was found that esomeprazole (a PPI), reduced the risk of POAG. This finding was of borderline significance but the authors hypothesized that it could be due to a reduction in *Helicobacter pylori* rates, and therefore reduced risk of POAG.[14,52] However, PPIs can also decrease production of NO, a vasodilator that plays a role in IOP regulation. POAG patients may already have a genetic and dietary susceptibility to reduced NO bioavailability.[53] In this regard, PPIs may be beneficial to those who do not have alterations in genes responsible for NO production, and harmful to those who do.

This study is limited by its retrospective design and its relatively small sample size. For medication ascertainment our primary metric was 'any use during follow-up' (a commonly used metric in pharmacoepidemiology), but we added duration of use information for the progression analysis and temporal information for the conversion analysis (by ascertaining that systemic medication exposure occurred prior to the conversion date). Obviously, this

metric is still limited by the absence of dosage information. Furthermore, we did not have BP measurements, and for this reason we could not perform a mediation analysis for BP. Instead, we used the number of BP medications as a crude proxy of disease severity. In spite of that, it is true that monotherapy is the traditional initial therapy for hypertension and subsequent medications are added depending on BP target and disease severity. The absence of BP measurements also did not allow us to examine overtreatment of hypertension, a situation that could lead to hypoperfusion of the RGCs and, hence, mask any protective effects. Nevertheless, our positive findings remain somewhat robust to this limitation, as they all lie on the protective side, whereas overtreatment is expected to have a negative effect on glaucoma progression or conversion. In addition, our population was predominantly Caucasian, so our results cannot be safely generalized, especially because of differential responses to cardiovascular agents among patients of different genetic ancestries. Last, our population's median age leans towards the younger side with regards to glaucoma populations, a limitation that we tried to address by assessing the interactions between systemic medication exposure and age in the models.

The main strength of this study is the long follow-up duration of the population. Furthermore, POAG patients and suspects were defined according to strict criteria, rather than being based on data from national registry or insurance claims. This ensures that the two groups are not cross-contaminated and that no other type of glaucoma is present in the dataset. Moreover, a novelty of this study is controlling the analysis for glaucoma medications, the surgical profile of each participant (operated/not operated), and mean IOP during follow-up. We believe that this reflects reality better, as it simulates the dynamic context of clinicians intervening in the process by trying to slow the glaucomatous progression.

Our study suggests that, within a glaucoma or glaucoma suspect population with regular follow-ups and well-controlled IOP, there exists some extra benefit added by BP medication, but its clinical relevance is unclear. A better study design and a larger sample size are both needed to strengthen these findings. Also interesting from a clinical perspective, a high pretreatment IOP is paradoxically almost beneficial on RoP (stays in the final model, but does not reach significance), whereas most studies show the opposite effect or no effect whatsoever.[26,54,55] This finding indicates that, in this population, the alarm of a higher baseline IOP could have resulted in early diagnosis and efficient, possibly more aggressive, treatment. As such, it is a marker of clinicians' responsiveness that is visible due to the

observational study design, rather than a disease property.

In this study, approximately 47% of glaucoma suspects converted to glaucoma within a median follow-up of 16 years. According to the Ocular Hypertension Treatment Study (OHTS), the expected percentage of converted cases within 5 years is 5% to 10%, so, assuming a linear relation, less than 30% of our suspects should have converted.[56] A possible explanation for this discrepancy could be the fact that a healthy optic disc at baseline was additionally required in the OHTS; we also included suspects based on a suspected optic disc (47 of 112). In addition, a positive family history was present in 44% of the participants in OHTS, to be compared with 58% in our study.[57] Together, these differences suggest that our participants were already 'further down the line' at baseline. Also, the OHTS used a stricter criterion for conversion (three consecutive abnormal last VF tests, rather than two); however, all of the converted suspects in our study actually had three consecutive abnormal last VF tests, as well. It must also be noted that 6 out of 59 nonconverted suspects in our study had (only) one abnormal last VF, but this was not enough to classify them as 'converted', since most of these cases are expected to yield a healthy VF on their next visit.[58] Our converters fulfilled the functional criteria of the OHTS, but we did not have data to also include the structural criteria of the OHTS. As such, the difference in conversion rate between both studies is larger than reported above.

In conclusion, we found no overall significant association of glaucomatous VF progression with systemic medication exposure, but ARBs appeared to significantly delay progression in older patients. ACEIs and ARBs were significantly associated with a lower risk of suspect conversion to POAG. Because this study was limited by its design, further investigations, ideally RCTs, are needed to examine these relationships; should they be proven true, their exact pathophysiology is yet to be disentangled.

2.6. References

1. Airaksinen PJ, Alanko HI. Effect of retinal nerve fibre loss on the optic nerve head configuration in early glaucoma. *Graefes Arch Clin Exp Ophthalmol*. 1983;220:193-196.

2. Schuman JS. Quantification of Nerve Fiber Layer Thickness in Normal and Glaucomatous Eyes Using Optical Coherence Tomography. *Arch Ophthal*. 1995;113:586.

3. Garway-Heath DF, Crabb DP, Bunce C, et al. Latanoprost for open-angle glaucoma (UKGTS): a randomised, multicentre, placebo-controlled trial. *Lancet*. 2015;385:1295-1304.

4. Heijl A, Leske MC, Bengtsson B, et al. Reduction of intraocular pressure and glaucoma progression: results from the Early Manifest Glaucoma Trial. *Arch Ophthalmol*. 2002;120:1268-1279.

5. Gordon MO, Beiser JA, Brandt JD, et al. The Ocular Hypertension Treatment Study: baseline factors that predict the onset of primary open-angle glaucoma. *Arch Ophthalmol*. 2002;120:714-720; discussion 829-830.

6. Whigham B, Oddone EZ, Woolson S, et al. The influence of oral statin medications on progression of glaucomatous visual field loss: A propensity score analysis. *Ophthalmic Epidemiol*. 2017;25:207-214.

7. Stein JD, Newman-Casey PA, Talwar N, Nan B, Richards JE, Musch DC. The relationship between statin use and open-angle glaucoma. *Ophthalmology*. 2012;119:2074-2081.

8. Leung DYL, Li FCH, Kwong YYY, Tham CCY, Chi SCC, Lam DSC. Simvastatin and disease stabilization in normal tension glaucoma: a cohort study. *Ophthalmology*. 2010;117:471-476.

9. Talwar N, Musch DC, Stein JD. Association of Daily Dosage and Type of Statin Agent With Risk of Open-Angle Glaucoma. *JAMA Ophthalmol*. 2017;135:263-267.

10. Topouzis F, Founti P. Weighing in ocular perfusion pressure in managing glaucoma. *Open Ophthalmol J*. 2009;3:43-45.

11. Horwitz A, Klemp M, Jeppesen J, Tsai JC, Torp-Pedersen C, Kolko M. Antihypertensive Medication Postpones the Onset of Glaucoma: Evidence From a Nationwide Study. *Hypertension*. 2017;69:202-210.

12. Iskedjian M, Walker JH, Desjardins O, et al. Effect of selected antihypertensives, antidiabetics, statins and diuretics on adjunctive medical treatment of glaucoma: a population based study. *Curr Med Res Opin*. 2009;25:1879-1888.

13. Lundberg JO, Weitzberg E, Lundberg JM, Alving K. Intragastric nitric oxide production in humans: measurements in expelled air. *Gut*. 1994;35:1543-1546.

14. Zeng J, Liu H, Liu X, Ding C. The Relationship Between Helicobacter pylori Infection and Open-Angle Glaucoma: A Meta-Analysis. *Invest Ophthalmol Vis Sci*. 2015;56:5238-5245.

15. McCann P, Hogg RE, Fallis R, Azuara-Blanco A. The Effect of Statins on Intraocular Pressure and on the Incidence and Progression of Glaucoma: A Systematic Review and Meta-Analysis. *Invest Ophthalmol Vis Sci*. 2016;57:2729-2748.

16. Zheng W, Dryja TP, Wei Z, et al. Systemic Medication Associations with Presumed Advanced or Uncontrolled Primary Open-Angle Glaucoma. *Ophthalmology*. 2018;125:984-993.

17. Nagaoka T, Takahashi A, Sato E, et al. Effect of systemic administration of simvastatin on retinal circulation. *Arch Ophthalmol*. 2006;124:665-670.

18. Yang H, Hirooka K, Fukuda K, Shiraga F. Neuroprotective Effects of Angiotensin II Type 1 Receptor Blocker in a Rat Model of Chronic Glaucoma. *Invest Ophthalmol Vis Sci*. 2009;50:5800.

19. Topouzis F, Roy Wilson M, Harris A, et al. Association of Open-angle Glaucoma With Perfusion Pressure Status in the Thessaloniki Eye Study. *Am J Ophthalmol*. 2013;155:843-851.e1.

20. Heeg GP, Blanksma LJ, Hardus PLLJ, Jansonius NM. The Groningen Longitudinal Glaucoma Study. I. Baseline sensitivity and specificity of the frequency doubling perimeter and the GDx nerve fibre analyser. *Acta Ophthalmol Scand*. 2005;83:46-52.

21. Wesselink C, Heeg GP, Jansonius NM. Glaucoma monitoring in a clinical setting: glaucoma progression analysis vs nonparametric progression analysis in the Groningen Longitudinal Glaucoma Study. *Arch Ophthalmol*. 2009;127:270-274.

22. Heeg GP, Jansonius NM. The Groningen Longitudinal Glaucoma Study III. The predictive value of frequency-doubling perimetry and GDx nerve fibre analyser test results for the development of

glaucomatous visual field loss. *Eye*. 2009;23:1647-1652.

23. Junoy Montolio FG, Wesselink C, Gordijn M, Jansonius NM. Factors that influence standard automated perimetry test results in glaucoma: test reliability, technician experience, time of day, and season. *Invest Ophthalmol Vis Sci*. 2012;53:7010-7017.

24. Bengtsson B, Heijl A. False-negative responses in glaucoma perimetry: indicators of patient performance or test reliability? *Am J Ophthalmol*. 2000;130:689.

25. Jansonius NM. On the accuracy of measuring rates of visual field change in glaucoma. *Br J Ophthalmol*. 2010;94:1404-1405.

26. Leske MC, Heijl A, Hyman L, et al. Predictors of long-term progression in the early manifest glaucoma trial. *Ophthalmology*. 2007;114:1965-1972.

27. Garg A, Vickerstaff V, Nathwani N, et al. Primary Selective Laser Trabeculoplasty for Open Angle Glaucoma and Ocular Hypertension: Clinical Outcomes, Predictors of Success and Safety from the Laser in Glaucoma and Ocular Hypertension (LiGHT) Trial. *Ophthalmology*. 2019;126:1238-1248.

28. De Castro DK, Punjabi OS, Bostrom AG, et al. Effect of statin drugs and aspirin on progression in open-angle glaucoma suspects using confocal scanning laser ophthalmoscopy. *Clin Experiment Ophthalmol*. 2007;35:506-513.

29. Kang JH, Boumenna T, Stein JD, et al. Association of Statin Use and High Serum Cholesterol Levels With Risk of Primary Open-Angle Glaucoma. *JAMA Ophthalmol*. 2019;137:756-765.

30. McGwin G Jr, McNeal S, Owsley C, Girkin C, Epstein D, Lee PP. Statins and other cholesterol-lowering medications and the presence of glaucoma. *Arch Ophthalmol*. 2004;122:822-826.

31. Owen CG, Carey IM, Shah S, et al. Hypotensive Medication, Statins, and the Risk of Glaucoma. *Invest Ophthalmol Vis Sci*. 2010;51:3524-3530.

32. Marcus MW, Müskens RPH, Ramdas WD, et al. Cholesterol-Lowering Drugs and Incident Open-Angle Glaucoma: A Population-Based Cohort Study. *PLoS One*. 2012;7:e29724.

33. Chen H-Y, Hsu S-Y, Chang Y-C, et al. Association Between Statin Use and Open-angle Glaucoma in Hyperlipidemia Patients: A Taiwanese Population-based Case-control Study. *Medicine* . 2015;94:e2018.

34. Morishita S, Oku H, Horie T, et al. Systemic simvastatin rescues retinal ganglion cells from optic nerve injury possibly through suppression of astroglial NF-κB activation. *PLoS One*. 2014;9:e84387.

35. Krempler K, Schmeer CW, Isenmann S, Witte OW, Löwel S. Simvastatin improves retinal ganglion cell survival and spatial vision after acute retinal ischemia/reperfusion in mice. *Invest Ophthalmol Vis Sci*. 2011;52:2606-2618.

36. Hirooka K, Baba T, Fujimura T, Shiraga F. Prevention of visual field defect progression with angiotensin-converting enzyme inhibitor in eyes with normal-tension glaucoma. *Am J Ophthalmol*. 2006;142:523-525.

37. Müskens RPHM, de Voogd S, Wolfs RCW, et al. Systemic antihypertensive medication and incident open-angle glaucoma. *Ophthalmology*. 2007;114:2221-2226.

38. Langman MJS, Lancashire RJ, Cheng KK, Stewart PM. Systemic hypertension and glaucoma: mechanisms in common and co-occurrence. *Br J Ophthalmol*. 2005;89:960-963.

39. Miglior S, Torri V, Zeyen T, et al. Intercurrent factors associated with the development of open-angle glaucoma in the European glaucoma prevention study. *Am J Ophthalmol*. 2007;144:266-275.

40. Khawaja AP. Calcium Channel Blockers and Risk of Primary Open-angle Glaucoma. *J Glaucoma*. 2019.28:e49-e50.

41. Mayama C. Calcium channels and their blockers in intraocular pressure and glaucoma. *Eur J Pharmacol*.

2014;739:96-105.

42. Höhn R, Mirshahi A, Nickels S, et al. Cardiovascular medication and intraocular pressure: results from the Gutenberg Health Study. *Br J Ophthalmol*. 2017;101:1633-1637.

43. Khawaja AP, Chan MPY, Broadway DC, et al. Systemic Medication and Intraocular Pressure in a British Population. *Ophthalmology*. 2014;121:1501-1507.

44. Klein BEK, Klein R, Knudtson MD. Intraocular pressure and systemic blood pressure: longitudinal perspective: the Beaver Dam Eye Study. *Br J Ophthalmol*. 2005;89:284-287.

45. Ho H, Shi Y, Chua J, et al. Association of Systemic Medication Use With Intraocular Pressure in a Multiethnic Asian Population. *JAMA Ophthalmol*. 2017;135:196.

46. Foster PJ, Khawaja AP. The Association of Systemic Medication and Disease With Intraocular Pressure. *JAMA Ophthalmol*. 2017;135:203-204.

47. Hughes AD, Stanton AV, Jabbar AS, Chapman N, Martinez-Perez ME, McG Thom SA. Effect of antihypertensive treatment on retinal microvascular changes in hypertension. *J Hypertens*. 2008;26:1703-1707.

48. Hirooka K, Shiraga F. Potential role for angiotensin-converting enzyme inhibitors in the treatment of glaucoma. *Clin Ophthalmol*. 2007;1:217-223.

49. Fletcher EL, Phipps JA, Ward MM, Vessey KA, Wilkinson-Berka JL. The renin-angiotensin system in retinal health and disease: Its influence on neurons, glia and the vasculature. *Prog Retin Eye Res*. 2010;29:284-311.

50. Bowe A, Grünig M, Schubert J, et al. Circadian Variation in Arterial Blood Pressure and Glaucomatous Optic Neuropathy--A Systematic Review and Meta-Analysis. *Am J Hypertens*. 2015;28:1077-1082.

51. Slagter SN, van Waateringe RP, van Beek AP, van der Klauw MM, Wolffenbuttel BHR, van Vliet-Ostaptchouk JV. Sex, BMI and age differences in metabolic syndrome: the Dutch Lifelines Cohort Study. *Endocr Connect*. 2017;6:278-288.

52. Tulassay Z, Stolte M, Sjölund M, et al. Effect of esomeprazole triple therapy on eradication rates of Helicobacter pylori, gastric ulcer healing and prevention of relapse in gastric ulcer patients. *Eur J Gastroenterol Hepatol*. 2008;20:526-536.

53. Kang JH, Willett WC, Rosner BA, Buys E, Wiggs JL, Pasquale LR. Association of Dietary Nitrate Intake With Primary Open-Angle Glaucoma: A Prospective Analysis From the Nurses' Health Study and Health Professionals Follow-up Study. *JAMA Ophthalmol*. 2016;134:294-303.

54. Nouri-Mahdavi K, Hoffman D, Coleman AL, et al. Predictive factors for glaucomatous visual field progression in the Advanced Glaucoma Intervention Study. *Ophthalmology*. 2004;111:1627-1635.

55. Chauhan BC, Mikelberg FS, Balaszi AG, et al. Canadian Glaucoma Study: 2. risk factors for the progression of open-angle glaucoma. *Arch Ophthalmol*. 2008;126:1030-1036.

56. Kass MA, Heuer DK, Higginbotham EJ, et al. The Ocular Hypertension Treatment Study: a randomized trial determines that topical ocular hypotensive medication delays or prevents the onset of primary open-angle glaucoma. *Arch Ophthalmol*. 2002;120:701-713; discussion 829-830.

57. Gordon MO, Kass MA. The Ocular Hypertension Treatment Study: design and baseline description of the participants. *Arch Ophthalmol*. 1999;117:573-583.

58. Keltner JL, Johnson CA, Quigg JM, Cello KE, Kass MA, Gordon MO. Confirmation of visual field abnormalities in the Ocular Hypertension Treatment Study. Ocular Hypertension Treatment Study Group. *Arch Ophthalmol*. 2000;118:1187-1194.

Chapter 3

QUANTITATIVE OPTICAL COHERENCE TOMOGRAPHY ANGIOGRAPHY*

* Pappelis K, Jansonius NM. Quantification and Repeatability of Vessel Density and Flux as Assessed by Optical Coherence Tomography Angiography. *Transl Vis Sci Technol*. 2019;8(3):3.

3.1. Abstract

Purpose: To determine the intrasession repeatability (test-retest variability) of parafoveal and peripapillary perfused capillary density (PCD) and normalized flux index (NFI) as assessed with Canon OCT-HS100 angiography.

Methods: Pairs of optical coherence tomography angiography (OCTA) images were obtained from the parafoveal and peripapillary region of 30 eyes of 30 healthy subjects. PCD and NFI were calculated using generic image-processing software. Macular ganglion-cell complex thickness (GCC) and peripapillary retinal nerve fiber layer thickness (RNFLT) were also recorded. Bland-Altman analysis was performed and the coefficient of repeatability (CoR) and intraclass correlation coefficient (ICC) were calculated. Correlations of parafoveal PCD/NFI with GCC and of peripapillary PCD/NFI with RNFLT were also computed.

Results: Mean (standard deviation) parafoveal and peripapillary PCD were 40.0% (1.8%) and 44.5% (1.3%), respectively. Corresponding values for NFI were 151.2 (6.8) and 164.2 (3.9). For PCD, ICC was 0.76 for parafoveal and 0.79 for peripapillary measurements; corresponding CoRs were 2.7% and 1.8%. Corresponding values for NFI were 0.62 and 0.67 for ICC and 13.3 and 7.0 for CoR. Average measures ICC was 0.87/0.88 and 0.76/0.80 for the parafoveal/peripapillary PCD and NFI, respectively. PCD and NFI were weakly correlated with GCC (r = 0.39, P = 0.035; r = 0.33, P = 0.077) and moderately correlated with RNFLT (r = 0.43, P = 0.017; r = 0.55, P = 0.002).

Conclusions: Repeatability of a commercially available OCTA with generic image-processing software was good (NFI) to excellent (PCD). Our results indicate that changes surpassing the variability in healthy subjects should be easily detectable in a clinical setting.

Translational relevance: Repeatability estimates provide information regarding the relevance of changes in retinal perfusion.

3.2. Introduction

Optical coherence tomography angiography (OCTA) is a novel imaging modality enabling the fast, noninvasive, and depth-resolved visualization of the retinal and optic nerve head (ONH) microcirculation, thus potentially assisting in the diagnosis and follow-up of numerous ocular pathologies.[1,2] However, in order to interpret findings in an objective rather than qualitative manner, standardized quantitative metrics must be established, and their repeatability must enable the detection of clinically relevant changes.

The main principle behind OCTA is the detection of erythrocyte movement by comparing the static and dynamic signal properties between consecutive B-scans. Different image acquisition algorithms have been implemented in current commercial OCTA systems. Moreover, image post-processing and depiction as well as the quantitative measurements offered by some OCT manufacturers introduce discrepancies in the technique's reproducibility.[3] Thus, OCTA currently struggles with the proprietary nature of the metrics and therefore requires each instrument to be evaluated separately.

Perfused capillary density (PCD) is one of the most frequently used metrics within the context of OCTA: a reduction in PCD may be present in various ocular disorders, but particular interest has been taken in its potential use for evaluating glaucoma.[4] Even though the relationship between OCTA signal and blood flow is still unclear,[5] PCD can provide information not only on the structure but also on the function of the microvasculature,[6] since OCTA allows visualization of only the flowing capillaries. Another metric, namely Normalized Flux Index (NFI), has been regarded as even more informative by certain investigators.[7,8]

PCD is available as a parameter on several commercial OCTA devices and its repeatability has been reported as well.[9-11] However, other systems - such as the angiographic module of Canon OCT-HS100 - currently lack this quantitative analysis and therefore the (intradevice) repeatability has not been evaluated yet, at least not outside the foveal avascular zone.[12] NFI on the contrary is not available at the moment in any manufacturer's quantification software. Related to that, information regarding its repeatability is scarce.[8]

The aim of this study was to determine the intrasession repeatability (test-retest variability) of parafoveal and peripapillary PCD and NFI as assessed with Canon OCT-HS100. For this

purpose, we obtained OCTA images from a well-defined healthy sample and analyzed the data using generic image processing software in order to compensate for the system's absence of quantitative measurements and allow for harmonization of data across different OCTA brands.

3.3. Methods

3.3.1. Study Population

This is a prospective, cross-sectional study. All subjects between 50 and 65 years of age who responded to our advertisement received an information letter. We imaged one random eye of the first 34 participants who satisfied the following inclusion criteria after initial screening: best-corrected visual acuity ≥ 0.8; spherical refraction between -3 and +3 D and astigmatism not exceeding 2 D; intraocular pressure (IOP) ≤ 21 mmHg as assessed by a noncontact tonometer (Tonoref II, Nidek, Aichi, Japan); no reproducibly abnormal visual field test locations in Frequency Doubling Technology C20-1 screening mode (Carl Zeiss, Jena, Germany); no ophthalmic, vascular, cardiac, or blood disease (except for hypertension) as assessed by fundus imaging (TRC-NW400, Topcon Corporation, Tokyo, Japan) and a medical history questionnaire; no family history of glaucoma.

The ethics board of the University Medical Center Groningen (UMCG) approved the study protocol (no. NL61508.042.17). All participants provided written informed consent. The study followed the tenets of the Declaration of Helsinki.

3.3.2. Data Collection

Prior to the imaging session, the pupil of the chosen eye was dilated with tropicamide 0.5%. In addition, blood pressure (BP) was recorded twice in sitting position with an automatic BP monitor (Omron M6 Comfort, Omron Healthcare, Kyoto, Japan) from the brachial artery.

Subsequently, three 6 × 6 mm scans centered at the fovea and three 6 × 6 mm scans centered at the ONH were obtained in succession with the angiographic module of the Canon OCT-HS100 (Angio eXpert, OCTA version 2.0, Tokyo, Japan). In order to optimize image quality, while keeping at the same time scanning duration to tolerable levels (less than 10 seconds per

scan), the resolution was set to 'medium' (928 × 928 pixels) after repeats within each scan were set to '2'. Between the scans participants were asked to remove and reposition their head on the chinrest. The interval between the scans was typically less than 1 minute, being the time needed for removing and repositioning the participant's chin on the chinrest and refocusing. All scans were obtained in the late afternoon (5:00 PM-6:00 PM).

Out of the six angiographic scans obtained, the first two parafoveal and the first two peripapillary scans with sufficient quality (≥7 as assessed by the device itself) and free of motion or blinking artifacts were included in the repeatability analysis. Participants whose images did not satisfy the aforementioned criteria were excluded from the study.[13] Of the included scans, the median image quality was 8 (range 7- 9) for the parafoveal scans and 7 (7-8) for the peripapillary scans. To elucidate whether the angiographic imaging signal and its subsequent analysis are truly informative, we also recorded as a secondary outcome the parafoveal ganglion-cell complex thickness (GCC) and the peripapillary retinal nerve fiber layer thickness (RNFLT) which have been previously shown to positively correlate with PCD even in healthy subjects.[14]

3.3.3. Image Segmentation and Analysis

The angiographic images containing information from the maximum intensity projection signal of the superficial capillary plexus (top: inner limiting membrane; bottom: ganglion cell/inner plexiform border; offset: +50 μm) as determined by the manufacturer's segmentation were stored in an uncompressed format (bitmap). Even though the device can visualize the deep capillary plexus with a projection-resolved algorithm, we limited the analysis to the inner retinal layers to ensure that the signal is not a result of projection artifacts.[15]

Pairs of images from the same subject corresponding to the same region (parafoveal or peripapillary) were registered by means of a rigid body transformation matrix (rotation and translation) so that their structural features coincide (ImageJ; public domain software, National Institutes of Health, Bethesda, MD[16]). Local Otsu's thresholding algorithm was then applied in 14 × 14 pixel blocks to binarize each image in signal of flow and nonflow. Additionally, the big blood vessels were masked out of the images centered at the ONH through a combination of Hessian-based Frangi vesselness filtering algorithm[17] (made

available to the public by Dirk-Jan Kroon, 2009) and global thresholding. Our analysis was confined to a well-defined ring around the ONH with inner and outer radii of 1.03 and 1.84 mm respectively[18] and a 3-mm-diameter disc around the fovea (Fig. 1).[19] An experienced grader (KP) determined the center of the ONH and of the foveal avascular zone.

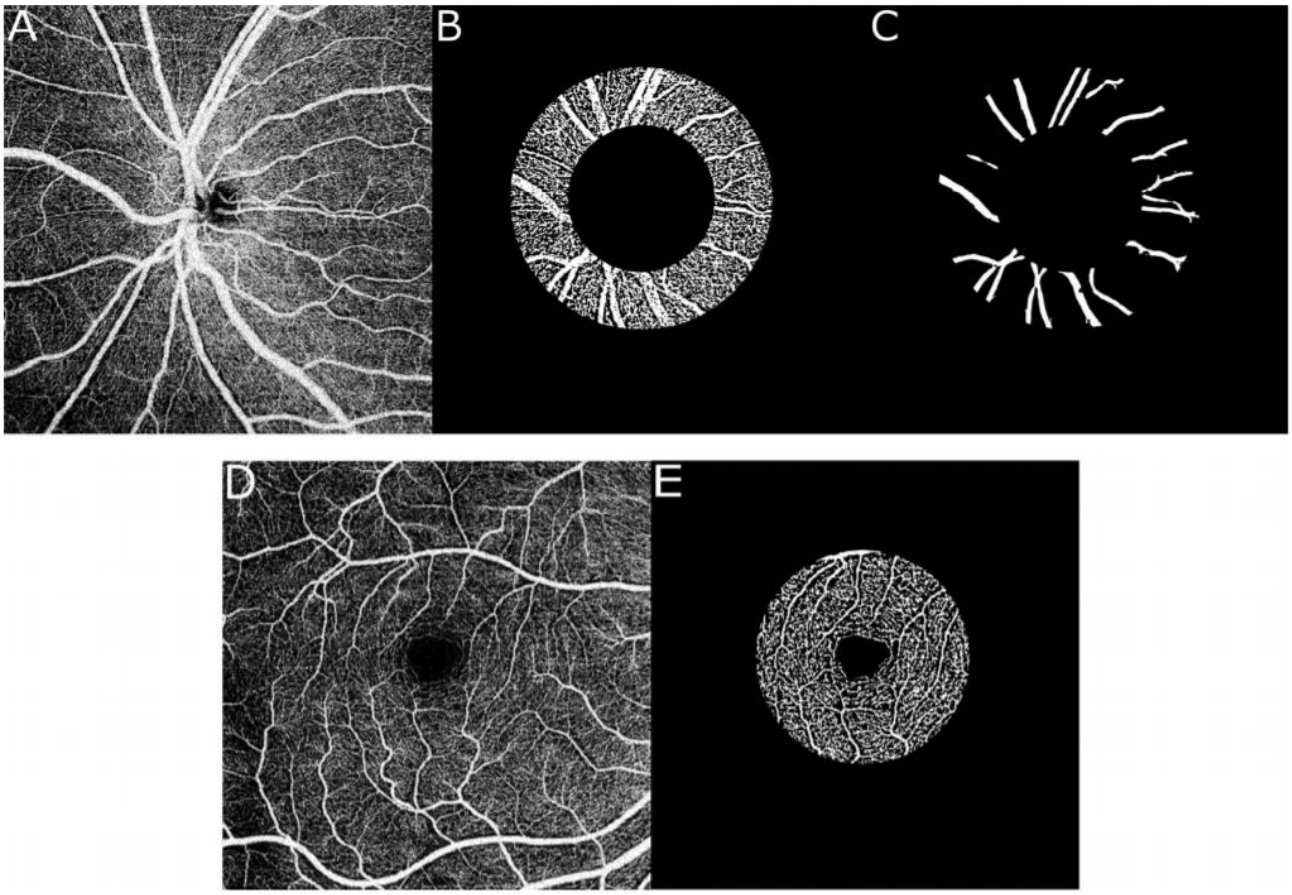

Figure 1. Regions of interest defined. (A) Peripapillary OCT-A image; (B) Peripapillary region of interest after local thresholding; (C) Peripapillary large vessel mask; (D) Parafoveal OCT-A image; (E) Parafoveal region of interest after local thresholding (no large vessel mask applied parafoveally).

We calculated PCD as the percentage of pixels occupied by capillaries inside the total measurement area. NFI was calculated as the average signal strength (grayscale intensity) of the pixels associated with perfused capillaries and is a unitless number between 0 and 255 (being the 8-bit intensity coding in the raw image, before binarization). For the peripapillary scan, the area occupied by large vessels was not included in these calculations.

Image processing was performed in MATLAB R2014a (The MathWorks, Natick, MA). The scripts are available on request.

3.3.4. Data Analysis

Means and standard deviations (SDs) were used to describe normally distributed variables. Variables with a skewed distribution were described by median and interquartile range (IQR). We generated scatterplots of the second measurement as a function of the first as well as the corresponding Bland-Altman plots[20] both for the parafoveal and peripapillary PCD and NFI.

We computed the mean difference in the two repeated scans for the parafoveal and peripapillary PCD and NFI. For these variables we also calculated (1) the coefficient of repeatability (CoR) as twice the standard deviation of the difference in two repeated scans[20] and (2) the two-way mixed intraclass correlation coefficient, both for single and average measures [ICC(2,1)/ICC(2,2);[21]]. For the interpretation of ICC values, we used the guidelines of Cicchetti *et al.*[22] Additionally, we computed Pearson's correlation coefficient for parafoveal PCD/NFI versus GCC as well as peripapillary PCD/NFI versus RNFLT. All analysis was performed using R (version 3.4.2; R Foundation for Statistical Computing, Vienna, Austria) and WINPEPI (PAIRSetc version 3.59; Abramson JH, 2004). A *P* value of 0.05 or less was considered statistically significant.

3.4. Results

Of the 34 participants satisfying the screening criteria, four were excluded due to significant image artifacts. Therefore, a total of 30 participants were included in the analysis. Table 1 shows the demographics and characteristics of the study population.

Table 1. Characteristics of Study Population

Age, median (IQR), y	58 (53–61)
Gender, % female	53
IOP, mean (SD), mm Hg	13 (3)
SBP, mean (SD), mm Hg	130 (14)
DBP, mean (SD), mm Hg	85 (8)
GCC, mean (SD), µm	92 (5)
RNFLT, mean (SD), µm	100 (10)

SBP, systolic blood pressure; DBP, diastolic blood pressure.

Table 2 summarizes mean values for PCD and NFI in both regions of interest, mean differences between the two consecutive scans, and the repeatability estimates. Based on the ICC, repeatability was excellent for PCD and good for NFI. A one-sample *t*-test ensured that the difference between the two consecutive scans was not significantly different from 0 (all *P* values ≥ 0.4). Moreover, the absolute interscan difference for the various outcomes did not depend on age, BP, or body mass index, as assessed by the significance of Pearson's correlation coefficient corrected for multiple testing with the Bonferroni method (all *P* values

> 0.2). Figures 2 and 3 present the scatterplots of the second measurement metrics plotted as a function of the first measurement metrics and the corresponding Bland-Altman plots, for the PCD and NFI, respectively.

Table 2. Repeatability Estimates for Parafoveal and Peripapillary PCD and NFI

	Mean (SD)	Mean (SD) Difference	CoR (95% CI)	ICC[2,1] (95% CI)	ICC[2,2] (95% CI)
Parafoveal PCD (%)	40.0 (1.8)	0.1 (1.4) [$P = 0.8$]	2.7 (1.8–3.6)	0.76* (0.56–0.88)	0.87* (0.72–0.94)
Peripapillary PCD (%)	44.5 (1.3)	−0.1 (0.9) [$P = 0.4$]	1.8 (1.2–2.4)	0.79* (0.60–0.89)	0.88* (0.75–0.94)
Parafoveal NFI	151.2 (6.8)	1.0 (6.7) [$P = 0.4$]	13.3 (9.1–17.5)	0.62* (0.34–0.80)	0.76* (0.51–0.89)
Peripapillary NFI	164.2 (3.9)	0.4 (3.5) [$P = 0.6$]	7.0 (4.8–9.2)	0.67* (0.41–0.83)	0.80* (0.58–0.91)

CI, confidence interval.
* Significant at $P = 0.001$.

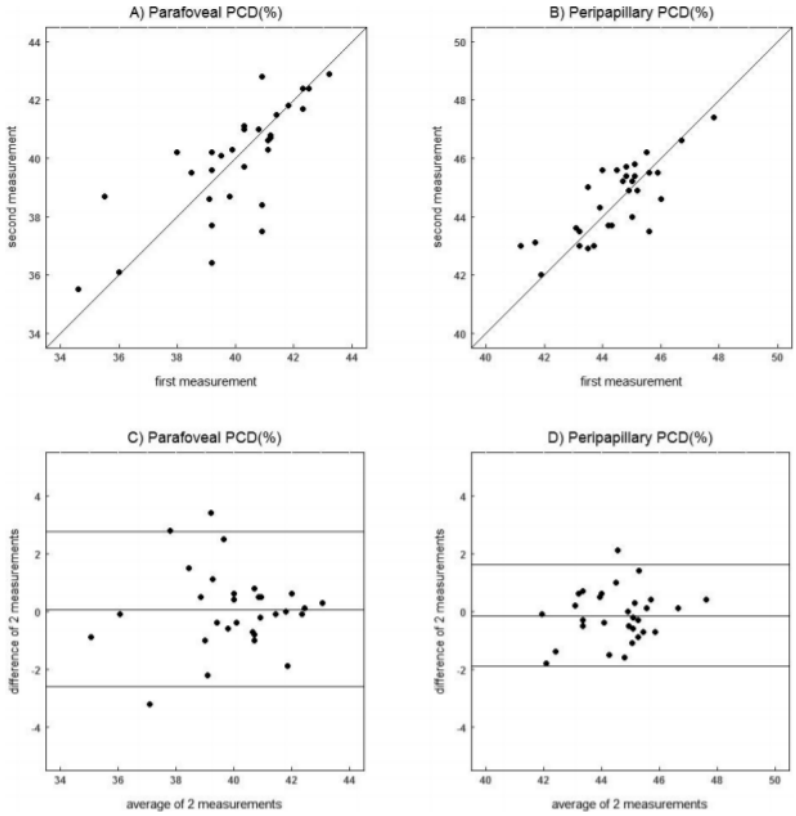

Figure 2. Scatterplots (A, B) of second PCD measurement as a function of the first measurement and the corresponding Bland-Altman plots (C, D) showing the difference of the two measurements as a function of the average. *Horizontal lines* denote mean difference (bias) and 95% limits of agreement.

Regarding our secondary outcome, only PCD but not NFI was significantly correlated with GCC in the parafoveal region [r = 0.39 (P = 0.035) and r = 0.33 (P = 0.077), respectively]. In the peripapillary region, both PCD and NFI were significantly correlated with RNFLT [r= 0.43 (P = 0.017) and r = 0.55 (P = 0.002), respectively].

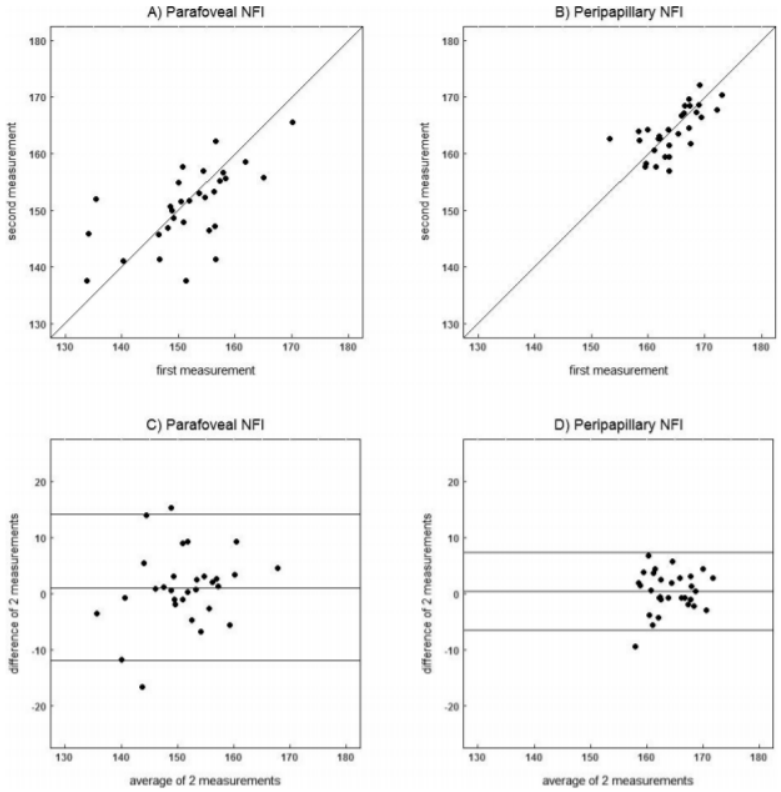

Figure 3. Scatterplots (A, B) of second NFI measurement as a function of the first measurement and the corresponding Bland-Altman plots (C, D) showing the difference of the two measurements as a function of the average. *Horizontal lines* denote mean difference (bias) and 95% limits of agreement.

3.5. Discussion

Parafoveal and peripapillary PCD measurements obtained by the Canon OCT-HS100 within the same session and from the same subject are in excellent agreement when considering the ICC values; upon retest their absolute values may differ up to 2.7% and 1.7%, respectively. NFI measurements are in good agreement; upon retest they may differ up to 13.1 and 6.9, respectively. Reliability from average measures is higher than reliability from single measures among all metrics in both regions. The angiographic metrics are weakly to moderately correlated with the corresponding retinal layer thicknesses.

A number of other studies have evaluated the intrasession repeatability of OCTA metric PCD, albeit with different devices. Regarding the parafoveal region, Alnawaiseh *et al*. found the CoR and ICC(2,1) for the PCD to be 3.4% and 0.72, respectively,[11] to be compared with 2.7% (95% CI: 1.8%-3.6%) and 0.76 (0.56-0.88) in our study. Fang *et al.*[23] reported a CoR of 3.2% and an ICC of 0.86, while the same repeatability variables reported by Coscas *et al*.[24] were 3.3% and 0.78 and by Al-Sheikh *et al*.[9] 3.4% and 0.90. The latter three studies did not

clarify which ICC was presented. An ICC of 0.89 without further specification was also reported by Lei *et al*.[10] A larger CoR of 4.9% was reported by Chen *et al*.[25] because they included multiplication by the square root of 2 in the calculation; the corrected value is 3.4%. Venugopal *et al*.[26] presented a CoR of 4.4% together with an ICC of 0.87 for the parafoveal region, as well as the corresponding values of 4.1% and 0.86 for the peripapillary region. Hence, the CoR for PCD that we report here as assessed by the angiographic module of Canon OCT HS-100 with customized software is at least as good as the ones reported in most of the aforementioned studies for different devices. Venugopal *et al*.,[26] using a different device in their study, found the measurements to be significantly less repeatable than ours both in the parafoveal and the peripapillary region. This could be attributed to improved results of our customized software, to different inclusion criteria, or to differences between devices in terms of scanning and segmentation.

Chen *et al*.[8] evaluated the repeatability of NFI, but with a different statistical approach. They found a coefficient of variation (CV) of 3.3% and 4.2% for the parafoveal and peripapillary region, respectively. For the sake of comparison, we also calculated the CV (SD of differences divided by the mean), which was 2.3% (CI: 1.7%-2.9%) for the parafoveal and 1.2% (CI: 0.9%-1.5%) for the peripapillary region. This might suggest improved repeatability of our methods; however, using exclusively the CV might spuriously suggest that repeatability is worse (higher CV) in ocular diseases where the mean angiographic metrics decrease (e.g., in glaucoma) or in devices with lower average signal intensity. Indeed, a recent study found some differences between glaucoma and healthy in the CV of the inferotemporal region of the peripapillary scan, but not in the CoR.[26]

Variation among consecutive scans could in general be a consequence of signal strength (even within the high quality scans), floaters, or measurement noise. Importantly, since OCTA is only able to image capillaries that are perfused and visible given the resolution of the system, it is possible that a portion of the variation between consecutive scans could be attributed to physiological reasons such as small changes in perfusion pressure due to, for example, cardiac cycle related variability in IOP.[27]

To our knowledge, this is the first study that addressed the PCD and NFI intrasession repeatability with the Canon OCT-HS100, and the first report of CoR and ICC for OCTA metric NFI. Importantly, the Canon OCT-HS100 is currently the only device using a full-spectrum amplitude decorrelation algorithm, therefore a separate evaluation was also deemed

necessary.[28] A strength of this study is the fact that the calculation of the quantification parameters and reasoning are described in detail. This generic approach avoids obscurities involved in metrics belonging to proprietary algorithms and thus allows for harmonization. For example, it is unclear if other algorithms include the larger vessels originating from the ONH in their calculations. A limitation of this study is the restriction to the superficial capillary plexus. Additionally, other metrics such as fractal dimension and foveal avascular zone were not considered in this analysis. Lastly, it is possible that the small sample size of the study affects the weak correlations of PCD and NFI with the GCC. A larger sample size could, for example, result in measured differences regressing towards the mean. However, our results are in agreement with Yu *et al*.[29] who reported stronger correlations in the peripapillary than the parafoveal sector.

The results suggest that it is possible to quantify the retinal microvasculature through OCTA with a satisfactory degree of accuracy. The additional information provided by OCTA metrics can be helpful in differentiating between healthy and diseased eyes within the clinical setting, should the effect size be sufficiently large. However, this study shows that one single OCTA image, which is most frequently obtained within the clinical setting, is not enough to guarantee a reliable absolute value estimation. Consequently, the use of these measurements for the evaluation and follow-up on an individual basis is not recommended. Instead, averaging of consecutive images or measurements might be a more informative approach,[30] and this is also suggested in our study when comparing average measures versus single measures ICC values.

In conclusion, by applying a generic quantification algorithm to the images obtained with a commercially available OCTA, we were able to quantify perfusion and estimate its intra-session repeatability. Small changes in perfusion fall within the test-retest variability; changes surpassing the variability in healthy subjects should be easily detectable in a clinical setting. This is important, since it provides insight on how the output of the specific device can be interpreted and handled in the clinic. Metrics with improved test-retest variability and diagnostic accuracy together with quantified blood velocity could potentially not only serve as additional clinical markers, but also help unravel underlying pathophysiological mechanisms.

3.6. References

1. Jia Y, Tan O, Tokayer J, et al. Split-spectrum amplitude-decorrelation angiography with optical coherence tomography. *Opt Express.* 2012;20:4710–25.

2. Kashani AH, Chen C-L, Gahm JK, et al. Optical coherence tomography angiography: A comprehensive review of current methods and clinical applications. *Prog Retin Eye Res.* 2017;60:66–100.

3. Corvi F, Pellegrini M, Erba S, et al. Reproducibility of Vessel Density, Fractal Dimension, and Foveal Avascular Zone Using 7 Different Optical Coherence Tomography Angiography Devices. *Am J Ophthalmol.* 2018;186:25–31.

4 . Rao HL, Kadambi SV, Weinreb RN, et al. Diagnostic ability of peripapillary vessel density measurements of optical coherence tomography angiography in primary open-angle and angle-closure glaucoma. *Br J Ophthalmol.* 2017;101:1066–70.

5. Ploner SB, Moult EM, Choi W, et al. Toward quantitative optical coherence tomography angiography: Visualizing Blood Flow Speeds in Ocular Pathology Using Variable Interscan Time Analysis. *Retina.* 2016;36(suppl 1):S118–26.

6. Pechauer AD, Jia Y, Liu L, et al. Optical Coherence Tomography Angiography of Peripapillary Retinal Blood Flow Response to Hyperoxia. *Invest Ophthalmol Vis Sci.* 2015;56:3287–91.

7. Bojikian KD, Chen C-L, Wen JC, et al. Optic Disc Perfusion in Primary Open Angle and Normal Tension Glaucoma Eyes Using Optical Coherence Tomography-Based Microangiography. *PLoS One.* 2016;11:e0154691.

8. Chen C-L, Bojikian KD, Xin C, et al. Repeatability and reproducibility of optic nerve head perfusion measurements using optical coherence tomography angiography. *J Biomed Opt.* 2016;21(6):65002.

9. Al-Sheikh M, Tepelus TC, Nazikyan T, et al. Repeatability of automated vessel density measurements using optical coherence tomography angiography. *Br J Ophthalmol.* 2017;101:449–52.

10. Lei J, Durbin MK, Shi Y, et al. Repeatability and Reproducibility of Superficial Macular Retinal Vessel Density Measurements Using Optical Coherence Tomography Angiography En Face Images. *JAMA Ophthalmol.* 2017;135:1092–8.

11. Alnawaiseh M, Brand C, Bormann E, et al. Quantification of macular perfusion using optical coherence tomography angiography: repeatability and impact of an eye-tracking system. *BMC Ophthalmol.* 2018;18(123).

12. Mihailovic N, Brand C, Lahme L, et al. Repeatability, reproducibility and agreement of foveal avascular zone measurements using three different optical coherence tomography angiography devices. *PLoS One.* 2018;13:e0206045

13. Fenner BJ, Tan GSW, Tan ACS, et al. Identification of imaging features that determine quality and repeatability of retinal capillary plexus density measurements in OCT angiography. *Br J Ophthalmol.* 2018;102:509–14.

14. She X, Guo J, Liu X, et al. Reliability of Vessel Density Measurements in the Peripapillary Retina and Correlation with Retinal Nerve Fiber Layer Thickness in Healthy Subjects Using Optical Coherence Tomography Angiography. *Ophthalmologica.* 2018;25:1–8.

15. Takusagawa HL, Liu L, Ma KN, et al. Projection-Resolved Optical Coherence Tomography Angiography of Macular Retinal Circulation in Glaucoma. *Ophthalmology.* 2017;124:1589–99.

16. Thévenaz P, Ruttimann UE, Unser M. A pyramid approach to subpixel registration based on intensity. *IEEE Trans Image Process* 1998;7:27–41.

17. Frangi AF, Niessen WJ, Vincken KL, et al. Multiscale vessel enhancement filtering. In: Wells WM, Colchester A, Delp S, eds. *Medical Image Computing and Computer-Assisted Intervention — MICCAI'98. MICCAI 1998. Lecture Notes in Computer Science*. Vol 1496. Berlin, Heidelberg: Springer; 1998:130-137.

18. Springelkamp H, Lee K, Ramdas WD, et al. Optimizing the information yield of 3-D OCT in glaucoma. *Invest Ophthalmol Vis Sci.* 2012;53:8162–71.

19. Ho J, Dans K, You Q, et al. Comparison of 3 mm × 3 mm versus 6 mm × 6 mm optical coherence tomography angiography scan sizes in the evaluation of non-proliferative diabetic retinopathy. *Retina.* 2019;39:259-264.

20. Bland JM, Altman DG. Measuring agreement in method comparison studies. *Stat Methods Med Res.* 1999;8:135–60.

21. Shrout PE, Fleiss JL. Intraclass correlations: Uses in assessing rater reliability. *Psychol Bull.* 1979;86:420–428.

22. Cicchetti DV. Guidelines, criteria, and rules of thumb for evaluating normed and standardized assessment instruments in psychology. *Psychol Assess.* 1994;6:284–90.

23. Fang D, Tang FY, Huang H, et al. Repeatability, interocular correlation and agreement of quantitative swept-source optical coherence tomography angiography macular metrics in healthy subjects. *Br J Ophthalmol.* 2019;103:4115-420.

24. Coscas F, Sellam A, Glacet-Bernard A, et al. Normative Data for Vascular Density in Superficial and Deep Capillary Plexuses of Healthy Adults Assessed by Optical Coherence Tomography Angiography. *Invest Ophthalmol Vis Sci.* 2016;57:OCT211–23.

25. Chen FK, Menghini M, Hansen A, et al. Intrasession Repeatability and Interocular Symmetry of Foveal Avascular Zone and Retinal Vessel Density in OCT Angiography. *Transl Vis Sci Technol.* 2018;7:6.

26. Venugopal JP, Rao HL, Weinreb RN, et al. Repeatability of vessel density measurements of optical coherence tomography angiography in normal and glaucoma eyes. *Br J Ophthalmol.* 2018;102:352–357.

27. Kaizu Y, Nakao S, Wada I, et al. Imaging of Retinal Vascular Layers: Adaptive Optics Scanning Laser Ophthalmoscopy Versus Optical Coherence Tomography Angiography. *Transl Vis Sci Technol.* 2017;6:2.

28. Rodríguez FJ, Staurenghi G, Gale R, et al. The role of OCT-A in retinal disease management. *Graefes Arch Clin Exp Ophthalmol.* 2018;256:2019–2026.

29. Yu J, Gu R, Zong Y, et al. Relationship Between Retinal Perfusion and Retinal Thickness in Healthy Subjects: An Optical Coherence Tomography Angiography Study. *Invest Ophthalmol Vis Sci.* 2016;57: OCT204–10.

30. Mo S, Phillips E, Krawitz BD, et al. Visualization of Radial Peripapillary Capillaries Using Optical Coherence Tomography Angiography: The Effect of Image Averaging. *PLoS One.* 2017;12:e0169385.

Chapter 4

A MODEL FOR STATIC RETINAL BLOOD FLOW AUTOREGULATION*

* Pappelis K, Choritz L, Jansonius N. Microcirculatory model predicts blood flow and autoregulation range in the human retina: in vivo investigation with Laser Speckle Flowgraphy. *Am J Physiol Heart Circ Physiol*. 2020;319(6):H1253-1273.

4.1. Abstract

In this study, we mathematically predict retinal vascular resistance (RVR) and Retinal Blood Flow (RBF), we test predictions using Laser Speckle Flowgraphy (LSFG), we estimate the range of vascular autoregulation, and we examine the relationship of RBF with the retinal nerve fiber layer (RNFL) and ganglion cell complex (GCC). Fundus, optical coherence tomography (OCT), and OCT-angiography images, systolic/diastolic blood pressure (SBP/DBP), and intraocular pressure (IOP) measurements were obtained from 36 human subjects. We modeled two circulation markers (RVR and RBF) and estimated individualized lower/higher autoregulation limits (LARL/HARL), using retinal vessel calibers, fractal dimension, perfusion pressure, and population-based hematocrit values. Quantitative LSFG waveforms were extracted from vessels of the same eyes, before and during IOP elevation. LSFG metrics explained most variance in RVR ($R^2 = 0.77/P = 6.9 \cdot 10^{-9}$) and RBF ($R^2 = 0.65/P = 1.0 \cdot 10^{-6}$), suggesting that the markers strongly reflect blood flow physiology. Higher RBF was associated with thicker RNFL ($P = 4.0 \cdot 10^{-4}$) and GCC ($P = 0.003$), thus also verifying agreement with structural measurements. LARL was at SBP/DBP of 105/65 mmHg for the average subject without arterial hypertension, and at 115/75 mmHg for the average hypertensive subject. Moreover, during IOP elevation, changes in RBF were more pronounced than changes in RVR. These observations physiologically imply that healthy subjects are already close to LARL, thus prone to hypoperfusion. In conclusion, we modeled two clinical markers and described a novel method to predict individualized autoregulation limits. These findings could improve understanding of retinal perfusion and pave the way for personalized intervention decisions, when treating patients with coexisting ophthalmic and cardiovascular pathologies.

New & Noteworthy

We describe and test a new approach to quantify retinal blood flow, based on standard clinical examinations and imaging techniques, linked together with a physiological model. We use these findings to generate individualized estimates of the autoregulation range. We provide evidence that healthy subjects are closer to the lower autoregulation limit than thought before. This suggests that some retinas are less prepared to withstand hypoperfusion, even after small intraocular pressure rises or blood pressure drops.

4.2. Introduction

The retinal microcirculation is involved in many ophthalmic pathologies, but particular attention has been given to its role in leading causes of blindness, such as age-related macular degeneration, diabetic retinopathy, and glaucoma.[1] In addition, it is often an indicator of cardiovascular or cerebrovascular disease.[2,3] To date, there is only partial understanding of the regulation of blood supply in the retina and the optic nerve head (ONH), partially due to the lack of a gold-standard, noninvasive way to quantify blood flow (BF).[4]

The main advantage of the retinal vasculature is that it can be a direct source of physiological insight in humans, as a result of the transparent anterior ocular structures. However, there still are numerous caveats in assessing the retinal circulation. Despite its advantages, fluorescein angiography is an invasive procedure that only provides limited, qualitative information about tissue perfusion.[5] With the development of optical coherence tomography angiography (OCTA), many additional characteristics of the retinal microvasculature can now be quantified noninvasively, but, when considered alone, they still do not describe BF in its entirety.[6,7] In addition, laser speckle flowgraphy (LSFG) is one among several promising techniques currently used for relative retinal BF dynamic evaluation.[8-10] Details of this technique, as well as its application in the retina and the ONH, have been described elsewhere.[9,11,12] In short, it calculates the mean blur rate (MBR) of the speckle pattern, which is caused by moving red blood cells and is roughly proportional to BF velocity. Its ability to quantify BF characteristics has already been demonstrated, but considerable technical limitations have to be overcome before LSFG can be introduced to the clinical setting.[13,14]

Consequently, there is no direct way to predict how individual microcirculatory determinants interact to determine tissue blood supply in the bigger picture. This interaction is complex: BF is driven by a pressure difference [ocular perfusion pressure (OPP)] but also depends on numerous properties of the vascular bed, such as autoregulation. Autoregulation is the intrinsic ability of certain blood vessels to actively modify their caliber in response to changes in circumferential wall stress.[15] Hence, the use of oversimplified perfusion surrogates such as OPP is a common shortcoming in ophthalmology. Indeed, not only does this approach run into serious statistical limitations in population studies, but it also disregards physiological compensatory mechanisms.[16,17]

In an attempt to complement the current assessment of retinal hemodynamics, current research mainly focuses on two approaches. First, the emergence of Doppler OCT allows for absolute retinal blood flow quantification, which has been regarded as informative in describing physiological phenomena, as well as in detecting pathological changes.[18,19] Absolute retinal blood flow is a metric that partly addresses the limitations raised in the previous paragraph and is also the penultimate step in estimating tissue oxygenation.[20] While the reproducibility of Doppler OCT is constantly being improved, it could still pose significant challenges in pathological conditions, since it requires considerably more expertise than standard imaging methods.[21] Consequently, it has not found its way to the clinical routine yet. Second, mathematical models have been proposed, especially with regards to glaucoma, where a vascular component has long been thought to pertain to the disease pathogenesis.[22-27]

However, these models have not attempted to describe quantitative BF metrics that could be easily obtained in everyday clinical care, hence immediately useful not only in physiological research, but also in diagnostic and treatment decisions. In addition, even though autoregulation in the retina has been established as a general principle, each individual vasculature is unique. As such, it has distinct autoregulation capacity that depends on its phenotype at a given point in time (extent of dilation/contraction, structural complexity, viscous forces, perfusion pressure, etc.). Neither approach is currently able to quantitatively predict the effect of blood pressure (BP) changes on BF physiology, taking into account these individual phenotypical characteristics.

Therefore, the primary aims of this study were (1) to mathematically predict retinal vascular resistance (RVR) and absolute retinal blood flow (RBF), given individualized input collected with a proposed clinically feasible protocol, (2) to test these predictions against *in vivo* BF measurements from human retinal vessels, and (3) to provide individualized estimates for the range of retinal vascular autoregulation. For this purpose, in the theoretical part of the study, we extended a model for the retinal microcirculation based on fractal geometry[28]; in the experimental part, we examined the relationship of the theoretical predictions with BF information obtained from a human population in a clinical setting by means of LSFG. As a secondary aim, we looked into whether the model predictions for blood supply also reflect structural (nerve tissue) measurements.

4.3. Methods

4.3.1. Study Population

The experimental part had a prospective, cross-sectional design. We included 36 eyes from 36 adult subjects. Participants underwent screening to exclude ocular pathologies. We did not exclude glaucoma, ocular hypertension, mild cataract (with best-corrected visual acuity ≥ 0.8), mild/moderate refractive error (-6 D to +3 D), and astigmatism of 2 D or less. In order for the model to be tested over the full dynamic range of its variables, we encouraged participation of subjects with arterial hypertension (AHT), albeit no hypertensive retinopathy, and glaucoma. We used the standard AHT definition: current use of antihypertensive medication, or systolic blood pressure (SBP) ≥ 140 mmHg, or diastolic blood pressure (DBP) ≥ 90 mmHg.[29] Glaucoma was defined as an already established clinical diagnosis, in accordance with the European Glaucoma Society guidelines.[30] As a result, 15 of 36 subjects had AHT and 5 of 36 were patients from the ophthalmology clinic, already diagnosed with glaucoma [4 high-tension, primary open angle (POAG) cases, 1 primary closed angle case]. Eleven of 15 subjects with AHT were using antihypertensive medication, while all 5 glaucoma patients were using at least one topical antiglaucoma medication. The age of the participants ranged from 22 to 77 yr (median 54 yr).

Screening comprised a detailed slit lamp examination, best-corrected visual acuity (on a standardized letter chart), and C20-1 screening mode frequency doubling perimetry (Carl Zeiss, Jena, Germany). Additional documentation of ophthalmic health was performed with the imaging session (fundus photography, OCT, and OCTA; see 4.3.2A and 4.3.2C). Apart from the glaucoma patients, all other participants had healthy eyes, while there were no subjects with diagnosed diabetes or cardiovascular disease (except for AHT). All tests were performed in the ophthalmology clinic, under similar conditions (room temperature 22.5-23.5°C), and with undilated pupils, since some mydriatic drops (alpha-adrenergic agonists) could affect certain BF metrics.[12] Other studies have used muscarinic antagonists for pupil dilation, without any notable effect on BF.[14]

The ethics board of the Otto von Guericke University Magdeburg approved the study protocol (no. 32/19). All participants received an information letter and provided written informed consent. The study followed the tenets of the Declaration of Helsinki.

4.3.2. Model Variables and Parameters

A) Central retinal artery and vein radii

We obtained 45° fundus photographs centered at the ONH in high resolution from all subjects with a nonmydriatic digital camera (nonmyd WX-3D, Kowa Company, Ltd., Japan). We used the revised Parr-Hubbard formulas proposed by Knudtson *et al*. and a freely available, semiautomatic software [Automated Retinal Image Analyzer (ARIA), Peter Bankhead] to derive the central retinal artery and vein equivalents (CRAE and CRVE).[31,32] Details of this procedure have been described elsewhere.[32] In short, a standardized number of six largest arteriolar and six largest venular branches were identified within a ring with borders at 0.5- and 1.0-optic-disc diameters from the ONH margin (Fig. 1A); subsequently, an iterative mathematical procedure, using the area expansion ratio of the daughter branches to the mother branch, returned the expected radii of the CRA and CRV (r_{a_0}, r_{v_0}).

B) Branch length exponent (α) and branch length coefficient (β)

The microvascular bed can be decomposed into two distinct fractal patterns: one with regards to the exponential decay in branch radius *r* and one with regards to the decay in the corresponding branch length *l*, as the order *i* of the branches increases. Assuming symmetric, dichotomous branching (see 4.3.3), we may write:

$$\begin{cases} r_i = r_0 \, \mathrm{e}^{-i\tau} \\ l_i = l_0 \, \mathrm{e}^{-i\sigma} \end{cases} \tag{1}$$

where *i* is an integer representing the branch order and τ and σ are rate parameters. It follows that:

$$l_i = \beta \, r_i^{\alpha} \tag{2}$$

$$\text{where } \beta = \frac{l_0}{r_0^{\alpha}} \text{ and } \alpha = \frac{\sigma}{\tau}.$$

For the branch length exponent α, we use the constant suggested by Takahashi *et al.* for the retinal vasculature, $\alpha = 1.15$, which is based on data from cerebral vessels.[28] Regarding the

branch length coefficient β, *Eq.* 2 suggests that it is dependent on the stem radius; hence, its baseline value can be altered in conditions such as AHT or glaucoma.[33-35] Takahashi *et al.* use the value $\beta = 7.4$, but this was calculated from an average of young, healthy individuals.[28] Assuming vasodilation/vasoconstriction are length-preserving, collective, and uniform transformations of the vessels, we calculate the corrected branch length coefficients β_a and β_v from each individual CRA and CRV, based on their deviation from the average radii r_{a_0} and r_{v_0}, determined from the 18 healthy normotensives in our study:

$$\begin{cases} \beta_a = 7.4 \left(\dfrac{\overline{r_{a_0}}}{r_{a_0}} \right)^{\alpha} \\ \beta_v = 7.4 \left(\dfrac{\overline{r_{v_0}}}{r_{v_0}} \right)^{\alpha} \end{cases} \tag{3}$$

C) Fractal dimension

Fractal dimension (D) is a measure of microvascular complexity. Subjects underwent spectral domain OCT and OCTA imaging (SPECTRALIS Flex Module, Heidelberg Engineering, Inc., Heidelberg, Germany). We calculated D from 20° OCTA images centered at the macula (Fig. 1B), by means of customized image processing software. Details and repeatability of this method have been described elsewhere.[36] In short, we extracted the vasculature corresponding to the superficial vascular plexus (SVP) from a 3-mm-diameter circle centered at the fovea (Fig. 1C), by means of a local Otsu binarization algorithm. Subsequently, we defined D as the Minkowski-Bouligand (boxcounting) dimension:

$$D = \lim_{\varepsilon \to 0} \frac{\log [N(\varepsilon)]}{\log \left(\frac{1}{\varepsilon} \right)} \tag{4}$$

where N and ε describe the number and size of the superpixels needed to cover the vascular area, respectively. In practice, D can be approximated by the slope of the corresponding log-log plot (Fig. 1D).

For the secondary aim of the study, peripapillary retinal nerve fiber layer (pRNFL) thickness and ganglion cell complex (GCC) volume (full 6 × 6 mm ETDRS grid) were also recorded from regular ONH and macular OCT scans.

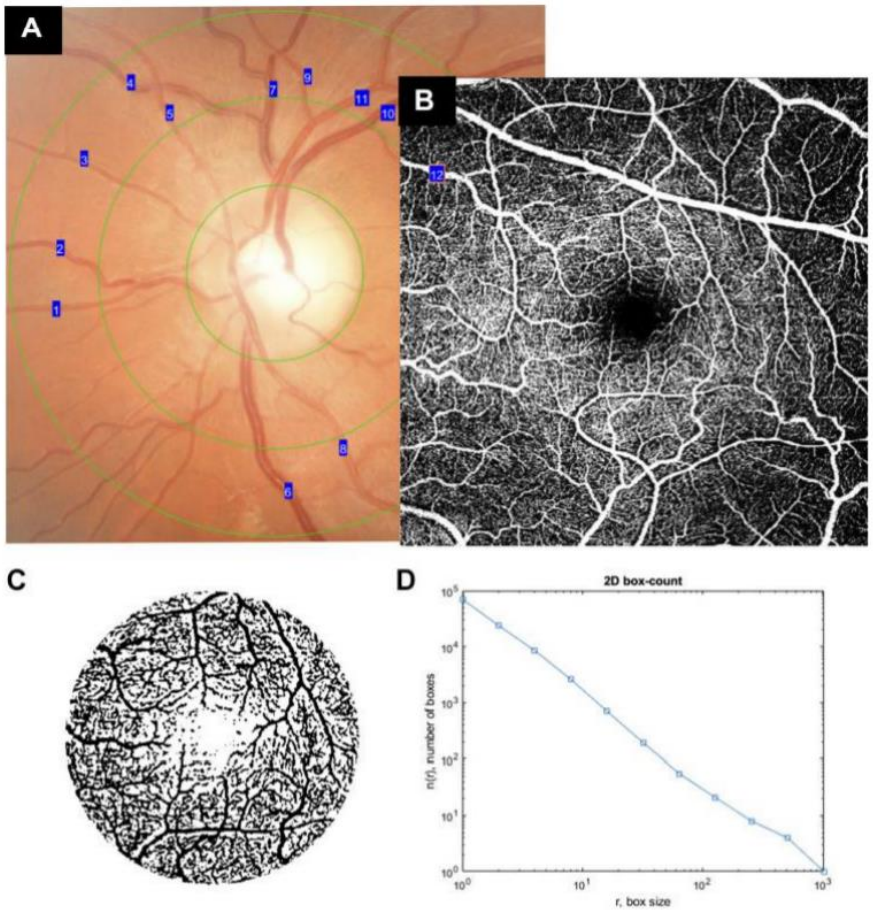

Fig. 1. *A*: cropped 45° fundus image centered at the optic disk. According to the Knudtson-Parr-Hubbard algorithm, the 6 largest arteries and 6 largest veins within the region of interest are marked with blue labels. *B*: overlayed 20° optical coherence tomography angiography (OCTA) image of the superficial vascular plexus of the same eye centered at the macula. *C*: OCTA image from *B* binarized within a 3-mm-diameter circle centered at the macula. Flowing blood vessels, recognized as thresholded pixels, appear in black. *D*: number of superpixels needed to cover the flowing blood vessels plotted against the size of the superpixels in a log-log graph. Fractal ("boxcounting") dimension is equal to the slope of the trend line.

D) Blood viscosity (μ)

In the retinal microcirculation (where for the Womersley number Wo < 0.05 holds, hence viscous forces are much more important than inertial forces), viscosity follows the Fåhræus-Lindqvist effect.[37] This effect concerns a decrease in viscosity with a decrease in vessel diameter. Haynes proposed the following formula to account for decreasing radii:

$$\mu\,(r) = \mu_{\infty} \frac{r^2}{(r+\delta)^2} \tag{5}$$

where $\mu\,(r)$ is the viscosity in a branch with radius r, μ_{∞} is the asymptotic viscosity in large vessels, and δ is a red-cell-size order of magnitude constant.[38]

Kamiya and Takahashi used the data of Fåhræus and Lindqvist to calculate δ = 4.29 μm. μ_{∞} can be estimated by the formula of Chien *et al.*:

$$\mu_{\infty} = 0.0016209\ e^{2.0795\frac{\mathrm{Hct}(\%)}{100}}\ \mathrm{Pa{\cdot}s} \tag{6}$$

where Hct is the hematocrit expressed as a percentage.[39,40]

An *in vitro* study suggested that a multiplication by a factor of 1.08 in *Eq.* 6 should be used when calculating venous viscosity, due to differences in shear rates compared to arterioles of the same radius.[41] In this study, we did not obtain blood samples; instead, we used the average Hct values reported in the Gubbio Population Study, stratified for age, gender, and BP status (treated vs. untreated AHT).[42]

E) Capillary parameters

For the three capillary parameters (r_c, l_c, μ_c), we used the values of Takahashi *et al.*.[28] The radius r_c and length l_c of the capillaries are assumed constant (r_c = 2.5 μm, l_c = 500 μm), that is, they do not autoregulate or undergo significant structural remodeling. An inverse Fåhræus-Lindqvist effect with an increase in viscosity is expected in branches with a diameter of less than 6 μm, since they are smaller than the diameter of a single red blood cell.[43] We assume μ_c = 0.0046 Pa·s.

F) Ocular perfusion pressure

Ocular perfusion pressure (OPP) is the difference between the pressures in the arterial P_a and venous P_v ends. Mean P_a is usually approximated by 2/3 MAP, where MAP is the mean arterial pressure, calculated as MAP = 1/3 SBP + 2/3 DBP, where SBP and DBP are the systolic and diastolic BP, respectively.[44] In this study, we use Takahashi's slightly different definition for mean P_a, being 7/10 MAP − 19.5 mmHg, because it results in a more accurate representation of the pressure in the CRA.[28,45] P_v is taken as equal to the intraocular pressure (IOP). Therefore:

$$\overline{OPP} = \overline{P_a} - P_v = \left(\frac{7}{10}MAP - 19.5\right) - IOP \text{ mmHg}. \quad (7)$$

The BP was measured twice, in sitting position, immediately before the LSFG imaging, with an automated monitor (BM 85, Beurer medical, Beurer GmbH, Ulm, Germany). IOP was measured with a rebound tonometer (Icare TA01i, Icare Finland Oy, Vantaa, Finland), after the subject had placed his or her chin on the chinrest of the LSFG apparatus.

4.3.3. Model Building

We adopt the dichotomous symmetrical branching structure proposed by Takahashi *et al*.[28] In our model, the CRA and CRV are the stem generation of the arteriolar and venular generations of radius r_{a_0} and r_{v_0}, respectively. In addition, each generation of radius r_i is a compartment of 2^i parallel, congruent resistors with total resistance R_{a_i} (arterioles), R_{v_j} (venules), or R_c (capillaries) as shown in Fig. 2. In agreement with Takahashi *et al.*, 15 generations (including the stem) of arterioles and 15 generations of venules were needed for the radii to drop to capillary level; in addition, the terminal arteriole is assumed to give rise to 4 capillaries, which then reunite into 1 terminal venule.[28] This parallel structure allows R_{a_i}, R_{v_j}, and R_c to be calculated similarly to electrical circuits. We can now compute the first outcome variable, RVR, by summing in series all the arteriolar, venular, and capillary resistive generations. This calculation is provided in the box below.

Calculation of RVR

We first calculate the resistance of each vessel generation R_{a_i} in the arterial compartment, as a function of its radius. Similar reasoning applies to the venous compartment.

$$R_a(r) = \frac{R_b(r)}{N_b(r)} \tag{B1}$$

where $R_b(r)$ is the resistance of a single branch with radius r and $N_b(r)$ is the expected number of branches of radius r.

$R_b(r)$ can be calculated from Poiseuille's law and *Eqs*. 2, 3, and 5 (main text). For an arteriole, it will be:

$$R_b(r) = \frac{8\,\mu(r)\,l(r)}{\pi\, r^4} = \ldots = \frac{8\,\mu_\infty\,\beta\left(\frac{\overline{r_{a_0}}}{r_{a_0}}\right)^\alpha}{\pi\, r^{2-\alpha}\,(r+\delta)^2} \tag{B2}$$

where δ = 4.29 μm is the red-cell-size order of magnitude constant defined in *Eq*. 5.

$N_b(r)$ has been estimated by Kamiya and Takahashi.[40] Again, for an arteriole:

$$N_{\mathrm{b}}(r) = \left(\frac{r}{r_{\mathrm{a}_0}}\right)^{-D-\alpha}. \tag{B3}$$

From *Eq*. B3, it is not difficult to show that, for symmetric and dichotomous branching, r_i is a geometric sequence. Hence:

$$r_i = \lambda^i \, r_0 \tag{B4}$$

where $\lambda = 2^{-\frac{1}{D+\alpha}}$ (which equals $e^{-\tau}$ as can be seen in *Eq*. 1 of the main text) and, again, *i* is an integer representing the branch order.

The resistance of the capillaries R_{c} is constant:

$$R_{\mathrm{c}} = \frac{8\,\mu_{\mathrm{c}}\,l_{\mathrm{c}}}{\pi\, r_{\mathrm{c}}^4}\; 2^{-16} \tag{B5}$$

where we assume 4 branches per terminal arteriole/venule.

In the last step, we use *Eqs*. B1-B5 to compute RVR:

$$\mathrm{RVR} = \sum_{i=0}^{14} R_{\mathrm{a}_i} + \sum_{j=0}^{14} R_{\mathrm{v}_j} + R_{\mathrm{c}} = \ldots = \tag{B6}$$

$$= \frac{8\beta}{\pi}\left[\mu_{\mathrm{a}_\infty}\frac{\overline{r_{\mathrm{a}_0}}^{\alpha}}{r_{\mathrm{a}_0}^2}\sum_{i=0}^{14}\frac{2^{\frac{D+2\alpha-2}{D+\alpha}i}}{\left(2^{-\frac{1}{D+\alpha}i}\,r_{\mathrm{a}_0}+\delta\right)^2} + \mu_{\mathrm{v}_\infty}\frac{\overline{r_{\mathrm{v}_0}}^{\alpha}}{r_{\mathrm{v}_0}^2}\sum_{j=0}^{14}\frac{2^{\frac{D+2\alpha-2}{D+\alpha}j}}{\left(2^{-\frac{1}{D+\alpha}j}\,r_{\mathrm{v}_0}+\delta\right)^2}\right] + \frac{8\,\mu_{\mathrm{c}}\,l_{\mathrm{c}}}{\pi\, r_{\mathrm{c}}^4}\,2^{-16}$$

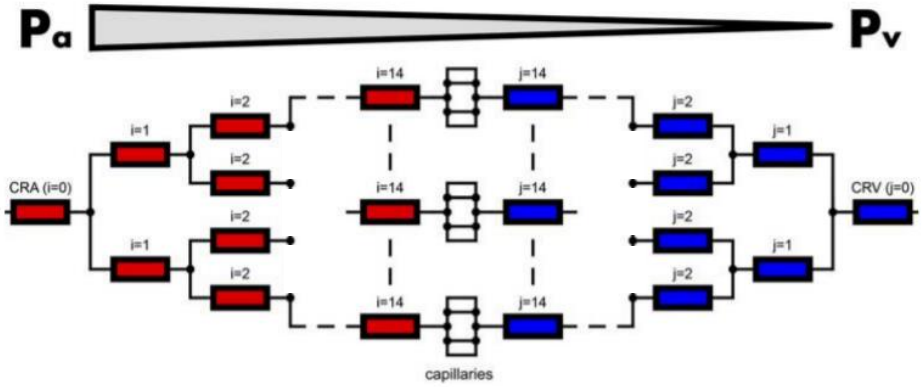

Fig. 2. Geometry of the retinal microcirculatory network, as proposed by Takahashi et al. (128). Dichotomous, symmetric branching is assumed throughout. Central retinal artery (CRA) and central retinal vein (CRV) are set as generation 0 vessels ($i = 0$, $j = 0$). Generation 14 corresponds to the terminal arterioles/venules, each 1 being connected with 4 true capillaries. Flow is driven by the difference between pressures at the arteriolar (P_{a}) and venular level (P_{v}).

We can simultaneously express resistance with Ohm's law, analogously to an electrical circuit:

$$RVR = \frac{\overline{OPP}}{\overline{RBF}} \quad (8)$$

where RBF is the mean retinal blood flow.

From this equation, the second outcome variable, RBF, can be directly calculated.

All image processing and calculations were performed in MATLAB R2018a (The MathWorks, Natick, MA). Scripts are freely available and will be personalized for each OCT device upon request to the corresponding author.

4.3.4. LSFG Imaging

We performed LSFG imaging (RetFlow, Nidek Co., Ltd., Gamagori, Aichi, Japan) in the standard orthogonal (22° by 11°) area centered at the ONH (Fig. 3A). Measurements were performed in a dark room, following a break of ~15 minutes, to stabilize systemic and ocular blood flow variables. As already mentioned, no topical mydriasis was applied. We obtained one reliable scan from each patient; upon detection of blinking or motion artifacts, the scan was repeated. An elliptic region of interest (ROI) was manually set to coincide with the ONH borders and the area within the ROI corresponding to large vessels was automatically identified by the apparatus based on histogram thresholding. The device acquires 30 frames per second over a 4-s measurement period, and for each pixel, the average MBR of all frames over one heartbeat is calculated.

The 10 following waveform metrics were extracted within the ROI: mean velocity in large vessels (MV), flow acceleration index (FAI), skew, fluctuation, heart rate (HR), resistivity index (RI), blowout time, acceleration time index, rising rate, and falling rate. The derivation protocol and the interpretation of these metrics have been described elsewhere.[14,46] In brief, they quantify mean BF velocity (in relative units) and additional characteristics obtained from waveform analysis, which depend on pulsatile BF and vessel caliber. The separate arterial and venous velocity components can be estimated from the *in vivo* measurements, by making use of the LSFG velocity information, as well as the cross section of the vessels:

$$\overline{\mathrm{RBF}_{\mathrm{iv}}} = \pi\, \overline{u_{\mathrm{a}_0}}\, r_{\mathrm{a}_0}^2 = \pi\, \overline{u_{\mathrm{v}_0}}\, r_{\mathrm{v}_0}^2 \tag{9}$$

where iv is short for *in vivo*, $\overline{u_{\mathrm{a}_0}}$, $\overline{u_{\mathrm{v}_0}}$ are the mean velocities in the CRA and CRV, respectively, and r_{a_0}, r_{v_0} have been previously defined, from which it follows that:

$$\frac{\overline{u_{\mathrm{a}_0}}}{\overline{u_{\mathrm{v}_0}}} = \frac{r_{\mathrm{v}_0}^2}{r_{\mathrm{a}_0}^2}\,. \tag{10}$$

Importantly, LSFG was used as an independent experimental validation of the theoretical predictions. As such, it is not part of the theoretical model itself.

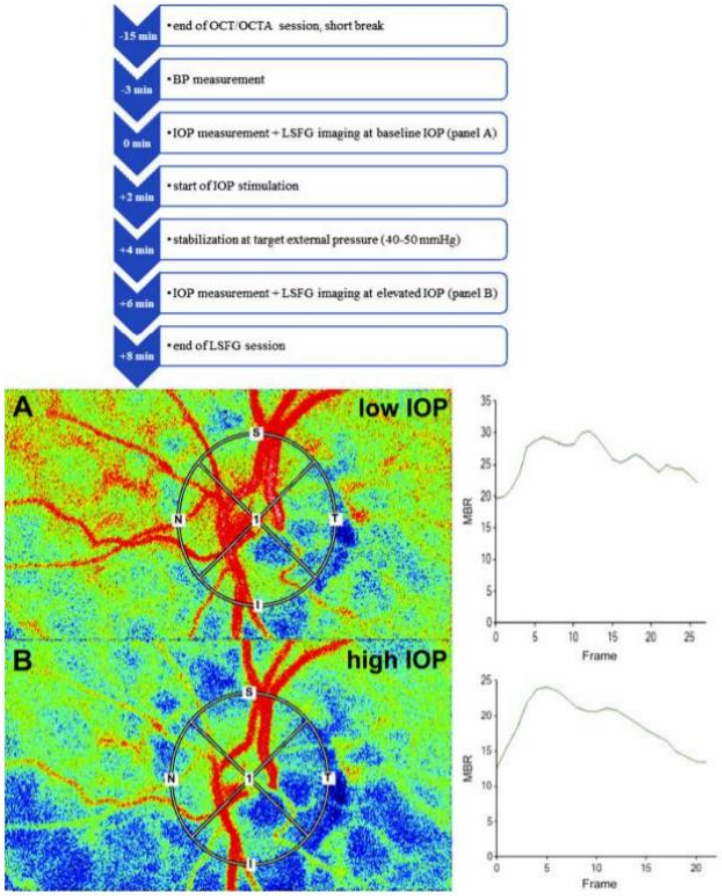

Fig. 3. Laser speckle flowgraphy (LSFG) snapshots of the same eye as in Fig. 1, centered at the optic disk. Graphs on the right display the mean blur rate (MBR) during 1 heartbeat, averaged from all pixels within the region of interest. Pixels with higher MBR are colored in red and correspond to higher blood velocity. Pixels with lower MBR are colored in blue. *A*: LSFG snapshot obtained at baseline venous pressure (P_v), with intraocular pressure (IOP) at 11 mmHg. *B*: LSFG snapshot of the same eye obtained at high P_v, after controlled increase of IOP to 21 mmHg. OCTA, optical coherence tomography angiography; BP, blood pressure.

4.3.5. IOP Stimulation

We used a subset of the study population (n = 12, of which 5 subjects had AHT and 1 had both glaucoma and AHT) to repeat the LSFG measurements following IOP increase, by means of $\mathrm{IOP}_{\mathrm{stim}}$ (IMEDOS Systems GmbH, Jena, Germany). Defined external pressure (40-50 mmHg) was applied directly to the sclera at the lateral canthus proximity, while the

subjects still had their chin placed on the LSFG apparatus and were gazing forward; IOP was measured again with rebound tonometry. LSFG imaging was repeated with the same laser intensity and at the same location, as registered by the device itself (Fig. 3B), within 2 min of established IOP elevation (which itself was reached within 2 min after the onset of stimulation). The metrics described in 4.3.4 were extracted for comparison.

4.3.6. Data Analysis-Statistics

D) Correlation of model predictions with *in vivo* blood flow metrics

Multivariable linear regression was performed to examine the relationship between each theoretical model output (either RVR or RBF; dependent variable) and the 10 LSFG waveform metrics (before IOP stimulation; independent variables). By contrast to RBF, where OPP is already incorporated in the theoretical calculation (*Eq*. 8), the regression model for RVR additionally contained MAP and IOP as independent variables. Initially, two saturated models (1 for RVR and 1 for RBF) were built and, subsequently, backwards elimination was implemented in each model. Specifically, the least significant variable was removed and the models with and without this variable were compared using the Akaike Information Criterion (AIC). If the model without the concerning variable had a lower AIC, the same process was repeated for the next least significant variable. The procedure was terminated when the minimal AIC was reached (reduced model). For both reduced models, the coefficient of determination (R^2), regression coefficients, and *P* values were reported.

We also rebuilt the theoretical model replacing the formula by Haynes *et al.* (see 4.3.2D and 4.3.2E) with two alternative viscosity calculations proposed by Pries *et al.*[47-49] The *in vivo* viscosity calculation accounts for the presence of the endothelial glycocalyx, while the *in vitro* viscosity calculation does not.[49] The formulas are shown in the following box. We subsequently performed the same fitting analysis, in order to assess robustness against assumptions related to viscosity.

In vivo viscosity calculation

$$\mu(r) = \mu_p \left[1 + (\mu_{45} - 1)\frac{(1 - Hct)^C - 1}{0.55^C - 1}\left(\frac{2r}{2r - 1.1}\right)^2\right]\left(\frac{2r}{2r - 1.1}\right)^2 \quad \text{(B7)}$$

where $\mu_p = 0.0012$ Pa·s is the plasma viscosity, r is the radius, Hct is the hematocrit, and:

$$C = (0.8 + e^{-0.15r})\left[-1 + \frac{1}{1 + 10^{-11}(2r)^{12}}\right] + \frac{1}{1 + 10^{-11}(2r)^{12}} \quad \text{(B8)}$$

$$\mu_{45} = 6\, e^{-0.17r} - 2.44\, e^{-0.094r^{0.645}} + 3.2 \quad (\textit{in vivo} \text{ viscosity at Hct} = 0.45). \quad \text{(B9)}$$

In vitro viscosity calculation

$$\mu'(r) = \mu_p\left[1 + (\mu_{45}' - 1)\frac{(1 - \text{Hct})^C - 1}{0.55^C - 1}\right] \quad \text{(B10)}$$

where:

$$\mu_{45}' = 220\, e^{-2.6r} - 2.44\, e^{-0.094r^{0.645}} + 3.2 \quad (\textit{in vitro} \text{ viscosity at Hct} = 0.45). \quad \text{(B11)}$$

E) Contribution of the various factors to the theoretical model

Subsequently, a sensitivity analysis was performed for the model variables contributing to the theoretical model, in two different ways. First, to assess how strongly each contributing variable (vessel radius, viscosity, etc.) affects the outcome values, two new linear models (one for RVR and one for RBF) were built, now using the model input variables as predictors. We directly looked at the magnitude and statistical significance of the standardized regression coefficients in the saturated models to assess the importance of each predictor. Since the more linear the relationships the more accurate results this method yields, we first transformed the independent variables by using *Eqs*. B6 and 8 (for example, if variable x contributes as x^{-1} to RVR, it is entered as x^{-1} in the regression analysis).[50] For the second sensitivity analysis, to assess how important (or redundant) each variable is to the model fit, we recalculated the theoretical predictions with consecutive, independent imputations of the input variables to constant values, one at a time. The constant values assigned were either average values coming from our study sample or theoretical expectations. The new RVR and RBF were fitted again over the LSFG metrics and the resulting R^2 were successively compared with the ones corresponding to the original models.

F) Autoregulation

Our *in vivo* investigation of the RBF model was based on a regression analysis of RBF versus the LSFG variables. In this analysis, OPP, which is part of RBF (*Eqs.* B6 and 8), was based on an assumed contribution of MAP (a factor of 0.70), and on IOP (*Eq.* 7). A presumably more accurate estimate of MAP contribution can be obtained from the investigation of the RVR model, which was based on a regression analysis of RVR versus the LSFG variables, MAP, and IOP. The resulting regression coefficient of MAP was used to optimize the perfusion pressure calculation. Specifically, according to *Eqs.* 7 and 8, a 1-mmHg increase in MAP, holding RBF constant at its central value of x µl·min^{-1} (assuming perfect autoregulation), should produce a $0.7x^{-1}$ mmHg·min·µl^{-1} increase in RVR. If now the RVR regression model predicts a y mmHg·min·µl^{-1} increase in RVR per mmHg increase in MAP (with y the regression coefficient of MAP), this would correspond to a MAP factor of xy in the OPP calculation (instead of 0.70 as used in *Eq.* 7 or 0.67 as in the classical OPP definition). The resulting optimized OPP was called retinal perfusion pressure (RPP). The constant (−19.5 mmHg in *Eq.* 7) was subsequently updated to ensure that RPP = OPP (as in the OPP definition implemented in our study), so that the magnitude of RPP still accurately reflects the magnitude of the pressure in the CRA. To verify optimality, we refitted the RBF values (now calculated from RVR and RPP rather than from RVR and OPP) over the LSFG metrics and compared the resulting R^2 with the original.

We then used RPP and our subjects' (excluding glaucoma subjects) vessel characteristics to theoretically calculate the autoregulation limits. For each subject, the lowest and highest autoregulation limits (LARL and HARL) were calculated. This was done for normotensive ($LARL_N$/$HARL_N$) and hypertensive ($LARL_H$/$HARL_H$) subjects separately. Starting with a subject's own r_{a_0} and RPP, $LARL_N$ ($HARL_N$) was defined as the RPP needed to keep RBF constant at simultaneously maximal (minimal) r_{a_0} and minimal (maximal) β_a, as observed in the normotensive sample, ceteris paribus. Similarly, we defined $LARL_H$ ($HARL_H$) for the hypertensive subjects. An example of this calculation can be found in the following box. Glaucoma subjects were excluded from this analysis because, in these subjects, perfect autoregulation is less safe as an assumption.[51,52]

Calculation of autoregulation limits

We provide the full example of a 47-year-old female with normal BP (115/73 mmHg), and a normal IOP of 15 mmHg, yielding together an RPP of 29.0 mmHg.

At baseline (measured) arteriolar radius (97 μm), a total RVR of 0.54 mmHg·min·μl^{-1} was predicted. At 29.0 mmHg of RPP, this corresponds to an RBF of 54 μl·min^{-1} (*Eq.* 8). At maximal arteriolar radius (102 μm, taken in this case from the normotensive sample; normative data should be used, when available) a total RVR of 0.51 mmHg·min·μl^{-1} was predicted. Working backwards, at an RBF of 54 μl·min^{-1}, this RVR value corresponds to an RPP of 27.4 mmHg (*Eq.* 8). Hence, for this subject, $LARL_N$ = 27.4 mmHg.

Similarly, by making use of the minimal arteriolar radius, HARL can be calculated.

We also examined the ability for autoregulation on the basis of the LSFG *in vivo* measurements before and during stimulation. First, Wilcoxon signed-rank tests with the Bonferroni correction were used for individual comparisons of all relevant LSFG metrics (i.e., metrics that stayed in at least one of the reduced RVR or RBF models), before and during IOP elevation. Next, we studied the effect of IOP elevation on RVR and RBF. In the absence of vessel diameter measurements during IOP elevation, RVR_{stim} was approximated using the reduced RVR model (see 4.3.6A). RBF_{stim} was then calculated from *Eq.* 8. First, we used Wilcoxon signed-rank tests to compare RVR_{stim} with baseline RVR and RBF_{stim} with baseline RBF. Ideally, that is, within autoregulation limits, RVR would change in response to stimulation, yielding an unchanged RBF. However, if the IOP elevation will bring a subject below LARL, RVR will change less than expected and RBF will show some decrease. To further explore this, we defined the autoregulatory reserve (AR) to this stimulation (maximal percentage of 'within autoregulation' RPP change that can be induced by the stimulation), being:

$$AR = \frac{RPP - LARL}{RPP} 100\% \qquad (11a)$$

for those subjects where the stimulation went below LARL. For those who stayed within the autoregulation range, the relevant change in RPP (AC) is given by:

$$\mathrm{AC} = \frac{\mathrm{RPP} - \mathrm{RPP}_{\mathrm{stim}}}{\mathrm{RPP}} 100\% \,. \tag{11b}$$

We used Spearman's rank correlation coefficient (ρ) to examine to what extent the percentage change in RVR is influenced by the AR or AC of each subject (again, excluding glaucoma subjects) during this stimulation. Ideally, percentage change in RVR plotted against percentage AR or AC should yield datapoints scattering around the minus identity line.

Similarly, we defined the autoregulatory deviation (AD) to this stimulation (percentage of 'below LARL' change induced by the stimulation), according to the following equation:

$$\mathrm{AD} = \frac{\mathrm{LARL} - \mathrm{RPP}_{\mathrm{stim}}}{\mathrm{LARL}} 100\% \,. \tag{11c}$$

For those subjects where the stimulation went below LARL, AD will be positive, whereas it will be zero or negative in those where the IOP stimulation respects LARL. The same correlation analysis as in the previous paragraph was performed, this time for percent change in RBF versus AD.

The mathematical arguments behind the aforementioned are presented in the following box.

Autoregulation and RPP manipulation

Let us call a system 'autoregulating within A' if and only if there exists a non-trivial interval of RPPs A = [LARL, HARL] over which, for any RPP, RPP' ∈ A, the following holds:

$$\mathrm{RBF}' = \mathrm{RBF} \Leftrightarrow \ldots \Leftrightarrow \frac{\mathrm{RPP}' - \mathrm{RPP}}{\mathrm{RPP}} = \frac{\mathrm{RVR}' - \mathrm{RVR}}{\mathrm{RVR}} \tag{B12}$$

where during the algebraic manipulations we made use of *Eq*. 8 (main text).

Let us also call a system 'non-autoregulating beyond A' if and only if, for any RPP, RPP' ∉ A, the following holds:

$$\mathrm{RVR}' = \mathrm{RVR} \Leftrightarrow \ldots \Leftrightarrow \frac{\mathrm{RPP}' - \mathrm{RPP}}{\mathrm{RPP}} = \frac{\mathrm{RBF}' - \mathrm{RBF}}{\mathrm{RBF}} \tag{B13}$$

It can be seen from these equations that percentage change in RPP will correlate with either percentage change in resistance or percentage change in blood flow, depending on whether the manipulation takes place within or beyond the autoregulation limits.

G) Blood flow and retinal layer thicknesses

Lastly, as a secondary analysis, we examined the relationship of RBF with the thickness of the pRNFL and the volume of the GCC of the same eyes, by means of age-adjusted linear regression models. For comparison, the regression model with the original RBF calculation as predictor and the regression model with the optimized (RPP-based) RBF calculation as predictor are both reported.

Normally distributed variables are described by mean (SD), while skewed variables are described by median [interquartile range (IQR)]. All analyses were performed in R (version 3.4.2; R Foundation for Statistical Computing, Vienna, Austria). $P \leq 0.05$ was considered statistically significant. For nested models, AIC-based inclusion in the model implies $P < 0.16$.[53]

4.4. Results

4.4.1. General Characteristics

Table 1 summarizes the characteristics of the population on which the model predictions were tested *in vivo*.

Table 1. *Characteristics of the population used for in vivo investigation*

General characteristics	
Age, yr [median (IQR)]	54 (47 to 56)
Sex, %Female	69.4
BMI, kg·m^{-2} [mean (SD)]	27.5 (5.6)
AHT	
Prevalence, %	41.7
Use of antihypertensive medication, %	73.3
Glaucoma	
Prevalence, %	13.9
Use of antiglaucoma medication, %	100.0
Visual field MD, dB [median (IQR)]	−4.4 (−8.8 to −1.6)
pRNFL, µm [median (IQR)]	103 (92 to 109)
GCC, mm^3 [mean (SD)]	2.79 (0.29)
Theoretical model input variables	
CRAE, µm [mean (SD)]	167 (20)
CRVE, µm [mean (SD)]	239 (21)
β_a [median (IQR)]	7.81 (7.18 to 8.48)
β_v [mean (SD)]	7.77 (0.75)
D [median (IQR)]	1.596 (1.572 to 1.605)
μ_∞ Arterial, Pa s [median (IQR)]	0.0038 (0.0037 to 0.0042)
μ_∞ Venous, Pa s [median (IQR)]	0.0041 (0.0040 to 0.0045)
SBP, mmHg [mean (SD)]	134 (21)
DBP, mmHg [mean (SD)]	83 (12)
IOP, mmHg [mean (SD)]	16.3 (3.8)
Theoretical model outcome variables	
RVR, mmHg·min·µl^{-1} [median (IQR)]	0.71 (0.65 to 0.91)
RBF, µl·min^{-1} [mean (SD)]	45 (12)

Values are as indicated; n = 36. BMI, body mass index; AHT, arterial hypertension; pRNFL, peripapillary retinal nerve fiber layer; GCC, ganglion cell complex; MD, mean deviation; IQR, interquartile range; CRAE, central retinal artery equivalent; CRVE, central retinal vein equivalent; β_a, arteriolar branch length coefficient; β_v, venular branch length coefficient; D, fractal dimension; μ_∞, viscosity in large vessels; SBP, systolic blood pressure; DBP, diastolic blood pressure; IOP, intraocular pressure; RVR, retinal vascular resistance; RBF, retinal blood flow.

4.4.2. Relationship with In Vivo Data

Table 2 displays the reduced multivariable models showing the relationship of the theoretical predictions with the *in vivo* LSFG measurements. LSFG metrics are obtained by operations in MBR relative

units (see 4.3.4). Holding other variables constant, a one MBR-unit decrease in MV results in an increase of 0.015 mmHg·min·µl^{-1} in RVR. In the same model, an increase in FAI and MAP and a decrease in s*kew* and *fluctuation* result in an increase in resistance. Interestingly, IOP is not present in the reduced RVR model. Similarly, holding other variables constant, a one MBR-unit increase in MV results in an increase of 0.7 µl·min^{-1} in RBF. In the same model, a decrease in FAI and HR and an increase in *skew* result in an increase in BF.

Table 2. *Reduced multivariable fitting models for RVR and RBF with LSFG metrics*

	RVR, mmHg·min·µl^{-1}			RBF, µl·min^{-1}		
	β	*P* value	R^2 (*P*)	β	*P* value	R^2 (*P*)
			0.77 ($6.9\cdot10^{-9}$)			0.56 ($3.1\cdot10^{-5}$)
MV	−0.015	$1.0\cdot10^{-6}$		0.7	$2.1\cdot10^{-4}$	
FAI	0.116	$2.2\cdot10^{-5}$		−6.5	$2.0\cdot10^{-4}$	
Skew	−0.039	$1.0\cdot10^{-5}$		2.5	$2.1\cdot10^{-5}$	
Fluctuation	−0.026	0.045			NA	
HR		NA		−0.3	0.026	
MAP	0.009	$2.0\cdot10^{-6}$			NA	

LSFG, laser speckle flowgraphy; MV, mean velocity in large vessels; FAI, flow acceleration index; MAP, mean arterial pressure; HR, heart rate; NA, not applicable; RBF, retinal blood flow; RVR, retinal vascular resistance.

According to the R^2, 77% and 56% of the variation in the theoretical values for RVR and RBF, respectively, could be explained solely by the LSFG waveform metrics. Supplementary Table S3 is similar to Table 2, after implementation of alternative viscosity calculations (see 4.3.6A). Similar proportion of variation for RVR and RBF could be explained by LSFG metrics; RVR and RBF values remained at the same order of magnitude (Table 1), as did the beta values (Table 2); all beta values kept the same sign.

Figure 4 shows the corresponding scatterplots (rotated residual plots) for RVR (Fig. 4A) and RBF (Fig. 4B). Visual inspection suggests that subjects with AHT tend to cluster towards higher RVRs than subjects without AHT, as expected;

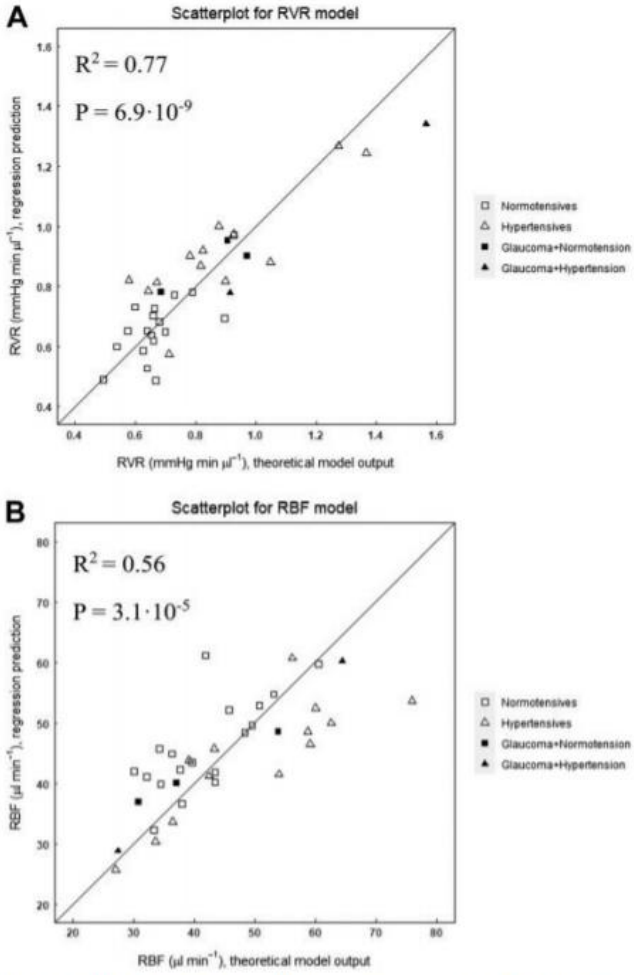

Fig. 4. Scatterplots (n = 36) for multivariable regression models fitting laser speckle flowgraphy metrics to the theoretical output: retinal vascular resistance (*A*; RVR) and retinal blood flow (*B*; RBF). Regression-predicted values (equivalently: theoretical model values minus corresponding residuals) are plotted against the theoretical model values. Diagonal line represents perfect fit (no residuals).

this was confirmed as significant in a Mann-Whitney *U* test ($P = 0.005$). RBF was similar for both groups (P = 0.11); that said, when MAP is high, RBF tends to be overestimated by the theoretical model, since most hypertensives (11 of 15) are found below the diagonal line. Indeed, a Wilcoxon signed ranks test revealed that, in hypertensives, the regression-predicted value was on average 5.8 $\mu l \cdot min^{-1}$ lower than the theoretical model output ($P = 0.039$).

4.4.3. Sensitivity Analysis

The results of the regression-based sensitivity analysis are given in Table 3. The CRA radius is the most important variable in the RVR calculation ($b_{stand} = 0.79$, $P = 2.0 \cdot 10^{-29}$), while MAP is the most important variable in the RBF calculation ($b_{stand} = 1.06$, $P = 8.6 \cdot 10^{-13}$). The magnitude of RBF is not really affected by venular diameter and fractal dimension. For both sensitivity models, we merged each vessel caliber predictor with the corresponding branch length coefficient into one single predictor (e.g., $\beta_a r_a^{-4}$) and additionally, we did not differentiate viscosity in arteries and veins, to avoid collinearity issues (see *Eqs*. 3 and 6).

Table 3. *Sensitivity analysis for the theoretical model predictions*

	RVR			RBF			Imputed variable(s)	
	Stand. β	*P* value	R^2	Stand. β	*P* value	R^2	R^2 (RVR)	R^2 (RBF)
Regression-based sensitivity analysis			0.99 $P = 7.1 \cdot 10^{-33}$			0.88 $P = 6.8 \cdot 10^{-12}$		
$\beta_a r_a^{-4}$	0.79	$2.0 \cdot 10^{-29}$						
$\beta_v r_v^{-4}$	0.26	$2.1 \cdot 10^{-15}$						
$r_a^4 \beta_a^{-1}$				0.76	$2.8 \cdot 10^{-8}$			
$r_v^4 \beta_v^{-1}$				0.00	0.97			
e^{-D}	0.07	$2.9 \cdot 10^{-4}$						
e^{D}				0.03	0.70			
μ_∞	0.11	$5.7 \cdot 10^{-7}$						
μ_∞^{-1}				0.17	0.037			
MAP				1.06	$8.6 \cdot 10^{-13}$			
IOP				−0.42	$1.6 \cdot 10^{-5}$			
Imputation-based sensitivity analysis								
Baseline (from Table 2)							0.77	0.56
$r_a = 176$ μm, $r_v = 248$ μm, $\beta_a = \beta_v = 7.4$							0.55	0.22
$\beta_a = \beta_v = 7.4$							0.80	0.46
$D = 1.7$							0.75	0.53
μ_∞(art) = 0.0043 Pa s, μ_∞(ven) = 0.0046 Pa s							0.69	0.49
MAP = 95 mmHg							*NA*	0.38
IOP = 15 mmHg							*NA*	0.41

r_a, central retinal artery radius; r_v, central retinal vein radius; β_a, arterial branch length coefficient; β_v, venous branch length coefficient; *D*, fractal dimension; μ_∞, blood viscosity in large vessels; MAP, mean arterial pressure; IOP, intraocular pressure; NA, not applicable.

Table 3 also demonstrates the extent to which imputations affect the model fit. The new RVR and RBF models that demonstrated the smallest fit were the ones with all fundus variables imputed with -22% and -24% of variance explained, respectively, compared with baseline. Imputation of solely the branch length coefficient resulted in a small increase in the RVR fit (+3%), but a more substantial drop in the RBF fit (-10%). The variable whose imputation

induced the smallest change from baseline was fractal dimension (-2% and -3% for RVR and RBF, respectively).

Figure 5 displays the tornado plots corresponding to the RVR and RBF models. RVR and RBF are displayed as a function of the full dynamic range (minimum to maximum, as observed in our study sample) of each individual component. As shown in the RBF plot, the MAPs of our sample would be able to produce a wide RBF dynamic range (25.0 µl·min^{-1} to 80.1 µl·min^{-1} around the central value of 47.5 µl·min^{-1}), ceteris paribus. For visualization purposes, variables in the figure are permitted to vary independently; however, as expected, the arterial diameter is, in fact, dependent on MAP (Pearson's r = -0.46, P = 0.004); together with the collinear arterial branch length coefficient, they have an important, compensatory effect on RBF values (see 4.3.6C).

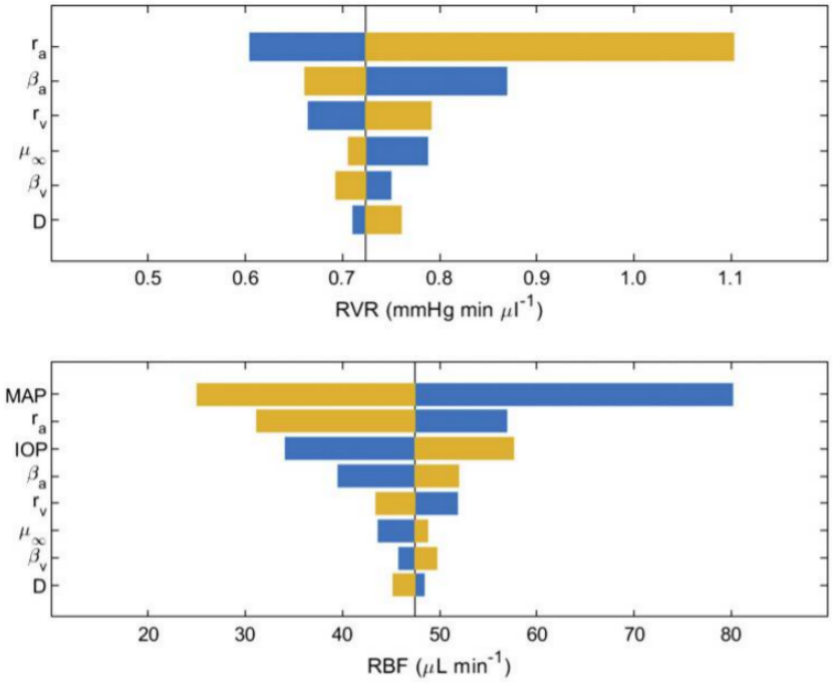

Fig. 5. Tornado plots for the simulated retinal vascular resistance (RVR) and retinal blood flow (RBF) models. Vertical line gives the outcome value at the central value of all predictors. Horizontal bars display the outcome values at the full range of each predictor, all other predictors being at their central value. Blue and orange colors correspond to the high and low values of each predictor, respectively.

4.4.4. Retinal Perfusion Pressure

Since OPP is only an approximation of the pressure difference between the arterial and venous components of the retinal circulation, we additionally looked for the RPP that optimizes the RBF model fit. This is given by the following formula:

$$\overline{\mathrm{RPP}} = \left(\frac{39}{100}\mathrm{MAP} + 10.1\right) - \mathrm{IOP\ mmHg.} \qquad (12)$$

With this calculation, the new (optimal) R^2 for RBF was 65% (to be compared with the previous 56%). Interestingly, 65% is actually the global maximum R^2, given a MAP factor of 0.39, and is achieved at a range of MAP constants containing the predicted +10.1 (+7.7 to +11.1). Lastly, with this RPP calculation, there was no longer an overestimation of the theoretically predicted RBF in hypertensive patients, as seen above (see 4.4.2; Wilcoxon signed rank test, $P = 0.55$).

4.4.5. Autoregulation and IOP Stimulation

Figure 6 displays the theoretically predicted autoregulation plateaus (i.e., the RPP span between LARL and HARL) for each individual nonglaucomatous subject (n = 31), as well as the full autoregulation curves for the average cases with (red) and without (blue) AHT, in healthy eyes. All subjects are autoregulating, hence, as shown in the graph, their baseline status can be found inside their individual plateau. Beyond the autoregulation limits, RBF is proportional to RPP. $LARL_N$ for the average case was estimated from Fig. 6 at 25 mmHg (SD: 4 mmHg). This, according to *Eq*. 12, corresponds to a MAP of 77 mmHg (i.e., a BP reading of 105/65 mmHg) at mean IOP (15 mmHg in the non-AHT group) or to an IOP of 20 mmHg at mean MAP (89 mmHg). In fact, a BP 1 SD below average together with an IOP 1 SD above average bring a subject already at or below $LARL_N$. $LARL_H$ for the average case was estimated at 27 mmHg (SD: 6 mmHg). Similarly, this corresponds to a MAP of 88 mmHg (i.e., a BP reading of 115/75 mmHg) at mean IOP (17 mmHg in the AHT group) or to an IOP of 26 mmHg at mean MAP (111 mmHg). $HARL_N$ and $HARL_H$ were estimated as 39 mmHg (SD: 7 mmHg) and 54 mmHg (SD: 13 mmHg), respectively. This rightward shift of the autoregulation limits in AHT was only significant for HARL according to the Mann Whitney *U* test (LARL: $P = 0.12$; HARL: $P = 0.001$).

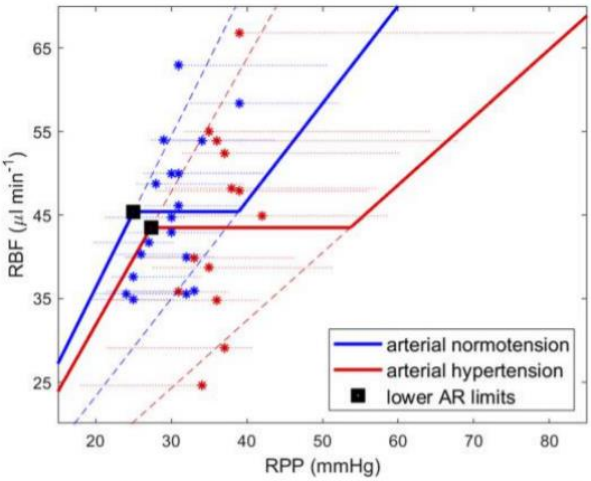

Fig. 6. Predicted autoregulation (AR) curves for arterial normotension (n = 18) and arterial hypertension (n = 13), each centered at mean retinal blood flow (RBF). Dashed lines (extended) meet at the origin. Retinal perfusion pressure (RPP) is calculated according to *Eq. 12*. Star-shape markers denote baseline RBF, as estimated from vascular caliber, viscosity, fractal dimension, and RPP. Dotted lines represent individual AR plateau approximations, extending from the lower to the higher AR limit (LARL, HARL). LARL and HARL for each subject are theoretically predicted, according to a standardized procedure (see METHODS, *Data Analysis-Statistics*, *Autoregulation*). If the subject is close to maximum arteriolar dilation, the baseline marker will be found close to LARL. If the subject is close to maximum arteriolar constriction, the baseline marker will be found close to HARL.

After stimulation, IOP increased (hence RPP decreased, assuming MAP remained relatively unchanged) in all 12 subjects by a median of 9 mmHg (IQR: 4.5 to 14.8 mmHg; $P = 0.002$). Among relevant LSFG metrics (i.e., metrics included in Table 2), MV decreased ($P = 0.002$), whereas *skew* and *fluctuation* increased ($P = 0.006$ and $P = 0.002$, respectively). These differences were significant even at the Bonferroni-adjusted threshold of $P = 0.01$. It is important to mention here that, in univariable analysis at baseline (n = 36), *skew* was the one parameter most strongly associated with arterial diameter at an interindividual level, and this was in a positive direction (Pearson's $r = 0.59$, $P = 1.6 \cdot 10^{-4}$); age did not play a role in this association, as shown in the bivariable model ($P = 0.63$). FAI and HR did not change ($P = 0.26$ and $P = 0.45$, respectively), after IOP stimulation. Figure 7 depicts changes in *skew*, MV, and IOP before and after IOP stimulation in individual subjects.

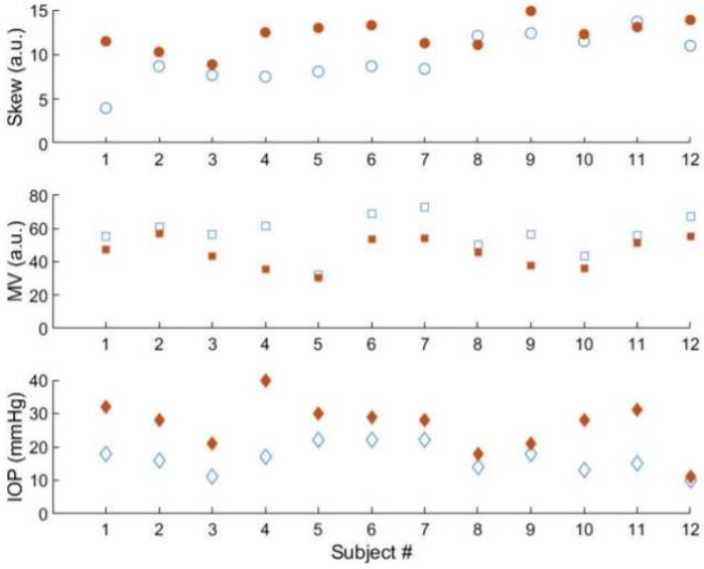

Fig. 7. Skew, mean velocity in large vessels (MV), and intraocular pressure (IOP) values in individual subjects ($n = 12$) plotted before (empty blue markers) and after (filled red markers) IOP stimulation. Subjects are ranked from highest to lowest autoregulatory (AR) reserve/change (*Eqs. 11a* and *11b*). *Subject 5* is a primary open angle glaucoma subject. Wilcoxon signed-rank tests revealed simultaneous increase in skew and decrease in MV, following IOP elevation, which is an indication of AR capacity with conservation of flow; a.u., arbitrary units.

Regarding the effect of stimulation on RVR, RVR_{stim} was not significantly different compared with baseline, regardless of whether baseline RVR was calculated from the theoretical variables ($P = 0.94$) or the regression coefficients in Table 2 ($P = 0.75$). However, within overall nonsignificance, RVR percentage change was more negative with larger AR/AC ($\rho = -0.66$, $P = 0.026$). On the other hand, RBF_{stim} was lower by a median of 17.9 $\mu l \cdot min^{-1}$ compared with baseline ($P = 0.019$). In addition, RBF percentage change was more negative with larger AD ($\rho = -0.91$, $P = 1.1 \cdot 10^{-4}$). These observations can be visualized in Figure 8.

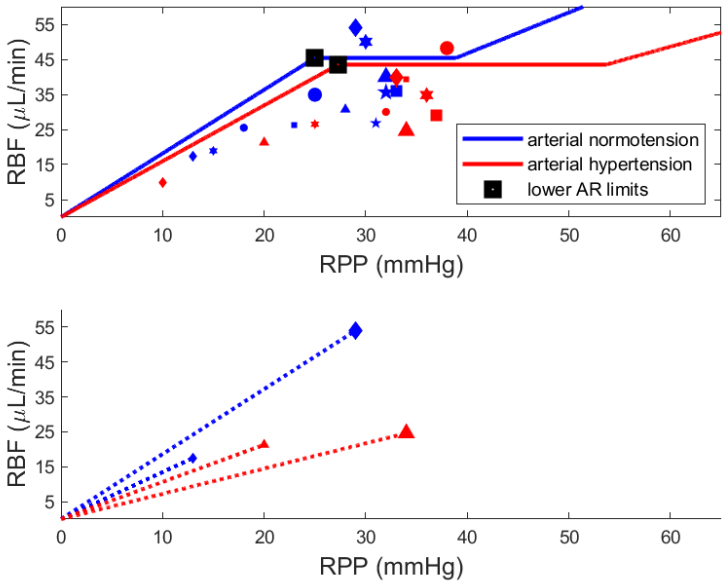

Fig. 8. Upper panel: Retinal blood flow (RBF) before (larger markers) and after (smaller markers) IOP stimulation. Markers of the same type and color represent the same subject. Scatterpoints are overlayed on the average autoregulation curves for normotension and hypertension, as predicted in Fig. 6 (each scatterpoint actually belonging to its own autoregulation curve, as shown in Fig. 6). Lower panel: Visualization of LARL properties on two subjects undergoing similar retinal perfusion pressure (RPP) decrease. Blue rhombus represents a subject already close to LARL, at baseline. Red triangle represents a subject further away from LARL, at baseline. Absence of autoregulatory reserve in the former case resulted in a large decrease in RBF and a decrease in slope (RVR^{-1}), due to venular compression. Presence of autoregulatory reserve in the latter case resulted in only a slight decrease in RBF and an increase in slope, despite venular compression.

4.4.6. Resistivity Index

As a secondary observation, RI (which did not appear in the reduced final models) also showed an increase after IOP elevation ($P = 0.002$). In addition, its baseline value exhibited a correlation with the pulse pressure index (n = 36, Spearman's $\rho = 0.49$, $P = 0.002$), which is defined according to the following equation:

$$\mathrm{PPI} = \frac{\mathrm{SBP} - \mathrm{DBP}}{\mathrm{SBP}} = 1 - \frac{\mathrm{DBP}}{\mathrm{SBP}}. \qquad (13)$$

Blowout score is an additional metric offered by the LSFG, but was not considered at all in this study, since it can be directly calculated from the RI. Indeed, our *in vivo* data also confirmed that the two metrics are collinear (n = 36, Spearman's $\rho = 0.90$, $P = 1.8 \cdot 10^{-13}$). Notably, RI and *fluctuation* were also highly correlated (n = 36, Spearman's $\rho = 0.87$, $P = 3.8 \cdot 10^{-12}$).

4.4.7. Model Predictions and Structural Measurements

Table 4 displays the age-adjusted linear regression models for the relationship between blood supply (RBF) and inner retinal structural measures (pRNFL thickness, GCC volume). In the optimized RBF model, 1 $\mu l \cdot min^{-1}$ increase in RBF is associated with a 0.69-μm increase in

pRNFL and a 0.012-mm^3 increase in GCC. Associations remained significant, albeit weaker, after exclusion of the glaucoma subjects.

Table 4. *Age-adjusted linear models for structural SD-OCT metrics as a function of RBF*

	pRNFL, µm			GCC, mm^3		
	β	*P* value	R^2 (*P*)	β	*P* value	R^2 (*P*)
Models with original RBF calculation			0.46 ($3.7 \cdot 10^{-5}$)			0.35 (0.001)
RBF, µl·min^{-1}	0.53	0.002		0.009	0.011	
Age, yr	−0.76	$5.6 \cdot 10^{-5}$		−0.013	0.001	
Models with optimized RBF calculation			0.51 ($7.0 \cdot 10^{-6}$)			0.40 ($4.0 \cdot 10^{-4}$)
RBF, µl·min^{-1}	0.69	$4.0 \cdot 10^{-4}$		0.012	0.003	
Age, yr	−0.65	$1.8 \cdot 10^{-4}$		−0.011	0.003	

pRNFL, peripapillary retinal nerve fiber layer; GCC, ganglion cell complex; RBF, retinal blood flow; SD-OCT, spectral domain optical coherence tomography.

4.5. Discussion

In this study, we proposed and tested a physiological model, coupled with a clinical protocol, that predicts the behavior of retinal vascular networks on an individual level by means of two clinical markers, RVR and RBF. Investigation in human subjects showed that a considerable proportion of the variation in the theoretical predictions could be explained by *in vivo* BF metrics, as given by LSFG. MV, FAI, and *skew* were the LSFG metrics exhibiting the strongest associations with both outcomes. According to the sensitivity analysis, all variables included a priori in the theoretical model were confirmed to range from very important to at least mild determinants of RVR and RBF. Using the model and the *in vivo* data, we proposed autoregulation curves and predicted LARL for subjects with and without AHT. We then verified that changes in RVR and RBF induced by IOP elevation are, indeed, dependent on the AR/AC and AD, respectively. Lastly, we demonstrated that the amount of nerve tissue present in the inner layers of the human retina is strongly correlated with blood supply.

4.5.1. Model Investigation Results: Literature Comparison and Physiological Interpretation

A) Retinal blood flow and retinal vascular resistance

The proposed model predicted a mean RBF of 45 (12) µl·min^{-1} in our sample (Table 1), which is in agreement with values reported in the vast majority of studies using Doppler OCT and laser-Doppler velocimetry.[19,20,54-58] Older studies using laser-Doppler velocimetry

reported higher RBF values, possibly because previous hardware versions of this technique overestimated blood velocity.[59,60] Contrary to the previous methods, the LSFG apparatus does not yield an absolute BF estimate; hence, all waveform metrics were a priori given an equal opportunity to be included in the reduced multivariable models (see 4.5.1B).

According to *Eq*. 8, high RVR mathematically implies either high OPP or low RBF. Our results clearly demonstrate this (Table 2), since increased RVR (which reflects narrower arterioles) was associated with an increased MAP, as well as decreased MV, when the other is held constant. To calculate RVR, previous studies relied on first estimating RBF with one of the aforementioned, usually challenging, dynamic techniques and then applying *Eq*. 8.[61-63] In our study, we demonstrated that it is possible to quantify resistance by static imaging and simple clinical examinations, without any information on BF as a prerequisite. After RVR is constructed from its individual components, RBF can be obtained with a simple calculation from *Eq*. 8.

In this regard, RI, which is calculated according to the following formula:

$$RI = \frac{u_{max} - u_{min}}{u_{max}} = 1 - \frac{u_{min}}{u_{max}} \quad (14)$$

where u_{max} and u_{min} are the peak systolic velocity (PSV) and end diastolic velocity (EDV), respectively, has been previously shown to not be an adequate standalone representation of vascular resistance. Instead, it reflects combined effects of resistance and compliance, a phenomenon that has also been observed in the circulation of other organs.[64-67] Our data second that: first, *fluctuation*, which is a more detailed computational quasi-equivalent highly correlating with RI, possibly masked the effect of RI in the reduced multivariable RVR model and still was only of borderline significance (Table 2). Moreover, the strong correlation between RI and PPI that we replicated suggests that RI also depends on central impulse, in addition to downstream flow characteristics.[68]

B) Laser speckle flowgraphy metrics

Overall, LSFG metrics explained considerable proportion of variance in the RVR and RBF calculations, exhibiting some very strong correlations in multivariable analysis (Table 2). This suggests that the theoretical approximations implemented in this study were able to capture individual variations in blood flow physiology, as measured *in vivo*. In this

subsection, we discuss the physiological meaning of each (significant) LSFG component and its relationship with the theoretical predictions.

MV represents blood velocity in large retinal vessels, which, according to *Eq*. 9, is a primary component of RBF and is segmented separately from the signal of surrounding tissues.[8,13] It also incorporates information from both the arteriolar and venular component; hence, it is informative in conditions where velocity is affected due to changes in vascular caliber (e.g., in glaucoma). For these reasons, it has been used as a surrogate for BF in a number of LSFG studies.[12,46,69,70] In particular, Iwase *et al*. showed that OPP reduction by means of IOP stimulation induced a drop in MV, a finding that was also confirmed in our study. In addition, another study revealed that MV was significantly lower in normal tension glaucoma (NTG), compared with healthy controls.[46] These findings suggest that MV is sensitive to both physiological and pathological BF changes. We note here that, in our study, there was no correlation between MV and ONH size (Pearson's r = -0.08, P = 0.62) and that ONH size did not confound any of the associations uncovered in the reduced multivariable LSFG models. Hence, there was no artifactual component related to the area of measurement in the MV-driven associations.

According to *Eq*. 9, a predictor related to vessel diameter was also reasonably expected to show up in the models, after adjusting for MV (Table 2). *Skew* was the LSFG metric that best reflected arteriolar caliber, since it was the predictor that was most strongly, positively associated with CRAE in univariable analysis (and also bivariable age-adjusted analysis), as well as negatively with RVR and positively with RBF in the reduced multivariable models. In addition, *skew* significantly increased after IOP elevation, with a concomitant decrease in MV, most likely indicating autoregulation-driven vasodilation with conservation of flow (Fig. 7). Results from other LSFG studies corroborate this finding. Shiga *et al.* showed a decrease in *skew* in NTG, compared to controls, while Gardiner *et al.* found the same effect when comparing POAG patients to controls, only when the eyes had detectable functional deficit.[71,72] Additionally, Bhatti *et al.* reported a mild increase in *skew* 40 min after challenging IOP with the water drinking test in healthy individuals.[73] They did not report IOP values before and after the challenge, but this test is expected to increase IOP by 3-4 mmHg.[74] However, the opposite effect was observed by Kiyota *et al.*, with *skew* decreasing after a 20-mmHg controlled IOP elevation, with a procedure similar to ophthalmodynamometry.[75] This discrepancy with our data could possibly be explained as

follows: firstly, such a big IOP increase is unlikely to have been confined within the autoregulation limits in most of their subjects (Fig. 6); as such, decreased *skew* in this case might indicate decreased RBF more than it indicates increased RVR. In addition, the compressive force exerted by high IOP to passively reacting venules and capillaries (and at very high IOP, even arterioles, as was suggested in a recent study) might partly cancel out the autoregulatory effect of arterial vasodilation.[76,77] Lastly, Kiyota *et al.* obtained measurements from the ONH tissue area, not including the large retinal vessels; this area is characterized by more complex vascular supply and, therefore, might exhibit different autoregulation properties.[75,78] Despite the multiple indications present in our data, we believe that additional studies are needed to clarify the relationship between *skew* and arteriolar caliber.

In addition to MV and *skew*, increased FAI was found to be an independent predictor of higher RVR and lower RBF (Table 2). There are a number of explanations for this commonly reported phenomenon.[79-81] First, the shear stimulus for flow-mediated dilation (FMD) is known to also depend on flow acceleration, triggering a transient initial burst of nitric oxide (NO) production at the endothelium, before the slower NO release attributed to flow velocity.[82,83] Specifically, increased acceleration is expected to attenuate FMD. Second, flow acceleration in the microcirculation exhibits a more complex behaviour than in the macrocirculation. Indeed, in large vessels, where the effects of inertance on flow acceleration dominate the effects of resistance on flow velocity, Newton's second law of motion is generally sufficient for an estimate of acceleration.[49] We illustrate this in the box below.

Flow acceleration

Let us consider a pressure difference $P(t)$ varying through the cardiac cycle as a single harmonic and accelerating blood of mass m inside a vessel of length l and radius r, with r large enough:

$$P(t) = M\cos(\omega t) + P_0, \;\; t \in [0, \frac{60}{\mathrm{HR}}] \qquad \text{(B14)}$$

where M is the pulse amplitude, ω is the angular velocity ($2\pi\frac{\mathrm{HR}}{60}$), and P_0 is the average pressure difference. For the time-varying acceleration $\alpha(t)$, it follows that:

$$a\,(\mathrm{t}) = \frac{[M\cos(\omega t) + \mathrm{P}_0]\,\pi r^2}{m} = \frac{M\cos(\omega t) + P_0}{\varrho l} \tag{B15}$$

where ϱ is the blood density.

Therefore, FAI, which is the maximum acceleration during the systolic phase, in this case would largely depend on individual SBP values (central impulse) and would be independent from RVR[84]:

$$\mathrm{FAI} = a_{\mathrm{max_{syst}}} = \frac{M + P_0}{\varrho l} \tag{B16}$$

Due to the interdependence of *Eqs*. 13 and 14, in *Eq*. B14, M can be considered a partial determinant of $u_{\max} - u_{\min}$, while P_0 can be seen as a partial determinant of $\bar{u}$. When adjusting for MV in the RVR regression model, the FAI-induced increase in RVR translates to increased PSV and decreased EDV.

However, Doppler ultrasound studies in other organs revealed that, downstream in the circulation, increased distal resistance is associated with higher early systolic acceleration, possibly due to interference of reflections with the dampened wave.[81,85] To our knowledge, this is the first study to demonstrate that this phenomenon holds true in the ocular circulation, since FAI was positively associated with RVR in the reduced model (Table 2). Lastly, flow acceleration can introduce an error in velocity measurements, especially in stenotic segments or areas of turbulent flow.[86,87] Hence, adjusting for an acceleration term in the RVR and RBF models is expected to increase precision. This artificial normalization could also be especially beneficial for reducing variability in LSFG measurements, where univariable interindividual comparisons are difficult to interpret, due to the effect of pigmentation.[88] Notably, again shown in the box above, the presence of FAI in the model also provides an explanation for the *in vivo* documented differential effect of distal resistance on PSV and EDV values, which sometimes can even lead to diastolic flow reversal.[85]

Univariable analysis in the study of Gardiner *et al.* showed increased FAI in early POAG, compared to controls, but only in eyes with no detectable functional deficit; FAI values dropped back to baseline when functional deficit was present.[71] Another study revealed decreased FAI in NTG, compared to controls.[46] At first, this seems paradoxical, as it points towards lower RVR and higher RBF, while the opposite is expected.[89] However, in our

multivariable regression models (Table 2), interpretation of these effects required other LSFG metrics to be held constant. Indeed, using the regression coefficients in Table 2 and the average values for LSFG metrics provided in their study, we reverse-engineered approximations for average RVR and RBF values in their population: 0.77 mmHg·min·μl^{-1} and 50.5 μl·min^{-1} for NTG patients, versus 0.59 mmHg·min·μl^{-1} and 54.3 μl·min^{-1} for controls. These values reflect the physiological expectations and are somewhat comparable to the average values we report, despite the fact that they used a different LSFG apparatus, yielding considerably different MBR values. We invite researchers to use this approach to re-analyze their LSFG data.

A faster HR was also weakly associated with reduced RBF (Table 2). Womersley's model for oscillatory BF predicts that, in large vessels, HR would affect maximal, but not average, BF during the cardiac cycle.[90] In the microcirculation, where Womersley number Wo is small and BF tends to approximate steady-state behaviour, HR is theoretically not expected to profoundly influence BF. That said, it is apparent from the LSFG waveforms (Fig. 3) that retinal BF still has a transient component. In addition, peripheral resistance has been shown to not be an accurate representation of impedance at nonzero frequencies, because of wave reflections and the fact that viscous drag increases with increasing oscillation frequency.[91,92] These observations could explain our findings.

4.5.2. Quantitative Vascular Analysis: Literature Comparison and Physiological Interpretation

In the sensitivity analysis, the CRAE (r_a) was the most important variable in determining RVR and the second most important (after MAP) in determining RBF (Table 3 and Fig. 5). This is not unexpected, since it is mostly the arterioles that are responsible for short-term (autoregulation) or long-term (structural remodeling) control of circumferential wall stress, in response to acute or chronic changes in perfusion pressure.[93,94] In this study, we estimated vascular caliber from fundus images. Semiautomatic retinal vascular caliber measurements have not been fully standardized and are known to be influenced by the measurement software and the choice of formula.[95,96] We used the most widely accepted Parr-Hubbard formulas, revised by Knudtson *et al.*; the CRAE and CRVE mean values and ranges observed in our study sample agree with the outcomes of the Beaver Dam Study, when the same formulas are applied.[32] They also agree with the values reported by Dorner *et al.*, who used a

reverse approach to quantify diameters from flow values.[97] We excluded eyes with high refractive error, in order to keep variability introduced by magnification to a minimum. Upon imputation of central retinal vessel caliber values in the theoretical model, a significant proportion of variance in the *in vivo* data could no longer be explained (Table 3). This highlights that the use of individualized values is paramount, despite the fact that the indirect caliber estimation of the otherwise inaccessible central retinal vessels could introduce some degree of uncertainty to the model predictions.

It is worth noticing here that the formulas by Knudtson *et al.* are derived by extracting the branching coefficient B (also known as area expansion ratio) from human retinal vessel bifurcations, a quantity that is calculated as follows:

$$B = \frac{r_S^2 + r_L^2}{r_P^2} \tag{15}$$

where r_S is the small daughter branch, r_L is the large daughter branch, and r_P is the parent trunk. Let us also define an asymmetry index I as:

$$I = \frac{r_S}{r_L}\,. \tag{16}$$

Using *Eq*. B3, as well as the fact that the number of terminal vessels corresponding to a mother vessel upstream is always equal to the sum of the terminal vessels corresponding to each of the two daughters, Kamiya and Takahashi obtained[40]:

$$r_P^{D+\alpha} = r_S^{D+\alpha} + r_L^{D+\alpha}\,. \tag{17}$$

From *Eqs*. 15, 16, and 17, we get (after some algebra):

$$B = \frac{I^2 + 1}{\left(I^{D+\alpha} + 1\right)^{\frac{2}{D+\alpha}}} \tag{18}$$

Pooled data from the studies of Knudtson *et al.* and Patton *et al.* suggest that B is ~1.27 (CI: 1.21 to 1.33) for arterioles and 1.15 (CI: 1.10 to 1.21) for venules.[32,98] Moreover, Aschinger *et al*. provided mean (SD) values for the bifurcation exponent (here $D+\alpha$) using a power fitting approach based on data from Doppler OCT.[18] A value of 3.01 (0.22) was proposed for arterioles, while 2.62 (0.26) was proposed for venules. When no differentiation is made

between arterial and venous bifurcation exponents, Murray's law predicts a value of 3.00, based on a minimum work principle, while Takahashi *et al.* suggest an exponent of 2.85 based on the theoretical values $D = 1.70$ and $\alpha = 1.15$.[28,99]

Our study assumes symmetrical dichotomous branching ($I = 1$), as well as equal $D+\alpha$ (median: 2.75) for arterioles and venules (since, at the moment, microvessels are not differentiated by OCTA). For the sake of comparison, we calculated B using these values, yielding 1.21 (exactly halfway between the arteriole and venule values, pooled from the studies of Knudtson *et al.* and Patton *et al.*).[32,98] In addition, Popel showed that, although heterogeneous models are more precise in accounting for flow rate within individual branches of the same tree, a symmetric series-parallel network is not inferior when it comes to mean total flow predictions.[100] These observations together suggest that, since in our study the required outcomes were (or were derived from) total blood flow and total resistance, the branching structure implemented can be considered as equivalent to more complex networks.

Notably, according to Patton *et al.*, asymmetry index I is roughly 0.76 for arterioles and 0.75 for venules, when calculated from the first few generations.[98] This is indeed high, but still indicates at least some degree of asymmetry, when based on upstream vessels. However, in the following box, in support of the aforementioned, we provide a mathematical argument as to why-asymmetry in the upstream branches is not expected to profoundly affect our main endpoints. In the same argument, we use a simple optimization principle to justify why, as we move towards the terminal vessels, branching is reportedly less asymmetric than upstream.[101] In any case, previous research indicates that, at this terminal level, total flow rate has mostly been determined by the upstream arterioles.[101]

Branching optimization

Consider a given (fixed) parent branch and let its two daughter branches (of unknown caliber) be two approximately parallel resistors R_S and R_L. Using *Eq*. B2, we introduce the following quantity:

$$\frac{1}{R_{\text{daughters}}} = \frac{1}{R_S} + \frac{1}{R_L} = K\left[r_S^{2-\alpha}(r_S+\delta)^2 + r_L^{2-\alpha}(r_L+\delta)^2\right] =$$

$$= K\left[z_S^{\frac{2-\alpha}{D+\alpha}}\left(z_S^{\frac{1}{D+\alpha}}+\delta\right)^2 + z_L^{\frac{2-\alpha}{D+\alpha}}\left(z_L^{\frac{1}{D+\alpha}}+\delta\right)^2\right] \qquad \text{(B17)}$$

where $z_S = r_S^{D+\alpha}$, $z_L = r_L^{D+\alpha}$ (with $z_S + z_L$ fixed according to *Eq*. 17), and K is a constant.

It can be shown that $f: [0, +\infty) \rightarrow \mathrm{R}$, defined as:

$$f(x) = K\, x^{\frac{2-\alpha}{D+\alpha}} \left(x^{\frac{1}{D+\alpha}} + \delta \right)^2 \tag{B18}$$

is concave for all physiologically possible choices of D and α. Hence, from Jensen's inequality:

$$f(z_S) + f(z_L) \leq 2 f\left(\frac{z_S + z_L}{2} \right) \tag{B19}$$

where the left-hand side is precisely the quantity in *Eq*. B17 and the right-hand side is a fixed number.

The upper bound in Jensen's inequality is attained if and only if $z_S = z_L$ (hence $r_S = r_L$) or f is linear; this equality case results in minimal total daughter resistance for a given parent branch (optimization principle). Upstream in the retinal circulation, perfectly symmetrical branching is not necessary for optimization: indeed, it can be shown that f is almost linear for large x (f'' approaches zero). Towards the terminal vessels, f is more concave, hence symmetrical branching will favour BF optimization. Importantly, without the Fåhræus-Lindqvist effect (i.e., without δ in the equation), concavity of f is not guaranteed over all physiologically possible D and α (f would now become convex when $D+2\alpha > 4$). Therefore, this particular optimization principle cannot be safely generalized to other fluids and branching structures.

4.5.3. Autoregulation: Literature Comparison and Physiological Interpretation

A) Retinal perfusion pressure

After RVR is obtained, RBF calculation significantly relies on an accurate OPP estimate. In the classical OPP definition, $P_a \approx \frac{2}{3}$MAP is assumed (see 4.3.2F), according to ophthalmodynamometric guidelines; Stodtmeister *et al.* recommend an additional age correction to account for arterial stiffening, thus avoiding OPP underestimation in the elderly.[102,103] However, it is known that the arterial pressure measured by ophthalmodynamometry actually reflects the pressure somewhere upstream, in the much

larger ophthalmic artery, rather than in the CRA.[104] Werff estimated the pressure in the CRA to be roughly 14-17 mmHg lower, due to the large pressure gradient produced by its small lumen; in this study we initially used the offset suggested by Takahashi (19.5 mmHg).[28] Comparing *Eq*. 12 to $\frac{2}{3}$MAP-IOP, our results suggest that this offset is more likely MAP dependent (rather than constant, as assumed in the aforementioned studies), which is also intuitive, since subjects with AHT should exhibit higher pressure drops from the ophthalmic artery to the CRA. The same phenomenon has also been predicted for cerebral vessels of similar diameters.[105] Also pointing towards the superiority of the optimized calculation, results in Table 4 suggest that its implementation also improves the accuracy in pRNFL and GCC predictions.

At this point, we should highlight that IOP was not a significant predictor in the reduced RVR model (Table 2), suggesting it might not be a satisfactory surrogate for P_v. This is supported by the observation that the RBF model fit (which includes IOP in the calculation) was worse than the RVR model fit, even after optimizing the OPP formula for P_a. Indeed, several studies report discrepancy between IOP and CRV pressure (the latter is always higher) in patients with glaucoma (or other ocular diseases), vascular dysregulation, and metabolic syndrome but also in healthy subjects with no spontaneous venous pulsation, as well as animal models.[106-110]

B) Estimation of autoregulation limits

When generating autoregulation curves, we distinguished between subjects with and without AHT. Indeed, there is evidence (mostly coming from the cerebral circulation) that structural remodeling due to AHT shifts the curve to the right, because of the higher transmural pressures needed to achieve a given value of circumferential wall stress.[111-113] This shift was observed in our data, albeit only reaching significance for HARL.

Autoregulation plateaus are assumed flat in our study (Fig. 6); hence autoregulation limits are strictly defined: they are the marginal pressures slightly below or over which a minute decrease or increase in RBF is expected to take place (or equivalently the pressures corresponding to maximal vasodilation or vasoconstriction). For the sake of comparison, we also calculated $LARL_N$ and $LARL_H$ using the suboptimal, classical OPP definition at 37 mmHg and 43 mmHg, respectively. Most experimental studies in the literature use binned

data and define the autoregulation limits to be the pressures below or over which either a statistically significant or pre-determined percentage change from baseline BF is observed.[15,77,114,115] As such, these studies likely result in a looser LARL and HARL estimation; thus, comparisons between these numbers and the predictions of this study are to be interpreted with caution. For example, in the Doppler-OCT study by Puchner *et al.* (n = 15), their Fig. 5 indicates that the drop in BF after IOP elevation only becomes statistically significant at OPP ≃ 23 mmHg, when, at that point, BF has been reduced by almost 40%.[77] However, their data shows that autoregulation might not be in effect already at OPP ≃ 38 mmHg (in agreement with our prediction of 37 mmHg), upon appearance of the steep linear slope expected from *Eq*. 8 (Fig. 6). Similarly, in the LSFG study of Witkowska *et al.* [this time regarding HARL in normotensive subjects (n = 27)], Fig. 6 suggests that autoregulation starts to fail when OPP ≃ 60 mmHg [which almost coincides with our $HARL_N$ prediction, calculated according to the classical OPP definition (58 mmHg)], this time reaching significance almost immediately (OPP ≃ 62 mmHg).[115]

As expected (see 4.4.5), percent change in RVR correlated negatively with autoregulatory reserve/change (*Eqs*. 11a and 11b); similarly, percent change in RBF correlated negatively with autoregulatory deviation. These observations verify that the retinal vessels are an autoregulating system and also provide evidence in favor of the specific autoregulation limit approximation implemented in this study. Indeed, we showed that the predicted LARL dichotomizes the perfusion pressure range: below LARL, perfusion pressure drives BF; conversely, above LARL (while below HARL), perfusion pressure drives resistance. However, RVR_{stim} was not significantly different from RVR: this could be due to a simultaneous increase in resistance during IOP elevation, due to the compressive effect of IOP in retinal venules taking over (see next paragraph), or it could indicate that, in the majority of subjects, AR is close to 0 (i.e., the subject is already close to its LARL). From a teleological point of view, this could imply that most eyes are better prepared to counteract rises in RPP (for example related to physical activity, stress, diet, etc.), rather than RPP drops, being closer to LARL than to HARL (Fig. 6). This is also intuitive given the skewed distribution of BP: larger deviations from the mean are to be expected due to increases in BP. The fact that subjects are usually closer to LARL than to HARL and are better prepared for transient hypertension than hypotension has been observed in the cerebral circulation.[116-118]

4.5.4. Comparison with Previous Physiological Models

For the sake of comparison with other models, we also calculated the average (SD) velocities in the CRA and CRV, according to *Eq*. 9: 3.3 (0.5) cm/s and 1.6 (0.3) cm/s, respectively, in line with values reported in the literature.[119] The observation that venous velocity is roughly one half of the arterial velocity is a consequence of *Eq*. 10 and was also confirmed by Malek *et al.* by means of a fundus-based mathematical model.[27]

Following IOP elevation, we reported a decrease in MV, mostly due to conservation of flow after autoregulation-induced vasodilation. Guidoboni *et al.* showed that this decrease can be also partially attributed to the effect of IOP on the retinal venules (especially when it is considerably above the normal range) and much less to the compressive stress due to the lamina cribrosa.[25] This implies that triggering OPP by inducing changes in IOP is not equivalent to inducing changes in MAP; therefore, they might result in slightly different autoregulatory responses, a hypothesis that has been confirmed in experimental studies.[114,120] In the mathematical model of Guidoboni *et al.*, Table 2 reports total resistance of 0.71 mmHg·min·μl^{-1} from the CRA to the CRV at the control state, which corresponds to a 28.9-mmHg pressure drop, as reported in Table 3 of the same study.[26] These values are in excellent agreement with our median RVR theoretical prediction [0.71 (IQR: 0.65 to 0.91) mmHg·min·μl^{-1}] and the mean RPP [33.1 (SD: 5.1) mmHg], respectively. However, their model relies on a given, mean RBF control value (41 μl·min^{-1}), whereas we are additionally able to predict this value on an individual basis, accounting for variations in mean perfusion pressure, vessel caliber, hematocrit, and complexity of the microvascular network. The same study predicted LARLs equivalent to RPP = 24 mmHg and RPP = 23 mmHg for normotensives and hypertensives with intact autoregulation, respectively (to be compared with 25 mmHg and 27 mmHg, respectively, in our study). The 4-mmHg discrepancy in $LARL_H$ between their results and ours is somewhat expected, since they used the same baseline CRA radius for the normotensive and the hypertensive condition. This means their approach describes newly-established AHT, prior to structural remodeling, with the curve exhibiting no rightward shift. Interestingly, their model also predicts an increase in RI following IOP elevation, which we were able to replicate *in vivo*.

Lastly, Ganesan *et al.* used the formulas by Pries *et al.* to demonstrate that taking into account downstream changes in viscosity is paramount to calculating precise pressure drops

on the intraindividual level.[24,47-49] Our model was shown to be robust to the choice of formula (Table 2 and Supplementary Table S3), as long as the same formula is used for all subjects. In our study, we implemented the viscosity corrections by Haynes *et al*., since the model of Takahashi *et al*. was built and validated around them (see 4.3.2D). Absolute RVR and RBF values resulting from this calculation were more in agreement with previous literature.[19,20,54-58] Using these values, we subsequently showed that prediction accuracy increases when interindividual asymptotic viscosity is taken into account (Table 3).[28] This is further supported by a recent study, showing that blood viscosity was the mediator of sex-related differences in LSFG metrics.[70]

4.5.5. Physiological Implications and Clinical Relevance

To the best of our knowledge, this is the first study examining the association of LSFG metrics with theoretical predictions that are based on a multitude of vascular characteristics; hence, it allows for additional insight regarding properties and interpretation of LSFG outcomes. This is also the first study proposing such a multimodal approach for absolute, individualized predictions of vascular resistance and BF through simple clinical tests: fundus imaging, OCTA scans, BP and IOP measurements (or ophthalmodynamometry), and a blood sample.

With respect to physiology, this study implies that by assessing the phenotype of the perfused vasculature (extent of dilation/contraction, structural complexity, viscous forces, and perfusion pressure) at a specific timepoint, we are able to draw significant quantitative conclusions on its autoregulatory reserve, i.e., its ability to withstand transient BP drops or increases. Importantly, we used these findings to provide evidence that LARL in healthy subjects is closer to resting state than thought before; thus, big drops in perfusion pressure are not necessary for hypoperfusion to become relevant. It is noteworthy that such drops in perfusion pressure are not only linked to disease (e.g., glaucoma) but can also occur as episodes of orthostatic hypotension or nocturnal blood pressure dipping (see below). As already discussed, this implies that the retinal vasculature is better prepared to counteract transient rises rather than decreases in perfusion pressure.

Regarding clinical relevance, a recent study on diabetic retinopathy showed that a combination of fundus and OCTA measurements can already improve assessment of the

disease.[121] Another study used a fundus-based model to generate a fixed length feature vector as an index that can be used to successfully discriminate between healthy and glaucoma.[122] However, since they used constant, non-individualized inlet values and relied on the vessel structure to guide the outcome, the endpoint parameters are not easily interpretable. Our study showed that RBF predicted pRNFL thickness and GCC volume and this effect was independent of age (Table 4). Therefore, aside from its potential merit in understanding pathophysiological mechanisms, the model possibly also offers useful clinical markers in diagnosing ocular pathologies.

In this regard, a low blood pressure (especially during the night), sometimes even when resulting from aggressive treatment of pre-existing AHT (J-shape phenomenon), has been suggested as a risk factor for glaucoma development or progression in several studies.[123-129] It is hypothesized that this association is mediated by hypoperfusion of the retinal ganglion cells, leading to their death; that said, since the retina exhibits autoregulation properties, the subjects really at risk are probably the ones at the extremities of low BP or the ones with vascular dysregulation, that is, impaired autoregulation.[130,131] Notably, in all of the aforementioned studies regarding low BP and glaucoma, risk starts to increase around perfusion pressures comparable to LARL (37 mmHg with the classical definition). Our study suggests that subjects with low BP (or even with a BP ~1 SD lower than average, combined with an IOP ~1 SD higher than average) might already be below their LARL, suggesting these observations are of considerable clinical relevance. Importantly, a recent longitudinal study showed that the clinical entity of NTG (i.e., glaucomatous damage with IOP measured within the normal range) displayed faster progression in patients whose DBP dips low during the night.[132] As previously mentioned, the fact that LARL lies within the spectrum of values relevant to clinical management has already been suggested for the cerebral circulation.[116,118,133,134]

AHT has also been suggested itself as a risk factor for glaucoma, but a meta-analysis showed there exists significant heterogeneity across studies, sometimes even reporting protective associations.[128] Increased glaucoma risk in patients with AHT could be, first of all, directly mediated by elevated IOP.[135] In addition, both aggressive antihypertensive treatment (as previously mentioned) and poorly controlled, chronic AHT (resulting in endothelial damage, compromised autoregulation, and disproportionately increased RVR) could also make certain subjects more susceptible to BF reduction, thus explaining this association.[131,136,137] In this

regard, our study estimated the lower perfusion pressure levels (43 mmHg with the classical OPP definition) that should be respected, in order to avoid overtreating AHT, especially in glaucoma patients or suspects. Regarding the protective associations between AHT and glaucoma that are sometimes reported, some studies provide evidence in favour of certain categories of antihypertensive medication with a potential neuroprotective effect.[138-141] Additionally, we hypothesize that well-controlled or newly established AHT could offer an initial protection to perfusion deficits, as has been observed in rodents.[142] Results from our study second that, since the AHT group had reduced susceptibility to IOP elevation, as far as perfusion is concerned (IOP = 26 mmHg was needed to bring the average subject with AHT to LARL, to be compared with IOP = 20 mmHg for the subjects without AHT).

4.5.6. Study Limitations

This study has several limitations. With regards to the model build, firstly, we did not obtain individualized information for Hct. Instead, we relied on reference values, adjusted for age, sex, and blood pressure status (see 4.3.2D). Nevertheless, the sensitivity analysis (Table 3) revealed that Hct was still an important determinant of RVR and RBF, suggesting that analyzing blood samples in future studies might be a worthwhile consideration, with the potential to increase the accuracy of the model predictions.

Secondly, fractal dimension was considered as a global index, as measured from the SVP, inside a 3-mm-diameter circular ROI, centered at the fovea (see 4.3.2C and Fig. 1B). Therefore, it might ignore local variations attributed to anatomy or to disease-related focal microvascular dropout, outside the ROI.[143-145] A more accurate representation of the vasculature would contribute to the understanding of crucial phenomena, such as localized flow deficits or tissue oxygen extraction and diffusion.[146] However, adapting more heterogeneous or three-dimensional theoretical models to account for individualized estimations in the human eye would require further improvements in visualization and quantification of the interconnectivity between different capillary plexus. Again, the sensitivity analysis (Table 3) suggests that, even with this suboptimal calculation, fractal dimension slightly improves the model predictions.

Lastly, as already discussed, we only used approximations of the pressures in the CRA and CRV, based on the MAP and the IOP, respectively (see 4.3.2F); ophthalmodynamometric measurements could further refine the model predictions.

As far as the *in vivo* investigation limitations are concerned, we used a small sample size (n = 36) containing mostly healthy eyes. The small sample size does not provide optimal power for detecting low or medium effect sizes when fitting multivariable backward regression models.[147] However, we made sure the saturated models contained only pre-selected variables, based on physiological expectations and previous literature reports. In addition, only a small number of variables with very strong associations ended up in the reduced models, while the effect size (R^2) was large; hence, our findings can be considered robust to this limitation. Notably, implementing forward regression with the same LSFG metrics yielded the exact same results.

According to the Windkessel effect, BF at any point throughout a cardiac cycle is the sum of resistive ('outlet') and capacitive ('storage') flow.[148] Despite the fact that compliance is not expected to affect the mean blood flow estimate (i.e., RBF), as shown in the box below, our IOP stimulation poses some limitations, one of which is that it can only investigate static autoregulation.[52] Static autoregulation describes the overall effect of the autoregulatory activity and is examined cross-sectionally before and after the stimulation. Notably, in dynamic autoregulation (where the vascular response latency is also evaluated), compliance buffering has been shown to be more important than resistance changes in explaining blood velocity fluctuations, at least in cerebral vessels.[149,150] In addition, an experimental study revealed that chronic IOP elevation in glaucomatous eyes could also affect dynamic autoregulation; therefore, considering solely static autoregulation would likely underestimate the extent of hypoperfusion.[151] This could enhance our findings, since it highlights the fact that the clinically relevant location of LARL can be even more alarming when we also consider potential defects in dynamic autoregulation.

Vascular compliance

The simplest Windkessel equation (two-element) is displayed below:

$$Q(t) = \frac{P(t)}{\mathrm{RVR}} + CP'(t) = \frac{M\cos(\omega t) + P_0}{\mathrm{RVR}} - \omega C \sin(\omega t), \; t \in [0, \frac{60}{\mathrm{HR}}] \qquad \text{(B20)}$$

where we have kept the single-harmonic notation of *Eq*. B14, $Q(t)$ is the time-varying BF, and C is the vascular compliance (change in blood volume for a given change in perfusion pressure).

Clearly, since $\int_0^{2\pi} \cos x = \int_0^{2\pi} \sin x = 0$, compliance is not expected to affect the mean blood flow estimate (i.e., RBF), because *Eq*. B20 reduces to *Eq*. 8 (main text) when integrated over the complete Fourier series within one cardiac cycle.

4.5.7. Conclusions

In summary, we used a novel approach to characterize two markers of the human retinal circulation (vascular resistance and blood flow), by combining standard clinical tests, quantitative static imaging techniques, and physiological modeling. We demonstrated that these predictions correlate strongly with dynamic blood flow metrics, as offered by laser speckle flowgraphy. We used these findings to generate autoregulation curves and estimated that the lower autoregulation limit is well inside the range of clinical significance, both in healthy subjects and in subjects receiving antihypertensive treatment. This suggests that autoregulatory mechanisms in the retina are more effective in counteracting increases, rather than decreases in perfusion pressure. Therefore, some retinas are more liable to hypoperfusion than previously thought, even after relatively small intraocular pressure rises or blood pressure drops. By using intraocular pressure stimulation, we showed that this lower autoregulation limit prediction was in agreement with *in vivo* physiological observations.

These findings could enhance our understanding of the vascular component in ophthalmic diseases and improve treatment decisions in patients with coexisting ophthalmic and cardiovascular pathology, especially arterial hypertension. In particular, monitoring retinal blood flow in longitudinal designs could elucidate the ‘chicken-egg’ dilemma in glaucoma, according to which it is unknown whether reduced BF is the cause or consequence of RGC death. Further studies are needed to assess the diagnostic value of this approach, its efficacy in personalized intervention, such as antihypertensive treatment, and its applicability in other vascular networks.

4.6. References

1. Kur J, Newman EA, Chan-Ling T. Cellular and physiological mechanisms underlying blood flow regulation in the retina and choroid in health and disease. *Prog Retin Eye Res* 2012;31:377–406.

2. Cabrera DeBuc D, Somfai GM, Koller A. Retinal microvascular network alterations: potential biomarkers of cerebrovascular and neural diseases. *Am J Physiol* 2017;312:H201–H212.

3. Guo S, Yin S, Tse G, Li G, Su L, Liu T. Association Between Caliber of Retinal Vessels and Cardiovascular Disease: a Systematic Review and Meta-Analysis. *Curr Atheroscler Rep* 2020;22:16.

4. Vosborg F, Malmqvist L, Hamann S. Non-invasive measurement techniques for quantitative assessment of optic nerve head blood flow. *Eur J Ophthalmol* 2019;30:235-244.

5. Keane PA, Sadda SR. Imaging chorioretinal vascular disease. *Eye* 2010;24:422–427.

6. Jia Y, Morrison JC, Tokayer J, et al. Quantitative OCT angiography of optic nerve head blood flow. *Biomed Opt Express* 2012;3:3127–3137.

7. Spaide RF, Fujimoto JG, Waheed NK, Sadda SR, Staurenghi G. Optical coherence tomography angiography. *Prog Retin Eye Res* 2018;64:1–55.

8. Heeman W, Steenbergen W, van Dam G, Boerma EC. Clinical applications of laser speckle contrast imaging: a review. *J Biomed Opt* 2019;24:1–11.

9. Sugiyama T. Basic Technology and Clinical Applications of the Updated Model of Laser Speckle Flowgraphy to Ocular Diseases. *Photonics* 2014;1:220–234.

10. Tamaki Y, Araie M, Kawamoto E, Eguchi S, Fujii H. Noncontact, two-dimensional measurement of retinal microcirculation using laser speckle phenomenon. *Invest Ophthalmol Vis Sci* 1994;35:3825–3834.

11. Draijer M, Hondebrink E, van Leeuwen T, Steenbergen W. Review of laser speckle contrast techniques for visualizing tissue perfusion. *Lasers Med Sci* 2009;24:639–651.

12. Luft N, Wozniak PA, Aschinger GC, et al. Ocular Blood Flow Measurements in Healthy White Subjects Using Laser Speckle Flowgraphy. *PLoS One* 2016;11:e0168190.

13. Briers D, Duncan DD, Hirst E, et al. Laser speckle contrast imaging: theoretical and practical limitations. *J Biomed Opt* 2013;18:066018.

14. Luft N, Wozniak PA, Aschinger GC, et al. Measurements of Retinal Perfusion Using Laser Speckle Flowgraphy and Doppler Optical Coherence Tomography. *Invest Ophthalmol Vis Sci* 2016;57:5417–5425.

15. Riva CE, Grunwald JE, Petrig BL. Autoregulation of human retinal blood flow. An investigation with laser Doppler velocimetry. *Invest Ophthalmol Vis Sci* 1986;27:1706–1712.

16. Khawaja AP, Crabb DP, Jansonius NM. The role of ocular perfusion pressure in glaucoma cannot be studied with multivariable regression analysis applied to surrogates. *Invest Ophthalmol Vis Sci* 2013;54:4619–4620.

17. Pournaras CJ, Rungger-Brändle E, Riva CE, Hardarson SH, Stefansson E. Regulation of retinal blood flow in health and disease. *Prog Retin Eye Res* 2008;27:284–330.

18. Aschinger GC, Schmetterer L, Fondi K, et al. Effect of Diffuse Luminance Flicker Light Stimulation on Total Retinal Blood Flow Assessed With Dual-Beam Bidirectional Doppler OCT. *Invest Ophthalmol Vis Sci* 2017;58:1167–1178.

19. Lee B, Novais EA, Waheed NK, et al. En Face Doppler Optical Coherence Tomography Measurement of Total Retinal Blood Flow in Diabetic Retinopathy and Diabetic Macular Edema. *JAMA Ophthalmol* 2017;135:244–251.

20. Werkmeister RM, Schmidl D, Aschinger G, et al. Retinal oxygen extraction in humans. *Sci Rep* 2015;5:15763.

21. Szegedi S, Hommer N, Kallab M, et al. Repeatability and Reproducibility of Total Retinal Blood Flow Measurements Using Bi-Directional Doppler OCT. *Transl Vis Sci Tech* 2020;9:34.

22. Cherecheanu AP, Garhofer G, Schmidl D, Werkmeister R, Schmetterer L. Ocular perfusion pressure and ocular blood flow in glaucoma. *Curr Opin Pharmacol* 2013;13:36–42.

23. Flammer J, Orgül S, Costa VP, et al. The impact of ocular blood flow in glaucoma. *Prog Retin Eye Res* 2002;21:359–393.

24. Ganesan P, He S, Xu H. Analysis of retinal circulation using an image-based network model of retinal vasculature. *Microvasc Res* 2010;80:99–109.

25. Guidoboni G, Harris A, Carichino L, Arieli Y, Siesky BA. Effect of intraocular pressure on the hemodynamics of the central retinal artery: a mathematical model. *Math Biosci Eng* 2014;11:523–546.

26. Guidoboni G, Harris A, Cassani S, et al. Intraocular pressure, blood pressure, and retinal blood flow autoregulation: a mathematical model to clarify their relationship and clinical relevance. *Invest Ophthalmol Vis Sci* 2014;55:4105–4118.

27. Malek J, Azar AT, Nasralli B, Tekari M, Kamoun H, Tourki R. Computational analysis of blood flow in the retinal arteries and veins using fundus image. *Comput Math Appl* 2015;69:101–116.

28. Takahashi T, Nagaoka T, Yanagida H, et al. A mathematical model for the distribution of hemodynamic parameters in the human retinal microvascular network. *J Biorheol* 2009;23:77–86.

29. Williams B, Mancia G, Spiering W, et al. 2018 ESC/ESH Guidelines for the management of arterial hypertension. The Task Force for the management of arterial hypertension of the European Society of Cardiology (ESC) and the European Society of Hypertension (ESH). *G Ital Cardiol* 2018;19:3–73.

30. Anonymous. European Glaucoma Society Terminology and Guidelines for Glaucoma, 4th Edition - Chapter 3: Treatment principles and options Supported by the EGS Foundation: Part 1: Foreword; Introduction; Glossary; Chapter 3 Treatment principles and options. *Br J Ophthalmol* 2017;101:130-195.

31. Bankhead P, Scholfield CN, McGeown JG, Curtis TM. Fast retinal vessel detection and measurement using wavelets and edge location refinement. *PLoS One* 2012;7:e32435.

32. Knudtson MD, Lee KE, Hubbard LD, Wong TY, Klein R, Klein BEK. Revised formulas for summarizing retinal vessel diameters. *Curr Eye Res* 2003;27:143–149.

33. Kawasaki R, Wang JJ, Rochtchina E, Lee AJ, Wong TY, Mitchell P. Retinal vessel caliber is associated with the 10-year incidence of glaucoma: the Blue Mountains Eye Study. *Ophthalmology* 2013;120:84–90.

34. King LA, Stanton AV, Sever PS, Thom SA, Hughes AD. Arteriolar length-diameter (L:D) ratio: a geometric parameter of the retinal vasculature diagnostic of hypertension. *J Hum Hypertens* 1996;10:417–418.

35. Thom S. Arterial structural modifications in hypertension: Effects of treatment. *Eur Heart J* 1997;18:2–4.

36. Pappelis K, Jansonius NM. Quantification and Repeatability of Vessel Density and Flux as Assessed by Optical Coherence Tomography Angiography. *Transl Vis Sci Technol* 2019;8:3.

37. Fåhræus R, Lindqvist T. THE VISCOSITY OF THE BLOOD IN NARROW CAPILLARY TUBES. *Am J Physiol Legacy Content* 1931;96:562–568.

38. Haynes RH. Physical basis of the dependence of blood viscosity on tube radius. *Am J Physiol* 1960;198:1193–1200.

39. Chien S, Usami S, Skalam R. Blood flow in small tubes. In: *Handbook of Physiology*, edited by Renkin EM, Michel CC. Bethesda, MD: American Physiological Society; 1984:217–249.

40. Kamiya A, Takahashi T. Quantitative assessments of morphological and functional properties of biological trees based on their fractal nature. *J Appl Physiol* 2007;102:2315–2323.

41. Nagaoka T, Yoshida A. Noninvasive evaluation of wall shear stress on retinal microcirculation in humans. *Invest Ophthalmol Vis Sci* 2006;47:1113–1119.

42. Cirillo M, Laurenzi M, Trevisan M, Stamler J. Hematocrit, blood pressure, and hypertension. The Gubbio Population Study. *Hypertension* 1992;20:319–326.

43. Skalak R, Ozkaya N, Skalak TC. Biofluid Mechanics. *Annu Rev of Fluid Mech* 1989;21:167–200.

44. Leske MC. Ocular perfusion pressure and glaucoma: clinical trial and epidemiologic findings. *Curr Opin Ophthalmol* 2009;20:73–78.

45. Arciero J, Harris A, Siesky B, et al. Theoretical analysis of vascular regulatory mechanisms contributing to retinal blood flow autoregulation. *Invest Ophthalmol Vis Sci* 2013;54:5584–5593.

46. Mursch-Edlmayr AS, Luft N, Podkowinski D, Ring M, Schmetterer L, Bolz M. Laser speckle flowgraphy derived characteristics of optic nerve head perfusion in normal tension glaucoma and healthy individuals: a Pilot study. *Sci Rep* 2018;8:5343.

47. Pries AR, Secomb TW, Gaehtgens P, Gross JF. Blood flow in microvascular networks. Experiments and simulation. *Circ Res* 1990;67:826–834.

48. Pries AR, Secomb TW, Gessner T, Sperandio MB, Gross JF, Gaehtgens P. Resistance to blood flow in microvessels in vivo. *Circ Res* 1994;75:904–915.

49. Secomb TW. Hemodynamics. *Compr Physiol* 2016;6:975–1003.

50. Saltelli A, Andres TH, Homma T. Sensitivity analysis of model output. *Comput Stat Data Anal* 1993;15:211–238.

51. Binggeli T, Schoetzau A, Konieczka K. In glaucoma patients, low blood pressure is accompanied by vascular dysregulation. *EPMA J* 2018;9:387–391.

52. Schmidl D, Garhofer G, Schmetterer L. The complex interaction between ocular perfusion pressure and ocular blood flow – Relevance for glaucoma. *Exp Eye Res* 2011;93:141–155.

53. Heinze G, Wallisch C, Dunkler D. Variable selection - A review and recommendations for the practicing statistician. *Biom J*. 2018;60(3):431-449.

54. Dai C, Liu X, Zhang HF, Puliafito CA, Jiao S. Absolute retinal blood flow measurement with a dual-beam Doppler optical coherence tomography. *Invest Ophthalmol Vis Sci* 2013;54:7998–8003.

55. Fuchsjager-Mayrl G, Schmetterer L. Characterization of retinal blood flow in healthy subjects (Abstract). *Acta Ophthalmol* 2011;89.

56. Garhofer G, Werkmeister R, Dragostinoff N, Schmetterer L. Retinal Blood Flow in Healthy Young Subjects. *Invest Ophthalmol Vis Sci* 2012;53:698.

57. Srinivas S, Tan O, Wu S, et al. Measurement of retinal blood flow in normal Chinese-American subjects by Doppler Fourier-domain optical coherence tomography. *Invest Ophthalmol Vis Sci* 2015;56:1569–1574.

58. Wang Y, Fawzi AA, Tan O, Zhang X, Huang D. Flicker-induced changes in retinal blood flow assessed by Doppler optical coherence tomography. *Biomed Opt Express* 2011;2:1852–1860.

59. Feke GT, Tagawa H, Deupree DM, Goger DG, Sebag J, Weiter JJ. Blood flow in the normal human retina. *Invest Ophthalmol Vis Sci* 1989;30:58–65.

60. Garcia JP Jr, Garcia PT, Rosen RB. Retinal blood flow in the normal human eye using the canon laser blood flowmeter. *Ophthalmic Res* 2002;34: 295–299.

61. Kannenkeril D, Harazny JM, Bosch A, et al. Retinal vascular resistance in arterial hypertension. *Blood Press* 2018;27:82–87.

62. Nagaoka T, Mori F, Yoshida A. Retinal artery response to acute systemic blood pressure increase during cold pressor test in humans. *Invest Ophthalmol Vis Sci* 2002;43:1941–1945.

63. Omae T, Nagaoka T, Yoshida A. Relationship Between Retinal Blood Flow and Serum Adiponectin Concentrations in Patients with Type 2 Diabetes Mellitus. *Invest Ophthalmol Vis Sci* 2015;56:4143–4149.

64. Bardelli M, Veglio F, Arosio E, Cataliotti A, Valvo E, Morganti A. New intrarenal echo-Doppler velocimetric indices for the diagnosis of renal artery stenosis. *Kidney Int* 2006;69:580–587.

65. Heine GH, Reichart B, Ulrich C, Köhler H, Girndt M. Do ultrasound renal resistance indices reflect systemic rather than renal vascular damage in chronic kidney disease? *Nephrol Dial Transplant* 2007;22:163–170.

66. O'Neill WC. Renal resistive index: a case of mistaken identity. *Hypertension* 2014;64:915–917.

67. Polska E, Kircher K, Ehrlich P, Vecsei PV, Schmetterer L. RI in central retinal artery as assessed by CDI does not correspond to retinal vascular resistance. *Am J Physiol Heart Circ Physiol* 2001;280:H1442–H1447.

68. Akaishi T, Abe M, Miki T, et al. Ratio of diastolic to systolic blood pressure represents renal resistive index. *J Hum Hypertens* 2020;34:512-519.

69. Iwase T, Akahori T, Yamamoto K, Ra E, Terasaki H. Evaluation of optic nerve head blood flow in response to increase of intraocular pressure. *Sci Rep* 2018;8:17235.

70. Iwase T, Yamamoto K, Yanagida K, et al. Investigation of causes of sex-related differences in ocular blood flow in healthy eyes determined by laser speckle flowgraphy. *Sci Rep* 2017;7:13878.

71. Gardiner SK, Cull G, Fortune B, Wang L. Increased Optic Nerve Head Capillary Blood Flow in Early Primary Open-Angle Glaucoma. *Invest Ophthalmol Vis Sci* 2019;60:3110–3118.

72. Shiga Y, Omodaka K, Kunikata H, et al. Waveform analysis of ocular blood flow and the early detection of normal tension glaucoma. *Invest Ophthalmol Vis Sci* 2013;54:7699–7706.

73. Bhatti MS, Tang TB, Laude A. Effects of water drinking test on ocular blood flow waveform parameters: A laser speckle flowgraphy study. *PLoS One* 2017;12:e0181512.

74. Susanna R Jr, Hatanaka M, Vessani RM, Pinheiro A, Morita C. Correlation of asymmetric glaucomatous visual field damage and water-drinking test response. *Invest Ophthalmol Vis Sci* 2006;47:641–644.

75. Kiyota N, Shiga Y, Ichinohasama K, et al. The Impact of Intraocular Pressure Elevation on Optic Nerve Head and Choroidal Blood Flow. *Invest Ophthalmol Vis Sci* 2018;59:3488–3496.

76. Nagel E, Vilser W. Autoregulative behavior of retinal arteries and veins during changes of perfusion pressure: a clinical study. *Graefes Arch Clin Exp Ophthalmol* 2004;242:13–17.

77. Puchner S, Schmidl D, Ginner L, et al. Changes in Retinal Blood Flow in Response to an Experimental Increase in IOP in Healthy Participants as Assessed with Doppler Optical Coherence Tomography. *Invest Ophthalmol Vis Sci* 2020;61:33.

78. Prada D, Harris A, Guidoboni G, Siesky B, Huang AM, Arciero J. Autoregulation and neurovascular coupling in the optic nerve head. *Surv Ophthalmol* 2016;61:164–186.

79. Crutchfield KE, Razumovsky AY, Tegeler CH, Robert Mozayeni B. Differentiating Vascular Pathophysiological States by Objective Analysis of Flow Dynamics. *J Neuroimaging* 2004;14:97–107.

80. Sainz A, Cabau J, Roberts VC. Deceleration vs. acceleration: a haemodynamic parameter in the assessment of vascular reactivity. A preliminary study. *Med Eng Phys* 1995;17:91–95.

81. Sung CK, Lee KH, Kim SH. Evaluation of factors influencing arterial Doppler waveforms in an in vitro flow phantom. *Ultrasonography* 2017;36:39–52.

82. Stoner L, McCully KK. Velocity acceleration as a determinant of flow-mediated dilation. *Ultrasound Med Biol* 2012;38:580–592.

83. Stoner L, Young JM, Fryer S, Sabatier MJ. The Importance of Velocity Acceleration to Flow-Mediated Dilation. *Int J Vasc Med* 2012;2012:589213.

84. Chemla D, Démolis P, Thyrault M, Annane D, Lecarpentier Y, Giudicelli JF. Blood flow acceleration in the carotid and brachial arteries of healthy volunteers: respective contributions of cardiac performance and local resistance. *Fundam Clin Pharmacol* 1996;10:393–399.

85. Halpern EJ, Merton DA, Forsberg F. Effect of distal resistance on Doppler US flow patterns. *Radiology* 1998;206:761–766.

86. Ku DN. Blood flow in arteries. *Annu Rev Fluid Mech* 1997;29:399–434.

87. Oshinski JN, Ku DN, Bohning DE, Pettigrew RI. Effects of acceleration on the accuracy of MR phase velocity measurements. *J Magn Reson Imaging* 1992;2:665–670.

88. Nagahara M, Tamaki Y, Tomidokoro A, Araie M. In vivo measurement of blood velocity in human major retinal vessels using the laser speckle method. *Invest Ophthalmol Vis Sci* 2011;52:87–92.

89. Yoo E, Yoo C, Lee B-R, Lee T-E, Kim YY. Diagnostic Ability of Retinal Vessel Diameter Measurements in Open-Angle Glaucoma. *Invest Ophthalmol Vis Sci* 2015;56:7915–7922.

90. Womersley JR. Method for the calculation of velocity, rate of flow and viscous drag in arteries when the pressure gradient is known. *J Physiol* 1955;127:553–563.

91. Attinger EO. The physics of pulsatile blood flow with particular reference to small vessels. *Invest Ophthalmol Vis Sci* 1965;4:973–987.

92. Hale JF, McDonald DA, Womersley JR. Velocity profiles of oscillating arterial flow, with some calculations of viscous drag and the Reynolds number. *J Physiol* 1955;128: 629–640.

93. Lehmann MV, Schmieder RE. Remodeling of retinal small arteries in hypertension. *Am J Hypertens* 2011;24:1267–1273.

94. Russell RW. Evidence for autoregulation in human retinal circulation. *Lancet* 1973;2:1048–1050.

95. Heitmar R, Kalitzeos AA, Panesar V. Comparison of Two Formulas Used to Calculate Summarized Retinal Vessel Calibers. *Optom Vis Sci* 2015;92:1085–1091.

96. Yip W, Tham YC, Hsu W, et al. Comparison of Common Retinal Vessel Caliber Measurement Software and a Conversion Algorithm. *Transl Vis Sci Tech* 2016;5:11.

97. Dorner GT, Polska E, Garhöfer G, Zawinka C, Frank B, Schmetterer L. Calculation of the diameter of the central retinal artery from noninvasive measurements in humans. *Curr Eye Res* 2002;25:341–345.

98. Patton N, Aslam T, Macgillivray T, Dhillon B, Constable I. Asymmetry of retinal arteriolar branch widths at junctions affects ability of formulae to predict trunk arteriolar widths. *Invest Ophthalmol Vis Sci* 2006;47:1329–1333.

99. Murray CD. The Physiological Principle of Minimum Work: I. The Vascular System and the Cost of Blood Volume. *Proc Natl Acad Sci* 1926;12:207–214.

100. Popel AS. A Model of Pressure and Flow Distribution in Branching Networks. *J Appl Mech* 1980;47:247–253.

101. McClatchey PM, Schafer M, Hunter KS, Reusch JE. The endothelial glycocalyx promotes homogenous blood flow distribution within the microvasculature. *Am J Physiol Heart Circ Physiol*. 2016;311(1):H168-H176.

102. Stodtmeister R, Oppitz T, Spoerl E, Haustein M, Boehm AG. Contact lens dynamometry: the influence of age. *Invest Ophthalmol Vis Sci* 2010;51:6620–6624.

103. Ulrich W-D. *Grundlagen und Methodik der Ophthalmodynamometrie (ODM), Ophthalmodynamographie (ODG), Temporalisdynamographie (TDG)*. Leipzig, Germany: VEB Georg Thieme; 1976.

104. Werff TJV. The Pressure Measured in Ophthalmodynamometry. *Arch Ophthalmol* 1972;87:290–292.

105. Blanco PJ, Müller LO, Spence JD. Blood pressure gradients in cerebral arteries: a clue to pathogenesis of cerebral small vessel disease. *Stroke Vasc Neurol* 2017;2:108–117.

106. Attariwala R, Giebs CP, Glucksberg MR. The influence of elevated intraocular pressure on vascular pressures in the cat retina. *Invest Ophthalmol Vis Sci* 1994;35:1019–1025.

107. Flammer J, Konieczka K. Retinal venous pressure: the role of endothelin. *EPMA J* 2015;6:21.

108. Kim KE, Kim DM, Flammer J, Kim KN. Central retinal venous pressure in eyes of normal-tension glaucoma patients with optic disc hemorrhage. *PLoS One* 2015;10:e0127920.

109. Mustur D, Vahedian Z, Bovet J, Mozaffarieh M. Retinal venous pressure measurements in patients with Flammer syndrome and metabolic syndrome. *EPMA J* 2017;8:339–344.

110. Stodtmeister R, Ventzke S, Spoerl E, et al. Enhanced pressure in the central retinal vein decreases the perfusion pressure in the prelaminar region of the optic nerve head. *Invest Ophthalmol Vis Sci* 2013;54:4698–4704.

111. Barry DI. Cerebral blood flow in hypertension. *J Cardiovasc Pharmacol* 1985;7 Suppl 2:S94–S98.

112. Hayreh SS. Blood flow in the optic nerve head and factors that may influence it. *Prog Retin Eye Res* 2001;20:595–624.

113. Pires PW, Dams Ramos CM, Matin N, Dorrance AM. The effects of hypertension on the cerebral circulation. *Am J Physiol Heart Circ Physiol* 2013;304:H1598–H1614.

114. Tani T, Nagaoka T, Nakabayashi S, Yoshioka T, Yoshida A. Autoregulation of retinal blood flow in response to decreased ocular perfusion pressure in cats: comparison of the effects of increased intraocular pressure and systemic hypotension. *Invest Ophthalmol Vis Sci* 2014;55:360–367.

115. Witkowska KJ, Bata AM, Calzetti G, et al. Optic nerve head and retinal blood flow regulation during isometric exercise as assessed with laser speckle flowgraphy. *PLoS One* 2017;12:e0184772.

116. Armstead WM. Cerebral Blood Flow Autoregulation and Dysautoregulation. *Anesthesiol Clin* 2016;34:465–477.

117. Brassard P, Ferland-Dutil H, Smirl J, et al. Evidence for hysteresis in the cerebral pressure-flow relationships in healthy men. *Am J Physiol* 2017;312:H701-H704.

118. Czosnyka M, Miller C. Monitoring of Cerebral Autoregulation. *Neurocrit Care* 2014;21:95–102.

119. Pemp B, Cherecheanu AP, Garhofer G, Schmetterer L. Calculation of central retinal artery diameters from non-invasive ocular haemodynamic measurements in type 1 diabetes patients. *Acta Ophthalmol* 2013;91:e348–e352.

120. Wang L, Cull GA, Fortune B. Optic nerve head blood flow response to reduced ocular perfusion pressure by alteration of either the blood pressure or intraocular pressure. *Curr Eye Res* 2015;40(4):359-367.

121. Tan T-E, Nguyen Q, Chua J, et al. Global Assessment of Retinal Arteriolar, Venular and Capillary Microcirculations Using Fundus Photographs and Optical Coherence Tomography Angiography in Diabetic Retinopathy. *Sci Rep* 2019;9:11751.

122. Orlando JI, Breda JB, van Keer K, Blaschko MB, Blanco PJ, Bulant CA. Towards a Glaucoma Risk Index Based on Simulated Hemodynamics from Fundus Images. In: *Medical Image Computing and Computer Assisted Intervention*. Berlin, Germany: Springer; 2018:65–73.

123. Bowe A, Grünig M, Schubert J, et al. Circadian Variation in Arterial Blood Pressure and Glaucomatous Optic Neuropathy—A Systematic Review and Meta-Analysis. *Am J Hypertens* 2015;28:1077–1082.

124. Leske MC, Heijl A, Hyman L, et al. Predictors of long-term progression in the early manifest glaucoma trial. *Ophthalmology* 2007;114:1965–1972.

125. Leske MC, Wu S-Y, Hennis A, Honkanen R, Nemesure B, BESs Study Group. Risk factors for incident open-angle glaucoma: the Barbados Eye Studies. *Ophthalmology* 2008;115:85–93.

126. Melgarejo JD, Lee JH, Petitto M, et al. Glaucomatous Optic Neuropathy Associated with Nocturnal Dip in Blood Pressure: Findings from the Maracaibo Aging Study. *Ophthalmology* 2018;125:807–814.

127. Topouzis F, Wilson MR, Harris A, et al. Association of open-angle glaucoma with perfusion pressure status in the Thessaloniki Eye Study. *Am J Ophthalmol* 2013;155:843–851.

128. Zhao D, Cho J, Kim MH, Guallar E. The association of blood pressure and primary open-angle glaucoma: a meta-analysis. *Am J Ophthalmol* 2014;158:615–627.e9.

129. Zheng Y, Wong TY, Mitchell P, Friedman DS, He M, Aung T. Distribution of ocular perfusion pressure and its relationship with open-angle glaucoma: the singapore malay eye study. *Invest Ophthalmol Vis Sci* 2010;51:3399–3404.

130. Flammer J, Konieczka K, Flammer AJ. The primary vascular dysregulation syndrome: implications for eye diseases. *EPMA J* 2013;4:14.

131. He Z, Vingrys AJ, Armitage JA, Bui BV. The role of blood pressure in glaucoma. *Clin Exp Optom* 2011;94:133–149.

132. Kwon J, Jo YH, Jeong D, Shon K, Kook MS. Baseline Systolic versus Diastolic Blood Pressure Dip and Subsequent Visual Field Progression in Normal-Tension Glaucoma. *Ophthalmology* 2019;126:967–979.

133. Donnelly J, Czosnyka M, Adams H, et al. Individualizing Thresholds of Cerebral Perfusion Pressure Using Estimated Limits of Autoregulation. *Crit Care Med* 2017;45:1464–1471.

134. Drummond JC. The lower limit of autoregulation: time to revise our thinking? *Anesthesiology* 1997;86:1431–1433.

135. Hennis A, Wu SY, Nemesure B, Leske MC, Barbados Eye Studies Group. Hypertension, diabetes, and longitudinal changes in intraocular pressure. *Ophthalmology* 2003;110:908–914.

136. He Z, Vingrys AJ, Armitage JA, Nguyen CT, Bui BV. Chronic hypertension increases susceptibility to acute IOP challenge in rats. *Invest Ophthalmol Vis Sci* 2014;55:7888–7895.

137. van Koeverden AK, He Z, Nguyen CTO, Vingrys AJ, Bui BV. Systemic hypertension is not protective against chronic intraocular pressure elevation in a rodent model. *Sci Rep* 2018;8:7107.

138. Hirooka K, Baba T, Fujimura T, Shiraga F. Prevention of Visual Field Defect Progression with Angiotensin-Converting Enzyme Inhibitor in Eyes With Normal-tension Glaucoma. *Am J Ophthalmol* 2006;142:523–525.

139. Horwitz A, Klemp M, Jeppesen J, Tsai JC, Torp-Pedersen C, Kolko M. Antihypertensive Medication Postpones the Onset of Glaucoma: Evidence From a Nationwide Study. *Hypertension* 2017;69:202–210.

140. Pappelis K, Loiselle AR, Visser S, Jansonius NM. Association of Systemic Medication Exposure with Glaucoma Progression and Glaucoma Suspect Conversion in the Groningen Longitudinal Glaucoma Study. *Invest Ophthalmol Vis Sci* 2019;60:4548–4555.

141. Yang H, Hirooka K, Fukuda K, Shiraga F. Neuroprotective Effects of Angiotensin II Type 1 Receptor Blocker in a Rat Model of Chronic Glaucoma. *Invest Ophthalmol Vis Sci* 2009;50:5800.

142. He Z, Nguyen CTO, Armitage JA, Vingrys AJ, Bui BV. Blood pressure modifies retinal susceptibility to intraocular pressure elevation. *PLoS One* 2012;7:e31104.

143. Campbell JP, Zhang M, Hwang TS, et al. Detailed Vascular Anatomy of the Human Retina by Projection-Resolved Optical Coherence Tomography Angiography. *Sci Rep* 2017;7:42201.

144. Nesper PL, Fawzi AA. Human Parafoveal Capillary Vascular Anatomy and Connectivity Revealed by Optical Coherence Tomography Angiography. *Invest Ophthalmol Vis Sci* 2018;59:3858–3867.

145. Yarmohammadi A, Zangwill LM, Diniz-Filho A, et al. Optical Coherence Tomography Angiography Vessel Density in Healthy, Glaucoma Suspect, and Glaucoma Eyes. *Invest Ophthalmol Vis Sci* 2016;57:OCT451.

146. Fry BC, Coburn EB, Whiteman S, Harris A, Siesky B, Arciero J. Predicting retinal tissue oxygenation using an image-based theoretical model. *Math Biosci* 2018;305:1-9.

147. Green SB. How Many Subjects Does It Take To Do A Regression Analysis. *Multivariate Behav Res* 1991;26:499–510.

148. Frank O. The basic shape of the arterial pulse. First treatise: mathematical analysis. 1899. *J Mol Cell Cardiol* 1990;22:255–277.

149. Tzeng Y-C, Chan GSH, Willie CK, Ainslie PN. Determinants of human cerebral pressure-flow velocity relationships: new insights from vascular modelling and Ca2 channel blockade. *J Physiol* 2011;589:3263–3274.

150. Zhang R, Behbehani K, Levine BD. Dynamic pressure-flow relationship of the cerebral circulation during acute increase in arterial pressure. *J Physiol* 2009;587:2567–2577.

151. Wang L, Cull GA, Burgoyne CF, Thompson S, Fortune B. Longitudinal Alterations in the Dynamic Autoregulation of Optic Nerve Head Blood Flow Revealed in Experimental Glaucoma. *Invest Ophthalmol Vis Sci* 2014;55:3509-351.

Chapter 5

BLOOD PRESSURE, RETINAL PERFUSION, AND STRUCTURAL OCT*

* Pappelis K, Jansonius NM. U-shaped Effect of Blood Pressure on Structural OCT Metrics and Retinal Perfusion in Ophthalmologically Healthy Subjects. *Invest Ophthalmol Vis Sci*. 2021;62(12):5.

5.1. Abstract

Purpose: We wanted to investigate the association of blood pressure (BP) status with the ganglion cell-inner plexiform layer (GCIPL) and retinal nerve fiber layer (RNFL) thickness of non-glaucomatous eyes and to elucidate whether this effect is related to vascular metrics proxying retinal perfusion.

Methods: For this case-control study, we prospectively included 96 eyes of 96 healthy subjects (age 50-65) from a large-scale population-based cohort in the northern Netherlands (n = 167,000) and allocated them to four groups (low BP, normal BP [controls], treated arterial hypertension [AHT], untreated AHT). We measured macular GCIPL and RNFL (mRNFL) and peripapillary RNFL (pRNFL) thicknesses with optical coherence tomography (OCT). We estimated retinal blood flow (RBF), retinal vascular resistance (RVR), and autoregulatory reserve (AR) from quantitative OCT-angiography, fundus imaging, BP, and intraocular pressure. We compared structural and vascular metrics across groups and performed mediation analysis.

Results: Compared to controls, GCIPL was thinner in the low BP group ($P = 0.013$), treated hypertensives ($P = 0.007$), and untreated hypertensives ($P = 0.007$). Treated hypertensives exhibited the thinnest mRNFL ($P = 0.001$), temporal pRNFL ($P = 0.045$), and inferior pRNFL ($P = 0.034$). The association of GCIPL thickness with BP was mediated by RBF within the combined low BP group and controls ($P = 0.003$), by RVR and AR within the combined treated hypertensives and controls ($P = 0.001$, $P = 0.032$), and by RVR within the combined untreated antihypertensives and controls ($P = 0.022$).

Conclusions: Inner retinal thinning was associated with both tails of the BP distribution and with ineffective autoregulation. Longitudinal studies could clarify whether these defects can explain the reported glaucomatous predisposition of these population groups.

5.2. Introduction

Glaucoma is a chronic optic neuropathy characterized by thinning of the retinal nerve fiber layer (RNFL), loss of retinal ganglion cells (RGCs), and progressive visual function decline.[1] Although elevated intraocular pressure (IOP) is considered as the most important modifiable risk factor, glaucoma may also manifest in those with apparently normal IOP (normal-tension glaucoma [NTG]).[2–4] Therefore, certain components of the disease remain elusive or insufficiently addressed.

It has been proposed that low or unstable blood supply could lead to reduced oxygenation of the RGCs.[4,5] From a hemodynamic perspective, blood flow is determined by the balance between ocular perfusion pressure (OPP) and vascular resistance.[6] Therefore, low blood pressure (BP) could result in low OPP, thus increasing the risk for glaucoma incidence and progression, possibly because of flow-mediated damage to the RGCs. Indeed, this has been observed in some cross-sectional and longitudinal population-based studies.[7–10] However, other studies do not confirm this finding, and there is also evidence that this association becomes relevant only when low BP manifests as pronounced nocturnal dipping.[11,12] On the other hand, although arterial hypertension (AHT) is also frequently reported as a risk factor for glaucoma, conflicting results exist on whether BP reduction exacerbates or protects from glaucomatous optic neuropathy (GON), possibly depending on individual medication effects and on how aggressive the treatment strategy is.[13–20]

Current assessment of RGC structure is based on optical coherence tomography (OCT), whereas its more recent extensions, OCT-angiography (OCTA) and Doppler OCT, enable the noninvasive evaluation of retinal perfusion.[21–23] These imaging modalities have already revealed that, in glaucoma patients, reduced blood flow is associated with visual field (VF) deterioration, independently of neural tissue damage.[24–26] However, perfusion deficits could, at the same time, be the cause (low supply) or consequence (low demand) of GON. This realization is known as the ‘chicken-egg’ dilemma in glaucoma. Therefore, without first establishing a clear picture of the baseline interplay between vascular risk factors (in this case BP status), perfusion, and structure in healthy eyes, it is difficult to objectively assess GON for a potential vascular component.

The retinal microcirculation normally demonstrates the ability of autoregulation, i.e., active modification of vascular caliber in response to local signals, keeping retinal blood flow (RBF) essentially constant.[27] This property protects the tissue from ischemia, in case of OPP drops. BP status can interfere with this process: BP lowering brings subjects closer to their lower autoregulation limit (LARL), thus at risk of hypoperfusion, whereas AHT may cause endothelial damage and flow dysregulation.[28] In this study, we hypothesized an inverse U-shaped association between BP status and structural OCT measures in nonglaucomatous eyes. Although the detrimental effect of AHT to the RGCs and their axons has been previously documented, this effect has not been studied in subjects with low BP, nor has it been examined in combination with RBF autoregulation.[29–32] Studies until now have used linear models to describe the association between BP and structural OCT measures, thus potentially neglecting any signal coming from the left tail of the distribution.[33,34]

Therefore, the aims of this study were to investigate the effect of low BP, treated AHT, and untreated AHT on the inner retinal layer thicknesses of non-glaucomatous eyes and to elucidate whether this effect is related to retinal perfusion and to crossing the lower limit of RBF autoregulation. For this purpose, we performed multimodal structural and vascular imaging in ophthalmically healthy normotensive controls, treated arterial hypertensives, and individuals belonging to the lower and higher (untreated) tails of the BP distribution. Participants were selected from the large-scale population-based Lifelines cohort, which enabled us to study the real extremes, especially from the low BP tail, in an unbiased manner.

5.3. Methods

5.3.1. Study Design and Population

For this cross-sectional, case-control study, we prospectively recruited subjects via targeted invitation among the participants of a large-scale prospective cohort study of the northern Netherlands (Lifelines Biobank; n = 167,000).[35] Subjects were invited solely on the basis of their BP status and age. After a strict selection procedure, 105 participants between 50 and 65 years of age satisfied both the BP criteria (see next paragraph) and the ophthalmic and medical history inclusion criteria: unoperated eyes; best-corrected visual acuity ≥ 0.8; spherical refractive error between -3 and +3 D; cylinder not exceeding 2 D; IOP ≤ 21 mmHg

(non-contact tonometer Tonoref II; Nidek, Aichi, Japan); no reproducibly abnormal VF test locations (Frequency Doubling Technology [C20-1 screening mode]; Carl Zeiss, Jena, Germany); no family history of glaucoma; no ophthalmic, hematologic, or cardiovascular disease (except for AHT), and no diabetes. We performed additional documentation of ophthalmic health with the subsequent imaging sessions (see 5.3.3). We allocated participants to one of four non-overlapping groups: (1) low BP, (2) normal BP (controls), (3) treated AHT, and (4) untreated AHT (see next paragraph).

All participants provided written informed consent. The ethics board of the University Medical Center Groningen approved the study protocol (no. NL61508.042.17). The study followed the tenets of the Declaration of Helsinki.

5.3.2. Blood Pressure Group Definitions

We defined low BP (group 1) as both systolic and diastolic BP (SBP, DBP) lower than the 10th percentiles of the Lifelines Biobank age-matched population (110 mmHg and 65 mmHg, respectively), without any AHT record. This criterion had to be confirmed on at least two previous, separate occasions (ascertaining that subjects truly belonged to the tail of the distribution and did not regress towards the mean). We defined untreated AHT (group 4) similarly, with the criteria being both SBP and DBP higher than the 90th percentiles of the Lifelines Biobank age-matched population (149 mmHg and 88 mmHg, respectively), verified at least twice previously. Subjects of this group were aware of their BP status, but never made use of antihypertensive medication, by choice. For the aforementioned groups, recruitment started from the tails of the SBP and DBP distributions (outside the first and ninety-ninth percentile), moving upwards towards the tenth percentile bound for group 1 and downwards towards the ninetieth percentile bound for group 4. For treated AHT (group 3), we randomly invited participants documented as receiving (and still making uninterrupted use of) antihypertensive medication for at least one year. Lastly, we defined normal BP (group 2) as both SBP and DBP within 1 standard deviation (SD) from the mean of the age-matched population (SBP: 113 mmHg to 143 mmHg and DBP: 67 mmHg to 85 mmHg, measured on site) and no previous record of AHT.

For all groups, recruitment ended upon group completion or upon unavailability or unresponsiveness of participants with the required characteristics. Specifically, the power

analysis for a one-way ANOVA design (power, 0.8; alpha level, 0.05; effect size f, 0.35; groups, 4) recommended 24 subjects per group, which was rounded up to 25.

The definitions used for group 1 (low BP) and group 4 (untreated AHT) are based on predetermined cutoffs of an otherwise continuous variable (BP), based on multiple previous measurements. To verify the robustness of statistical findings and allow for direct comparison with relevant studies, for these groups we also used the standard, cross-sectional definition, based on the on-site BP measurement. Specifically, low/high SBP was defined as SBP outside the 5th/95th percentile of the Lifelines Biobank population (105 mmHg and 155 mmHg, respectively). The same definition was used for low/high DBP (61 mmHg and 92 mmHg, respectively).

5.3.3. Data Collection

All participants were examined at the same time of the day (5:00 PM-6:30 PM) and were not given any instructions regarding their routine before their visit. Following screening (see previous section), we applied mydriatic drops that have been shown not to affect RBF (tropicamide 0.5%).[36] After the participants had rested in a quiet room for 20 minutes, we recorded BP from the brachial artery, in sitting position, with an automatic monitor (Omron M6 Comfort, Omron Healthcare, Kyoto, Japan). We averaged two readings, unless there was a discrepancy of at least 10 mmHg in SBP or 5 mmHg in DBP, in which case we averaged three readings. We also measured the weight and height of each participant.

For the imaging session, we selected, randomly if both eyes fulfilled the inclusion criteria, one eye per participant. We performed macular and optic nerve head (ONH) structural OCT imaging, as well as parafoveal OCTA (Canon HS100 SD-OCT; Canon, Inc., Tokyo, Japan). The device automatically segments and quantifies macular RNFL (mRNFL) thickness and ganglion cell-inner plexiform layer (GCIPL) thickness within a 10-mm diameter circular region of interest (ROI) centered at the fovea (Fig. 1A), a region that has been shown to be advantageous over the commonly used 5-mm diameter ROI for mRNFL measurements.[37] It also reports peripapillary RNFL (pRNFL) thickness at a 3.45-mm diameter circle centered at the ONH (Fig. 1B). We further subdivided pRNFL into temporal, superior, nasal, and inferior and also recorded values for the neuroretinal rim (NRR) area and the vertical cup-to-disc ratio (VCDR). We additionally acquired two 6 × 6 mm OCTA scans centered at the fovea (Fig.

1C). We required an image quality of 7/10 or better, as well as the absence of any artifacts or segmentation errors for all OCT and OCTA scans, resulting in the exclusion of 9 out of the 105 subjects.

After registering and binarizing the signal of the en face OCTA images, we calculated the fractal dimension (FD) of the superficial vascular plexus, inside a 3-mm diameter circle centered at the fovea (Fig. 1C). We have previously provided details on FD and its calculation, as well as on the specifications and repeatability of the Canon OCTA.[38,39] In short, FD represents the complexity of the branching pattern and is lower in conditions with sparser vasculature, such as glaucoma.[40]

Lastly, we acquired two 45° high-quality and artifact-free fundus images (TRC-NW400; Topcon Corporation, Tokyo, Japan), centered at the ONH (Fig. 1D). For Gullstrand's schematic eye, that is, not accounting for variations in corneal curvature or axial length and assuming a distance of 17 mm between the secondary nodal point and the retina, the resolution of this camera is ~6.9 μm per pixel. For each image, we derived the central retinal artery and vein equivalents (CRAE, CRVE; i.e., diameters) using the standardized Knudtson-Parr-Hubbard iteration, whose details and validation can be found elsewhere.[38,41] In short, we back-calculated vessel diameters using the six largest arteriolar and six largest venular branches, identified within a ring centered at the ONH (2 and 3 optic disc diameters). We recorded the average CRAE and CRVE of two images.

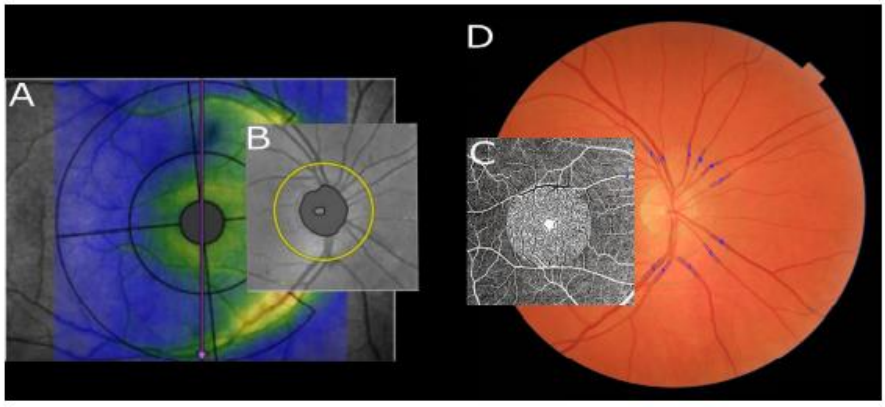

FIGURE 1. Structural (**A, B**) and vascular (**C, D**) regions of interest. (**A**) The mRNFL and GCIPL thicknesses measured within the larger (10 mm diameter) circle centered at the fovea, excluding the innermost 1 mm diameter circle and the nasal sector of the outer ring. (**B**) The pRNFL measured at a circle of 3.45 mm diameter centered at the ONH. (**C**) OCT-A scan of 6 × 6 mm centered at the fovea. Signal intensity inside the innermost 3-mm diameter circle is binarized in flow (*black*) and non-flow (*white*). (**D**) A 45° fundus image centered at the ONH. The six largest arterioles and six largest venules between rings of two and three optic disc diameters are marked in *blue*.

5.3.4. Retinal Blood Flow and Lower Autoregulation Limit

We calculated total retinal vascular resistance (RVR) using the measured FD, CRAE, and CRVE of each participant, as well as population-based hematocrit values (Lifelines Biobank), adjusted for age, sex, and blood pressure status. We have previously documented the mathematics behind this Poiseuille-based model and its validation *in vivo*, by means of Laser Speckle Flowgraphy (LSFG).[38,42] Subsequently, we computed total RBF, using RVR and retinal perfusion pressure (RPP), a more precise estimation of OPP for the retinal circulation:[38]

$$\mathrm{RBF} = \frac{\mathrm{RPP}}{\mathrm{RVR}} \tag{1}$$

where RPP = (0.39·MAP + 10.1) - IOP mmHg and MAP = $\frac{1}{3}$SBP + $\frac{2}{3}$DBP is the mean arterial pressure.

We defined LARL as the lowest RPP value for which RBF can be maintained constant (Fig. 2). At this critical point, the vasculature has reached its maximal autoregulatory capacity and any further pressure drop will not trigger compensatory vasodilation, resulting in flow reduction. We have previously shown and experimentally validated, by means of LSFG, that LARL can be approximated as:

$$\mathrm{LARL} = \mathrm{RBF}\cdot\mathrm{RVR}_{max} \tag{2}$$

where RVR_{max} is an upper bound observed in a population.[38]

In this study, we defined RVR_{max} as the 95th percentile of the RVR distribution. Due to the possible occurrence of structural remodeling in retinal vessels belonging to subjects with AHT, we separated the RVR distributions of the non-hypertensives (groups 1 and 2) and hypertensives (groups 3 and 4).[6]

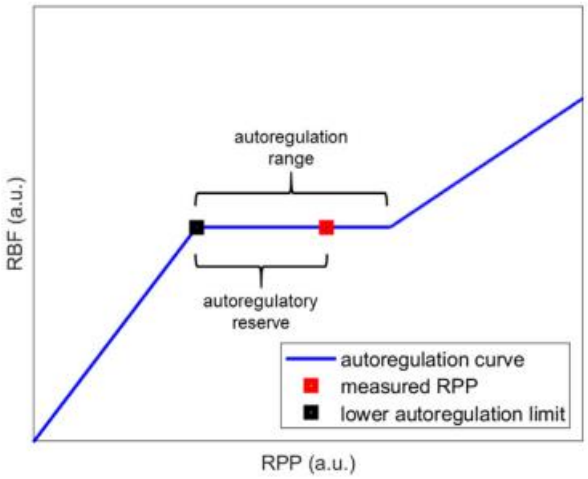

Figure 2. Theoretical autoregulation curve (axes in arbitrary units). RBF is displayed as a function of RPP. Within the autoregulation range, blood flow is maintained constant. The distance of the actual (measured) RPP from the LARL is the AR.

Lastly, for each participant, we defined the *autoregulatory reserve* (AR) as the difference between measured RPP and predicted LARL (Fig. 2).

5.3.5. Statistical Analysis

This study is divided in three parts. For the first part of the analysis (structural OCT analysis), to establish the existence of a U-shaped association (if any), we univariably compared structural OCT metrics (mRNFL, GCIPL, and pRNFL) between the four BP groups, without accounting at this point for any vascular factors. For the second part of the analysis, to investigate whether any vascular factors could possibly explain this association, we univariably compared RVR, RBF, and AR between the groups. For the last part of the analysis, we performed mediation analysis to examine whether the vascular metrics lie in the explanatory pathway of the relationship between MAP and the structural OCT metrics that were significant in the first part of the analysis. All analyses were initially performed using the recruitment BP definitions and were reiterated using the standard, cross-sectional definitions based on the fifth and ninety-fifth percentiles of the SBP and DBP distributions (see 5.3.2).

We described normally distributed variables with the mean and standard deviation (SD) and variables with a skewed distribution with the median and interquartile range (IQR). We used one-way ANOVA with post hoc tests for group mean comparisons, adjusting for potential confounders. To account for multiple testing, we implemented the Tukey HSD correction. We applied Levene's test to check for equality of variances. Whenever ANOVA assumptions were not met, we used nonparametric tests, Welch's one-way ANOVA with the Games-Howell correction, or quantile regression.

To determine a mediation effect, we used Baron and Kenny's mediation steps.[43] In short, a vascular factor M was considered a mediator of the effect of MAP (X) on structural OCT (Y), if the following were true in linear regression analysis:

a) X was a significant predictor of Y (Y~X).
b) X was a significant predictor of M (M~X).
c) When M was added to the model (Y~X+M), M was a significant predictor of Y and the significance of X as a predictor of Y was reduced.

We verified these findings by using the Sobel test for indirect effects. Mediation analysis was performed separately for the low BP group together with the controls, the treated AHT group together with the controls, and the untreated AHT group together with the controls. RBF, RVR, and AR were examined as potential mediators.

All analyses were performed using R (version 3.3.3; R Foundation for Statistical Computing, Vienna, Austria) and SPSS (version 26; IBM Corp., Armonk, NY). A *P* value of 0.05 or less was considered statistically significant.

5.4. Results

In total, 96 eyes of 96 subjects fulfilled all the criteria and were included in the analysis. Table 1 displays the characteristics of the population, stratified by BP status. Sex and body mass index (BMI) were significantly different between groups, aside from BP. As expected, the low BP group comprised almost exclusively females, whereas higher BMI was present in the hypertensive groups.[44,45] Other factors that could affect the comparisons, such as age, IOP, spherical equivalent (SEQ), and ONH area, were similar between groups.

Table 1. Characteristics of the Study Population

	Group 1 (Low BP)	Group 2 (Normal BP)	Group 3 (Treated AHT)	Group 4 (Untreated AHT)	*P* Value
Group size *(N)*	31	21	26	18	
Age (y), mean (SD)	56.1 (4.4)	55.9 (4.7)	56.4 (4.8)	57.2 (4.6)	0.81
Sex, % female	93.5	47.6	42.3	44.4	**<0.001**
SBP (mm Hg), mean (SD)	106 (9)	126 (6)	142 (18)	159 (22)	**<0.001**
DBP (mm Hg), mean (SD)	66 (6)	79 (6)	86 (11)	99 (8)	**<0.001**
BMI (kg · m^{-2}), median (IQR)	22.1 (21.2 to 24.3)	23.3 (22.1 to 26.5)	26.9 (24.7 to 29.8)	27.3 (24.3 to 28.4)	**<0.001**
Smoking, % exposed	22.6	38.1	30.8	38.9	0.57
IOP (mm Hg), mean (SD)	13.9 (3.0)	13.2 (3.1)	14.3 (3.0)	14.6 (3.7)	0.56
SEQ (D), mean (SD)	−0.10 (1.41)	0.27 (1.67)	−0.23 (1.55)	−0.68 (1.69)	0.31
ONH area (mm^2), median (IQR)	1.89 (1.69 to 2.24)	1.96 (1.71 to 2.20)	1.94 (1.72 to 2.31)	2.00 (1.78 to 2.29)	0.75

5.4.1. Structural Metrics

Table 2 and Figure 3 present the comparison of structural OCT metrics across the four BP groups (recruitment BP definitions). Adjusted post hoc comparisons revealed that, compared to the controls, GCIPL was significantly thinner in the low BP group (P_{adj} = 0.013), the treated AHT group (P_{adj} = 0.007), and the untreated AHT group (P_{adj} = 0.007). The mRNFL was also thinner, but this was only significant for the treated AHT group (P_{adj} = 0.001). Interestingly, mRNFL in treated hypertensives was even significantly thinner than in

untreated hypertensives (P_{adj} = 0.033). Figure 3 shows the characteristic (inverse) U shape for the macular OCT metrics. There was no clear effect of BP group on the mean pRNFL, the NRR area, or the VCDR. However, treated hypertensives had a thinner temporal pRNFL (P_{adj} = 0.045) than normotensives. Also, inferior pRNFL was borderline thinner in subjects

Table 2. Structural OCT Metrics as a Function of BP Status

	Group 1 (Low BP)	Group 2 (Normal BP)	Group 3 (Treated AHT)	Group 4 (Untreated AHT)	*P* Value
GCIPL (µm), mean (SD)	53.6 (2.7)	56.2 (3.0)	53.4 (3.3)	53.1 (2.5)	**0.002**
mRNFL (µm), mean (SD)	37.7 (3.3)	39.8 (3.4)	36.0 (2.8)	38.7 (3.4)	**0.001**
Total pRNFL (µm), mean (SD)	99.4 (8.2)	103.1 (10.1)	96.9 (9.2)	100.3 (8.8)	0.14
Temporal pRNFL (µm), mean (SD)	71.8 (10.5)	74.0 (8.1)	65.5 (9.5)	72.6 (15.3)	**0.038**
Superior pRNFL (µm), mean (SD)	119.6 (14.7)	124.1 (16.7)	119.5 (13.5)	126.1 (16.6)	0.36
Nasal pRNFL (µm), mean (SD)	82.2 (11.2)	80.6 (14.1)	81.4 (11.4)	80.6 (14.0)	0.96
Inferior pRNFL (µm), mean (SD)	124.5 (12.9)	134.0 (13.3)	122.7 (14.3)	121.5 (15.7)	**0.019**
NRR area (mm^2), median (IQR)	1.43 (1.21 to 1.63)	1.37 (1.27 to 1.74)	1.35 (1.18 to 1.64)	1.52 (1.41 to 1.69)	0.50
VCDR, median (IQR)	0.54 (0.42 to 0.60)	0.49 (0.39 to 0.55)	0.47 (0.42 to 0.60)	0.51 (0.39 to 0.59)	0.82

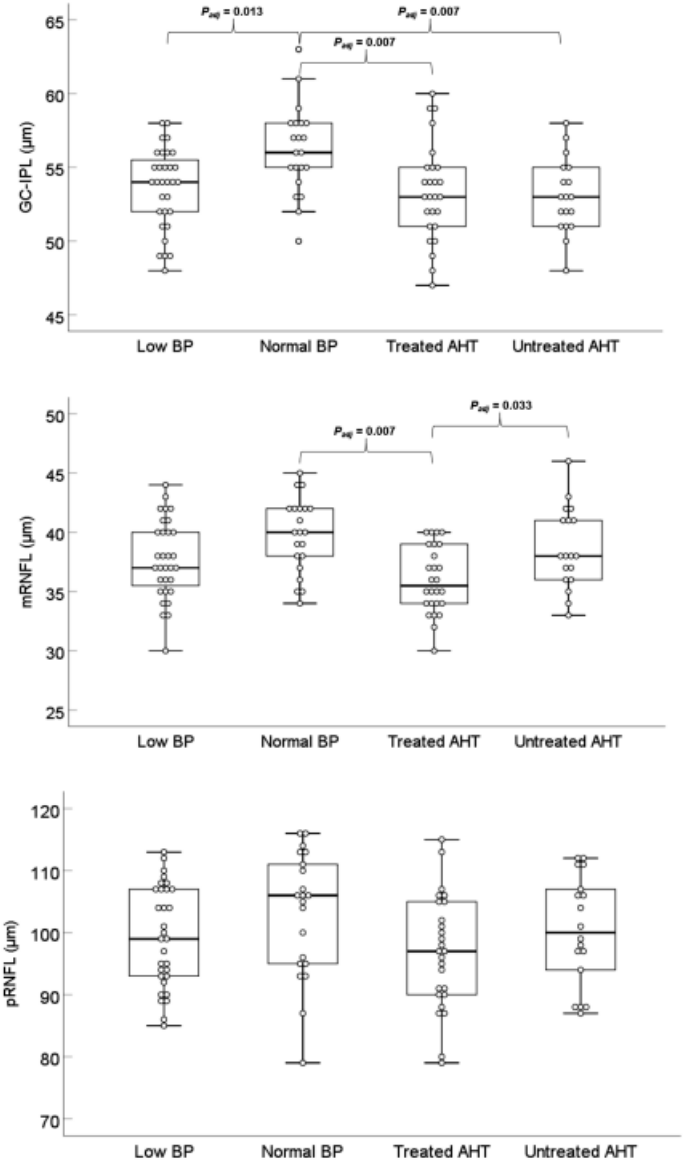

Figure 3. GCIPL, mRNFL, and pRNFL as a function of BP status. Significant differences after post hoc comparisons (adjusted for multiple testing) are marked. The thicker layers observed in the control group (normal BP) than in the low BP or AHT groups create a characteristic (inverse) U shape.

with low BP (P_{adj} = 0.083) and clearly thinner in both treated and untreated hypertensives (P_{adj} = 0.034 and 0.033, respectively). Sex, SEQ, and BMI did not confound any of the associations (all *P* values > 0.05) and this was still true after the omission of any group from the analysis.

The structural comparisons using the 5th/95th percentile definition cutoffs are presented in Supplementary Tables S4 (SBP) and S5 (DBP). Associations were consistent and adjusted significances remained essentially unchanged.

5.4.2. Vascular Metrics

Figure 4 displays the vascular outcome variables (RBF, RVR, and AR) as a function of BP status (recruitment BP definitions). For reference, Table 3 presents RPP, hematocrit, and the components measured by fundus imaging (CRAE, CRVE) and OCTA (FD) that were used in the calculation of the vascular outcome variables.

There were differences in RBF between groups (*P* = 0.034), but after adjusting for multiple comparisons RBF was only significantly lower in the low BP group when compared to the untreated AHT group (P_{adj} = 0.043). RVR was also different between groups ($P = 9.0 \cdot 10^{-9}$), with the additional presence of a larger variance in the treated AHT group (Levene's test: *P* = 0.002). With regards to AR, the unequal variances were also statistically significant (Levene's test: *P* = 0.0002), showing that, unlike any other group, treated hypertensives could have either a large or a small AR. As can be better seen in Figure 5 and Supplementary Table S6, the low BP group had a significantly smaller AR than the control group, regardless of AR quantile compared. Conversely, the untreated hypertensives had a significantly larger AR than the control group, regardless of quantile compared. However, there was a mixed response in the treated AHT group: the AR was significantly smaller than that of the controls for small quantiles, although it was similar or larger for larger quantiles. In addition, correlation analysis within the treated AHT group revealed that the smaller AR quantiles corresponded to the lowest MAP values (Pearson's r = 0.45, *P* = 0.020), that is., to the most intensively controlled hypertensives. Again, sex, SEQ, and BMI did not confound these associations. The use of the fifth/ninety-fifth percentile-based BP definitions resulted, again, in almost identical findings (data not shown).

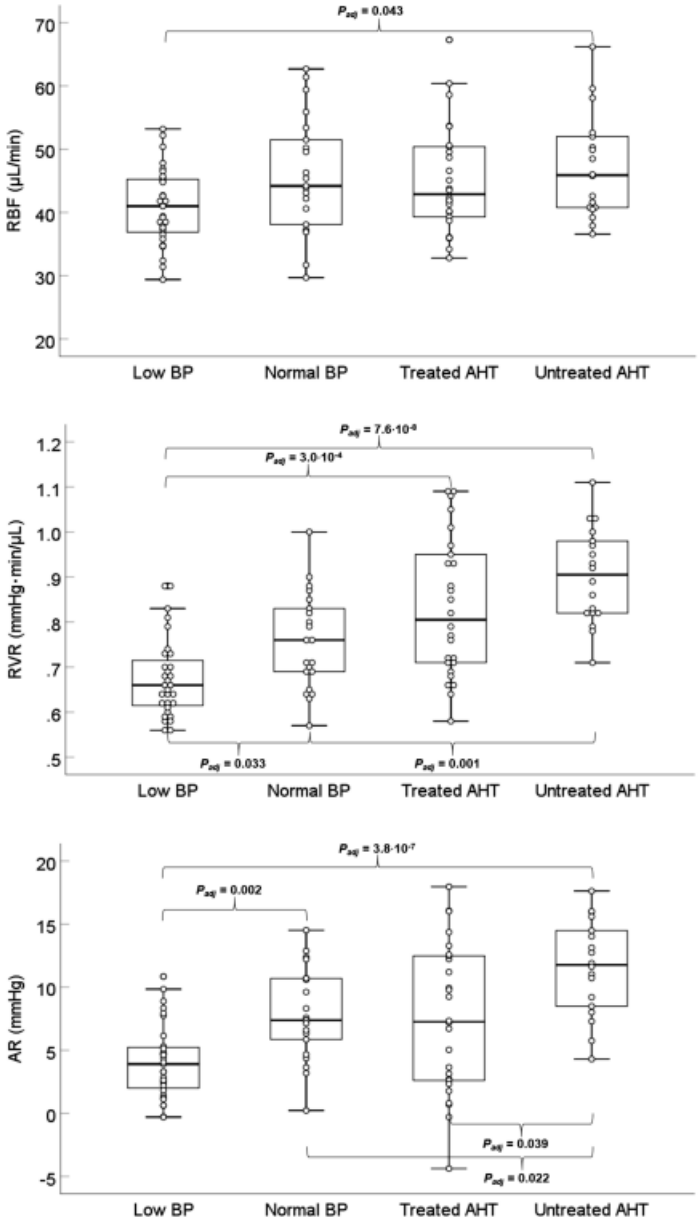

Figure 4. Absolute total RBF, RVR, and AR as a function of BP status. Significant differences after post hoc comparisons (adjusted for multiple testing) are marked. With increasing BP, RBF increases less than RVR, resulting in an autoregulation effect visible in the *first panel*. A statistically significant larger variability is observed for the AR of treated hypertensives (*third panel*), suggesting that subjects in this group can be very close or very far from the lower autoregulation limit.

Table 3. Components Used in the Calculation of Vascular Outcomes, as a Function of BP Status

	Group 1 (Low BP)	Group 2 (Normal BP)	Group 3 (Treated AHT)	Group 4 (Untreated AHT)	*P* Value
RPP (mm Hg), mean (SD)	27.2 (2.9)	33.8 (4.1)	36.6 (4.7)	42.0 (4.9)	**<0.001**
Hematocrit,* mean (SD)	0.408 (0.025)	0.428 (0.025)	0.427 (0.026)	0.441 (0.025)	**<0.001**
CRAE (µm), mean (SD)	172 (12)	162 (12)	154 (13)	147 (7)	**<0.001**
CRVE (µm), mean (SD)	228 (17)	228 (16)	229 (18)	222 (12)	0.49
OCT-A FD, mean (SD)	1.626 (0.005)	1.626 (0.007)	1.625 (0.006)	1.626 (0.006)	0.85

* Data from Lifelines. Individualized values adjusted for age, sex, and BP status were used.

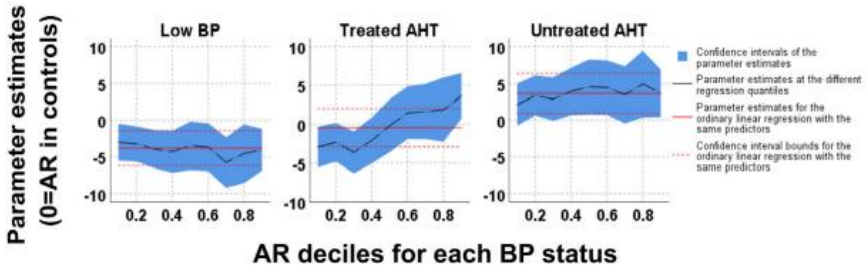

Figure 5. Quantile regression models for AR at each BP status. Parameter estimates (y-axis) represent the relative AR (compared to controls) for every AR decile (x-axis). Low BP individuals (*left panel*) have a smaller AR than controls ($y < 0$), whereas individuals with untreated AHT (*right panel*) have a larger AR than controls ($y > 0$). Individuals with treated AHT (*middle panel*) have a smaller AR only when intensively treated (leftmost deciles).

5.4.3. Mediation Analysis

Results from mediation analysis regarding the effect of BP status on GCIPL are presented in Table 4 (recruitment BP definitions). RBF was mediating the association of GCIPL with BP within the combined low BP group and controls, while RVR was mediating the same association within the combined untreated AHT group and controls. RVR and AR were both independently mediating the association of GCIPL with BP within the combined treated AHT group and controls. In the complete model (GCIPL~MAP+RVR+AR), which accounts for the covariance between RVR and AR, the opposite, real effect of AR became visible, that is, small AR was associated with thinner GCIPL (see Discussion section). We did not observe any vascular mediation for the effect of BP status on RNFL metrics.

Table 4. Effect of BP Status on GCIPL: Mediation Analysis

	Controls + Low BP (Group 2 + Group 1)		Controls + Treated AHT (Group 2 + Group 3)		Controls + Untreated AHT (Group 2 + Group 4)	
	Effect	***P***	**Effect**	***P***	**Effect**	***P***
Mediation Step 1						
GCIPL ~ MAP	$b_{MAP} = 0.09$	0.052	$b_{MAP} = -0.10$	**0.043**	$b_{MAP} = -0.07$	**0.032**
Mediation Step 2						
RBF ~ MAP	$b_{MAP} = 0.27$	**0.020**				
RVR ~ MAP			$b_{MAP} = 0.005$	**0.008**	$b_{MAP} = 0.005$	**0.0003**
AR ~ MAP			$b_{MAP} = 0.17$	**0.015**		
Mediation Step 3						
GCIPL ~ MAP + RBF	$b_{MAP} = 0.05$	0.30				
	$b_{RBF} = 0.16$	**0.003**				
GCIPL ~ MAP + RVR			$b_{MAP} = -0.04$	0.42	$b_{MAP} = -0.03$	0.51
			$b_{RVR} = -11.87$	**0.001**	$b_{RVR} = -10.23$	**0.022**
GCIPL ~ MAP + AR			$b_{MAP} = -0.06$	0.21		
			$b_{AR} = -0.21$	**0.042**		
GCIPL ~ MAP + RVR + AR			$b_{MAP} = -0.04$	0.40		
			$b_{RVR} = -27.37$	**0.001**		
			$b_{AR} = 0.47$	**0.032**		
Sobel test	0.059		RVR: **0.041**; AR: 0.095		**0.031**	

Supplementary Tables S7 and S8 present the results of the same mediation analysis, using the fifth/ninety-fifth percentile-based BP definitions. Interestingly, similar associations, but with

slightly different patterns were present in the GCIPL-SBP analysis (Table S7) versus the GCIPL-DBP analysis (Table S8). Although low RBF can account for the association of low SBP with GCIPL thinning, it does not account as much for the association of low DBP with GCIPL thinning. In addition, in the AHT groups, DBP is a more important determinant of RVR and AR, compared to SBP.

5.5. Discussion

In this study, we reported three main findings. In the first part of the analysis (structural OCT analysis) we uncovered an inverse U-shaped association between blood pressure status and OCT metrics (GCIPL and RNFL), with both low and high blood pressure being associated with thinning of the inner retinal layers. In the second part of the analysis (analysis of vascular metrics), we showed that, despite the existence of retinal blood flow autoregulation, only a small autoregulatory reserve is present in individuals with low blood pressure, as well as in individuals with intensively treated arterial hypertension. In the last part of the analysis (mediation analysis) we showed that this compromised capacity for retinal blood flow regulation explains (mediates) the effect of blood pressure status on the GCIPL.

5.5.1. Low Blood Pressure

This is, to our knowledge, the first study to uncover an association between low BP and thinning of the inner retina in ophthalmologically healthy subjects. This relationship and its vascular mediation were more pronounced for the GCIPL, which has been shown to be the main layer of early NTG manifestation.[46] In addition, the association was entirely mediated by RBF (no effect of sex, BMI, or other confounders in our population).

Indeed, we have previously shown that LARL for subjects without AHT corresponds to a realistic SBP/DBP of ~105/65 mmHg (or even higher if IOP is above average).[38] Because, in the present study, the average BP reading for the low BP group was at 106/66 mmHg, our finding that this group had a borderline lower RBF (Fig. 4, Table 4) and a considerably smaller AR (Fig. 5, Supplementary Table S6) than controls is in line with our estimations and the general concept of autoregulation.

Population studies have failed to report this association between low BP and GCIPL thickness, possibly because of the implementation of linear models, but an explanation due to differences in genetic background cannot be excluded.[33,34] However, nonlinear models were used is studies with glaucoma as the outcome measure and, in line with our findings, there is evidence for the existence of increased glaucoma risk with low, usually diastolic or nocturnal, BP.[7–10,12,47,48] It is unknown why low DBP appears to be more frequently associated with glaucoma risk than low SBP.[9,10,12,47] In a study linking nocturnal DBP dips with glaucoma progression, Kwon *et al*. argued that DBP might better reflect retinal tissue perfusion, which mainly occurs during diastole.[49] That said, this finding is not consistent and could be ethnicity-dependent, since the Barbados Eye Study and the Early Manifest Glaucoma Trial (EMGT) reported that lower baseline SBP increases the risk for glaucoma incidence or progression.[7,8] In our study, daytime mean RBF could not account for GCIPL thinning associated with low DBP, further pointing towards the need to study the specific properties of blood flow during diastole or during DBP dips.

An intriguing observation is that some studies that use BP binning report unfavorable glaucoma outcomes already manifesting at a population level at apparently normal BP values (e.g., SBP ≤ 125 mmHg in the EMGT or the first quartile of DBP in the Singapore Malay Eye Study).[7,9] The Los Angeles Latino Eye study found that a trend for increased glaucoma prevalence starts at DBP ≤ 71 mmHg, but reported strong evidence only for DBP ≤ 61 mmHg, which corresponds approximately to the fifth DBP percentile in our population.[10] In our study, we used two different BP binning definitions: one using prospective recruitment criteria based on multiple previous measurements consistently outside the first and ninth BP deciles and one using the standard, cross-sectional fifth and ninety-fifth BP percentile cutoffs. Results were insensitive to the definition chosen and therefore could help interpret the findings of these population studies.

An interesting, albeit not unexpected, observation regarding the low BP group is the fact that it predominantly comprises females whose BMI is on the lower side. This description matches the central traits of a particular phenotype, sometimes referred to as ‘Flammer syndrome’, which has been shown to be associated with NTG, likely owing to deficient RBF or vascular dysregulation.[50]

As also expected, the same group was characterized, on a population basis, by lower hematocrit values. Hematocrit affects blood viscosity, which, in turn, affects RVR and RBF,

something that has been accounted for and validated in our estimations.[38,51] Not accounting for the correlation of BP with blood viscosity would erroneously underestimate RBF in the low BP group and overestimate RBF in the hypertensive groups. As such, the viscosity-related indirect effect on structural OCT measurements is actually incorporated in the complete vascular mediation effect presented in Table 4. It is a matter of debate in cardiovascular medicine whether BP is actively modified to compensate for this general effect of hematocrit on organ blood flow.[52] Hyperviscosity has been linked in the past to increased glaucoma risk, but, in our study, we did not find a protective effect of low hematocrit for the low BP group.[53-56] We hypothesize that, due to the stratification of the groups according to BP status and the range of BP examined, BP is the dominant player in our population and a protective effect of hypoviscosity, if any, is masked by the detrimental effect of low BP. Future studies with appropriate, controlled design are needed to elucidate this ambiguity.

5.5.2. Hypertension

Despite a slightly higher RBF and a considerably higher AR (Figs. 4 and 5), untreated hypertensives had thinner GCIPL, which has also been shown to be the location of first progression in glaucoma patients with AHT.[46] This was mediated by RVR (Table 4), i.e., the negative effect of increased BP to the GCIPL is explained by increased vascular resistance (but not by reduced blood flow - see below). Nevertheless, it was the treated AHT group that exhibited the most pronounced thinning and this was present in the majority of structural OCT metrics (GCIPL, mRNFL, temporal pRNFL, inferior pRNFL). For this group, GCIPL thinning was independently mediated by RVR and AR (Fig. 5, Table 4). In the univariable models, large RVR and large AR were both associated with thinner GCIPL, because of substantial covariance. After controlling for the confounding effect of RVR, small AR was associated with thinner GCIPL. This suggests that, in treated AHT, a combination of increased resistance and being close to the autoregulatory tipping point explain the negative effect to the GCIPL.

GCIPL thinning without a decrease in RBF seems counterintuitive. However, even when total RBF is largely unaffected, increased RVR results in increased blood velocity (i.e., reduced transit time), shunting of flow, and reduced capillary density.[57,58] This could affect red blood cell distribution and retinal oxygen extraction. Smaller AR was additionally present in

intensively treated subjects (Fig. 4C, Fig. 5, Supplementary Table S6), which could mimic low BP and lead to hypoperfusion of the RGCs. In this regard, our results reflect a possible effect of the combined rightward shift of the autoregulation curve (due to atherosclerosis and arteriosclerosis) and the variations of the measured RPP (Fig. 2), due to BP fluctuations throughout the day. Last, chronic AHT also results in endothelial dysfunction and, therefore, impaired autoregulation.[59]

A number of previous studies have also shown an effect of AHT on GCIPL and RNFL thickness.[15,29–32] However, some population-based studies did not detect this relationship.[33,34] Again, study design and analysis methods seem to be the most likely explanations for this discrepancy. Regarding glaucoma risk, the role of AHT is controversial. Most evidence points towards at least some benefit of timely AHT treatment, possibly due to the prevention of microvascular damage, in combination with a slight IOP lowering.[18,60] However, it has been suggested that aggressive treatment of AHT, resulting in low DBP, could negatively affect glaucoma and we observed a structural effect with the same direction in this healthy population.[14] The confounding contribution of individual antihypertensive medications, whether neuroprotective or detrimental, remains inconclusive.[15–19]

In all, the existence of thinner GCIPL in both low BP and AHT creates the characteristic inverse U-shaped association. Although, theoretically, structural thinning could be attributed to thinner and sparser vasculature contributing to the OCT layer segmentation, it is highly unlikely that this U-shaped association is artificial for two reasons. Firstly, the low BP group had significantly lower RVR, due to significantly broader vascular caliber. This would have led to overestimation, if anything, rather than underestimation of structural metrics. Therefore, caliber-related segmentation inaccuracies cannot explain this U-shaped association. Second, associations remained identical before and after compensating for these anatomic confounders in a recent study on antihypertensive medication.[15] The effect of image magnification is also likely negligible, since only mildly ametropic eyes (-3 D to +3 D, see 5.3.1) were included and SEQ was similar between groups. Indeed, using the SEQ values reported in Table 1, it can be estimated that the error in the observed differences attributed to magnification is 0.6% to 1.5%.[61] SEQ was also never significant when adjusted for as a potential confounder, further corroborating this claim.

5.5.3. Study Strengths and Limitations

The main strength of this study was the strict selection process which allowed us to look at the true extremes of BP. This reduces the noise that usually characterizes larger population studies and results in indirect loss of power. In addition, our linearity-free assumptions and the categorizing of BP (rather than considering it as a continuous variable) allowed us to differentiate between BP status and uncover a U-shaped association that was previously elusive. Last, to our knowledge, this study is the first to provide a rigorous explanation of the differential effect of BP status on retinal structure, by directly linking it to total RBF and its autoregulation.

With regards to limitations, there is certainly error associated with RBF, RVR, and AR estimations in the second and third part of our study. In the absence of a gold standard way to quantify these variables, it is difficult to predict the deviation from their actual values. Overall, the physiological component of these variables can be seen in our results and the range of values we report is in very good agreement with that reported in Doppler OCT studies.[62–67] In addition, we have previously shown, in an independent population, that these outcomes strongly correlate with *in vivo* blood flow metrics, as assessed by LSFG.[38] Compared to Doppler OCT or LSFG, our approach has the advantage of using more reproducible imaging techniques to quantify vascular caliber and, most importantly, allows for estimation of autoregulation limits. However, it is likely inferior in estimating blood velocity, since velocities are inferred from the calculation of pressures, calibers, viscosities, and branching complexities (see Table 3), rather than directly measured. Combining these methods could therefore further finetune estimations.

It should be also noted that our approach provides information on the effect of static RBF autoregulation, but it is possible that BP status also results in impairment of the autoregulatory latency, that is, dynamic autoregulation, which our study cannot evaluate. As such, our results might only be part of a bigger underlying effect. Similarly, the absence of 24-hour BP monitoring could also result in underestimation of the true effect, since, as already mentioned, individuals in the risk groups might also be prone to nocturnal hypotension.[12] We postulate that these unobserved variables might explain why structural differences were more pronounced than differences in RBF. Because of the cross-sectional nature of our study, absence of data on the first occurrence of AHT is a limitation. However,

our threshold of an at least one-year-old diagnosis, together with the selection procedure using multiple previous visits from another database, ensured no newly-diagnosed cases (almost all cases had been diagnosed before at least three years). Last, our population was predominantly Caucasian; it is to be determined whether the results can be generalized to other ethnicities.

5.5.4. Further Considerations

From a theoretical standpoint, there exists a point in the predisease time course when the very first vascular deficits or the very first structural deficits manifest. A subsequent causal cascade of events would then result in further mutually mediated vascular and structural deterioration, sometimes leading to a glaucoma diagnosis. In this regard, one novelty of this study lies in demonstrating that interdependent structural and vascular deficits related to a long-debated cardiovascular risk factor (especially low BP) can even be traced back to whom we perceive as ophthalmologically healthy subjects. Therefore, while this cross-sectional study cannot fully resolve the 'chicken-egg' dilemma (we showed that vascular deficits are present without glaucoma, but not necessarily without smaller structural deficits), it provides evidence towards a possible pathophysiological mechanism that warrants further investigation.

Related to that, a similar mediation analysis approach has revealed that structural deficits mediate, in turn, the effect of vascular deficits on glaucoma risk itself.[68] Interestingly, the structural deficits that we report were much more prominent on the macular OCT scans than the ONH scans. It is possible that the initial spatial manifestation of glaucomatous-like damage attributed to vascular factors (NTG phenotype) differs from that of high-tension glaucoma.[46] However, the subject matter is much more complex, since it is beyond doubt that the pathology of NTG itself is still highly dependent on IOP levels and thus vascular etiology is likely only secondary.[69] Therefore, with the existing evidence, vascular factors should be regarded as additional risk factors, rather than primary driving forces in glaucomatous pathogenesis. The key question for future research is which vascular outcomes can identify increased vulnerability to structural/functional deficit onset and progression.

We would like to stress here that, since there are benefits to intensive BP control with regards to cardiovascular disease, our results should only be seen as such and should not be

considered as a case for milder treatment of AHT in general.[70,71] However, since a J- or U-shaped effect is reported in both fields when intensive treatment becomes too intensive, it could be a starting point for discussion with cardiologists in individual cases where, for example, glaucoma continues to deteriorate despite adequate IOP control.[72]

In conclusion, on examination of structural metrics, we uncovered a previously elusive, inverse U-shaped thinning of the GCIPL and RNFL associated with both tails of the blood pressure distribution and with intensive treatment of arterial hypertension, in ophthalmologically healthy individuals. Upon subsequent examination of vascular metrics, we additionally found that GCIPL thinning was differentially associated with reduced retinal blood flow, increased vascular resistance, or insufficient static autoregulatory capacity, depending on blood pressure status. It remains to be seen whether these defects could explain the recurring epidemiological finding of increased glaucoma risk in certain population subgroups, especially subjects with nocturnal blood pressure dipping or intensively treated arterial hypertension. Longitudinal studies are needed to examine this postulation.

5.6. References

1. Schuman JS, Hee MR, Puliafito CA, et al. Quantification of nerve fiber layer thickness in normal and glaucomatous eyes using optical coherence tomography. *Arch Ophthalmol*. 1995;113(5):586-596.

2. Garway-Heath DF, Crabb DP, Bunce C, et al. Latanoprost for open-angle glaucoma (UKGTS): a randomised, multicentre, placebo-controlled trial. *Lancet*. 2015;385(9975):1295-1304.

3. Heijl A, Leske MC, Bengtsson B, et al. Reduction of intraocular pressure and glaucoma progression: results from the Early Manifest Glaucoma Trial. *Arch Ophthalmol*. 2002;120(10):1268-1279.

4. Drance SM. Some factors in the production of low tension glaucoma. *Br J Ophthalmol*. 1972;56(3):229-242.

5. Flammer J, Orgül S, Costa VP, et al. The impact of ocular blood flow in glaucoma. *Prog Retin Eye Res*. 2002;21(4):359-393.

6. Hayreh SS. Blood flow in the optic nerve head and factors that may influence it. *Prog Retin Eye Res*. 2001;20(5):595-624.

7. Leske MC, Heijl A, Hyman L, et al. Predictors of long-term progression in the early manifest glaucoma trial. *Ophthalmology*. 2007;114(11):1965-1972.

8. Leske MC, Wu S-Y, Hennis A, Honkanen R, Nemesure B, BESs Study Group. Risk factors for incident open-angle glaucoma: the Barbados Eye Studies. *Ophthalmology*. 2008;115(1):85-93.

9. Zheng Y, Wong TY, Mitchell P, Friedman DS, He M, Aung T. Distribution of Ocular Perfusion Pressure and Its Relationship with Open-Angle Glaucoma: The Singapore Malay Eye Study. *Invest Ophthalmol Vis Sci*. 2010;51(7):3399.

10. Memarzadeh F, Ying-Lai M, Chung J, Azen SP, Varma R, Los Angeles Latino Eye Study Group. Blood pressure, perfusion pressure, and open-angle glaucoma: the Los Angeles Latino Eye Study. *Invest Ophthalmol Vis Sci*. 2010;51(6):2872-2877.

11. Ramdas WD, Wolfs RCW, Hofman A, de Jong PTVM, Vingerling JR, Jansonius NM. Ocular perfusion pressure and the incidence of glaucoma: real effect or artifact? The Rotterdam Study. *Invest Ophthalmol Vis Sci*. 2011;52(9):6875-6881.

12. Bowe A, Grünig M, Schubert J, et al. Circadian Variation in Arterial Blood Pressure and Glaucomatous Optic Neuropathy—A Systematic Review and Meta-Analysis. *Am J Hypertens*. 2015;28(9):1077-1082.

13. Zhao D, Cho J, Kim MH, Guallar E. The association of blood pressure and primary open-angle glaucoma: a meta-analysis. *Am J Ophthalmol*. 2014;158(3):615-627.e9.

14. Topouzis F, Wilson MR, Harris A, et al. Association of open-angle glaucoma with perfusion pressure status in the Thessaloniki Eye Study. *Am J Ophthalmol*. 2013;155(5):843-851.

15. Chong RS, Chee M-L, Tham Y-C, et al. Association of Antihypertensive Medication with Retinal Nerve Fiber Layer and Ganglion Cell-Inner Plexiform Layer Thickness. *Ophthalmology*. 2020;31:S0161-6420(20)30739-9.

16. Müskens RPHM, de Voogd S, Wolfs RCW, et al. Systemic antihypertensive medication and incident open-angle glaucoma. *Ophthalmology*. 2007;114(12):2221-2226.

17. Zheng W, Dryja TP, Wei Z, et al. Systemic Medication Associations with Presumed Advanced or Uncontrolled Primary Open-Angle Glaucoma. *Ophthalmology*. 2018;125(7):984-993.

18. Horwitz A, Klemp M, Jeppesen J, Tsai JC, Torp-Pedersen C, Kolko M. Antihypertensive Medication Postpones the Onset of Glaucoma: Evidence From a Nationwide Study. *Hypertension*. 2017;69(2):202-210.

19. Pappelis K, Loiselle AR, Visser S, Jansonius NM. Association of Systemic Medication Exposure With Glaucoma Progression and Glaucoma Suspect Conversion in the Groningen Longitudinal Glaucoma Study. *Invest Ophthalmol Vis Sci*. 2019;60(14):4548-4555.

20. Asefa NG, Neustaeter A, Jansonius NM, Snieder H. Autonomic Dysfunction and Blood Pressure in Glaucoma Patients: The Lifelines Cohort Study. *Invest Ophthalmol Vis Sci*. 2020;61(11):25.

21. Huang D, Swanson EA, Lin CP, et al. Optical coherence tomography. *Science*. 1991;254(5035):1178-1181.

22. Jia Y, Tan O, Tokayer J, et al. Split-spectrum amplitude-decorrelation angiography with optical coherence tomography. *Opt Express*. 2012;20(4):4710.

23. Wojtkowski M, Leitgeb R, Kowalczyk A, Bajraszewski T, Fercher AF. In vivo human retinal imaging by Fourier domain optical coherence tomography. *J Biomed Opt*. 2002;7(3):457.

24. Yarmohammadi A, Zangwill LM, Diniz-Filho A, et al. Relationship between Optical Coherence Tomography Angiography Vessel Density and Severity of Visual Field Loss in Glaucoma. *Ophthalmology*. 2016;123(12):2498-2508.

25. Yoshioka T, Song Y, Kawai M, et al. Retinal blood flow reduction in normal-tension glaucoma with single-hemifield damage by Doppler optical coherence tomography. *Br J Ophthalmol*. 2021;105(1):124-130.

26. Hwang JC, Konduru R, Zhang X, et al. Relationship among visual field, blood flow, and neural structure measurements in glaucoma. *Invest Ophthalmol Vis Sci*. 2012;53(6):3020-3026.

27. Riva CE, Grunwald JE, Petrig BL. Autoregulation of human retinal blood flow. An investigation with laser

Doppler velocimetry. *Invest Ophthalmol Vis Sci*. 1986;27(12):1706-1712.

28. He Z, Vingrys AJ, Armitage JA, Bui BV. The role of blood pressure in glaucoma. *Clin Exp Optom*. 2011;94(2):133-149.

29. Lee SH, Lee WH, Lim HB, Jo YJ, Kim JY. THICKNESSES OF CENTRAL MACULAR, RETINAL NERVE FIBER, AND GANGLION CELL INNER PLEXIFORM LAYERS IN PATIENTS WITH HYPERTENSION. *Retina*. 2019;39(9):1810-1818.

30. Lim HB, Lee MW, Park JH, Kim K, Jo YJ, Kim JY. Changes in Ganglion Cell–Inner Plexiform Layer Thickness and Retinal Microvasculature in Hypertension: An Optical Coherence Tomography Angiography Study. *Am J Ophthalmol*. 2019;199:167-176.

31. Akay F, Gündoğan FC, Yolcu U, Toyran S, Tunç E, Uzun S. Retinal structural changes in systemic arterial hypertension: an OCT study. *Eur J Ophthalmol*. 2016;26(5):436-441.

32. Sahin OZ, Sahin SB, Ayaz T, et al. The impact of hypertension on retinal nerve fiber layer thickness and its association with carotid intima media thickness. *Blood Press*. 2015;24(3):178-184.

33. Tham Y-C, Chee ML, Dai W, et al. Profiles of Ganglion Cell-Inner Plexiform Layer Thickness in a Multi-Ethnic Asian Population. *Ophthalmology*. 2020;127(8):1064-1076.

34. Koh VT, Tham Y-C, Cheung CY, et al. Determinants of Ganglion Cell–Inner Plexiform Layer Thickness Measured by High-Definition Optical Coherence Tomography. *Invest Ophthalmol Vis Sci*. 2012;53(9):5853.

35. Ende MY van der, van der Ende MY, Hartman MHT, et al. The LifeLines Cohort Study: Prevalence and treatment of cardiovascular disease and risk factors. *Int J Cardiol*. 2017;228:495-500.

36. Luft N, Wozniak PA, Aschinger GC, et al. Measurements of Retinal Perfusion Using Laser Speckle Flowgraphy and Doppler Optical Coherence Tomography. *Invest Ophthalmol Vis Sci*. 2016;57(13):5417-5425.

37. Heikka T, Cense B, Jansonius NM. Retinal layer thicknesses retrieved with different segmentation algorithms from optical coherence tomography scans acquired under different signal-to-noise ratio conditions. *Biomed Opt Exp*. 2020;11(12):7079.

38. Pappelis K, Choritz L, Jansonius N. Microcirculatory model predicts blood flow and autoregulation range in the human retina: in vivo investigation with Laser Speckle Flowgraphy. *Am J Physiol Heart Circ Physiol*. 2020;319(6):H1253-1273.

39. Pappelis K, Jansonius NM. Quantification and Repeatability of Vessel Density and Flux as Assessed by Optical Coherence Tomography Angiography. *Transl Vis Sci Technol*. 2019;8(3):3.

40. Al-Nosairy KO, Prabhakaran GT, Pappelis K, Thieme H, Hoffmann MB. Combined Multi-Modal Assessment of Glaucomatous Damage With Electroretinography and Optical Coherence Tomography/Angiography. *Transl Vis Sci Technol*. 2020;9(12):7.

41. Knudtson MD, Lee KE, Hubbard LD, Wong TY, Klein R, Klein BEK. Revised formulas for summarizing retinal vessel diameters. *Curr Eye Res*. 2003;27(3):143-149.

42. Takahashi T, Nagaoka T, Yanagida H, et al. A mathematical model for the distribution of hemodynamic parameters in the human retinal microvascular network. *J Biorheol*. 2009;23(2):77-86.

43. Baron RM, Kenny DA. The moderator-mediator variable distinction in social psychological research: conceptual, strategic, and statistical considerations. *J Pers Soc Psychol*. 1986;51(6):1173-1182.

44. Tigchelaar EF, Zhernakova A, Dekens JAM, et al. Cohort profile: LifeLines DEEP, a prospective, general population cohort study in the northern Netherlands: study design and baseline characteristics. *BMJ Open*.

2015;5(8):e006772.

45. Slagter SN, van Waateringe RP, van Beek AP, van der Klauw MM, Wolffenbuttel BHR, van Vliet-Ostaptchouk JV. Sex, BMI and age differences in metabolic syndrome: the Dutch Lifelines Cohort Study. *Endocr Connect*. 2017;6(4):278.

46. Marshall HN, Andrew NH, Hassall M, et al. Macular Ganglion Cell–Inner Plexiform Layer Loss Precedes Peripapillary Retinal Nerve Fiber Layer Loss in Glaucoma with Lower Intraocular Pressure. *Ophthalmology*. 2019;126(8):1119-1130.

47. Melgarejo JD, Lee JH, Petitto M, et al. Glaucomatous Optic Neuropathy Associated with Nocturnal Dip in Blood Pressure: Findings from the Maracaibo Aging Study. *Ophthalmology*. 2018;125(6):807-814.

48. Tielsch JM, Katz J, Sommer A, Quigley HA, Javitt JC. Hypertension, perfusion pressure, and primary open-angle glaucoma. A population-based assessment. *Arch Ophthalmol*. 1995;113(2):216-221.

49. Kwon J, Jo YH, Jeong D, Shon K, Kook MS. Baseline Systolic versus Diastolic Blood Pressure Dip and Subsequent Visual Field Progression in Normal-Tension Glaucoma. *Ophthalmology*. 2019;126(7):967-979.

50. Flammer J, Konieczka, Flammer AJ. The primary vascular dysregulation syndrome: implications for eye diseases. *EPMA J*. 2013;4(1):14.

51. Iwase T, Yamamoto K, Yanagida K, et al. Investigation of causes of sex-related differences in ocular blood flow in healthy eyes determined by laser speckle flowgraphy. *Sci Rep*. 2017;7(1):13878.

52. Atsma F, Veldhuizen I, de Kort W, van Kraaij M, Pasker-de Jong P, Deinum J. Hemoglobin level is positively associated with blood pressure in a large cohort of healthy individuals. *Hypertension*. 2012;60(4):936-941.

53. Klaver JH, Greve EL, Goslinga H, Geijssen HC, Heuvelmans JH. Blood and plasma viscosity measurements in patients with glaucoma. *Br J Ophthalmol*. 1985;69(10):765-70. .

54. Trope GE, Salinas RG, Glynn M. Blood viscosity in primary open-angle glaucoma. *Can J Ophthalmol*. 1987;22(4):202-204.

55. Cheng HC, Chan CM, Yeh SI, Yu JH, Liu DZ. The hemorheological mechanisms in normal tension glaucoma. *Curr Eye Res*. 2011;36(7):647-53.

56. Kim YK, Choi HJ, Jeoung JW, Park KH, Kim DM. Five-year incidence of primary open-angle glaucoma and rate of progression in health center-based Korean population: the Gangnam Eye Study. *PLoS One*. 2014;9(12):e114058.

57. Leskova W, Warar R, Harris NR. Altered Retinal Hemodynamics and Mean Circulation Time in Spontaneously Hypertensive Rats. *Invest Ophthalmol Vis Sci*. 2020;61(10):12.

58. Chua J, Chin CWL, Hong J, et al. Impact of hypertension on retinal capillary microvasculature using optical coherence tomographic angiography. *J Hypertens*. 2019;37(3):572-580.

59. Delles C, Michelson G, Harazny J, Oehmer S, Hilgers KF, Schmieder RE. Impaired endothelial function of the retinal vasculature in hypertensive patients. *Stroke*. 2004;35(6):1289-1293.

60. Klein BEK, Klein R, Knudtson MD. Intraocular pressure and systemic blood pressure: longitudinal perspective: the Beaver Dam Eye Study. *Br J Ophthalmol*. 2005;89(3):284-287.

61. Bengtsson B, Krakau CE. Correction of optic disc measurements on fundus photographs. *Graefes Arch Clin Exp Ophthalmol.* 1992;230(1):24-8.

62. Dai C, Liu X, Zhang HF, Puliafito CA, Jiao S. Absolute retinal blood flow measurement with a dual-beam

Doppler optical coherence tomography. *Invest Ophthalmol Vis Sci*. 2013;54(13):7998-8003.

63. Garhofer G, Werkmeister R, Dragostinoff N, Schmetterer L. Retinal Blood Flow in Healthy Young Subjects. *Invest Ophthalmol Vis Sci*. 2012;53(2):698.

64. Lee B, Novais EA, Waheed NK, et al. En Face Doppler Optical Coherence Tomography Measurement of Total Retinal Blood Flow in Diabetic Retinopathy and Diabetic Macular Edema. *JAMA Ophthalmol*. 2017;135(3):244-251.

65. Wang Y, Fawzi AA, Tan O, Zhang X, Huang D. Flicker-induced changes in retinal blood flow assessed by Doppler optical coherence tomography. *Biomed Opt Express*. 2011;2(7):1852-1860.

66. Srinivas S, Tan O, Wu S, et al. Measurement of retinal blood flow in normal Chinese-American subjects by Doppler Fourier-domain optical coherence tomography. *Invest Ophthalmol Vis Sci*. 2015;56(3):1569-1574.

67. Werkmeister RM, Schmidl D, Aschinger G, et al. Retinal oxygen extraction in humans. *Sci Rep*. 2015;5:15763.

68. Tham YC, Siantar RG, Cheung CY, et al. Relationships Between Retinal Vascular Caliber, Retinal Nerve Fiber Layer Thickness, and Glaucoma: A Mediation Analysis Approach. *Invest Ophthalmol Vis Sci*. 2016;57(8):3803-3809.

69. Anderson DR; Normal Tension Glaucoma Study. Collaborative normal tension glaucoma study. *Curr Opin Ophthalmol*. 2003;14(2):86-90.

70. Ettehad D, Emdin CA, Kiran A, et al. Blood pressure lowering for prevention of cardiovascular disease and death: a systematic review and meta-analysis. *Lancet*. 2016;387(10022):957-967.

71. 2018 ESC/ESH Guidelines for the management of arterial hypertension. *J Hypertens*. 2019;37(1):226.

72. Böhm M, Schumacher H, Teo KK, et al. Achieved diastolic blood pressure and pulse pressure at target systolic blood pressure (120-140 mmHg) and cardiovascular outcomes in high-risk patients: results from ONTARGET and TRANSCEND trials. *Eur Heart J*. 2018;39(33):3105-3114.

Chapter 6

BLOOD PRESSURE AND RETINAL OXYGENATION*

* Pappelis K, Jansonius NM. Retinal Oxygen Delivery and Extraction in Ophthalmologically Healthy Subjects With Different Blood Pressure Status. *Transl Vis Sci Technol*. 2022;11(2):9.

6.1. Abstract

Purpose: To compare retinal oxygen delivery (DO_2) and oxygen extraction (VO_2) in ophthalmologically healthy subjects with different blood pressure (BP) status.

Methods: In this case-control study, we prospectively included 93 eyes of 93 subjects (aged 50-65 years) from a Dutch cohort (n = 167,000) and allocated them to four groups (low BP, normal BP [controls], treated arterial hypertension [AHT], untreated AHT). We estimated vascular calibers from fundus images and fractal dimension from optical coherence tomography angiography scans. We combined calibers, fractal dimension, BP, and intraocular pressure measurements in a proxy of retinal blood flow (RBF), using a Poiseuille-based model. We measured arterial and venous oxygen saturations (S_aO_2, S_vO_2) with a scanning laser ophthalmoscope. We calculated the DO_2 and VO_2 from RBF, S_aO_2, and S_vO_2. We compared the DO_2 and VO_2 between groups and investigated the DO_2-VO_2 association.

Results: DO_2 and VO_2 were different between groups ($P = 0.009$, $P = 0.036$, respectively). In a post hoc analysis, the low BP group had lower DO_2 than the untreated AHT group ($P = 4.9 \cdot 10^{-4}$). The low BP group and the treated AHT group had a lower VO_2 than the untreated AHT group ($P = 0.021$ and $P = 0.034$, respectively). There was a significant DO_2-VO_2 correlation ($R_{obs} = 0.65$, $b_{obs} = 0.51$, $P = 2.4 \cdot 10^{-12}$). After correcting for shared measurement error, the slope was not significant.

Conclusions: The DO_2 and VO_2 were altered in ophthalmologically healthy subjects with different BP status. Future studies could elucidate whether these changes can explain the increased risk of ophthalmic pathologies in those subjects.

Translational relevance: Understanding the baseline interplay between BP, retinal perfusion, and oxygenation allows for improved evaluation of retinal disease manifestation.

6.2. Introduction

Blood pressure (BP) is implicated as a risk factor in the pathogenesis of several ophthalmic diseases, including leading causes of irreversible blindness, such as glaucoma, age-related macular degeneration, and diabetic retinopathy.[1,2] Although each disease is characterized by distinct, complex pathogenetic mechanisms, the implication of blood flow and tissue oxygenation is considered to be a common denominator.[3] However, to this day, our understanding of the influence of BP on the retinal oxygenation is largely incomplete.

It has long been known that the retina is a metabolically active tissue, thus prone to reduced oxygen (O_2) supply owing to hypoperfusion.[4,5] Retinal blood flow (RBF) is mostly responsible for the O_2 supply of the inner retinal layers through the superficial and deep capillary plexus.[6] By diffusion, RBF also has a modest O_2 contribution to the photoreceptors.[7] BP is a major determinant of RBF, but, at the same time, its transient and chronic effects are dampened by tight autoregulatory mechanisms and vascular wall remodeling, which buffer the O_2 volume delivered to the tissues (DO_2).[8-10] In addition, even when DO_2 is eventually altered, human body tissues, including the retina, are still able to control the extraction of O_2 volume (VO_2) from the circulation, up to a certain extent.[11-13] Consequently, it is difficult to a priori predict the effect of BP on retinal metabolism.

There is evidence that the concept of BP status could be more relevant to tissue oxygenation than BP alone, at least for certain ophthalmic diseases, such as glaucoma or ischemic optic neuropathy.[14-17] A low BP (especially when presented as nocturnal dipping) can directly lead to hypoperfusion, whereas a high BP can cause chronic damage to the endothelium, resulting in RBF dysregulation.[10,18] Moreover, antihypertensive treatment may or may not fully protect the tissue from ischemic damage. This factor would depend on disease stage, on the individual contribution of certain medications, or even on low BP targets.[19-22] The latter could bring the retinal vessels closer to their critical (lower) autoregulation limit, below which significant hypoperfusion may occur.[23-25]

Regardless, after the onset of any disease, it is almost impossible to disentangle the temporal relationship between perfusion deficits related to BP status and tissue apoptosis. Impaired oxygenation could simultaneously be the cause (decreased supply) and consequence (decreased demand) of cellular death. Therefore, to understand the involvement of BP in

retinal disease, it is important, as a starting point, to establish how chronic BP status affects the oxygenation of the otherwise healthy retina.

The aim of this study was to compare absolute retinal O_2 delivery and extraction in ophthalmologically healthy subjects with low BP, normal BP (controls), treated arterial hypertension (AHT), and untreated AHT. For this purpose, we used previously described approaches to combine static imaging-based modeling of absolute RBF with dual-wavelength retinal oximetry.

6.3. Methods

6.3.1. Study Design and Population

This is a cross-sectional, case-control study. We prospectively recruited subjects participating in Lifelines Biobank, an ongoing cohort study of the northern Netherlands (n ≃ 167,000). The study comprised four groups, each one describing a distinct BP status: 'low BP' (group 1), 'normal BP' (Group 2), that is, controls, 'treated AHT' (group 3), and 'untreated AHT' (group 4). The group definitions were based on information from multiple (at least two) previous visits. The exact definitions and rationale have been extensively described in our recent study on the same population.[25] In short, we required both the systolic and diastolic BP (SBP, DBP) of subjects belonging to groups 1 and 4 to consistently belong to the lowest and highest deciles of the Lifelines distribution, respectively. We also required both SBP and DBP in group 2 to fall no more than 1 standard deviation (SD) away from their means. Last, for subjects in group 3, we required uninterrupted use of antihypertensive medication for at least the past year. Invitations were sent to participants between 50 and 65 years old satisfying these BP criteria. Subjects that responded to our invitation underwent further screening for ophthalmic conditions and a general medical history interview. For each study group, the achievement of predetermined power levels (or lack of participant availability) was considered as the end of the recruitment.

We excluded participants with best-corrected visual acuity less than 0.8 (20/25), spherical refractive error larger than +3 diopters (D) or -3 D, cylinder exceeding 2 D, IOP higher than 21 mmHg (noncontact tonometer Tonoref II, Nidek, Aichi, Japan), reproducibly abnormal visual field test locations (Frequency Doubling Technology [C20-1 screening mode], Carl

Zeiss, Jena, Germany), family history of glaucoma, and any ophthalmic pathology, including history of previous ophthalmic surgery. Absence of ophthalmic disease was confirmed with the subsequent imaging sessions (discussed elsewhere in this article). We also excluded participants with diabetes, cardiovascular disease (except for AHT in groups 3 and 4), hematologic disease, and lung disease. We did not exclude smokers, but, because early chronic obstructive pulmonary disease cannot be completely ruled out in these participants, we recorded any previous or current regular smoking.

All participants provided written informed consent. The ethics board of the University Medical Center Groningen approved the study protocol (#NL61508.042.17). The study followed the tenets of the Declaration of Helsinki.

6.3.2. RBF Measurements

In total, 105 participants satisfying the BP definitions and screening criteria qualified for the subsequent imaging session. Before the start of the imaging session, we performed standard on-site BP measurements. The collected imaging data relevant to this study were, in short: ONH-centered fundus images, 6 × 6 mm OCTA macula scans, and retinal images obtained with a scanning laser ophthalmoscope (SLO). The details behind fundus imaging and OCTA scans can be found in our related study on the same population, and the details behind the SLO scanning are provided elsewhere in this article.[25] For the imaging session, we selected one eye per participant. If both eyes satisfied the ophthalmic inclusion criteria, this selection was random.

RBF estimations were based on a static imaging model-based approach. This protocol has been shown to have very good agreement with *in vivo* RBF measurements of the human retina, assessed by Laser Speckle Flowgraphy.[24] Hereunder, we provide an outline of the procedure. After data collection, we first estimated the central retinal artery and vein equivalents, that is, vascular calibers, from fundus images and the microvascular branching complexity (fractal dimension [FD]) from en face OCTA scans, using standard methods.[26-28] In short, we used full-spectrum amplitude decorrelation angiography (Canon OCT-HS100 SD-OCT; Canon, Inc., Tokyo, Japan) to generate 6 × 6 mm images of the superficial vascular plexus, centered at the macula. We subsequently binarized the images in ‘flow’ and ‘nonflow’ pixels using a local Otsu thresholding algorithm.[27] The FD was ultimately

calculated from the binarized images with the standard box-counting technique.[28] We then calculated total retinal vascular resistance (RVR) for each subject, by combining these measurements with blood viscosity in a Poiseuille-based fractal branching model.[24,29] Lastly, we calculated RBF from RVR and refined estimates of the retinal perfusion pressure (RPP):

$$\mathrm{RBF} = \frac{\mathrm{RPP}}{\mathrm{RVR}} \tag{1}$$

$$\text{where RPP} = 0.39 \cdot [\mathrm{DBP} + \tfrac{1}{3}(\mathrm{SBP} - \mathrm{DBP})] - \mathrm{IOP} + 10.1 \text{ mmHg.} \tag{2}$$

OCT and OCTA scans with image quality less than 7 out of 10, segmentation errors, or artifacts were excluded.[30] This resulted in the exclusion of nine subjects. All subjects had high-quality fundus images.

6.3.3. Oxygen Saturation Measurements

An SLO (Optomap 200Tx, Optos PLC, Dunfermline, United Kingdom) was used to measure arterial and venous O_2 saturations (S_aO_2, S_vO_2), by means of a commonly used dual-wavelength technique.[31,32] The device simultaneously acquires two retinal images, one at a wavelength of 532 nm (oxygen insensitive; Fig. 1A) and the other at a wavelength of 633 nm (oxygen sensitive; Fig. 1B). Three images per eye were obtained with the ResMax option (approximately 60°), at the same laser intensity, and with the gain set at medium iris pigmentation. Images were exported and stored in uncompressed format (.tiff). Three more subjects were excluded, owing to persistent blinking artifacts.

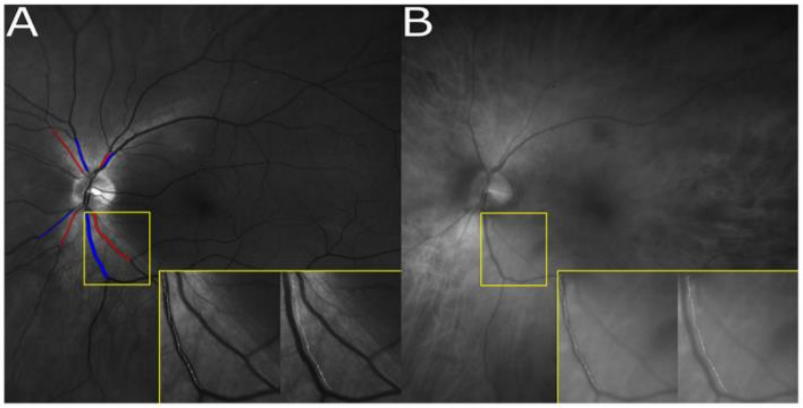

Figure 1. (A) SLO image at 532 nm. At this isosbestic ("oxygen-insensitive") wavelength, arteries and veins seem to be similar in terms of OD. Measured arterial and venous segments are marked in red and blue, respectively. The path of minimal intensity inside the vessel and a parallel path outside the vessel are shown for the IT vein. (B) SLO image at 633 nm. At this nonisosbestic ("oxygen-sensitive") wavelength, arteries appear brighter than veins, owing to higher O_2 content.

The optical density (OD) of a vessel at a given wavelength is defined as:

$$OD = \log\left(\frac{I_{out}}{I_{in}}\right) \quad (3)$$

where I_{out} is taken equal to the average grayscale intensity over a measurement area outside the vessel and I_{in} is taken equal to the average grayscale intensity inside the vessel.

The OD ratio (ODR) of a vessel at two given wavelengths (in this case, 633 nm and 532 nm) is defined as:

$$ODR = \frac{OD_{633}}{OD_{532}}. \quad (4)$$

By using the Beer-Lambert law, it can be shown that, under ideal conditions:

$$SO_2(\%) = \frac{\alpha_{r,532}\cdot ODR - \alpha_{r,633}}{(\alpha_{r,532} - \alpha_{o,532})\cdot ODR - (\alpha_{r,633} - \alpha_{o,633})} 100\% \quad (5)$$

where α_r is the absorption coefficient of reduced hemoglobin (Hb) and α_o is the absorption coefficient of oxyhemoglobin.

Because 532 nm is an almost isosbestic wavelength ($\alpha_{r,532} \simeq \alpha_{o,532}$) and the ODR is small, it is commonly assumed (and experimentally verified) that the SO_2 falls linearly with increasing ODR, that is:

$$SO_2(\%) = (k_1\cdot ODR + k_2)\cdot 100\% \quad (6)$$

where k_1, k_2 are constants determined after calibration.[31,33,34]

In order to obtain saturation values for the central retinal artery and vein, we first need to measure the saturation of their visible branches. We selected the largest artery and vein of each quadrant (superotemporal [ST], inferotemporal [IT], superonasal [SN], inferonasal [IN]) and ignored smaller vessels, because this approach has been found to minimally affect estimations.[35] To minimize O_2 diffusion losses, measurements were taken close to the border of the optic disc, according to a previously described, semiautomatic protocol.[34] In short, the path of minimal intensity (thus, avoiding the vessel light reflex) between the starting point of the vessel and the first major branching was automatically traced. A parallel path outside the vessel, at a fixed distance of 30 pixels was also traced automatically (Fig. 1). ODR was

subsequently calculated, according to *Eqs*. 3 and 4, with the image grayscale value as the standard proxy for intensity.[33] For each vessel, we recorded the median of three measurements. Feasibility, repeatability, and reproducibility of this approach have been previously established, also for an SLO.[36-40]

The obtained ODR values have to be corrected for the artifactual influence of factors other than O_2 saturation, mostly related to magnification errors, heterogeneous light absorption, and photon backscattering, before they can be used to calculate SO_2 via *Eq*. 6.[31,33,41] For each vessel segment, we implemented linear compensations by means of a backward regression model, with ODR serving as the dependent variable and the independent variables being potential confounders, that is, laterality, optic disc area, spherical error, cylinder, vessel diameter, and quadrant pigmentation index (PI). Only the significant variables of the reduced (final) model were subsequently used to construct the following correction formula:

$$ODR_{cor} = ODR - (b_0 + b_1X_1 + ... + b_nX_n) + \overline{ODR} \quad (7)$$

where ODR_{cor} is the corrected ODR, b_i are the regression coefficients, X_i are the confounders that remained in the reduced model, and $\overline{ODR}$ is the average ODR of the study population. The ODR_{cor} was evaluated for each quadrant separately.

PI was calculated based on extravascular reflection, as follows:

$$PI = \log\left(\frac{I_{out,633}}{I_{out,532}}\right). \quad (8)$$

Because the increase in light absorption with increasing melanin is more pronounced at longer wavelengths, lower PI values indicate increased pigmentation.[42]

The O_2 saturation in the central retinal artery can be calculated as the average measured saturation in the four major arterial arcades:

$$S_aO_2 = \frac{S_aO_{2,ST} + S_aO_{2,IT} + S_aO_{2,SN} + S_aO_{2,IN}}{4}. \quad (9)$$

The O_2 saturation in the central retinal vein can be calculated as the average measured saturation in the four major venous arcades, weighted by the relative flow contribution of each arcade. The weigh factor equals a power of the radius of the relevant venular segment[43]; the Poiseuille-based model used for absolute RBF estimations assumes that the power is

equal to FD + 1.15, where FD is the two-dimensional FD measured by OCTA (see 6.3.2) and 1.15 is a branch length coefficient.[24,29,44] Therefore:

$$S_vO_2 = \frac{r_{v,ST}^{FD+1.15} \cdot S_vO_{2,ST} + r_{v,IT}^{FD+1.15} \cdot S_vO_{2,IT} + r_{v,SN}^{FD+1.15} \cdot S_vO_{2,SN} + r_{v,IN}^{FD+1.15} \cdot S_vO_{2,IN}}{r_{v,ST}^{FD+1.15} + r_{v,IT}^{FD+1.15} + r_{v,SN}^{FD+1.15} + r_{v,IN}^{FD+1.15}} \quad (10)$$

where r_v denotes the radius of the relevant venular segment.

Owing to measurement artifacts, paradoxically different arteriolar saturations may be measured in each of the four retinal quadrants. Therefore, for the sake of comparison, the weighted average calculation proposed in *Eq*. 10 for the venules was also used for the arterioles, instead of *Eq*. 9. Henceforth, we refer to this calculation as the 'alternative S_aO_2 calculation'.

Using *Eqs*. 6, 7, 9, and 10, we can express S_aO_2 and S_vO_2 as a function of the regression coefficients b_i and the constants k_1 and k_2. As described elsewhere in this article, the b_i can be calculated from a standard linear fitting. Now, to determine k_1 and k_2, we need two distinct calibration values. The average S_aO_2 and S_vO_2 values for healthy eyes reported by Schweitzer *et al*. (92.2% and 57.9%, respectively) are the values most frequently used for calibration.[32] With these values, the calibration constants were $k_1 = -2.46$ and $k_2 = 1.26$. Calibration is unrestrictive and allows saturation measurements to exceed 100%, owing to variability.[37,45]

6.3.4. Total Retinal DO_2 and VO_2

We can now estimate the outcome variables, DO_2 and VO_2, from the Fick principle, as demonstrated by Werkmeister *et al*.[46]:

$$DO_2 = 1.35 \cdot [Hb_t] \cdot S_aO_2 \cdot RBF \quad (11)$$

$$VO_2 = 1.35 \cdot [Hb_t] \cdot (S_aO_2 - S_vO_2) \cdot RBF \quad (12)$$

where $[Hb_t]$ is the total Hb concentration.

In both formulas, we omitted a term for unbound O_2 content, because it is smaller than bound O_2 content by more than two orders of magnitude.[47] We did not obtain blood samples and we, therefore, used the average $[Hb_t]$ values reported in the Lifelines Biobank, stratified by age, sex, and BP status. For this reason, we also conducted a sensitivity analysis, repeatedly

replacing the average [Hb_t] values with random values taken from identical distributions. Last, the oxygen extraction fraction (OEF) was defined as:

$$OEF = \frac{VO_2}{DO_2} = \frac{S_aO_2 - S_vO_2}{S_aO_2}. \quad (13)$$

6.3.5. Statistical Analysis

We compared the general characteristics and outcome variables (DO_2 and VO_2) between the four groups, by means of analysis of variance (ANOVA) models. Potential confounding factors from the population general characteristics were included as covariates in the outcome variable models. In post hoc analysis, we used the Tukey honest significant differences correction to account for multiple comparisons. Whenever ANOVA assumptions were not met, we used Welch's ANOVA or nonparametric tests.

To examine the overall association between the DO_2 and VO_2, we used a linear regression analysis. The observed correlation of these two variables is inflated, owing to shared measurement error, stemming from the mathematical coupling of these variables. This phenomenon is commonly reported in other systems.[13] We used the method described by Stratton *et al*. to calculate the corrected regression coefficient.[48] In short, we calculated a reliability coefficient r_D:

$$r_D = \frac{var(DO_2) - var(err_{DO_2})}{var(DO_2)} \quad (14)$$

where var(DO_2) denotes the variance of DO_2 and var(err_{DO2}) denotes the variance attributable to measurement error.

The variance attributable to measurement error, var(err_{DO2}), was calculated from the error variances of RBF and S_aO_2, used in the calculation of DO_2 (Eq. 11). As described by Stratton *et al*., these error variances need to be derived from calibration.[48] In the absence of a gold calibration standard, the error variance of the RBF was approximated from a previous experiment in an independent population, from the residual variance of RBF fitted on *in vivo* Laser Speckle Flowgraphy measurements.[24] Because the physiological variation of S_aO_2 in healthy individuals is expected to be minimal, the error variance of S_aO_2 was set as equal to

the observed variance of S_aO_2. The corrected slope (b_{cor}) for VO_2 as a function of DO_2 can then be calculated as:

$$b_{cor} = \frac{b_{obs} - (1 - r_D)\, b_{err}}{r_D} \quad (15)$$

where b_{obs} is the observed slope and b_{err} the slope of measurement errors, which accounts for the covariance of the error in DO_2 and VO_2. We will not demonstrate here the detailed mathematical calculations of $var(err_{DO2})$ and b_{err}, as they are extensively provided in the aforementioned paper by Stratton *et al*.[48]

Henceforth, all normally distributed variables are described with the mean and standard deviation (SD). Variables with a skewed distribution are described with the median and interquartile range. All analyses were performed using R (version 3.3.3; R Foundation for Statistical Computing, Vienna, Austria) and SPSS (version 26; IBM Corp., Armonk, NY). A *P* value of 0.05 or less was considered statistically significant.

6.4. Results

6.4.1. General Characteristics

We excluded 12 out of 105 participants (3 from the low BP group, 3 from the control group, 4 from the treated AHT group, and 2 from the untreated AHT group), owing to artifacts or insufficient image quality at any stage of the imaging session. This resulted in a total of 93 eyes from 93 participants being included in the analysis. Their general characteristics are summarized in Table 1. The BP measurements in this table represent the actual on-site measurements preceding the scanning; the highly significant *P* values confirm the robustness of the inclusion procedure. Groups differed furthermore significantly in sex and body mass index (BMI), which is expected owing to the prevalence of low BP in females and high BMI among hypertensives, also verified in the Lifelines cohort.[49,50] Therefore, we adjusted subsequent analyses (discussed elsewhere in this article) for sex and BMI. We additionally adjusted DO_2 and VO_2 analyses for smoking status (despite not being significantly different among groups), because it could affect O_2 metrics.

Table 1. Characteristics of the Study Population

Group Size (*N*)	Group 1 (Low BP) 30	Group 2 (Normal BP) 20	Group 3 (Treated AHT) 26	Group 4 (Untreated AHT) 17	*P* Value
Age; years [median (IQR)]	56.0 (51.0–59.3)	53.5 (51.3–60.5)	55.5 (52.8–61.0)	58.0 (53.0–61.0)	0.74
Sex, % female	93.3	50.0	42.3	47.1	$\mathbf{2.2 \times 10^{-4}}$
SBP, mmHg [mean (standard deviation)]	107 (9)	125 (5)	142 (18)	159 (23)	$\mathbf{2.1 \times 10^{-14}}$
DBP, mmHg [mean (standard deviation)]	66 (6)	79 (6)	86 (11)	99 (8)	$\mathbf{4.1 \times 10^{-23}}$
BMI, kg/m^2 [median (IQR)]	22.4 (21.2–24.3)	23.4 (22.2–26.7)	26.9 (24.7–29.8)	27.4 (24.3–28.5)	$\mathbf{5.0 \times 10^{-6}}$
Smoking, % yes	23.3	35.0	30.8	41.2	0.62
IOP, mmHg [mean (standard deviation)]	14.0 (3.0)	13.4 (3.1)	14.3 (3.0)	14.5 (3.8)	0.72
SEQ, D [mean (standard deviation)]	−0.11 (1.44)	+0.19 (1.67)	−0.23 (1.55)	−0.65 (1.58)	0.45
ONH area, mm^2 [median (IQR)]	1.89 (1.68–2.24)	1.97 (1.71–2.20)	1.94 (1.72–2.31)	1.98 (1.78–2.15)	0.81

IOP, intraocular pressure; ONH, optic nerve head; IQR, interquartile range; SEQ, spherical equivalent.

Supplementary Table S9 displays the significant variables of the reduced linear models used for the ODR correction. Corrected ODR values per retinal quadrant and the global averages are provided in Supplementary Table S10. In general, aside from the O_2 content, ODR values were also influenced by measurement location (quadrant), pigmentation, refractive errors, and, in some cases, eye laterality (see the Discussion).

6.4.2. Associations with BP Status

Table 2 summarizes the measured components used in the estimation of DO_2 and VO_2, stratified by BP status. The reported mean (SD) [Hb_t] values are those of the age-matched Lifelines population. Groups were similar in terms of S_aO_2 and S_vO_2, but differed in terms of RBF, on univariable analysis. Sex, BMI, and smoking history did not confound this relationship when included as covariates, nor did they after omitting each one of the four groups from the analysis ($P >> 0.05$ in all cases). In a post hoc analysis, after adjusting for multiple comparisons, the low BP group had a significantly lower mean RBF than the untreated AHT group ($P = 0.032$).

Table 2. Group Summaries for Vascular and Oximetry Measurements

	Group 1 (Low BP)	Group 2 (Normal BP)	Group 3 (Treated AHT)	Group 4 (Untreated AHT)	*P* Value
Total RBF, µL/min [mean (standard deviation)]	40.7 (6.0)	45.7 (9.6)	45.1 (8.6)	47.6 (8.3)	**0.028**
RPP, mmHg [mean (standard deviation)]	27.2 (2.8)	33.5 (3.9)	36.6 (4.7)	41.2 (5.1)	$\mathbf{1.6 \times 10^{-19}}$
CRAE, µm [mean (standard deviation)]	172 (12)	162 (12)	154 (13)	148 (7)	$\mathbf{7.0 \times 10^{-10}}$
CRVE, µm [mean (standard deviation)]	228 (18)	229 (16)	229 (18)	223 (12)	0.57
OCTA FD [mean (standard deviation)]	1.625 (0.005)	1.626 (0.007)	1.624 (0.006)	1.626 (0.006)	0.67
[Hb_t]*, g/dL [mean (standard deviation)] (population-based data)	13.6 (0.8)	14.3 (0.8)	14.2 (0.9)	14.7 (0.8)	$\mathbf{5.3 \times 10^{-307}}$
S_aO_2 (%) [mean (standard deviation)]	94.7 (12.8)	88.6 (12.4)	89.3 (11.2)	96.3 (12.7)	0.12
S_aO_2 (%) [mean (standard deviation)] (alternative calculation)	91.5 (11.7)	87.7 (12.3)	87.5 (12.4)	94.2 (11.8)	0.22
S_vO_2 (%) [mean (standard deviation)]	59.1 (14.2)	53.2 (13.6)	60.2 (14.5)	56.3 (14.8)	0.36

CRAE, central retinal artery equivalent; CRVE, central retinal vein equivalent.
*Data and comparison taken from Lifelines ($n = 28,888$).

Figure 2 shows the final outcome variables, DO_2 and VO_2, stratified by BP status. Both variables were significantly different between groups ($P = 0.009$ and $P = 0.036$, respectively) in univariable analysis and the significance of this relationship was largely unaffected when

[Hb_t] values were repeatedly replaced with random values taken from the same distribution (DO_2: *P*[average] = 0.008, *P*[95% of repetitions] = 0.002-0.028; VO_2: *P*[average] = 0.025, *P*[95% of repetitions] = 0.014-0.044). The significance of this relationship was also unaffected when sex, BMI, and smoking history were included as covariates (Table 3). All three covariates had additional, independent effects, which are summarized in Table 3 (reported as coefficients from the equivalent generalized linear models). The significance of this relationship was also unaffected when the alternative S_aO_2 calculation was used inside the DO_2 and VO_2 formulas (*P* = 0.005 and *P* = 0.025, respectively). In a post hoc analysis, after adjusting for multiple comparisons, the low BP group had a significantly lower estimated marginal mean DO_2 than the untreated AHT group ($P = 4.9 \cdot 10^{-4}$), while both the low BP group and the treated AHT group had a significantly lower estimated marginal mean VO_2 than the untreated AHT group (*P* = 0.021 and *P* = 0.034, respectively).

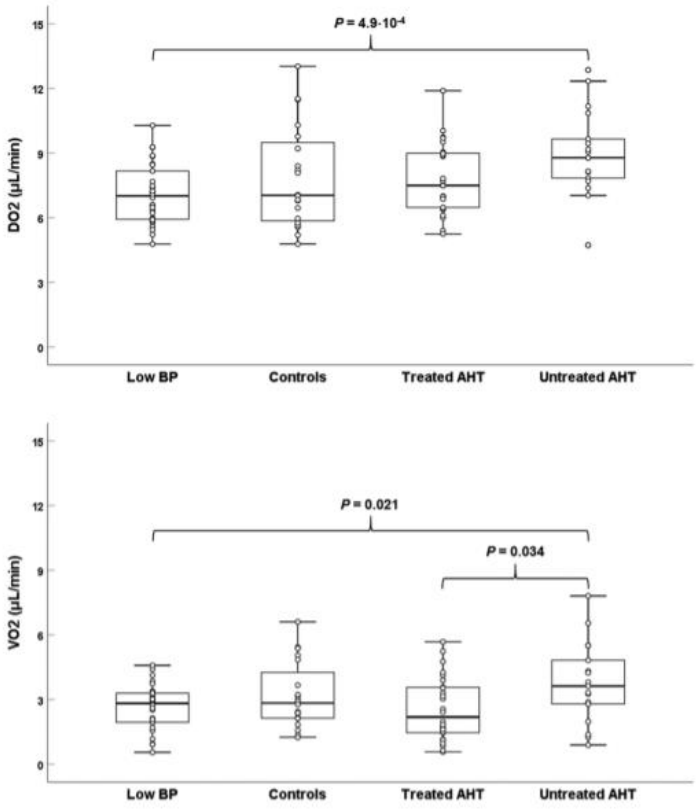

Figure 2. Total retinal DO_2 and extraction (VO_2) as a function of BP status. DO_2 is higher in subjects with untreated AHT, compared with the low BP group. The VO_2 is higher in subjects with untreated AHT, compared with both the low BP and the treated AHT group.

Table 3. Factors Associated With DO_2 and VO_2 in Multivariable Analysis

	DO_2 (µL/min)		VO_2 (µL/min)	
	Coefficient	*P* Value	Coefficient	*P* Value
BP status; ref.: untreated AHT				
Low BP	−2.4	**2.2×10^{-5}**	−1.4	**0.002**
Normal BP	−1.5	0.013	−0.9	0.042
Treated AHT	−1.1	0.041	−1.2	**0.003**
BMI; kg/m^2	−0.14	**0.027**	−0.13	**0.006**
Sex; female = 1	NS	NS	−0.7	**0.038**
Smoking; yes = 1	NS	NS	−0.7	**0.017**

NS, not significant.
For the BP status, *P* = 0.008 is taken as the adjusted threshold of significance.

The mean (SD) OEF was 0.37 (0.15) and was similar between groups (P = 0.20). In multivariable analysis, smoking was associated with a decrease in the OEF (b = -0.07, P = 0.039).

6.4.3. DO_2-VO_2 Relationship

The pooled (n = 93) association of DO_2 and VO_2 is plotted in Figure 3. Initially, there was a significant positive correlation between the two variables (R_{obs} = 0.65, b_{obs} = 0.51, $P = 2.4 \cdot 10^{-12}$; R_{obs} = 0.64, b_{obs} = 0.50, $P = 8.1 \cdot 10^{-12}$ with the alternative S_aO_2 calculation). However, after correcting for shared measurement error owing to mathematical coupling, the true slope was flatter and no longer statistically significant (b_{cor} = 0.19, P = 0.29), and the true correlation coefficient could not be calculated.[48]

6.5. Discussion

In this study, we showed that BP status was associated with altered total retinal DO_2 and VO_2 at rest in ophthalmologically healthy subjects. Specifically, we reported an increase in the DO_2 and VO_2 with increasing BP, which was more prominent at the tails of the BP distribution. In addition, the VO_2 was also higher in subjects with untreated AHT than in subjects with treated AHT. The true association between DO_2 and VO_2 was, at best, weak, suggesting these variables are mostly independent at rest.

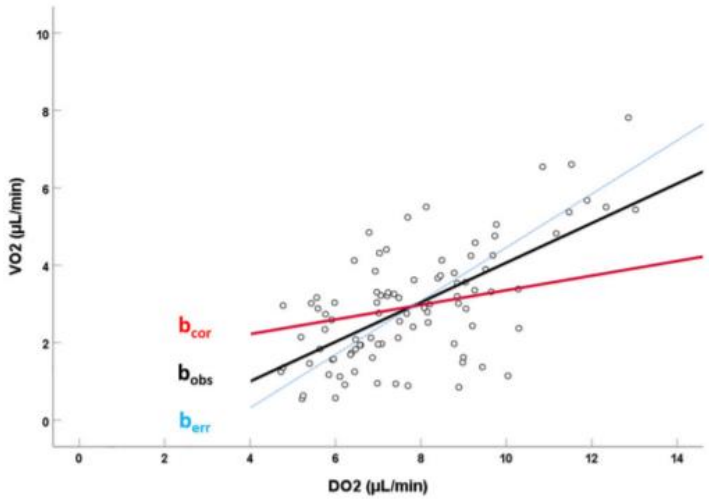

Figure 3. Pooled (n = 93) data for total retinal VO_2 plotted as a function of total retinal DO_2. The observed slope of the linear relationship (*continuous black line*) is denoted by b_{obs}. The component of the slope (*dashed blue line*) introduced purely via shared measurement error, owing to mathematical coupling of the two variables, is denoted by b_{err}. The true, corrected slope of the relationship (continuous red line), that is, adjusted for shared measurement error, is denoted by b_{cor}. The small, nonsignificant slope of the true relationship indicates little interdependency of resting DO_2 and VO_2.

6.5.1. Oxygen Delivery

Although the average RPP increased by 51% on the way from the low BP group to the untreated hypertensives (Table

3), the average RBF only increased by 17% (Table 3) and average DO_2 by 27% (Table 3, Fig. 2). As a result, the differences in the RBF and DO_2 were noted as significant only between the groups representing the tails of the BP distribution. This observation is not surprising, and it is consistent with the general concept of RBF autoregulation and with the subsequent structural remodeling of blood vessels, after chronic BP elevation.[8,10,51] Experimental studies and mathematical models have shown an increase in the tissue oxygen partial pressure with transient BP manipulations.[52,53] Our results suggest that chronic low or high, but still physiological, resting BP values can also have a subtle effect on the DO_2. The increase in DO_2 (which is the product of the RBF and O_2 content) with increasing BP was larger than that of RBF alone. Since S_aO_2 was similar between groups (Table 3), this is mostly owing to the increasing [Hb_t] with increasing BP (Table 3). This association is known from other population studies.[54,55]

A higher BMI was found to be independently associated with a reduced DO_2, but not RBF, which likely reflects the documented effects of obesity on lung function and pulmonary gas exchange.[56]

6.5.2. Oxygen Extraction

A significantly higher VO_2 was also observed in untreated hypertensives (Table 3, Fig. 2), relatively to subjects with a low BP (+41%) and treated hypertensives (+46%). Again, no group was significantly different from controls, after adjusting for multiple comparisons (Table 3). The smaller effect size, in combination with the high variability that is present in our estimates, seems to be the most likely explanation for this phenomenon. Indeed, although our average estimates for both DO_2 and VO_2 are similar to previously published values (and almost identical when the same calibration values are used), the variability we report is higher.[46,47] This outcome was owing to the larger error introduced by the SLO-based retinal oximetry (which is consistently present in all studies using the SLO), compared to the error yielded by tailored fundus cameras.[37,39,40]

The reported alterations in the VO_2 can have a number of pathophysiological explanations. We have recently shown that, in the same population, the low BP group and the treated hypertensives were characterized by subtle thinning of the ganglion cell-inner plexiform layer and the macular and peripapillary retinal nerve fiber layer.[25] Although we do not know for

sure if these insults are primary or secondary to a decreased DO_2, a lower VO_2 in these groups could, at least partially, suggest a current state of decreased O_2 demand. However, a thinning of the inner retina was also present (albeit less pronounced) in the untreated hypertensive group, which contradicts the higher average VO_2 reported for these subjects. In this regard, in the next paragraphs we speculate about potential mechanisms that could explain this finding.

First, it is estimated that about 15% of the O_2 extracted from the retinal circulation is not consumed by the inner retina, but actually complements the choroidal O_2 supply of the photoreceptors in the outer retina. As a result, any condition that compromises the choroidal supply could lead to a compensatory increase in the retinal VO_2.[7] This VO_2 increase has already been observed in mice with early diabetes, and it has also been reported that deficits of the deep retinal capillary plexus in human diabetics are associated with photoreceptor loss.[57,58] This could also apply to AHT, because it has been shown that AHT, especially when poorly controlled, has a detrimental effect on the choriocapillaris.[59] The magnitude of this effect is unknown, but it should be able to counteract opposing forces that would tend to decrease the VO_2, at least theoretically, such as a decreased mean circulation time, shunting of flow, and deep capillary rarefaction.[60,61]

Second, experimental evidence and mathematical models support that, in the presence of increased O_2 availability, the O_2 consumption of the inner retina (especially that of the inner and outer plexiform layers) increases, a mechanism that helps to keep inner retinal O_2 levels relatively stable.[6,52,62,63] This could pertain to subjects with untreated, chronic AHT. Indeed, while hyperoxic conditions such as 100% oxygen breathing achieve control of O_2 levels mostly by inducing RBF reduction through vasoconstriction, this is obviously not possible in conditions where RBF is a priori increased, despite vessels being already constricted.[64] Increased resting consumption in these subjects could, at least partially, explain increased VO_2.

That said, the true correlation analysis for DO_2-VO_2 indicates that this increase in resting O_2 consumption with increased resting delivery cannot be too pronounced, if any. Indeed, although mitochondrial oxidative phosphorylation could act as a sensor of O_2 tension, it also has a saturation ceiling.[65] It is not impossible, nevertheless, that a metabolic transition to a more oxidative state, with decreased glycolytic activity, occurs.[66] Other factors could also play a role in determining the DO_2-VO_2 slope. With constant consumption, an increase in BP

would initially cause an increase in RBF (and DO_2), which would be compensated by autoregulation. Now, with constant BP, an increase in consumption would cause an increase in local CO_2, inducing vasodilation, thus causing an increase in DO_2. The gain of this feedback loop at equilibrium is possibly a major determinant of this slope and is, therefore, likely close to zero.

A higher BMI was, again, independently associated with a decreased VO_2, possibly pointing towards reduced retinal function due to oxidative stress and inflammation.[67] The VO_2 was lower in females than males, on which conflicting evidence exists, and could reflect the lower systemic basal metabolic rate.[47,68] Smoking was also associated with a decreased VO_2 and could be related to the reported reduced O_2 uptake present in other systems. Last, although the average, resting OEF was consistent with previous reports, we found that it was lower in smokers.[11] Studies with a tailored design could shed more light on these secondary observations.

6.5.3. Study Strengths and Limitations

To our knowledge, this study is the first to describe alterations in DO_2 and VO_2 with different chronic BP status. The strict selection process that we implemented within the setting of a large-scale cohort (Lifelines Biobank) enabled us to investigate the true tails of the BP distribution. Another novelty of our study is the fact that we describe the true resting DO_2-VO_2 relationship in the retina, which avoids overestimations originating from mathematical coupling. However, there are several limitations that should be considered.

First, the calculation of the outcome variables (DO_2 and VO_2) is liable to propagation of error associated with their measured components. Similar to other systems, retinal DO_2 and VO_2 are not directly measured, but estimated from the multiplication of RBF with oxygen saturation (*Eqs.* 12 and 13). There is currently no gold standard way to measure these components in the clinic and there remain unresolved technical considerations with regards to acquisition and quantification. As such, any *in vivo* validation of these estimates remains liable itself to the same mathematical approximations. We only expect a small contribution of RBF measurements to this error for two reasons: first, RBF estimations are in very good agreement with Doppler OCT studies and, second, we have previously shown that RBF estimations strongly correlate with *in vivo* blood flow metrics across a large BP range, as

assessed by Laser Speckle Flowgraphy on an independent validation dataset.[24,46,69-73] However, elsewhere in this article, we discussed how the more substantial error introduced by variability in oximetry measurements could have affected certain results. A lot of this variability is likely of technical nature, owing to the documented presence of unaccounted nonuniform magnification, distortion, and illumination in particular parts of the retinal image, which can affect measurements, even with changes in the angle of gaze.[38,74] These observations can explain the unexpected between-eye ODR differences that were present in certain retinal quadrants (Supplementary Table S9). Device-specific preprocessing of the SLO images and suboptimal wavelengths are likely other sources of this increased variability. Of course, physiological effects could also result in additional optical artifacts.[75] That said, owing to the incorporation of this expected variability to our original power analysis, our study was still able to show significant effects, despite the noise introduced by measurement uncertainty.

Second, this cross-sectional study cannot conclude if and how these initial BP-related alterations in O_2 transport pertain to the development of ophthalmic pathologies. Owing to the cross-sectional nature of the study, we also did not have robust information regarding the onset and duration of AHT. However, the incorporation of BP measurements from multiple previous occasions in the group definitions, as well as the requirement of uninterrupted use of antihypertensive medication over (at least) the past year resulted in almost all diagnoses occurring before at least three years.

Last, this population was almost entirely Caucasian and, as such, any results derived from it should not be immediately generalized to other ethnicities.

6.5.4. Implications and Conclusions

By showing that BP-related alterations in O_2 transport may already exist in subjects with no signs of ophthalmic pathology, this study enhances our understanding of the baseline interplay between BP, RBF, and retinal oxygenation. This finding is important, but is merely a first step towards answering pertinent questions regarding the disease process. If hypoxia plays a role in complicated pathologies such as age-related macular degeneration and diabetic retinopathy, when does the retina really become hypoxic and how early can we detect it in clinical practice?[7] Can we use this information to evaluate treatments and slow disease

progression? A special mention should be made at this point for glaucoma: according to the 'chicken-egg' dilemma, structural loss could be both cause and consequence of impaired blood flow.[76] In this regard, future studies could examine whether deficits in perfusion and oxygenation related to known glaucoma risk factors, such as BP status, can be helpful in stratifying the risk of incidence and/or progression of the disease.

In conclusion, we reported alterations in retinal DO_2 and VO_2 in ophthalmologically healthy subjects with different BP status. Future studies should incorporate the vascular supply of the choroid to elucidate whether increased oxygen extraction in uncontrolled AHT could be the result of compensatory mechanisms in effect. Longitudinal studies could investigate whether compromised delivery and extraction in subjects with low BP and treated AHT can explain the increased risk of glaucomatous damage in these population groups.

6.6. References

1. GBD 2019 Blindness and Vision Impairment Collaborators, Vision Loss Expert Group of the Global Burden of Disease Study. Causes of blindness and vision impairment in 2020 and trends over 30 years, and prevalence of avoidable blindness in relation to VISION 2020: the Right to Sight: an analysis for the Global Burden of Disease Study. *Lancet Glob Health*. 2021;9(2):e144-e160.

2. Wong TY, Mitchell P. The eye in hypertension. *Lancet*. 2007;369:425–435.

3. Kur J, Newman EA, Chan-Ling T. Cellular and physiological mechanisms underlying blood flow regulation in the retina and choroid in health and disease. *Prog Retin Eye Res*. 2012;31:377–406.

4. Anderson B Jr, Saltzman HA. RETINAL OXYGEN UTILIZATION MEASURED BY HYPERBARIC BLACKOUT. *Arch Ophthalmol*. 1964;72:792–795.

5. Anderson B Jr. Ocular effects of changes in oxygen and carbon dioxide tension. *Trans Am Ophthalmol Soc*. 1968;66:423–474.

6. Yu DY, Cringle SJ. Oxygen distribution and consumption within the retina in vascularised and avascular retinas and in animal models of retinal disease. *Prog Retin Eye Res*. 2001;20:175–208.

7. Linsenmeier RA, Zhang HF. Retinal oxygen: from animals to humans. *Prog Retin Eye Res*. 2017;58:115–151.

8. Riva CE, Grunwald JE, Petrig BL. Autoregulation of human retinal blood flow. An investigation with laser Doppler velocimetry. *Invest Ophthalmol Vis Sci*. 1986;27:1706–1712.

9. Pournaras CJ, Rungger-Brändle E, Riva CE, Hardarson SH, Stefansson E. Regulation of retinal blood flow in health and disease. *Prog Retin Eye Res*. 2008;27:284–330.

10. Lehmann MV, Schmieder RE. Remodeling of retinal small arteries in hypertension. *Am J Hypertens*. 2011;24:1267–1273.

11. Felder AE, Wanek J, Blair NP, Shahidi M. Inner Retinal Oxygen Extraction Fraction in Response to Light Flicker Stimulation in Humans. *Invest Ophthalmol Vis Sci*. 2015;56:6633–6637.

12. Palkovits S, Told R, Schmidl D, et al. Regulation of retinal oxygen metabolism in humans during graded hypoxia. *Am J Physiol Heart Circ Physiol*. 2014;307:H1412–8.

13. Vincent J-L, De Backer D. Oxygen transport-the oxygen delivery controversy. *Intensive Care Med*. 2004;30:1990–1996.

14. Topouzis F, Wilson MR, Harris A, et al. Association of open-angle glaucoma with perfusion pressure status in the Thessaloniki Eye Study. *Am J Ophthalmol*. 2013;155:843–851.

15. Leeman M, Kestelyn P. Glaucoma and Blood Pressure. *Hypertension*. 2019;73:944–950.

16. Hayreh SS, Podhajsky P, Zimmerman MB. Role of nocturnal arterial hypotension in optic nerve head ischemic disorders. *Ophthalmologica*. 1999;213:76–96.

17. Memarzadeh F, Ying-Lai M, Chung J, Azen SP, Varma R, Los Angeles Latino Eye Study Group. Blood pressure, perfusion pressure, and open-angle glaucoma: the Los Angeles Latino Eye Study. *Invest Ophthalmol Vis Sci*. 2010;51:2872–2877.

18. Bowe A, Grünig M, Schubert J, et al. Circadian Variation in Arterial Blood Pressure and Glaucomatous Optic Neuropathy—A Systematic Review and Meta-Analysis. *Am J Hypertens*. 2015;28(9):1077-1082.

19. Zheng W, Dryja TP, Wei Z, et al. Systemic Medication Associations with Presumed Advanced or Uncontrolled Primary Open-Angle Glaucoma. *Ophthalmology*. 2018;125:984–993.

20. Chong RS, Chee M-L, Tham Y-C, et al. Association of Antihypertensive Medication with Retinal Nerve Fiber Layer and Ganglion Cell-Inner Plexiform Layer Thickness. *Ophthalmology*. 2021;128:393–400.

21. Pappelis K, Loiselle AR, Visser S, Jansonius NM. Association of Systemic Medication Exposure With Glaucoma Progression and Glaucoma Suspect Conversion in the Groningen Longitudinal Glaucoma Study. *Invest Ophthalmol Vis Sci*. 2019;60:4548–4555.

22. Horwitz A, Klemp M, Jeppesen J, Tsai JC, Torp-Pedersen C, Kolko M. Antihypertensive Medication Postpones the Onset of Glaucoma: Evidence From a Nationwide Study. *Hypertension*. 2017;69:202–210.

23. He Z, Vingrys AJ, Armitage JA, Bui BV. The role of blood pressure in glaucoma. *Clin Exp Optom*. 2011;94:133–149.

24. Pappelis K, Choritz L, Jansonius NM. Microcirculatory model predicts blood flow and autoregulation range in the human retina: in vivo investigation with laser speckle flowgraphy. *Am J Physiol Heart Circ Physiol*. 2020;319:H1253–H1273.

25. Pappelis K, Jansonius NM. U-Shaped Effect of Blood Pressure on Structural OCT Metrics and Retinal Perfusion in Ophthalmologically Healthy Subjects. *Invest Ophthalmol Vis Sci*. 2021;62:5.

26. Knudtson MD, Lee KE, Hubbard LD, Wong TY, Klein R, Klein BEK. Revised formulas for summarizing retinal vessel diameters. *Curr Eye Res*. 2003;27:143–149.

27. Pappelis K, Jansonius NM. Quantification and Repeatability of Vessel Density and Flux as Assessed by Optical Coherence Tomography Angiography. *Transl Vis Sci Technol*. 2019;8:3.

28. Al-Nosairy KO, Prabhakaran GT, Pappelis K, Thieme H, Hoffmann MB. Combined Multi-Modal Assessment of Glaucomatous Damage With Electroretinography and Optical Coherence Tomography/Angiography. *Transl Vis Sci Technol*. 2020;9:7.

29. Takahashi T, Nagaoka T, Yanagida H, et al. A mathematical model for the distribution of hemodynamic parameters in the human retinal microvascular network. *J Biorheol*. 2009;23:77–86.

30. Spaide RF, Fujimoto JG, Waheed NK. IMAGE ARTIFACTS IN OPTICAL COHERENCE TOMOGRAPHY ANGIOGRAPHY. *Retina*. 2015;35:2163–2180.

31. Beach JM, Schwenzer KJ, Srinivas S, Kim D, Tiedeman JS. Oximetry of retinal vessels by dual-wavelength imaging: calibration and influence of pigmentation. *J Appl Physiol*. 1999;86:748–758.

32. Schweitzer D, Hammer M, Kraft J, Thamm E, Königsdörffer E, Strobel J. In vivo measurement of the oxygen saturation of retinal vessels in healthy volunteers. *IEEE Trans Biomed Eng*. 1999;46:1454–1465.

33. Hammer M, Vilser W, Riemer T, Schweitzer D. Retinal vessel oximetry-calibration, compensation for vessel diameter and fundus pigmentation, and reproducibility. *J Biomed Opt*. 2008;13:054015.

34. Geirsdottir A, Palsson O, Hardarson SH, Olafsdottir OB, Kristjansdottir JV, Stefánsson E. Retinal Vessel Oxygen Saturation in Healthy Individuals. *Invest Ophthalmol Vis Sci*. 2012;53:5433-5442.

35. Heitmar R, Cubbidge RP. Retinal Vessel Oxygen Saturation Measurement Protocols and Their Agreement. *Transl Vis Sci Technol*. 2020;9:17.

36. Yip W, Siantar R, Perera SA, Milastuti N, Ho KK, Tan B, et al. Reliability and determinants of retinal vessel oximetry measurements in healthy eyes. *Invest Ophthalmol Vis Sci*. 2014;55:7104–7110.

37. Kristjansdottir JV, Hardarson SH, Halldorsson GH, Karlsson RA, Eliasdottir TS, Stefánsson E. Retinal oximetry with a scanning laser ophthalmoscope. *Invest Ophthalmol Vis Sci*. 2014;55:3120–3126.

38. Palsson O, Geirsdottir A, Hardarson SH, Olafsdottir OB, Kristjansdottir JV, Stefánsson E. Retinal oximetry images must be standardized: a methodological analysis. *Invest Ophthalmol Vis Sci*. 2012;53:1729–1733.

39. Blair NP, Wanek J, Felder AE, et al. Retinal Oximetry and Vessel Diameter Measurements With a Commercially Available Scanning Laser Ophthalmoscope in Diabetic Retinopathy. *Invest Ophthalmol Vis Sci*. 2017;58:5556–5563.

40. Vehmeijer WB, Magnusdottir V, Eliasdottir TS, Hardarson SH, Schalij-Delfos NE, Stefánsson E. Retinal Oximetry with Scanning Laser Ophthalmoscope in Infants. *PLoS One*. 2016;11:e0148077.

41. Lim LS, Lim XH, Tan L. Retinal Vascular Oxygen Saturation and Its Variation With Refractive Error and Axial Length. *Transl Vis Sci Technol*. 2019;8:22.

42. Delori FC, Pflibsen KP. Spectral reflectance of the human ocular fundus. *Appl Opt*. 1989;28:1061–1077.

43. Aschinger GC, Schmetterer L, Fondi K, et al. Effect of Diffuse Luminance Flicker Light Stimulation on Total Retinal Blood Flow Assessed With Dual-Beam Bidirectional Doppler OCT. *Invest Ophthalmol Vis Sci*. 2017;58:1167–1178.

44. Kamiya A, Takahashi T. Quantitative assessments of morphological and functional properties of biological trees based on their fractal nature. *J Appl Physiol*. 2007;102:2315–2323.

45. Garg AK, Knight D, Lando L, Chao DL. Advances in Retinal Oximetry. *Transl Vis Sci Technol*. 2021;10(2):5.

46. Werkmeister RM, Schmidl D, Aschinger G, et al. Retinal oxygen extraction in humans. *Sci Rep*. 2015;5:15763.

47. Bata AM, Fondi K, Szegedi S, et al. Age-Related Decline of Retinal Oxygen Extraction in Healthy Subjects. *Invest Ophthalmol Vis Sci*. 2019;60:3162–3169.

48. Stratton HH, Feustel PJ, Newell JC. Regression of calculated variables in the presence of shared measurement error. *J Appl Physiol*. 1987;62:2083–2093.

49. Tigchelaar EF, Zhernakova A, Dekens JAM, et al. Cohort profile: LifeLines DEEP, a prospective, general population cohort study in the northern Netherlands: study design and baseline characteristics. *BMJ Open*. 2015;5:e006772.

50. Slagter SN, van Waateringe RP, van Beek AP, van der Klauw MM, Wolffenbuttel BHR, van Vliet-Ostaptchouk JV. Sex, BMI and age differences in metabolic syndrome: the Dutch Lifelines Cohort Study. *Endocr Connect*. 2017;6:278–288.

51. Tani T, Nagaoka T, Nakabayashi S, Yoshioka T, Yoshida A. Autoregulation of retinal blood flow in response to decreased ocular perfusion pressure in cats: comparison of the effects of increased intraocular pressure and systemic hypotension. *Invest Ophthalmol Vis Sci*. 2014;55:360–367.

52. Yu DY, Cringle SJ, Alder VA, Su EN. Intraretinal oxygen distribution in rats as a function of systemic blood pressure. *Am J Physiol*. 1994;267:H2498–507.

53. Causin P, Guidoboni G, Malgaroli F, Sacco R, Harris A. Blood flow mechanics and oxygen transport and delivery in the retinal microcirculation: multiscale mathematical modeling and numerical simulation. *Biomech Model Mechanobiol*. 2016;15:525–542.

54. Atsma F, Veldhuizen I, de Kort W, van Kraaij M, Jong PP, Deinum J. Hemoglobin Level Is Positively Associated With Blood Pressure in a Large Cohort of Healthy Individuals. *Hypertension*. 2012;60(4):936-941.

55. Cirillo M, Laurenzi M, Trevisan M, Stamler J. Hematocrit, blood pressure, and hypertension. The Gubbio Population Study. *Hypertension*. 1992;20:319–326.

56. Kapur VK, Wilsdon AG, Au D, et al. Obesity is associated with a lower resting oxygen saturation in the ambulatory elderly: results from the cardiovascular health study. *Respir Care*. 2013;58:831–837.

57. Liu W, Wang S, Soetikno B, et al. Increased Retinal Oxygen Metabolism Precedes Microvascular Alterations in Type 1 Diabetic Mice. *Invest Ophthalmol Vis Sci*. 2017;58:981–989.

58. Scarinci F, Jampol LM, Linsenmeier RA, Fawzi AA. Association of Diabetic Macular Nonperfusion With Outer Retinal Disruption on Optical Coherence Tomography. *JAMA Ophthalmol*. 2015;133:1036–1044.

59. Chua J, Le T-T, Tan B, et al. Choriocapillaris microvasculature dysfunction in systemic hypertension. *Sci Rep*. 2021;11:4603.

60. Leskova W, Warar R, Harris NR. Altered Retinal Hemodynamics and Mean Circulation Time in Spontaneously Hypertensive Rats. *Invest Ophthalmol Vis Sci.* 2020;61:12.

61. Chua J, Chin CWL, Hong J, et al. Impact of hypertension on retinal capillary microvasculature using optical coherence tomographic angiography. *J Hypertens*. 2019;37:572–580.

62. Cringle SJ, Yu D-Y. A multi-layer model of retinal oxygen supply and consumption helps explain the muted rise in inner retinal Po2 during systemic hyperoxia. *Comp Biochem Physiol A Mol Integr Physiol*. 2002;132(1):61-66.

63. Wang S, Linsenmeier RA. Hyperoxia improves oxygen consumption in the detached feline retina. *Invest Ophthalmol Vis Sci*. 2007;48:1335–1341.

64. Palkovits S, Lasta M, Told R, et al. Retinal oxygen metabolism during normoxia and hyperoxia in healthy subjects. *Invest Ophthalmol Vis Sci*. 2014;55:4707–4713.

65. Wilson DF, Erecińska M. Effect of oxygen concentration on cellular metabolism. *Chest*. 1985;88:229S–232S.

66. Wang L, Kondo M, Bill A. Glucose metabolism in cat outer retina. Effects of light and hyperoxia. *Invest Ophthalmol Vis Sci*. 1997;38:48–55.

67. Natoli R, Fernando N, Dahlenburg T, et al. Obesity-induced metabolic disturbance drives oxidative stress and complement activation in the retinal environment. *Mol Vis*. 2018;24:201–217.

68. Liu X, He X, Yin Y, et al. Retinal oxygen saturation in 1461 healthy children aged 7–19 and its associated factors. *Acta Ophthalmol*. 2019;97(3):287-295.

69. Dai C, Liu X, Zhang HF, Puliafito CA, Jiao S. Absolute retinal blood flow measurement with a dual-beam Doppler optical coherence tomography. *Invest Ophthalmol Vis Sci*. 2013;54:7998–8003.

70. Garhofer G, Werkmeister R, Dragostinoff N, Schmetterer L. Retinal blood flow in healthy young subjects. *Invest Ophthalmol Vis Sci.* 2012;53:698–703.

71. Lee B, Novais EA, Waheed NK, et al. En Face Doppler Optical Coherence Tomography Measurement of Total Retinal Blood Flow in Diabetic Retinopathy and Diabetic Macular Edema. *JAMA Ophthalmol*. 2017;135:244–251.

72. Wang Y, Fawzi AA, Tan O, Zhang X, Huang D. Flicker-induced changes in retinal blood flow assessed by Doppler optical coherence tomography. *Biomed Opt Express*. 2011;2:1852–1860.

73. Srinivas S, Tan O, Wu S, et al. Measurement of retinal blood flow in normal Chinese-American subjects by Doppler Fourier-domain optical coherence tomography. *Invest Ophthalmol Vis Sci*. 2015;56:1569–1574.

74. Oishi A, Hidaka J, Yoshimura N. Quantification of the image obtained with a wide-field scanning ophthalmoscope. *Invest Ophthalmol Vis Sci*. 2014;55:2424–2431.

75. Jeppesen SK, Bek T. The Retinal Oxygen Saturation Measured by Dual Wavelength Oximetry in Larger Retinal Vessels is Influenced by the Linear Velocity of the Blood. *Curr Eye Res*. 2019;44:46–52.

76. Flammer J, Orgül S, Costa VP, et al. The impact of ocular blood flow in glaucoma. *Prog Retin Eye Res*. 2002;21:359–393.

Chapter 7

GENERAL DISCUSSION – OVERVIEW AND FUTURE PERSPECTIVES

7.1. (Instead of an) Abstract

"If in a discussion of many matters (…) we are not able to give perfectly exact and self-consistent accounts, do not be surprised: rather we would be content if we provide accounts that are second to none in probability." – Plato (Timaeus)

"I often quote myself. It adds spice to my conversation." – George Bernard Shaw

7.2. Summary of Main Results

Blood pressure (BP) has long been debated as an additional risk factor for glaucoma, but its exact contribution lacks lucidity, due to the abundance of conflicting findings.[1] As a whole, this dissertation constitutes a rigorous endeavor to present a cohesive story, explaining if and under what circumstances BP could indeed predispose to susceptibility for glaucomatous damage. To this end, even though each individual finding has already been extensively discussed elsewhere within this treatise, hereunder I summarize all the main findings collectively. I additionally provide some insight to the plot of this thesis, explaining how each finding paved the way for the next, giving rise to new questions and setting up subsequent studies.

7.2.1. Antihypertensive Medication and Glaucoma

In Chapter 2, we used data from the Groningen Longitudinal Glaucoma Study (GLGS) to examine (among others) the association between the reported use of antihypertensive (AH) medication and the rate of glaucomatous progression, as assessed by standard visual field testing. We also investigated the same relationship, now for the odds of conversion of glaucoma suspects to a definite glaucoma diagnosis. We found no overall effect, but we reported protective associations, specifically for AH medication belonging to the renin-angiotensin-system-acting agents, that is, angiotensin-converting enzyme inhibitors and angiotensin II receptor blockers.[2]

At first, this might sound counterintuitive. Arterial hypertension (AHT) is long known to be associated with elevated intraocular pressure (IOP), as well as with retinal nerve fiber layer (RNFL) and ganglion cell-inner plexiform layer (GCIPL) thinning, which both indicate proneness to glaucomatous optic neuropathy (GON).[3,4] In addition, aggressive treatment of AHT has also been linked to GON, likely not unrelated to ischemic insults to the retinal ganglion cells.[5] Do our findings then allegedly contradict a possible involvement of AHT in the pathogenesis of glaucoma? This is not the case, mainly for two reasons.

First, it must be noted that the GLGS population consists of glaucoma patients and suspects, hence creating selection bias, due to being already ‘further down the line’. Indeed, any possible contribution of AHT to glaucomatous optic neuropathy (GON) or to elevated

intraocular pressure (IOP) is likely already neutralized, because individuals receiving antihypertensive treatment are compared with individuals who share similar characteristics, in terms of GON. For instance, they are compared to patients who developed glaucoma without receiving AHT treatment, that is, to patients that may have untreated AHT or may be vulnerable to glaucoma due to another - yet unidentified - factor. Second, it may well be the case that the use of AH medication itself is harmful (from the perspective of glaucoma), but only in populations where it is being introduced aggressively or after years of untreated AHT, when chronic damage to the vessel walls renders regulation of blood flow problematic. Therefore, with the implemented study design, it is not surprising that the potential neuroprotective properties of certain AH medication categories that we discuss in Chapter 2 outshine any detrimental effect. The existence of a neuroprotective effect is supported by the fact that findings were confined to the renin-angiotensin-system-acting agents, which are already known to display such properties. It is also supported by the age-dependence of this protection, with older patients, who are more likely to display disturbances of the ocular circulation, benefiting more from their use. Table 1 summarizes the BP-related factors suggesting whether a subject is susceptible or not to GON.

Table 1. Factors conditioning the development of glaucomatous optic neuropathy (GON)

Low GON probability	High GON probability
timely AHT treatment	late AHT treatment
higher BP targets	lower BP targets
neuroprotective AH medication	retinal thinning or IOP elevation
nocturnal dipping absent	nocturnal dipping present

AHT, arterial hypertension; *BP*, blood pressure; *AH*, antihypertensive; *IOP*, intraocular pressure.

These realizations confirmed the considerable need to establish the baseline conditions of BP status, retinal perfusion, and retinal neural structure, in what we currently perceive as ophthalmologically healthy subjects, before we can claim a vascular component in the pathogenesis of glaucoma. A question still lingered though: how can we assess retinal perfusion, in order to find the missing link between BP and retinal structure?

7.2.2. Quantitative Optical Coherence Tomography Angiography

To answer this question, we first need to obtain reliable information on the morphology and perfusion density of the retinal microvascular network. On the one hand, the larger retinal

vessels are accessible and measurable by means of standard, validated fundus imaging techniques, which were utilized in subsequent studies (Chapters 4-6).[6] We have presented additional documentation on the reliability of these techniques, currently published in abstract form.[7] On the other hand, depicting the smaller vessels is a much more challenging task, which requires the use of optical coherence tomography angiography (OCTA), a high-resolution imaging modality, introduced over the last decade.[8]

In Chapter 3, we used image analysis techniques to develop an optimized method to quantify the density and flux index of the microvasculature, based on existing OCTA literature. We subsequently examined the test-retest variability and found that it ranged from good to excellent, depending on the metric examined.[9] In addition, we showed that these metrics correlated well with structural measurements obtained from healthy eyes, by means of OCT. Last, in a supporting publication (again, not part of this treatise), we showed that this microvascular information extracted from OCTA images was able to discriminate well between glaucoma subjects and healthy controls.[10] This software has been made freely accessible (https://figshare.com/articles/software/Image_Processing_Scripts/12982115) and it can be modified and tailored to OCT devices of different manufacturers.

Nevertheless, the metrics derived by OCTA mostly describe the structure of the vasculature, thus they do not sufficiently describe perfusion in its entirety. How can we combine all this information to predict retinal blood flow (RBF), that is, the volume of blood traversing the retinal microvascular network in the unit of time?

7.2.3. A Model for Static Retinal Blood Flow Autoregulation

In Chapter 4, we addressed this question by extending a Poiseuille-based, biophysical model for retinal vascular resistance (RVR) and RBF, based on the fractal geometry of the vasculature. We also proposed a method to estimate the autoregulation range of the retinal microcirculation, that is, the perfusion pressure range inside which RBF can be maintained relatively constant. We validated the outcomes of this model against *in vivo* flow metrics obtained from healthy and glaucomatous eyes, before and after IOP elevation, by means of Laser Speckle Flowgraphy. We found that the model had a high predictive ability and was in line with physiological expectations.[11]

Our results showed that, despite their ability to autoregulate by changing their caliber, the retinal vessels are still prone to flow reduction from perfusion pressure drops. This could potentially explain why low BP and nocturnal hypotension have both been associated with increased glaucoma risk in past studies.[12-14] Interestingly, in those studies, the BP values below which the risk for glaucoma starts to increase correspond well to our estimated lower autoregulation limit (LARL). This indicates, but does not yet prove that the association between low BP and glaucoma can be attributed, at least partially, to perfusion deficits, or if some other unknown, unaccounted factor is responsible for these population-based observations.

Having established a way to assess retinal perfusion, we were now ready to answer the most pertinent questions of this treatise: is there a link between BP status and retinal structure, already apparent in ophthalmologically healthy eyes? If yes, could this link be attributed to retinal perfusion?

7.2.4. Blood Pressure, Retinal Perfusion, and Structural OCT

In Chapter 5, we performed a rigorous, prospective recruitment of ophthalmologically healthy participants with different BP status (low BP, normal BP, treated AHT, and untreated AHT). Specifically, we recruited patients who had been documented to belong to the tails of the BP distribution of a large-scale Dutch cohort (Lifelines), over multiple previous visits. A significant amount of vascular, structural, and clinical data were subsequently acquired, combined, and analyzed, with the knowledge gained from the previous chapters. We then approached our hypothesis in steps.[15]

First, we showed that a U-shaped association was present between BP and retinal thinning, that is, the (otherwise healthy) retinas of subjects with low or high BP were thinner, compared to controls. Second, we showed that subjects with low BP, as well as subjects with intensively treated AHT (i.e., lower BP treatment targets), were close to their LARL, thus potentially prone to episodes of hypoperfusion. Last, we established that retinal perfusion mediates, indeed, the relationship between BP status and retinal thinning. In particular, decreased RBF and compromised autoregulatory capacity lied in the explanatory pathway between BP status and retinal thinning, in the low BP and the treated AHT groups, confirming our hypothesis.

However, we noted that increased vascular resistance was also a mediator of the same relationship in both AHT groups, without a concomitant decrease in RBF. This finding seemed somewhat puzzling. We hypothesized that this phenomenon could be attributed to the observed increase in blood flow velocity, which is known to shorten the time taken by red blood cells to traverse the retinal circulation.[16] The reduced transit time could theoretically result in suboptimal oxygen extraction, inducing tissue hypoxia. After all, if we can estimate oxygen extraction, this would likely provide a more complete picture than RBF alone. This observation brings us to our last chapter.

7.2.5. Blood Pressure and Retinal Oxygenation

In Chapter 6, we used the outcomes of the previous chapter, in combination with a customized retinal oximeter, to estimate the net volume of oxygen delivered (DO_2) and extracted (VO_2) by the retinas of the same healthy participants with different BP status. Contrary to what we expected, subjects in the untreated AHT group had the highest VO_2, compared to all other groups.[17]

We speculated on a number of potential mechanisms that could justify this apparently paradoxical finding. The explanation that is mostly supported by the literature suggests that this excess VO_2 is actually not consumed by the inner retina, but by the photoreceptors in the outer retina. This is already true in physiological conditions, but especially in conditions where the main supply of the photoreceptors, that is, the choroidal circulation, becomes compromised.[18] Indeed, there is recent evidence that uncontrolled AHT has a detrimental effect on the choriocapillaris.[19]

Last, in order to debunk a common fallacy reported in the retina and other systems, we used the same data to investigate the relationship between DO_2 and VO_2. From a physiological perspective, VO_2 should only depend on tissue needs, but numerous studies have reported that VO_2 is dependent on DO_2.[20] We argue that this was only due to the inflated correlation stemming from the mathematical coupling of these variables. Indeed, we used compensatory statistical techniques to rigorously demonstrate that the two variables are independent within their physiological range. DO_2 is already regulated through its RBF component, based on signals from the tissue. This lack of strong association between DO_2 and VO_2 suggests that, even when RBF and autoregulatory capacity are compromised, the oxygen extraction

mechanisms constitute an additional line of defense, opposing tissue hypoxia. Only when significant drops in RBF occur, for example during pronounced nocturnal BP dipping, do we eventually expect a drop in VO_2 with decreasing DO_2.

7.3. Impact and Future Directions

The vascular theory of glaucoma has been a subject of interest for many decades, with countless open problems yet to be solved and pertinent questions awaiting to be answered. Although this dissertation helped further the field by enhancing our current understanding on the topic of retinal perfusion, its completion only marks the beginning of a multitude of future possibilities.

It has long been known that the death of ganglion cells results in decreased oxygen demand and a concomitant decrease in RBF. In the ‘chicken-egg’ dilemma of glaucoma, this observation is known as the ‘egg’ component. This thesis concluded that there likely also exists a ‘chicken’ component in this causal cascade, according to which structural alterations could also be secondary to vascular insults. Indeed, subclinical retinal thinning was found without the presence of a glaucoma diagnosis and was associated with low and high BP, which are both recognized as risk factors of glaucoma. In addition, although the coinciding structural and vascular findings in these subjects still do not allow for disentangling temporality, the novel finding of a compromised autoregulatory capacity mediating this association contains the element of directionality, in the absence of an inverse explanatory pathway (structural deficits can lead to decreased RBF, but not to a smaller autoregulatory reserve). In the clinical setting, these observations could pertain to early detection of glaucoma or to the timely identification and targeting of subjects who are more at risk of developing the disease. However, future studies with a longitudinal design should verify whether higher odds exist that the reported deficits will convert to a glaucoma diagnosis.

In the next decades, the prevalence of glaucoma is expected to increase, due to the constantly aging population. In addition, based on recent interventional trial evidence, the guidelines for treating AHT have been revised to target lower BP values.[21] Therefore, based on the results of this thesis, glaucoma and hypertension specialists should opt for collaborative assessment and precision management of patients when both pathologies coexist. With regards to AH medication and glaucoma, there is arguably merit in focusing on the neuroprotective

properties that they have been shown to exhibit *in vitro*. However, it must be acknowledged that tailored designs in the form of randomized control trials are almost non-realistic, because these medications are widely used for the treatment of cardiovascular disease and their assignment is also subject to multiple concomitant indications and contraindications, based on coexisting clinical information.

Last, in view of the interesting results that we presented in the previous chapter, we hereby stress the need for more complex imaging and modeling studies, in order to understand the synergy between the retinal, choroidal, and retrobulbar circulation. It must be noted though that, with the introduction of OCTA, the additive value of vascular metrics in glaucoma management is not limited to the pathophysiological dimension. It has been shown that lots of useful information can be extracted for diagnostic purposes, when combined appropriately with structural and functional endpoints.[22] In this dissertation, we presented feasible methods for the rigorous assessment of the retinal circulation and oxygenation in the clinical setting. This could be meaningful, because vascular parameters relate to the majority of ophthalmic diseases, but currently there exists no gold standard for their objective evaluation. Our future work, which is currently supported by Oogfonds (Stichting Oogfonds Nederland), aims to expand on these topics. Our primary goal is to topographically combine vascular endpoints with structural and functional information, in order to improve predictions of future glaucomatous progression in the GLGS.

7.4. Major Findings

- The use of ARBs is associated with slower glaucomatous progression in older subjects. The use of ARBs or ACEIs is associated with decreased odds of conversion of glaucoma suspects to a definite glaucoma diagnosis.

- Quantitative OCTA with a customized image analysis tool showed good to excellent test-retest variability.

- A Poiseuille-based model for RVR and RBF built based on BP, IOP, vascular diameter, fractal branching dimension, and blood viscosity highly correlated with *in vivo* Laser Speckle Flowgraphy measurements. Predicted RBF autoregulation limits showed good concordance with measurements obtained before and after IOP

elevation. The retinal microvasculature is closer to its LARL than thought before, suggesting that drops in perfusion pressure are clinically relevant.

- A U-shaped association exists between BP status and RNFL or GCIPL thinning in ophthalmologically healthy subjects. A small autoregulatory reserve is present in patients with low BP and intensively treated AHT. Decreased RBF explains the association between low BP and GCIPL thinning, increased RVR explains the association between untreated AHT and GCIPL thinning, and increased RVR together with small autoregulatory reserve explains the association between treated AHT and GCIPL thinning.

- Ophthalmologically healthy subjects with untreated AHT have higher retinal VO2 than patients with treated AHT and higher retinal DO2 and VO2 than subjects with low BP.

7.5. References

1. Leeman M, Kestelyn P. Glaucoma and Blood Pressure. *Hypertension*. 2019;73:944–950.

2. Pappelis K, Loiselle AR, Visser S, Jansonius NM. Association of Systemic Medication Exposure With Glaucoma Progression and Glaucoma Suspect Conversion in the Groningen Longitudinal Glaucoma Study. *Invest Ophthalmol Vis Sci*. 2019;60:4548–4555.

3. Klein BEK, Klein R, Knudtson MD. Intraocular pressure and systemic blood pressure: longitudinal perspective: the Beaver Dam Eye Study. *Br J Ophthalmol*. 2005;89:284-287.

4. Chong RS, Chee M-L, Tham Y-C, et al. Association of Antihypertensive Medication with Retinal Nerve Fiber Layer and Ganglion Cell-Inner Plexiform Layer Thickness. *Ophthalmology*. 2021;128:393–400.

5. Topouzis F, Wilson MR, Harris A, et al. Association of open-angle glaucoma with perfusion pressure status in the Thessaloniki Eye Study. *Am J Ophthalmol*. 2013;155:843–851.

6. Knudtson MD, Lee KE, Hubbard LD, Wong TY, Klein R, Klein BEK. Revised formulas for summarizing retinal vessel diameters. *Curr Eye Res* 2003;27:143–149.

7. Pappelis K, Jansonius NM. Quantitative assessment of retinal blood vessels by means of a scanning laser ophthalmoscope (SLO) and a fundus camera (FC): a comparative study [abstract]. Invest Ophthalmol Vis Sci. 2020;61:528.

8. Jia Y, Tan O, Tokayer J, et al. Split-spectrum amplitude-decorrelation angiography with optical coherence tomography. *Opt Express.* 2012;20:4710–25.

9. Pappelis K, Jansonius NM. Quantification and Repeatability of Vessel Density and Flux as Assessed by Optical Coherence Tomography Angiography. *Transl Vis Sci Technol* 2019;8:3.

10. Al-Nosairy KO, Prabhakaran GT, Pappelis K, Thieme H, Hoffmann MB. Combined Multi-Modal

Assessment of Glaucomatous Damage With Electroretinography and Optical Coherence Tomography/Angiography. *Transl Vis Sci Technol*. 2020;9(12):7.

11. Pappelis K, Choritz L, Jansonius N. Microcirculatory model predicts blood flow and autoregulation range in the human retina: in vivo investigation with Laser Speckle Flowgraphy. *Am J Physiol Heart Circ Physiol*. 2020;319(6):H1253-1273.

12. Leske MC, Heijl A, Hyman L, et al. Predictors of long-term progression in the early manifest glaucoma trial. *Ophthalmology*. 2007;114:1965-1972.

13. Leske MC, Wu S-Y, Hennis A, Honkanen R, Nemesure B, BESs Study Group. Risk factors for incident open-angle glaucoma: the Barbados Eye Studies. *Ophthalmology* 2008;115:85–93.

14. Bowe A, Grünig M, Schubert J, et al. Circadian Variation in Arterial Blood Pressure and Glaucomatous Optic Neuropathy--A Systematic Review and Meta-Analysis. *Am J Hypertens*. 2015;28:1077-1082.

15. Pappelis K, Jansonius NM. U-Shaped Effect of Blood Pressure on Structural OCT Metrics and Retinal Perfusion in Ophthalmologically Healthy Subjects. *Invest Ophthalmol Vis Sci*. 2021;62:5.

16. Leskova W, Warar R, Harris NR. Altered Retinal Hemodynamics and Mean Circulation Time in Spontaneously Hypertensive Rats. *Invest Ophthalmol Vis Sci*. 2020;61(10):12.

17. Pappelis K, Jansonius NM. Retinal Oxygen Delivery and Extraction in Ophthalmologically Healthy Subjects With Different Blood Pressure Status. Transl Vis Sci Technol. 2022;11(2):9.

18. Linsenmeier RA, Zhang HF. Retinal oxygen: from animals to humans. *Prog Retin Eye Res*. 2017;58:115–151.

19. Chua J, Le T-T, Tan B, et al. Choriocapillaris microvasculature dysfunction in systemic hypertension. *Sci Rep*. 2021;11:4603.

20. Vincent J-L, De Backer D. Oxygen transport-the oxygen delivery controversy. *Intensive Care Med*. 2004;30:1990–1996.

21. Wright JT, Williamson JD, Whelton PK, et al. SPRINT Research Group. A randomized trial of intensive versus standard blood pressure control. *N Engl J Med*. 2015;373:2103-2116.

22. Wong D, Chua J, Lin E, et al. Focal Structure-Function Relationships in Primary Open-Angle Glaucoma Using OCT and OCT-A Measurements. *Invest Ophthalmol Vis Sci*. 2020;61(14):33.

Appendix A

SUPPLEMENTS

ABBREVIATIONS

SAMMENVATING

Supplements

Table S1. Saturated model with median rate of progression as dependent variable (Chapter 2)

	Coefficient	P value
Age (yrs)	-0.007	<0.001
Gender (female)	0.115	0.014
BMI (kg/m^2)	0.005	0.29
IOP before treatment (mmHg)	0.005	0.062
CCT (µm)	-0.0007	0.12
VF MD at baseline (0 = below median MD)	-0.016	0.71
Mean IOP during follow-up (mmHg)	-0.005	0.49
Glaucoma Surgery (0=No)	-0.020	0.69
Number of glaucoma medications	-0.037	0.041
Statins	-0.031	0.54
Diuretics	-0.009	0.88
Angiotensin II receptor blockers	0.102	0.063
ACE inhibitors	-0.028	0.54
Calcium channel blockers	-0.085	0.25
Beta blockers	0.046	0.41
Proton pump inhibitors	-0.052	0.32

BMI body mass index, *IOP* intraocular pressure, *CCT* central corneal thickness, *VF MD* standard automated perimetry mean deviation.

Table S2. Saturated model with glaucoma suspect conversion as dependent variable (Chapter 2)

	OR (95% CI)	P value
Age (yrs)	1.02 (0.98,1.07)	0.29
Gender (female)	1.12 (0.45,2.81)	0.80
BMI (kg/m^2)	0.97 (0.86,1.10)	0.60
IOP before treatment (mmHg)	1.01 (0.95,1.08)	0.65
CCT (µm)	0.99 (0.98,1.00)	0.11
Mean IOP during follow-up (mmHg)	0.94 (0.81,1.09)	0.42
Number of glaucoma medications	0.66 (0.40,1.09)	0.093
Statins	0.54 (0.14,2.12)	0.38
Diuretics	0.44 (0.10,1.96)	0.27
Angiotensin II receptor blockers	0.15 (0.01,1.75)	0.09
ACE inhibitors	0.37 (0.07,1.78)	0.20
Calcium channel blockers	1.70 (0.32,9.19)	0.54
Beta blockers	1.23 (0.28,5.44)	0.78
Proton pump inhibitors	1.08 (0.37,3.14)	0.89

OR Odds ratio, *CI* confidence interval, *BMI* body mass index, *IOP* intraocular pressure, *CCT* central corneal thickness.

Table S3. Reduced multivariable fitting models for retinal vascular resistance (RVR) and retinal blood flow (RBF) with laser speckle flowgraphy metrics (Chapter 4)

*Recalculation based on the **in vivo** viscosity formulas by Pries et al.*					
RVR (mmHg min µl^{-1})			**RBF (µl min^{-1})**		
R^2	0.76 (P=1.9·10^{-8})		**R^2**	0.63 (P=2.0·10^{-6})	
	Beta	**P value**		**Beta**	**P value**
MV	-0.067	4.1·10^{-7}	**MV**	0.3	3.1·10^{-5}
FAI	0.497	2.6·10^{-5}	**FAI**	-2.7	6.1·10^{-5}
Skew	-0.148	6.7·10^{-5}	**Skew**	1.1	1.0·10^{-6}
Fluctuation	-0.094	0.091	**HR**	-0.1	0.030
MAP	0.036	3.0·10^{-6}	*NA*		
Median (IQR): 1.81 (1.67 to 2.51)			*Mean (SD):* 17 (5)		
*Recalculation based on the **in vitro** viscosity formulas by Pries et al.*					
RVR (mmHg min µl^{-1})			**RBF (µl min^{-1})**		
R^2	0.76 (P=1.9·10^{-8})		**R^2**	0.60 (P=7.0·10^{-6})	
	Beta	**P value**		**Beta**	**P value**
MV	-0.018	1.0·10^{-6}	**MV**	0.9	3.7·10^{-4}
FAI	0.136	3.5·10^{-5}	**FAI**	-9.6	2.9·10^{-4}
Skew	-0.044	2.7·10^{-5}	**Skew**	4.6	1.0·10^{-6}
Fluctuation	-0.027	0.080	**HR**	-0.4	0.045
MAP	0.010	3.0·10^{-6}	*NA*		
Median (IQR): 0.52 (0.46 to 0.74)			*Mean (SD):* 61 (19)		
MV: mean velocity in large vessels, FAI: flow acceleration index, MAP: mean arterial pressure, HR: heart rate, *NA*: not applicable, IQR: interquartile range, SD: standard deviation					

Table S4. Structural OCT metrics as a function of blood pressure status with group definitions based on SBP 5th/95th percentiles (Chapter 5)

	Group 1 (SBP < 5th percentile)	**Group 2 (Normal BP)**	**Group 3 (Treated AHT)**	**Group 4 (SBP > 95th percentile)**	***P* value**
Group size *(N)*	15	21	26	11	
GCIPL; µm [mean (SD)]	53.9 (2.7)	56.2 (3.0)	53.4 (3.3)	53.3 (1.7)	**0.007**
mRNFL; µm [mean (SD)]	37.3 (3.7)	39.8 (3.4)	36.0 (2.8)	39.5 (3.9)	**0.001**
Total pRNFL; µm [mean (SD)]	100.1 (8.0)	103.1 (10.1)	96.9 (9.2)	101.6 (8.1)	0.13
Temporal pRNFL; µm [mean (SD)]	71.1 (11.5)	74.0 (8.1)	65.5 (9.5)	73.8 (13.1)	**0.025**
Superior pRNFL; µm [mean (SD)]	120.9 (13.1)	124.1 (16.7)	119.5 (13.5)	126.9 (14.5)	0.47
Nasal pRNFL; µm [mean (SD)]	83.3 (11.6)	80.6 (14.1)	81.4 (11.4)	83.3 (15.0)	0.91
Inferior pRNFL; µm [mean (SD)]	124.9 (13.8)	134.0 (13.3)	122.7 (14.3)	120.6 (14.5)	**0.024**
NRR area; mm^2 [median (IQR)]	1.40 (1.29 to 1.56)	1.37 (1.27 to 1.74)	1.35 (1.18 to 1.64)	1.51 (1.35 to 1.68)	0.78
VCDR [median (IQR)]	0.50 (0.42 to 0.55)	0.49 (0.39 to 0.55)	0.47 (0.42 to 0.60)	0.52 (0.42 to 0.59)	0.89
OCT, optical coherence tomography; BP, blood pressure; SBP, systolic blood pressure; AHT, arterial hypertension; GCIPL, ganglion cell-inner plexiform layer; SD, standard deviation; mRNFL, macular retinal nerve fiber layer; pRNFL, peripapillary retinal nerve fiber layer; NRR, neuroretinal rim; VCDR, vertical cup-to-disc ratio.					

Table S5. Structural OCT metrics as a function of blood pressure status with group definitions based on DBP 5th/95th percentiles (Chapter 5)

	Group 1 (DBP < 5th percentile)	Group 2 (Normal BP)	Group 3 (Treated AHT)	Group 4 (DBP > 95th percentile)	*P* value
Group size *(N)*	5	21	26	15	
GCIPL; µm [mean (SD)]	52.2 (2.0)	56.2 (3.0)	53.4 (3.3)	52.5 (2.2)	**0.001**
mRNFL; µm [mean (SD)]	36.0 (1.2)	39.8 (3.4)	36.0 (2.8)	38.4 (3.7)	**<0.001**
Total pRNFL; µm [mean (SD)]	91.2 (4.8)	103.1 (10.1)	96.9 (9.2)	99.6 (9.2)	**0.036**
Temporal pRNFL; µm [mean (SD)]	69.6 (14.5)	74.0 (8.1)	65.5 (9.5)	69.8 (13.6)	0.067
Superior pRNFL; µm [mean (SD)]	106.6 (9.1)	124.1 (16.7)	119.5 (13.5)	127.0 (16.5)	0.055
Nasal pRNFL; µm [mean (SD)]	76.2 (13.8)	80.6 (14.1)	81.4 (11.4)	82.6 (13.8)	0.81
Inferior pRNFL; µm [mean (SD)]	113.6 (7.0)	134.0 (13.3)	122.7 (14.3)	119.7 (13.4)	**0.002**
NRR area; mm² [median (IQR)]	1.22 (1.10 to 1.74)	1.37 (1.27 to 1.74)	1.35 (1.18 to 1.64)	1.51 (1.41 to 1.68)	0.31
VCDR [median (IQR)]	0.46 (0.16 to 0.59)	0.49 (0.39 to 0.55)	0.47 (0.42 to 0.60)	0.51 (0.40 to 0.58)	0.80

OCT, optical coherence tomography; BP, blood pressure; DBP, diastolic blood pressure; AHT, arterial hypertension; GCIPL, ganglion cell-inner plexiform layer; SD, standard deviation; mRNFL, macular retinal nerve fiber layer; pRNFL, peripapillary retinal nerve fiber layer; NRR, neuroretinal rim; VCDR, vertical cup-to-disc ratio.

Table S6. Autoregulatory reserve as a function of blood pressure status, compared to controls per decile (Chapter 5)

	Low BP (Group 1) *Baseline: Group 2*		Treated AHT (Group 3) *Baseline: Group 2*		Untreated AHT (Group 4) *Baseline: Group 2*	
	Effect (b)	***P* value**	**Effect (b)**	***P* value**	**Effect (b)**	***P* value**
Q10	-3.0	**0.019**	-3.0	**0.027**	2.1	0.15
Q20	-3.2	**0.009**	-2.3	0.065	3.3	**0.026**
Q30	-3.9	**0.003**	-3.6	**0.009**	2.9	0.057
Q40	-4.3	**0.004**	-2.1	0.16	3.9	**0.019**
Q50	-3.5	**0.038**	-0.2	0.91	4.5	**0.019**
Q60	-3.7	**0.027**	1.5	0.39	4.4	**0.020**
Q70	-5.8	**0.001**	1.6	0.36	3.4	0.083
Q80	-4.6	**0.025**	1.9	0.37	4.9	**0.034**
Q90	-4.0	**0.006**	3.6	**0.016**	3.6	**0.027**

AR, autoregulatory reserve; BP, blood pressure; AHT, arterial hypertension.

Table S7. Effect of blood pressure status on the GCIPL: mediation analysis with group definitions based on SBP 5th/95th percentiles (Chapter 5)

	Controls + SBP < 5th percentile (Group 2 + Group 1)		Controls + treated AHT (Group 2 + Group 3)		Controls + SBP > 95th percentile (Group 2 + Group 4)	
	Effect	*P*	Effect	*P*	Effect	*P*
Mediation step 1:						
GCIPL ~ SBP	b_{SBP}=0.07	0.069	b_{SBP}=-0.06	0.056	b_{SBP}=-0.05	**0.016**
Mediation step 2:						
RBF ~ SBP	b_{SBP}=0.21	**0.029**				
RVR ~ SBP			b_{SBP}=0.002	0.14	b_{SBP}=0.003	**0.002**
AR ~ SBP			b_{SBP}=0.04	0.35		
Mediation step 3:						
GCIPL ~ SBP + RBF	b_{SBP}=0.03	0.34				
	b_{RBF}=0.15	**0.017**				
GCIPL ~ SBP + RVR			b_{SBP}=-0.04	0.18	b_{SBP}=-0.03	0.21
			b_{RVR}=-12.00	**0.0005**	b_{RVR}=-7.30	0.089
GCIPL ~ SBP + AR			b_{SBP}=-0.05	0.095		
			b_{AR}=-0.24	**0.016**		
GCIPL ~ SBP + RVR + AR			b_{SBP}=-0.03	0.29		
			b_{RVR}=-26.53	**0.001**		
			b_{AR}=0.44	**0.048**		
Sobel test	0.092		RVR: 0.078; AR: 0.38		0.13	

BP, blood pressure; GCIPL, ganglion cell-inner plexiform layer; SBP, systolic blood pressure; AHT, arterial hypertension; RBF, retinal blood flow; RVR, retinal vascular resistance; AR, autoregulatory reserve.

Table S8. Effect of blood pressure status on the GCIPL: mediation analysis with group definitions based on DBP 5th/95th percentiles (Chapter 5)

	Controls + DBP < 5th percentile (Group 2 + Group 1)		Controls + treated AHT (Group 2 + Group 3)		Controls + DBP > 95th percentile (Group 2 + Group 4)	
	Effect	*P*	Effect	*P*	Effect	*P*
Mediation step 1:						
GCIPL ~ DBP	b_{DBP}=0.15	**0.019**	b_{DBP}=-0.10	0.070	b_{DBP}=-0.10	**0.017**
Mediation step 2:						
RBF ~ DBP	b_{DBP}=0.32	0.089				
RVR ~ DBP			b_{DBP}=0.007	**0.001**	b_{DBP}=0.006	**0.0001**
AR ~ DBP			b_{DBP}=0.26	**0.001**		
Mediation step 3:						
GCIPL ~ DBP + RBF	b_{DBP}=0.11	0.078				
	b_{RBF}=0.13	0.064				
GCIPL ~ DBP + RVR			b_{DBP}=-0.01	0.85	b_{DBP}=-0.04	0.44
			b_{RVR}=-12.62	**0.001**	b_{RVR}=-10.73	**0.035**
GCIPL ~ DBP + AR			b_{DBP}=-0.04	0.48		
			b_{AR}=-0.22	**0.050**		
GCIPL ~ DBP + RVR + AR			b_{DBP}=-0.03	0.60		
			b_{RVR}=-28.12	**0.001**		
			b_{AR}=0.49	**0.029**		
Sobel test	0.19		RVR: **0.013**; AR: 0.078		**0.039**	

BP, blood pressure; GCIPL, ganglion cell-inner plexiform layer; DBP, diastolic blood pressure; AHT, arterial hypertension; RBF, retinal blood flow; RVR, retinal vascular resistance; AR, autoregulatory reserve.

Table S9. Regression coefficients of confounding factors associated with optical density ratios in multivariable analysis, including only significant effects (Chapter 6)

		PI	Sphere	Cylinder (negative)	Disc area	Laterality (0=OD, 1=OS)
ST	**ODR_{art}**	-0.158	*NA*	*NA*	*NA*	*NA*
	ODR_{ven}	-0.159	*NA*	*NA*	*NA*	*NA*
IT	**ODR_{art}**	*NA*	0.016	*NA*	*NA*	-0.102
	ODR_{ven}	*NA*	*NA*	-0.062	*NA*	-0.093
SN	**ODR_{art}**	*NA*	*NA*	*NA*	*NA*	*NA*
	ODR_{ven}	*NA*	*NA*	*NA*	*NA*	-0.096
IN	**ODR_{art}**	*NA*	*NA*	*NA*	+0.064	+0.085
	ODR_{ven}	-0.139	*NA*	*NA*	*NA*	*NA*

ODR_{art}, arterial optical density ratio; ODR_{ven}, venous optical density ratio; ST, superotemporal; IT, inferotemporal; SN, superonasal; IN, inferonasal; PI, pigmentation index; OD, oculus dexter; OS, oculus sinister; *NA*, not applicable.

Table S10. Corrected optical density ratios per retinal quadrant (Chapter 6)

	Arterial ODR_{cor}	Venous ODR_{cor}	*P* value
Global [mean (SD)]	0.138 (0.052)	0.262 (0.052)	**$2.5 \cdot 10^{-37}$**
ST [mean (SD)]	0.178 (0.081)	0.269 (0.071)	**$2.6 \cdot 10^{-19}$**
IT [mean (SD)]	0.170 (0.103)	0.313 (0.109)	**$3.2 \cdot 10^{-20}$**
SN [mean (SD)]	0.078 (0.115)	0.202 (0.097)	**$2.0 \cdot 10^{-16}$**
IN [mean (SD)]	0.124 (0.118)	0.265 (0.086)	**$3.7 \cdot 10^{-14}$**
***P* value**	**$1.7 \cdot 10^{-10}$**	**$1.4 \cdot 10^{-13}$**	

ODR_{cor}, corrected optical density ratio; ST, superotemporal; IT, inferotemporal; SN, superonasal; IN, inferonasal; SD, standard deviation.

Abbreviations

AC	autoregulatory change
ACEI	angiotensin-converting enzyme inhibitor
AD	autoregulatory deviation
AH	antihypertensive
AHT	arterial hypertension
AIC	Akaike Information Criterion
ANOVA	analysis of variance
AR	autoregulatory reserve
ARB	angiotensin II receptor blocker
BF	blood flow
BMI	body mass index
BP	blood pressure
CCB	calcium channel blocker
CCT	central corneal thickness
CI	confidence interval
CoR	coefficient of repeatability
CRA	central retinal artery
CRAE	central retinal artery equivalent
CRV	central retinal vein
CRVE	central retinal vein equivalent
CV	coefficient of variation
DBP	diastolic blood pressure
DCP	deep capillary plexus
DO_2	oxygen delivery
EDV	end diastolic velocity
ELM	external limiting membrane
EMGT	Early Manifest Glaucoma Trial
FAI	flow acceleration index
FD	fractal dimension
FD-OCT	Fourier Domain optical coherence tomography
FMD	flow-mediated dilation
GCC	ganglion cell complex
GCIPL	ganglion cell-inner plexiform layer
GCL	ganglion cell layer
GLGS	Groningen Longitudinal Glaucoma Study
GON	glaucomatous optic neuropathy
HARL	higher autoregulation limit
HR	hazard ratio; heart rate
ICC	intraclass correlation coefficient
ICP	intermediate capillary plexus
ILM	inner limiting membrane
IN	inferonasal
INL	inner nuclear layer
IOP	intraocular pressure
IPL	inner plexiform layer
IQR	interquartile range
IT	inferotemporal
LARL	lower autoregulation limit
LSFG	laser speckle flowgraphy
MAP	mean arterial pressure

MBR	mean blur rate
MD	mean deviation
mRNFL	macular retinal nerve fiber layer
MV	mean velocity
NA	not applicable
NFI	normalized flux index
NO	nitric oxide
NRR	neuroretinal rim
NTG	normal tension glaucoma
OCT	optical coherence tomography
OCTA	optical coherence tomography angiography
OD	optical density
ODR	optical density ratio
OEF	oxygen extraction fraction
OHT	ocular hypertension
OHTS	Ocular Hypertension Treatment Study
ONH	optic nerve head
ONL	outer nuclear layer
OPL	outer plexiform layer
OPP	ocular perfusion pressure
OR	odds ratio
PCD	perfused capillary density
PI	pigmentation index
POAG	primary open angle glaucoma
PPI	proton pump inhibitor; pulse pressure index
pRNFL	peripapillary retinal nerve fiber layer
PSV	peak systolic velocity
RBF	retinal blood flow
RCT	randomized control trial
RGC	retinal ganglion cell
RI	resistivity index
RNFL	retinal nerve fiber layer
RNFLT	retinal nerve fiber layer thickness
ROI	region of interest
RoP	rate of progression
RPCP	radial peripapillary capillary plexus
RPE	retinal pigment epithelium
RPP	retinal perfusion pressure
RVR	retinal vascular resistance
S_aO_2	arterial oxygen saturation
SBP	systolic blood pressure
SCP/SVP	superficial capillary/vascular plexus
SD	standard deviation
SD-OCT	spectral domain optical coherence tomography
SEQ	spherical equivalent
SO_2	oxygen saturation
SLO	scanning laser ophthalmoscope
SN	superonasal
SS-OCT	swept-source optical coherence tomography
ST	superotemporal
S_vO_2	venous oxygen saturation
UMCG	University Medical Center Groningen
VA	visual acuity
VCDR	vertical cup-to-disc ratio
VF	visual field
VO_2	oxygen extraction

Samenvatting

De retina is een gelaagde structuur die achterin het oog ligt en verantwoordelijk is voor de complexe taak om visuele informatie op te vangen en door te geven aan de hersenen. De functie van de retina is afhankelijk van een efficiënte, goed gereguleerde perfusie (doorbloeding) en van voldoende zuurstoftoevoer. De binnenste cellaag van de retina is de ganglioncellaag. De axonen van de ganglioncellen vormen de oogzenuw en zijn verweven met de pathologie van een verraderlijke, neurodegeneratieve oogziekte, glaucoom.

Hoewel de pathogenese van glaucoom in wezen multifactorieel is, speelt een verhoogde oogdruk een centrale rol. Daarnaast leverde onderzoek in de afgelopen decennia bewijs op voor een vasculaire component van de ziekte. Vooral hypertensie (hoge bloeddruk) wordt in verband gebracht met glaucoom, omdat het de mechanismen zou kunnen verstoren waarmee de lokale microcirculatie voor voldoende weefselperfusie zorgt. De exacte bijdrage van hypertensie aan glaucoom is onduidelijk, vanwege vele tegenstrijdige bevindingen.

Recente ontwikkelingen in beeldvormingstechnieken hebben een gedetailleerde weergave van de retinale vascularisatie mogelijk gemaakt, samen met de neurale structuur van het netvlies. Hoewel er verschillende methoden zijn voorgesteld voor de kwantificering van de retinale perfusie en zuurstofextractie, heeft tot dusver geen enkele methode de weg naar de kliniek gevonden, voornamelijk vanwege technische tekortkomingen. Als gevolg hiervan is ons begrip van het samenspel tussen arteriële bloeddruk, retinale perfusie en oxygenatie, en hun relevantie voor glaucoom, vooralsnog grotendeels onvolledig. Als geheel vormt dit proefschrift een rigoureuze poging om een samenhangend verhaal te presenteren, waarin wordt uitgelegd of en onder welke omstandigheden bloeddruk inderdaad bijdraagt aan de gevoeligheid voor glaucoomschade.

In Hoofdstuk 2 hebben we gegevens uit de Groningen Longitudinal Glaucoma Study gebruikt om (onder andere) de associatie tussen het gebruik van antihypertensiva en de snelheid van glaucoomprogressie te onderzoeken, zoals bepaald met perimetrie (gezichtsveldonderzoek). Ook onderzochten we de relatie tussen het gebruik van

antihypertensiva en de kans op conversie van glaucoomverdachten naar een definitieve glaucoomdiagnose. We vonden geen effect van antihypertensiva in het algemeen, maar wel beschermende associaties specifiek voor de renine-angiotensinesysteem-beïnvloedende middelen, dat wil zeggen de ACE-remmers en de angiotensine II-receptor-blokkers. Omdat het gebruik van antihypertensiva wel schadelijk was gebleken in epidemiologische studies, vermoeden we dat het gebruik van antihypertensiva vooral schadelijk zou kunnen zijn (vanuit het perspectief van glaucoom) bij patiënten waarbij een al langer bestaande hypertensie, waardoor chronische schade aan de vaatwanden is ontstaan met een verminderde regulatie van de bloedstroming tot gevolg, te agressief wordt behandeld.

Voor een beter begrip van de rol van bloeddruk bij glaucoom is betrouwbare informatie over het retinale microvasculaire netwerk onmisbaar. **In Hoofdstuk 3** hebben we beeldanalysetechnieken gebruikt om een geoptimaliseerde methode te ontwikkelen om de dichtheid en fluxindex van de microvasculatuur te kwantificeren, door middel van OCT-angiografie (OCTA). Vervolgens hebben we de reproduceerbaarheid van deze beide maten onderzocht en vastgesteld dat deze varieerde van goed tot uitstekend. Ook toonden we aan dat deze maten goed correleerden met structurele metingen verkregen met OCT. Desalniettemin beschrijven deze maten toch vooral de structuur van het vaatstelsel, en niet de werkelijke perfusie. Hoe kunnen we al deze informatie combineren om de retinale perfusie te voorspellen, dat wil zeggen, het bloedvolume dat per tijdseenheid door het retinale microvasculaire netwerk gaat?

In Hoofdstuk 4 hebben we deze vraag beantwoord door een biofysisch model voor retinale vasculaire weerstand en retinale bloedstroom te ontwikkelen, gebaseerd op de wet van Poiseuille en de fractale geometrie van het vaatstelsel. We hebben daarbij ook een methode ontwikkeld om het autoregulatiebereik van de retinale microcirculatie te schatten, dat wil zeggen het perfusiedrukbereik waarbinnen de retinale bloedstroom relatief constant wordt gehouden. We hebben de resultaten van dit model gevalideerd met in vivo perfusiemetingen bij gezonde en glaucomateuze ogen, voor en na intraoculaire drukverhoging, door middel van Laser Speckle Flowgraphy. We ontdekten dat het model een hoog voorspellend vermogen had en in overeenstemming was met de fysiologische verwachtingen.

Onze resultaten toonden aan dat de retinale vaten, ondanks hun vermogen tot autoregulatie, toch gevoelig zijn voor bloeddrukdalingen, wat dan leidt tot een verminderde perfusie. Dat bracht ons op de meest relevante vraag van dit proefschrift: is er een verband

tussen de bloeddrukstatus en de structuur van het netvlies in oogheelkundig gezonde ogen? Zo ja, kan dit verband worden toegeschreven aan retinale perfusie?

In Hoofdstuk 5 hebben we prospectief oogheelkundig gezonde deelnemers gerekruteerd met verschillende bloeddrukstatus (lage bloeddruk, normale bloeddruk, behandelde arteriële hypertensie en onbehandelde arteriële hypertensie). In het bijzonder rekruteerden we patiënten waarvan was gedocumenteerd dat ze behoorden tot de extremen van de bloeddrukverdeling in de algemene bevolking (de deelnemers werden gerekruteerd uit een grootschalig Noord-Nederlands cohort, Lifelines).

Ten eerste toonden we aan dat er een U-vormig verband was tussen bloeddruk en een dunner netvlies, dat wil zeggen dat de netvliezen van (overigens gezonde) proefpersonen met lage of hoge bloeddruk dunner waren dan de netvliezen van proefpersonen met een normale bloeddruk. Ten tweede toonden we aan dat proefpersonen met een lage bloeddruk, evenals proefpersonen met een intensief behandelde arteriële hypertensie, dicht bij hun ondergrens van autoregulatie waren, dus mogelijk vatbaar zijn voor episodes van hypoperfusie. Als laatste hebben we vastgesteld dat retinale perfusie inderdaad de relatie tussen bloeddrukstatus en dunner netvlies medieert: een verminderde retinale perfusie en aangetast autoregulatievermogen lagen in de verklarende route tussen bloeddrukstatus en retinaverdunning in de groepen met lage bloeddruk en behandelde hoge bloeddruk, wat onze hypothese bevestigt.

We merkten echter op dat een verhoogde vaatweerstand ook een mediator was van dezelfde relatie in beide hypertensiegroepen (behandeld en onbehandeld), zonder een gelijktijdige afname van de retinale perfusie. Deze bevinding leek enigszins raadselachtig. We veronderstelden dat dit fenomeen zou kunnen worden toegeschreven aan de waargenomen toename van de bloedstroomsnelheid, wat de tijd verkort die rode bloedcellen nodig hebben om de retinale circulatie te doorkruisen. De kortere transittijd zou kunnen resulteren in een suboptimale zuurstofextractie, waardoor weefselhypoxie wordt veroorzaakt. Deze observatie brengt ons bij ons laatste hoofdstuk.

In Hoofdstuk 6 hebben we de uitkomsten van het vorige hoofdstuk gebruikt, in combinatie met een aangepaste retinale oximeter, om het netto volume van geleverde (DO_2) en geëxtraheerde (VO_2) zuurstof door het netvlies van dezelfde gezonde deelnemers met verschillende bloeddrukstatus te schatten. In tegenstelling tot wat we hadden verwacht,

hadden proefpersonen in de groep met onbehandelde arteriële hypertensie de hoogste VO_2, vergeleken met alle andere groepen.

We speculeerden over een aantal mogelijke mechanismen die deze schijnbaar paradoxale bevinding zouden kunnen verklaren. De verklaring die grotendeels door de literatuur wordt ondersteund, suggereert dat de extra VO_2 eigenlijk niet door het binnenste deel van het netvlies wordt geconsumeerd, maar door de fotoreceptoren in het buitenste deel van het netvlies. Dit is al het geval in fysiologische omstandigheden, maar vooral in omstandigheden waarin de hoofdtoevoer van de fotoreceptoren, dat wil zeggen de choroïdale circulatie, in gevaar komt, iets wat bij hypertensie gebeurt.

Als laatste hebben we dezelfde gegevens gebruikt om de relatie tussen DO_2 en VO_2 te onderzoeken. We gebruikten speciale statistische technieken om aan te tonen dat de twee variabelen onafhankelijk zijn binnen hun fysiologische bereik. Dit gebrek aan (sterke) associatie tussen DO_2 en VO_2 suggereert dat, zelfs wanneer de perfusie van het netvlies en het vermogen tot autoregulatie worden aangetast, de zuurstofextractiemechanismen een extra verdedigingslinie vormen tegen weefselhypoxie.

De vasculaire theorie van glaucoom is al tientallen jaren een onderwerp van debat, met vele, relevante openstaande vragen. Het is al lang bekend dat de dood van ganglioncellen resulteert in een verminderde zuurstofbehoefte en een daarmee gepaard gaande afname van de retinale perfusie. In het 'kip-ei'-dilemma van glaucoom staat deze waarneming bekend als de 'ei'-component. Dit proefschrift concludeert dat er waarschijnlijk ook een 'kip'-component bestaat, volgens welke de structurele veranderingen secundair zijn aan de vaatbeschadigingen. Hoewel samenvallende structurele en vasculaire bevindingen het niet mogelijk maken om volgordelijkheid te ontwarren, bevat de nieuwe bevinding van een gecompromitteerde autoregulatie die deze associatie medieert, het element van directionaliteit, in afwezigheid van een omgekeerde verklaringsroute (structurele defecten kunnen leiden tot een verminderde retinale perfusie, maar niet tot een kleinere autoregulatoire reserve). Toekomstige studies met een longitudinaal ontwerp zouden moeten nagaan of de gerapporteerde tekorten ook leiden tot een verhoogde kans op het ontwikkelen van glaucoom.

Appendix B

LAY SUMMARIES

EPILOGUE

ABOUT THE AUTHOR

Lay Summary

Glaucoma is a chronic eye disease characterized by thinning of the retina, death of ganglion cells, and progressive loss of vision, eventually leading to blindness. The prevalence of glaucoma is estimated at 1-3% of those over 40 years old. With a constantly aging population, this number is expected to increase significantly over the next 10 years. Even with treatment, about 15% of people with glaucoma currently develop residual vision or tunnel vision and eventually become blind or partially sighted.

The mechanisms behind ganglion cell death are poorly understood. Elevated eye pressure is the main risk factor for glaucoma, but treatment in the form of medication, laser, or surgery can only slow the decline, not stop it. In addition, high intraocular pressure is neither necessary nor sufficient for the development of glaucoma, indicating the existence of other unknown risk factors.

It has been established that the death of ganglion cells results in a decreased oxygen demand and a concomitant decrease in blood flow. However, there is also a hypothesis that reduced or unstable blood supply is not only a consequence, but also a cause of glaucoma. This is known as the ‘chicken-egg’ dilemma in glaucoma. It is supported by the observation that the risk of developing glaucoma is higher in people with very low blood pressure (sometimes even as a result of overtreatment of high blood pressure).

This dissertation is an attempt to methodically examine whether blood pressure can be linked to changes in the retina that could suggest susceptibility to glaucoma. For this purpose, we analyze epidemiological data from the Groningen Longitudinal Glaucoma Study, we use advanced imaging techniques to model the microcirculation, and we describe its relationship with the neural structure and oxygen consumption of the retina. We provide evidence leaning towards the existence of a vascular component, likely pertinent to glaucoma.

Publiekssamenvatting

Glaucoom is een chronische oogziekte die wordt gekenmerkt door dunner worden van het netvlies, afsterven van ganglioncellen en progressief verlies van het zien, wat uiteindelijk leidt tot blindheid. De prevalentie van glaucoom wordt geschat op 1-3% van de 40-plussers. Met een constant vergrijzende bevolking zal dit aantal naar verwachting de komende 10 jaar aanzienlijk toenemen. Zelfs met behandeling ontwikkelt momenteel ongeveer 15% van de mensen met glaucoom uiteindelijk blindheid of slechtziend.

De mechanismen onderliggend aan de dood van ganglioncellen worden slecht begrepen. Verhoogde oogdruk is de belangrijkste risicofactor voor glaucoom, maar behandeling in de vorm van medicatie, laser of chirurgie kan de achteruitgang alleen maar vertragen en niet stoppen. Bovendien is een hoge oogdruk niet nodig noch voldoende voor de ontwikkeling van glaucoom, wat wijst op het bestaan van andere, tot op heden onbekende risicofactoren.

Het is vastgesteld dat de dood van ganglioncellen resulteert in een verminderde zuurstofbehoefte en een gelijktijdige afname van de doorbloeding. Er is echter ook een hypothese dat een verminderde of onstabiele bloedtoevoer niet alleen een gevolg is, maar ook een oorzaak van glaucoom. Dit staat bekend als het ‘kip-en-eiprobleem’ bij glaucoom. Het wordt ondersteund door de waarneming dat het risico op het ontwikkelen van glaucoom hoger is bij mensen met een heel lage bloeddruk (soms zelfs als gevolg van overbehandeling van een hoge bloeddruk).

Dit proefschrift onderzoekt systematisch of bloeddruk kan worden gekoppeld aan veranderingen in het netvlies die kunnen wijzen op vatbaarheid voor glaucoom. Hiervoor analyseren we epidemiologische gegevens van de Groningen Longitudinal Glaucoma Study, gebruiken we geavanceerde beeldvormende technieken om de microcirculatie te modelleren en beschrijven we de relatie met de neurale structuur en het zuurstofverbruik van het netvlies. De resultaten pleiten voor het bestaan van een vasculaire component die waarschijnlijk relevant is voor glaucoom.

Περίληψη κοινού

Το γλαύκωμα είναι μια χρόνια οφθαλμική νόσος, η οποία χαρακτηρίζεται από λέπτυνση του αμφιβληστροειδούς, θάνατο γαγγλιακών κυττάρων και προοδευτική απώλεια όρασης, με κατάληξη την τύφλωση. Ο επιπολασμός του γλαυκώματος υπολογίζεται σε 1-3% των ατόμων άνω των 40 ετών. Λόγω του διαρκώς γηρασκόμενου πληθυσμού, αυτός ο αριθμός αναμένεται να αυξηθεί σημαντικά εντός της επόμενης δεκαετίας. Ακόμη και υπό θεραπεία, περίπου 15% των γλαυκωματικών αναπτύσσει ελλειμματική όραση ή όραση σήραγγας.

Οι μηχανισμοί πίσω από το θάνατο των γαγγλιακών κυττάρων δεν είναι πλήρως κατανοητοί. Η αυξημένη ενδοφθάλμια πίεση αποτελεί τον κυριότερο παράγοντα κινδύνου γλαυκώματος, αλλά η θεραπεία με τη μορφή φαρμακευτικής αγωγής, λέιζερ ή χειρουργείου μπορεί μόνο να καθυστερήσει την απόπτωση, και όχι να την αποτρέψει. Επιπρόσθετα, η υψηλή ενδοφθάλμια πίεση δεν είναι ούτε ικανή ούτε αναγκαία συνθήκη για την ανάπτυξη γλαυκώματος, καταδεικνύοντας την ύπαρξη άλλων άγνωστων παραγόντων κινδύνου.

Είναι γνωστό ότι ο θάνατος των γαγγλιακών κυττάρων οδηγεί σε μειωμένη ανάγκη για οξυγόνο και συνακόλουθη μείωση της αιματικής ροής. Ωστόσο, υπάρχει επίσης η υπόθεση πως η μειωμένη ή ασταθής αιμάτωση δεν αποτελεί μόνο συνέπεια, αλλά και αίτιο του γλαυκώματος. Αυτό είναι γνωστό ως το δίλημμα ‘αβγού-κότας’ στο γλαύκωμα. Υποστηρίζεται από την παρατήρηση πως ο κίνδυνος εμφάνισης γλαυκώματος είναι υψηλότερος σε άτομα με πολύ χαμηλή αρτηριακή πίεση (μερικές φορές ακόμα και ως αποτέλεσμα εντατικής θεραπείας της υπέρτασης).

Αυτή η διατριβή επιχειρεί να εξετάσει μεθοδικά εάν η αρτηριακή πίεση μπορεί να συνδεθεί με αλλαγές στον αμφιβληστροειδή που θα μπορούσαν να προδιαθέτουν στο γλαύκωμα. Για το σκοπό αυτό, αναλύουμε επιδημιολογικά δεδομένα από την Προοπτική Μελέτη Γλαυκώματος του Χρόνινγκεν, χρησιμοποιούμε προηγμένες τεχνικές απεικόνισης για να μοντελοποιήσουμε τη μικροκυκλοφορία και περιγράφουμε τη σχέση της με τη νευρική δομή και την κατανάλωση οξυγόνου του αμφιβληστροειδούς. Παρέχουμε ενδείξεις που κλίνουν προς την ύπαρξη μιας αγγειακής συνιστώσας, πιθανώς σχετιζόμενης με το γλαύκωμα.

Epilogue

At times, one might get lost wandering in the world of thoughts and ideas. One should never forget that it is people, not ideas, that guide us, support us, and motivate us to move forward. In place of an epilogue, I would like to use this space to acknowledge all these people in my life that made this piece of work possible.

To my mother, Hermione, and my father, Christos. Every step of the way, every hope and aspiration, everything I have come to expect has your loving signature. No parent could possibly top you. You have taught me everything, you have given me everything. There are no words to express my gratitude. I am forever in your debt.

To my grandmothers, Maria and Yota (†), and my grandfathers, Mimis (†) and Kostas (†). My childhood memories are entwined by your presence. Your faces, your voices, they hold the most beautiful and nostalgic place in my heart.

To my brother, Dimitris. To the endless times that we have found ourselves tackling open problems, discussing solutions, analyzing strategies. You are the most brilliant person I have ever met. Your ideas challenge me, your charisma inspires me. You are my greatest blessing, my younger self, my better self.

To my buddies from medical school, Romanos and Merkou. You are my long-time friends, the ones I would strive to see no matter what, with every bimonthly AMS-ATH return ticket. You made me feel like I never left. You never forgot me.

To my military medical ‘squad’. To the fruitful scientific and life discussions with Anastasis and Maj. Kostas, which always ended with me nagging about this PhD thesis.

To the Kounatidis family and their wonderful restaurant ‘Athene’. You were a Greek island of hospitality in Groningen. You were the place where I would feel like home. I will always reminisce about your good food, your warm hearts, and our constant Olympiakos-AEK grudge.

To my dear friends from Groningen, Azzu (who keeps refreshing submission portals, not unlike myself), Iris, Allison, and so many more. Our nights out, our trips, our discussions, they are so greatly missed. To the rest of my friends, colleagues, and mentors from Amsterdam, London, Magdeburg, Clermont-Ferrand, Turku, and every single person who made EGRET/EGRET(+) possible.

"I am indebted to my father for living; to my teacher for living well." – Alexander the Great
To Nomdo, my great mentor and supervisor, my friend. You are wise, you are diligent, yet you remain so humble. It is my greatest honour to know that half of everything in this work belongs to you. You are the clinician, the scientist, the person I look up to.

"So by day she'd weave at her great and growing web – by night, by the light of torches set beside her, she would unravel all she'd done. (…)What good sense resided in your Penelope – how well Icarius's daughter remembered you, Odysseus, the man she married once!" (Homer's 'Odyssey', excerpts)
To the 'Penelope' I left behind in this journey. To the 'Penelope' who sacrificed so much in my anticipation. To her beloved family and our poodle, Rocky. To the love of my life. To my Eleftheria.

About the Author

Konstantinos Pappelis was born in Amarousion (Athens, Greece), on September 1, 1991. From a very young age, he developed an aptitude for Mathematics and the Medical Sciences. Already since his high school years, Konstantinos was a member of the Mathematics, Physics, and Biology National Teams, and is still the only person in the history of the competitions having accomplished this achievement. In 2009, as a member of the Mathematics National Team, he won the bronze medal in the 26th Balkan Mathematical Olympiad (Kragujevac, Serbia) and in the 50th International Mathematical Olympiad (Bremen, Germany). In 2009, he graduated as a Valedictorian from the Hellenic-American Educational Foundation ('Athens College') and, following national examinations, he was granted entrance to the Medical School of the National & Kapodistrian University of Athens. Having achieved SAT perfect scores, he was also offered full-tuition scholarships for pre-medical studies by numerous Ivy League universities, including Harvard University, Princeton University, and the University of Pennsylvania, but decided to carry on with his studies in Greece.

During his medical studies, Konstantinos was the recipient of a six-year scholarship of Academic Excellence by the 'Antonios Papadakis' bequest of the University of Athens. In 2010, he was awarded the bronze medal in the 4th South-Eastern European Mathematics Olympiad for University Students (Plovdiv, Bulgaria) and in the 17th International Mathematics Competition (Blagoevgrad, Bulgaria), making him the only medical student in the history of the competitions having achieved this placement. Already before receiving his medical degree (M.D.) in 2016, Konstantinos had developed a strong interest in Ophthalmology, owing to the fascinating research and technological advancements in the field, to its underestimated interdisciplinary potential, but, most of all, owing to the complexity and almost mathematical precision characterizing visual function.

In January 2017, he joined the Rijksuniversiteit Groningen (RuG) as a Marie Curie fellow PhD student, under the supervision of Professor Nomdo M. Jansonius, head of the Ophthalmology Department of the University Medical Center Groningen (UMCG). His PhD

dissertation examines the implication of vascular factors in the pathogenesis of glaucoma, with a focus on optical coherence tomography. As an early-stage researcher of the European Glaucoma Research Education Training Plus consortium [EGRET(+); https://egret-plus.eu/], Konstantinos presented his research advancements to academic and industrial partners, during numerous international workshops and conferences. In 2017 and 2018 he served as an instructor for the Learning Community of Molecular Medicine of the RuG, teaching the Glaucoma Dissected course to medical and bioengineering students.

In 2019, parallel to his PhD studies, he joined the University Eye Clinic of the Otto von Guericke University (OvGU) Magdeburg as a visiting researcher. During this period, he specialized in advanced ophthalmic imaging (Laser Speckle Flowgraphy) and proposed a biophysical model for the autoregulating retinal microcirculation. During the same period, he collaborated with Heidelberg Engineering GmbH to develop quantitative analysis for the SPECTRALIS Flex OCT-angiography module. He subsequently implemented this technique to monitor vascular alterations during intraocular pressure stimulation in glaucoma patients with implanted intraocular pressure sensors. In 2020, Konstantinos began an external collaboration with the University Eye Clinic of the General Hospital of Athens ‘G. Gennimatas’, where he designed an ongoing project investigating retinal blood flow pathophysiology in diabetic retinopathy.

In 2021, Konstantinos was awarded a two-year research grant for postdoctoral research by Stichting Oogfonds Nederland. Since then, he holds a postdoctoral position at the UMCG, investigating the topographical association between structural, vascular, and visual function outcomes in the Groningen Longitudinal Glaucoma Study. He simultaneously fulfilled his one-year mandatory military service as a primary healthcare physician for the Medical Corps of the Hellenic Army. In September 2022 he will be undertaking the duties of resident ophthalmologist at the University General Hospital ‘Attikon’ in Athens, Greece.

Konstantinos is a regular member of the ARVO and EVER scientific societies and has an active presence in their annual meetings. He has published in several high-ranked journals in the fields of Ophthalmology and Physiology (refer to the Preface for a list of publications) and currently serves as a regular peer reviewer for twelve high-ranked scientific journals.

Aside from his scientific interests, Konstantinos is also a graduate of the National Conservatory of Athens, where he studied piano performance and contemporary composition.